NEW ADVENTURES IN SUPPORTED COPPER
NANOPARTICLES

M.ª Iris Martín García

Tesis Doctorales
UNIVERSIDAD de ALICANTE

Universitat d'Alacant
Universidad de Alicante

Instituto Universitario de Síntesis Orgánica (ISO)

NEW ADVENTURES IN SUPPORTED COPPER NANOPARTICLES

Thesis report to apply for a PhD degree with International Mention

at the University of Alicante submitted by:

Mª IRIS MARTÍN GARCÍA

Alicante, a certain day of a certain month in 2020
Doctoral Programme in Organic Synthesis

Scientific advisor:

FRANCISCO ALONSO VALDÉS

Instituto Universitario de Síntesis Orgánica (ISO), Universidad de Alicante
Ctra. Alicante-San Vicente s/n, 03690 San Vicente del Raspeig (Alicante), Spain
Tel. +34 965903400, ext. 2121; +34 965903549; Fax +34 965903549
http://iso.ua.es; iso@ua.es

Acknowledgements

Mi historia en Química empezó de manera un poco peculiar ya que me matriculé en la carrera simplemente porque me dijeron que no era capaz de aprobarla y que intentara cosas más fáciles y, sorprendentemente, estoy aquí, defendiendo mi trabajo de tesis y convirtiéndome en doctora en Química Orgánica. Simplemente tengo que agradecer a aquellos que no confiaron en mí al principio y por los cuales estoy aquí, gracias a ellos encontré mi lugar. Y como dijo una vez Albert Einstein "*Todos los grandes hechos y todos los grandes pensamientos tienen un comienzo ridículo*", tal y como empezó mi interés en este campo.

Antes de nada, quisiera mostrar mi agradecimiento al Instituto Universitario de Síntesis Orgánica y al Departamento de Química Orgánica por la oportunidad y los medios a los que me han dado acceso para llevar a cabo el proyecto de investigación que aquí se presenta.

En especial, agradecer a Francisco Alonso, mi "padre" en el mundo científico, por darme la oportunidad de trabajar en su grupo de investigación. Gracias por enseñarme todo lo que sé y animarme en mis momentos de frustración. Han sido años en los que te veía mucho más que a mi propia familia y más que un director, has sido un soporte y, en algunas ocasiones, hasta un psicólogo. Simplemente gracias.

Agradecer a J. C. Scaiano (Tito) por darme la oportunidad de realizar mi estancia internacional en su grupo de investigación y a Anabel por su apoyo y cuidado durante mis días allí. Sin duda alguna, una de las experiencias más enriquecedoras de mi vida.

También agradecer al resto de profesores que me han apoyado y amenizado mi estancia durante estos años como son Isidro, Diego A. y Álex, gracias por vuestros consejos y por las risas tanto fuera como dentro del laboratorio.

Hablando de profesores, no puedo olvidarme de ellos, Adela y Pedro, mis referentes desde el instituto. Hace 10 años me animaron a empezar mi carrera, y sólo puedo deciros: muchas gracias por confiar en mis posibilidades y por vuestra infinita paciencia. No os podéis imaginar la influencia positiva que han tenido vuestras palabras en mí.

La mejor manera de definir mi vida durante estos cinco años sería como una reacción oscilante. Sin embargo, no cambiaría nada de lo vivido, ya que, todos los momentos han servido para formar a la persona que soy actualmente. Además, he tenido la gran suerte de compartirlos con mi gran familia del laboratorio, que siempre han tenido los abrazos y las palabras adecuadas para cada momento. Muchas gracias por todo. En especial, a Juani, Diana, Jaisiel, Patri, Natalia, Bea, Edu, Diego, Nere, Mel, Llorenç, Óscar, Manu, Mario, Álex y

a las J. K. Rowling Stones; habéis sido un gran descubrimiento y ha sido un placer compartir estos años de aprendizaje con vosotros.

Agradecer también a mi Awatto Family por hacerme sentir en casa estando tan lejos de ella; gracias a ellos, el frío de Ottawa fue más llevadero. En especial, agradecer a Mica y a mis valencianos canadienses por cada uno de los momentos vividos juntos.

Las palabras de agradecimiento se me quedan cortas cuando tengo que hablar de ellos; son personas que te hacen ser mejor y sólo puedo decir que espero que no me falten nunca porque son parte de mí. Así que, María, María José y Xavi gracias por existir, por haber hecho más fáciles mis días en el laboratorio y por poner en mi vida a personas tan bonitas e imprescindibles como son Carla, Ángel y Luis.

También quiero agradecer a los de toda la vida, tanto a mi familia como a mis hermanas de otros padres. Muchas gracias a Mariajo, Ali, Cris, a mis cherries y a mis piñitas, por estar ahí cuando lo necesitaba y no soltarme nunca. En especial, a mis químicas viajeras y a mis petardas favoritas simplemente por estar en mi vida.

Agradecer todos los sacrificios que han hecho durante estos años los verdaderos pilares de mi vida, mis padres. Sin vosotros, nada de esto hubiera sido posible y sólo puedo deciros GRACIAS. Gracias por quererme, enseñarme, apoyarme, animarme y por los consejos que me habéis dado en cada uno de los aspectos de mi vida, pero, sobre todo, gracias por darme a la mejor hermana que se puede tener en este planeta. En definitiva, como dijo Ana, gracias por ser los cimientos de nuestras vidas, no podíamos tener más suerte.

Y qué decirte a ti Ana, gracias por sacarme una sonrisa hasta en los momentos más oscuros y por estar ahí siempre que lo necesito. Eres mi hermana pequeña, y me has enseñado mucho más a mí que yo a ti. La autodeterminación y la valentía que tienes es digna de admirar; decir que eres mi mayor orgullo se queda corto, te adoro.

Agradecerle a Carlos el ser mi medio melón, ya son 13 años juntos y no concibo una vida sin ti. Gracias por la paz que me das, por quererme de esa forma tan bonita, por ser mi lugar seguro en este mundo y por hacerme ser mi mejor versión.

En fin, esto llegó a su final y no puedo evitar sentir un poco de vértigo cuando pienso en el futuro. Pero bueno, como dijo una vez Gandhi *"Los grandes cambios siempre vienen acompañados de una fuerte sacudida. No es el fin del mundo, es el inicio de uno nuevo"*, y el mío me está esperando ahí fuera.

4

Preface

Preface

Over the last years, Alonso's group research has been focused on the development of new catalytic systems based on transition metal nanoparticles and their applications to develop new synthetic methods towards the synthesis of biologically active natural or synthetic compounds. The present thesis project was inspired by the same pivotal idea, more specifically, by the use of heterogeneous catalytic systems and their application in organic synthesis. Part of the results reported in this thesis have already been published:[†]

Chapter 1:

- o "Effect of morphology and support of copper nanoparticles on basic ovarian granulosa cell functions". Sirotkin, A. V.; Radosová, M.; Tarko, A.; Martín-García, I.; Alonso, F. *Nanotoxicology* **2020**, *14*, 683–695.
- o "Abatement of the stimulatory effect of copper nanoparticles supported on titania on ovarian cell functions by some plants and phytochemicals". Sirotkin, A. V.; Radosová, M.; Tarko, A.; Fabova, Z.; Martín-García, I.; Alonso, F. *Nanomaterials, (Accepted manuscript).*

Chapter 2:

- o "DNA-supported palladium nanoparticles as a reusable catalyst for the copper- and ligand-free Sonogashira reaction". Camacho, A. S.; Martín-García, I.; Contreras Celedón, C.; Chacón-García, L.; Alonso, F. *Catal. Sci. Technol*. **2017**, *7*, 2262–2273.
- o "Formation of C-C, C-S and C-N bonds catalysed by supported copper nanoparticles". Mitrofanov, A. Y.; Murashkina, A. V.; Martín-García, I.; Alonso, F.; Beletskaya, I. P. *Catal. Sci. Technol*. **2017**, *7*, 4401–4412.

Chapter 3:

- o "Cross-dehydrogenative coupling of tertiary amines and terminal alkynes catalysed by copper nanoparticles on zeolite". Alonso, F.; Arroyo, A.; Martín-García, I.; Moglie, Y. *Adv. Synth. Catal*. **2015**, *357*, 3549–3561.

Chapter 4:

"Synthesis of dihydroindoloisoquinolines through the copper-catalyzed cross-dehydrogenative coupling of tetrahydroisoquinolines and nitroalkanes". Martín-García, I.; Alonso, F. *Chem. Eur. J.* **2018**, *24*, 18857–18862. Highlighted article: Uozumi, Y.; Hamasaka, G. *Synfacts* **2019**, *15*, 0284.

Chapter 5:

"Synthesis of imines through the oxidative coupling of primary amines catalysed by sulfur-stabilised copper nanoparticles". Sloan, G.; Díaz, G.; Martín-García, I.; Moglie, Y.; Alonso, F. (*Manuscript in preparation).*

Other research developed during the doctoral period:

"Catalyst- and solvent-free hydrophosphination and multicomponent hydrothiophosphination of alkenes and alkynes". Moglie, Y.; González-Soria, M. J.; Martín-García, I.; Radivoy, G.; Alonso, F. *Green Chem*. **2016**, *18*, 4896–4907.

Summary

Summary

In this thesis, the development of new catalytic systems based on supported copper nanoparticles, the study of their biotoxicity and their applications in organic synthesis are described.

In **Chapter 1**, the effect of unsupported and supported (our catalytic systems) copper nanoparticles (CuNPs) on basic ovarian cell functions is studied. In this sense, the effect of the morphology (spherical, triangular and hexagonal) in unsupported CuNPs and the effect of the inorganic support [titanium dioxide (TiO_2), zeolite-Y (ZY) and active carbon (C)] in the supported ones are evaluated. For this purpose, cell-viability, accumulation of PCNA (proliferation marker), accumulation of BAX (apoptosis marker) and the release of steroid hormones (progesterone, testosterone and 17β-oestradiol) are analysed in cultured porcine ovarian granulosa cells, by the Trypan blue test, quantitative immunocytochemistry and the enzyme-linked immunosorbent assay (ELISA), respectively. By analysing the data of these experiments, promising results are concluded related to the reproduction field. Cell-viability increases for all the CuNPs, with the only exception being unsupported hexagonal CuNPs. Unsupported triangular and CuNPs/ZY improve the proliferation, whilst unsupported spherical and hexagonal CuNPs, together with CuNPs/TiO_2, deplete the accumulation of PCNA. Related to BAX accumulation, all CuNPs reduce the apoptosis except by CuNPs/ZY and hexagonal CuNPs. In general, the release of sexual hormones is promoted by CuNPs supported on ZY and C, whereas it is inhibited by CuNPs/TiO_2. All these results point to a direct impact of the morphology and support of the corresponding CuNPs in reproduction functions. Therefore, the proper modification of CuNPs might be a powerful tool for the control of reproductive processes.
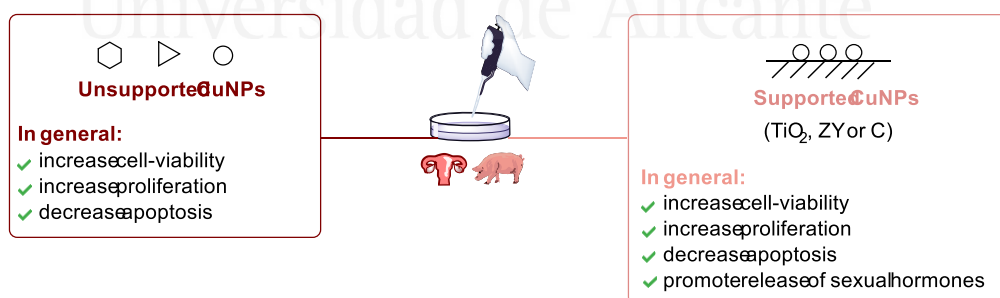
The following chapters describe the application of our catalytic systems (based on supported copper nanoparticles) in organic synthesis, paying special attention to cross-coupling, cross-dehydrogenative coupling (CDC) and some oxidation reactions.

In **Chapter 2**, the catalytic activity of four catalysts based on supported CuNPs (TiO$_2$, ZY, C and MK-10) is evaluated in three palladium- and ligand-free cross-coupling reactions for the construction of C-C, C-S and C-N bonds. Among these catalysts, CuNPs/ZY is the best one for the Sonogashira cross-coupling reaction of aryl iodides and terminal alkynes, as well as in the thiol arylation of aryl halides, being recyclable in both cases at least four times without losing any catalytic activity. On the other hand, CuNPs/TiO$_2$ shows the best results for the azoles' arylation. In this case, however, the recyclability of the catalyst is not effective due to the poisoning effect of the nitrogen-containing heterocycles (imidazole, pyrazole, benzimidazole and indole) on the catalyst surface. On the other hand, the catalytic activity of the nanostructured catalysts is compared with that of an array of copper-based commercial catalysts, being ours superior in the three cross-coupling reactions studied. Thus, a sustainable and cheaper alternative to palladium catalysis is described, showing similar behaviour in coupling reactions.
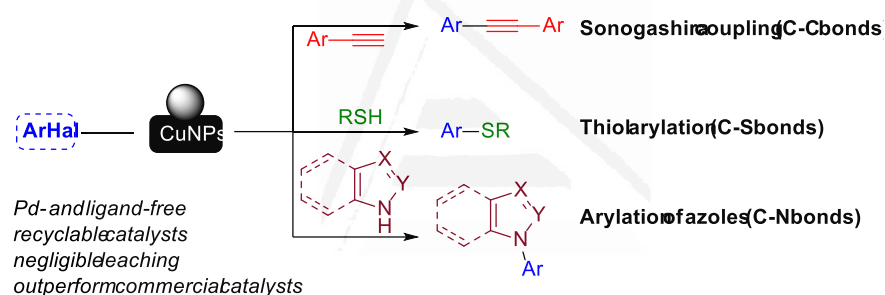
In **Chapter 3**, a large number of supported CuNPs catalysts is described and tested in the cross-dehydrogenative coupling of tertiary amines and terminal alkynes. CuNPs/ZY is the most effective catalyst in the presence of *tert*-butyl hydroperoxide (TBHP) as an oxidant at 70 ºC. In contrast to previous reported works, the reaction takes place without the need of an inert atmosphere under neat conditions, using 1.5 mol% catalyst loading. A variety of propargyl amines has been prepared from *N,N*-dialkylamines and terminal alkynes (including aromatic and aliphatic ones, in both cases) in moderate-to-excellent yields. The method has been equally effective even at 12 mmol scale. The catalyst can be reused in several cycles with no apparent loss of catalytic activity and has been shown to be superior to a wide variety of commercially available copper catalysts.
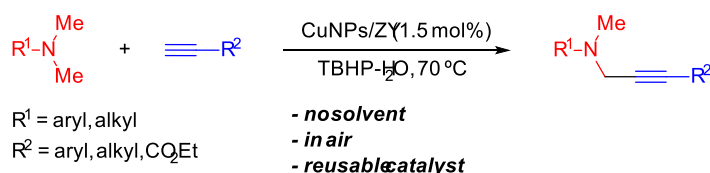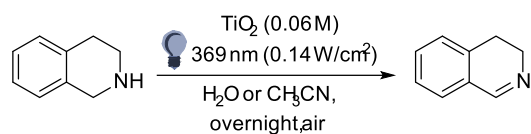
In **Chapter 4**, the CDC of 1,2,3,4-tetrahydroisoquinolines and nitroalkanes catalysed by supported CuNPs is evaluated. This reaction is one of the most studied CDCs in organic chemistry where, regardless of the catalyst and activation mode employed, only the corresponding β-nitroamines had been reported as products so far. A different behaviour has been observed when our catalytic system has been applied to this coupling. CuNPs/TiO$_2$ has been found to catalyse the CDC of 1,2,3,4-tetrahydroisoquinolines (THIQs) and nitroalkanes leading to the formation of 5,6-dihydroindolo[2,1-*a*]isoquinolines in good-to-excellent yields. Due to this particular behaviour, a thorough mechanism study has been performed and a reaction mechanism is proposed based on several control experiments. The recyclability of the catalyst has been found to be inefficient, due to the poisoning effect of the nitrocompounds on the catalyst surface. Nonetheless, the low catalytic loading deployed (1.5 mol%) and the superior performance of our catalytic system compared with that of commercial copper catalysts, support this methodology as an advantageous synthetic approach for the preparation of the aforementioned heterocyclic compounds.
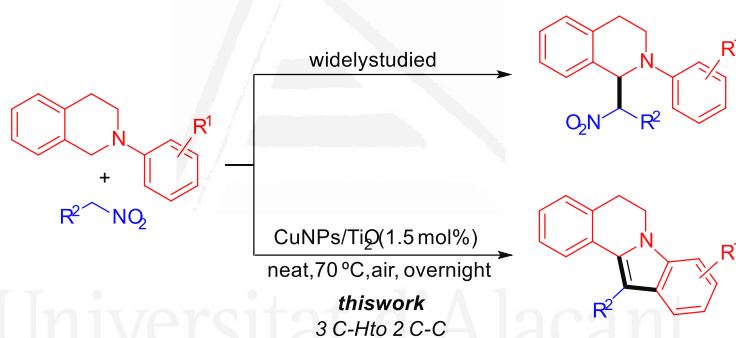
During the last year of this thesis, our research group decided to move on from conventional heterogeneous catalysis to heterogeneous photocatalysis. For this purpose, our catalytic systems have been tested in some organic transformations, employing light as mode of activation.

In **Chapter 5**, an array of MNPs supported on titania are compared in the dehydrogenative oxidation of 1,2,3,4-tetrahydroisoquinolines under photocatalytic activation. TiO$_2$ alone exhibits the highest catalytic activity, allowing the formation of the corresponding cyclic imines using low catalyst loading (0.06 M), in water or acetonitrile under air. The interaction between THIQs and TiO$_2$ has been analysed by different means, with the results pointing to the possible formation of an electron-transfer charge complex between them. Further experiments are required to better assess the scope and the reaction mechanism.

Index

Index

General Introduction

Antecedents

A.   Introduction to nanocatalysis

Although the word Nanotechnology is relatively new, alchemists and artisans had been using nanomaterials since ancient times.[1a] As an example, medieval artisans investigated the effect of the addition of different metals in glass for the preparation of stained-glass windows. Figure 1 shows the effect of size and shape of metal (M) nanoparticles (NPs) on their optical properties.
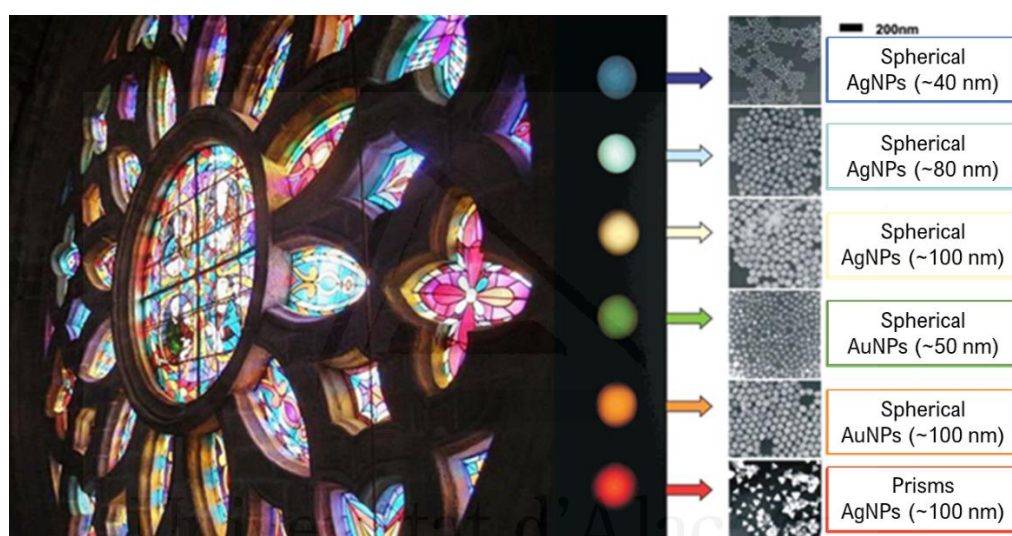
Figure 1. Effect of size and shape of Au and AgNPs on the colour properties. Figure reproduced from ref. 1b. Copyright 2005 Wiley-VCH.

Among the huge variety of MNPs discovered, colloidal gold nanoparticles (AuNPs)[2] have been the most studied ones, due to their applications in medicine since 1718. However, Michael Faraday was the first researcher to study, in a thoroughly way, the synthesis and properties of colloidal AuNPs in 1857. His systematic studies about light-AuNPs interactions can be considered as the very early stage of the emergence of Nanoscience and Nanotechnology. Afterwards, nanoparticles have had an amazing long history.

---

[1] (a) Loos, M. *Carbon Nanotube Reinforced Composites*; Elsevier: Amsterdam, 2015; pp. 1-36. (b) Mirkin, C. A. *Small* **2005**, *1*, 14-16.

[2] Reviews: (a) Daniel, M.-C.; Astruc, D. *Chem. Rev.* **2004**, *104*, 293-346. (b) Elahi, N.; Kamali, M.; Baghersad, M. H. *Talanta* **2018**, *184*, 537-556. (c) Ishida, T.; Murayama, T.; Taketoshi, A.; Haruta, M. *Chem. Rev.* **2020**, *120*, 464-525.

A.1. Nanoscience, Nanotechnology and nanoparticles

Generally, the starting point for the establishment of Nanoscience and Nanotechnology is attributed to the Nobel laureate Richard Feynman. In his 1959's lecture, *'There's plenty of room at the bottom'*, professor Feynman discussed on whether scientists could be able to control individual atoms and molecules.[3] This plenary session is widely considered as the first time where someone openly speculated about the matter manipulation at the atomic level. As such, it sparked off a huge interest in the field, with lots of theories and studies emerging from it during the following years and laying the foundations of what we know today as Nanoscience. For this reason, Professor Feynman is considered to be the 'father of Nanoscience'.

Based on the ideas that were discussed in this lecture, and with the invention of the scanning tunnelling microscope (1981), IBM scientists were able to manipulate 35 xenon atoms to create the IBM acronym (Figure 2). This experiment was the first evidence that proved Feynman's speculations.
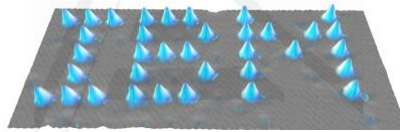
Figure 2. Xenon atoms, as arranged by IBM scientists, on a nickel substrate employing a scanning tunneling microscope. Credit: IBM. Image originally created by IBM Corporation.

Since its discovery, there have been a wide variety of definitions of Nanoscience and Nanotechnology, most of which relate them to the branch of science that deals with the manipulation of matter at the nanometre scale. Among these definitions, the most complete ones were those defined by *The Royal Society & The Royal Academy of Engineering*:[4]

'Nanoscience is the study of phenomena and manipulation of materials at atomic, molecular and macromolecular scales, where properties differ significantly from those at large scale. Nanotechnologies are the design, characterisation, production and application of structures, devices and systems by controlling shape and size at the nanometre scale.'

---

[3] Feynman, R. P. *Eng. Sci.* **1960**, 22-36.

[4] *Nanoscience and Nanotechnologies: Opportunities and Uncertainties*; The Royal Society and The Royal Academy of Engineering, Science Policy Section, The Royal Society: London, July 2004; p. 5.

The Greek prefix 'nano' implies a 10^{-9} factor for a given unit (it means that 1 nanometre is equal to 10^{-9} metres). In order to understand how small a nanometre (nm) is, Figure 3 shows the nanometre in context.
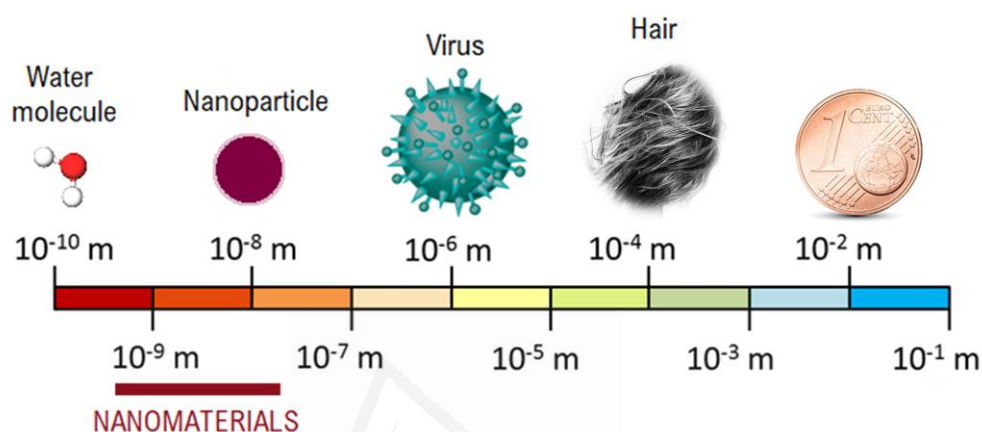
Figure 3. Comparison of the size of nanomaterials with that of some organisms and objects.

The particles in a size range from 1 to 100 nm can be considered nanoparticles (NPs).[5] These materials have different behaviour from the large ones, due to their high specific surface-to-volume ratio and the dominance of quantum effects. These two characteristics are the main reasons for their increased chemical reactivity, as well as their differences in optical, magnetic, thermal, mechanical and electrical properties, when compared to their homologous macroscale materials.[6]

During the last decade, the use of nanoparticles has emerged with practical applications in different fields such as medicine, biology, engineering, environment, physics and chemistry.[7] In the later, one of the main applications of nanoparticles is catalysis.[8]

---

[5] Reviews and monographs: (a) *Nanoparticles: From Theory to Application, 2nd Edn.*; Schmid, G., Ed.; Wiley-VCH: Weinheim, 2010. (b) Goesmann, H.; Feldmann, C. *Angew. Chem. Int. Ed.* **2010**, *49*, 1362-1395. (c) Vollath, D. *Nanomaterials: An Introduction to Synthesis, Properties and Applications, 2nd Edn.*; Wiley-VCH: Weinheim, 2013.

[6] Reviews and monographs: (a) *Inorganic Nanoparticles: Synthesis, Applications and Perspectives*; Altavilla, C.; Ciliberto, E., Eds.; CRC Press: London, 2010. (b) Review: An, K.; Alayoglu, S.; Ewers, T.; Somorjai, G. A. *J. Colloid Interface Sci.* **2012**, *373*, 1-13. (c) Horikoshi, S. A., Serpone, N. I. *Microwaves in Nanoparticle Synthesis: Fundamentals and Applications*; Wiley-VCH: Weinheim, 2013; pp. 1-24.

[7] Review: Khan, I.; Khalid, S.; Khan, I. *Arab. J. Chem.* **2019**, *12*, 908-931.

[8] For a special issue, see: (a) Nanoparticles for Catalysis. *Acc. Chem. Res.* **2013**, *46*, 1671-1910. (b) Asensio, J. M.; Bouzouita, D.; van Leeuwen, P. W. N. M.; Chaudret, B. *Chem. Rev.* **2020**, *120*, 1042-1084.

A.2. Synthesis of metallic nanoparticles

The preparation of NPs requires the total control of particle size, shape, composition, distribution and crystal structure. All protocols must be reproducible, paying special attention to the stabilisation of structural and physical properties avoiding, at the same time, the NPs aggregation.

Several strategies have been designed for the preparation of MNPs,[6c,9] all of which are included into two main families as *top down* and *bottom up* methods, being the second ones the most employed, due to their higher degree of control over the MNPs size that they provide.[10]

Table 1. Methodologies to prepare MNPs.

Top down Bulk » powder » NPs	*Bottom up* Atom » cluster » NPs	
Physical methods	**Chemical methods**	**Biological methods**
Arc discharge Electron beam lithography Ion implantation Inert-gas condensation Mechanical grinding Milling Spray pyrolysis Vapour-phase synthesis	Co-precipitation method Chemical reduction of metal salts Electrolysis Microemulsion method Pyrolysis Photochemical method Sonochemical method Sol-gel process Solvothermal synthesis	Using microorganisms Applying algae Employing enzymes and biomolecules Applying industrial and agricultural wastes

Chemical reduction of metal salts is considered the most widely used procedure within the huge variety of *bottom up* methods.[6b,10] Among the different reducing agents, the most

---

[9] Monographs: (a) *Metal Nanoclusters in Catalysis and Material Science. The Issue of Size Control;* Corain, B., Schmid, G., Toshima, N., Eds.; Elsevier: Amsterdam, 2008. (b) *Nanoparticles and Catalysis*; Astruc, D., Ed.; Wiley-VCH: Weinheim, 2008. (c) *Selective Nanocatalysts and Nanoscience;* Zecchina, A., Bordiga, S., Groppo, E., Eds.; Wiley-VCH: Weinheim, 2011. (d) *Nanocatalysis. Synthesis and Applications;* Polshettiwar, V., Asefa, T., Eds.; Wiley-VCH: Weinheim, 2013. (e) *Metal Nanoparticles for Catalysis: Advances and Applications*; Tao, F., Ed.; The Royal Society of Chemistry: Cambridge (UK), 2014. Review: (f) Jamkhande, P. G.; Ghule, N. W.; Bamer, A. H.; Klaskar, M. G. *J. Drug. Deliv. Sci. Technol.* **2019**, *53*, 101174.
[10] Reviews: (a) Roucoux, A.; Schulz, J.; Patin, H. *Chem. Rev.* **2002**, *102*, 3757-3778. (b) Cushing, B. L.; Kolesnichenko, V. L.; O'Connor, C. J. *Chem. Rev.* **2004**, *104*, 3893-3946. (c) Dahl, J. A.; Maddux, B. L. S.; Hutchison, J. E. *Chem. Rev.* **2007**, *107*, 2228-2269. (c) Xu, C.; De, S.; Balu, A. M.; Ojeda, M.; Luque, R. *Chem. Commun.* **2015**, *51*, 6698-6713.

outstanding ones are: oxidable solvents (such as alcohols),[11] H_2,[12] CO,[13] hydrides,[14] activated alkali metals (Rieke metals)[15] and organic salts.[16] The major drawback of this methodology is the difficulty in avoiding NPs aggregation, that is why it is important to maintain fine control (over the synthetic procedure) and understand the steps involved in NPs formation, from single atoms to the final particles.

In this sense, Turkevich and co-workers (1950) established the first standard procedure for the synthesis of controlled-size MNPs solutions, besides proposing the mechanism for the formation of MNPs through the growth of metallic clusters in solution.[16]
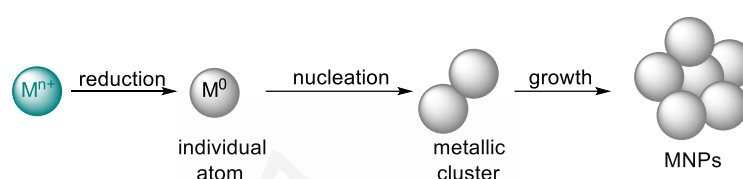
Figure 4. Turkevich's mechanism of MNPs formation.

Due to their high surface-volume ratio, NPs have an extra energy on their surface, which makes them thermodynamically unstable. For this reason, stabilising agents are compulsory to achieve a large interparticle separation. Depending on the nature of the corresponding agent, the type of interaction can be classified as electrostatic (including solvents), steric (including ligands) and electrosteric (Figures 5 and 6).[9b]

---

[11] Shiraishi, Y.; Arakawa, D.; Toshima, N. *Eur. Phys. J. E: Soft Matter Biol. Phys.* **2002**, *8*, 377-383.

[12] Boutonnet, M.; Kizling, J.; Touroude, R.; Maire, G.; Stenius, P. *Appl. Catal.* **1986**, *20*, 163-177.

[13] Kopple, K.; Meyerstein, D.; Meisel, D. *J. Phys. Chem.* **1980**, *84*, 870-875.

[14] (a) Mayer, A. B. R.; Johnson, R. W.; Hausner, S. H.; Mark, J. E. *J. Macromol. Sci. Pure Appl. Chem*. **1999**, *A36*, 1427-1441. (b) Crooks, R. M.; Zhao, M.; Sun, L.; Chechik, V.; Yeung, L. K. *Acc. Chem. Res.* **2001***, 34*, 181-190.

[15] Reviews: (a) Rieke, R. D. *Crit. Rev. Surf. Chem.* **1991**, *1*, 131-166. (b) Rieke, R. D.; Hanson, M. V. *Tetrahedron* **1997**, *53*, 1925-1956. (c) Rieke, R. D. *Aldrichimica Acta* **2000**, *33*, 52-60. (d) See, also: Schöttle, C.; Bockstaller, P.; Popescu, R.; Gerthsen, D.; Feldmann, C. *Angew. Chem. Int. Ed.* **2015**, *54*, 9866-9870.

[16] (a) Turkevich, J.; Stevenson, P. C.; Hillier, J. *Discuss. Faraday Soc.* **1951**, *11*, 55-75. (b) Turkevich, J.; Gim, G. *Science* **1970**, *169*, 873-879. (c) Turkevich, J. *Gold Bull.* **1985**, *18*, 86-91.
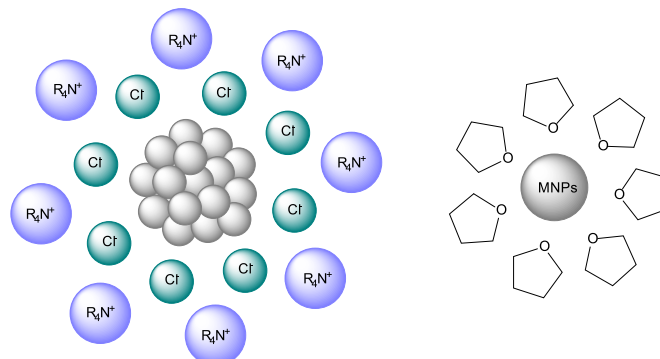
Figure 5. Electrostatic stabilising agents.
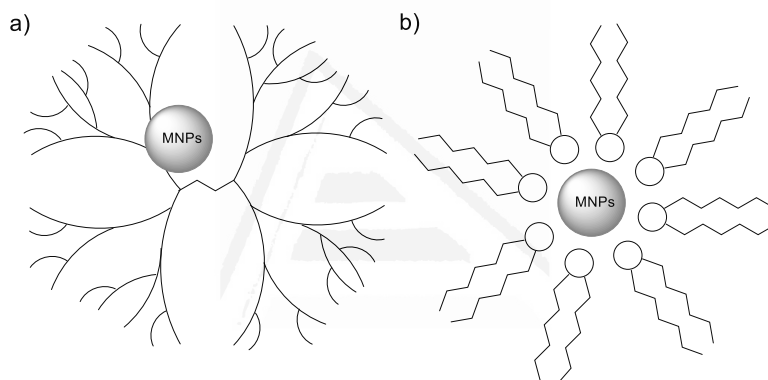
Figure 6. (a) Steric and (b) electrosteric stabilising agents.

Throughout the whole of the twentieth century, one of the main goals of organic chemistry has been to work within the framework of green chemistry.[17] In response to this, heterogeneous catalysis emerged as an attractive alternative to the traditional methodologies. Among the benefits of this kind of catalysis, the ease of separation of the catalyst from the reaction medium, which enables its regeneration, recycling and reuse, together with the thermal and oxidation stability that these catalysts exhibit, are the most remarkable ones.[18]

---

[17] Reviews: (a) Kidwai, M. in *Handbook of Green Chemistry*; Anastas, P. T., Crabtree, R. H., Eds.; Wiley-VCH: Weinheim, 2009; Vol. 2, pp. 81-92. (b) Yan, N.; Xiao, C.; Kou, Y. *Coord. Chem. Rev.* **2010**, *254*, 1179-1218. (c) Polshettiwar, V.; Varma, R. S. *Green Chem.* **2010**, *12*, 743-754. (d) Anastas, P.; Eghbali, N. *Chem. Soc. Rev.* **2010**, *39*, 301-312. (e) Gilbertson, L. M.; Zimmerman, J. B.; Plata, D. L.; Hutchinson, J. E.; Anastas, P. T. *Chem. Soc. Rev.* **2015**, *44*, 5758-5777. (f) Duan, H.; Wang, D.; Li, Y. *Chem. Soc. Rev.* **2015**, *44*, 5778-5792.

[18] (a) Burrington, J. D. *Industrial Catalysis: Chemistry and Mechanism*; Imperial College Press: London, 2017. (b) Wang, A.; Li, J.; Zhang, T. *Nat. Rev. Chem.* **2018**, *2*, 65-81.

Due to that, heterogeneous catalysts have the potential to be more environmentally friendly than their homogeneous counterparts.

In this sense, the exceptional properties of nanocatalysis and the inherent characteristics of heterogeneous catalysis can be combined to develop new efficient catalytic systems. Thus, heterogeneous catalysts[19] based on supported MNPs are attractive tools for the synthesis of organic molecules due to the reactivity and selectivity that they possess with the additional advantage of the MNPs stabilisation.

A.3. Synthesis of supported MNPs

In these kinds of catalysts, MNPs are generated *in situ* or deposited on fitting supports such as polymers,[20] metal oxides,[21] carbon materials[22] or mesoporous solids.[23] Among the supports that can be used, inorganic materials are considered the best ones because of their easy preparation, great dispersion, high catalytic efficiency and thermal stability.[9c]

Additionally, inorganic supports demonstrate a synergetic effect between the metal and the corresponding support, increasing their catalytic activity. Furthermore, the support plays a crucial role in the size and shape of the MNPs and, in turn, prevents their agglomeration.[19d]

The sustainable approaches for the synthesis of supported MNPs can be classified as physical, chemical and physicochemical,[24] some of which are shown in Table 2.

---

[19] Reviews: (a) Descorme, C.; Gallezot, P.; Geantet, C.; George, C. *ChemCatChem* **2012**, *4*, 1897-1906. (b) Friend, C. M.; Xu, B. *Acc. Chem. Res.* **2017**, *50*, 517-521. (c) Liu, L.; Corma, A. *Chem. Rev.* **2018**, *118*, 4981-5079. (d) Deelen, T. W.; Hernández Mejía, C.; Jong, K. P. *Nat. Catal.* **2019**, *2*, 955-970.

[20] Reviews: (a) Kralik, M.; Biffis, A. *J. Mol. Catal. A* **2001**, *177*, 113-138. (b) Akagi, T.; Baba, M.; Akashi, M. *Polymer* **2007**, *48*, 6729-6747. (c) Tamami, B.; Borujeni, K. P. *Iran. Polym. J.* **2009**, *18*, 191-206. (d) Ohtaka, A. *Chem. Rec.* **2013**, *13*, 274-285. (e) Kobayashi, S.; Miyamura, H. *Aldrichimica Acta* **2013**, *46*, 3-19.

[21] Reviews: (a) Risse, T.; Shaikhutdinov, S.; Nilius, N.; Sterrer, M.; Freund, H.-J. *Acc. Chem. Res.* **2008**, *41*, 949-956. (b) Chen, M. S.; Goodman, D. W. *Chem. Soc. Rev.* **2008**, *37*, 1860-1870. (c) *Nanomaterials in Catalysis*; Serp, P., Philippot, K., Eds.; Wiley-VCH: Weinheim, 2013; pp. 375-403.

[22] Reviews: (a) Lee, K.; Zhang, J. J.; Wang, H. J.; Wilkinson, D. P. *J. Appl. Electrochem.* **2006**, *36*, 507-522. (b) Georgakilas, V.; Otyepka, M.; Bourlinos, A. B.; Chandra, V.; Kim, N.; Kemp, K. C.; Hobza, P.; Zboril, R.; Kim, K. S. *Chem. Rev.* **2012**, *112*, 6156-6214. (c) *Carbon Materials for Catalysis*; Serp, P., Figueiredo, J. J., Eds.; Wiley-VCH: Weinheim, 2009.

[23] Reviews and monographs: (a) Stein, A. *Adv. Mater.* **2003**, *15*, 763-775. (b) Bronstein, L. M. *Top. Curr. Chem.* **2003**, *266*, 55-89. (c) *Catalyst for Fine Chemical Synthesis. Microporous and Mesoporous Solid Catalysis*; Derouane, E. G., Ed.; Wiley-VCH: Weinheim, 2007.

[24] Reviews: (a) Campelo, J. M.; Luna, D.; Luque, R.; Marinas, J. M.; Romero, A. A. *ChemSusChem* **2009**, *2*, 18-45. (b) Munnik, P.; Jongh, P. E.; Jong, K. P. *Chem. Rev.* **2015**, *115*, 6687-6718.

Table 2. Synthetic approaches of supported MNPs.

Physical	Chemical	Physicochemical
Sonication Microwaves UV Laser Plasma Supercritical fluids	Co-precipitation Impregnation Deposition-precipitation Reverse-micelle emulsions Photochemical Chemical vapour deposition Electrochemical reduction	Sonoelectrochemical Pyrolysis

In general, the catalytic activity of supported MNPs depends on the composition-distribution, size, shape and oxidation state of the corresponding metals. This is the reason why a thorough characterisation of the catalysts is necessary to understand their selectivity and reactivity.

A.4. Characterisation techniques

There is a wide range of surface-sensitive imaging and spectroscopic techniques to perform a complete characterisation of supported MNPs. Some of them are summarised in Figure 7, followed by a brief description of each one.[25]
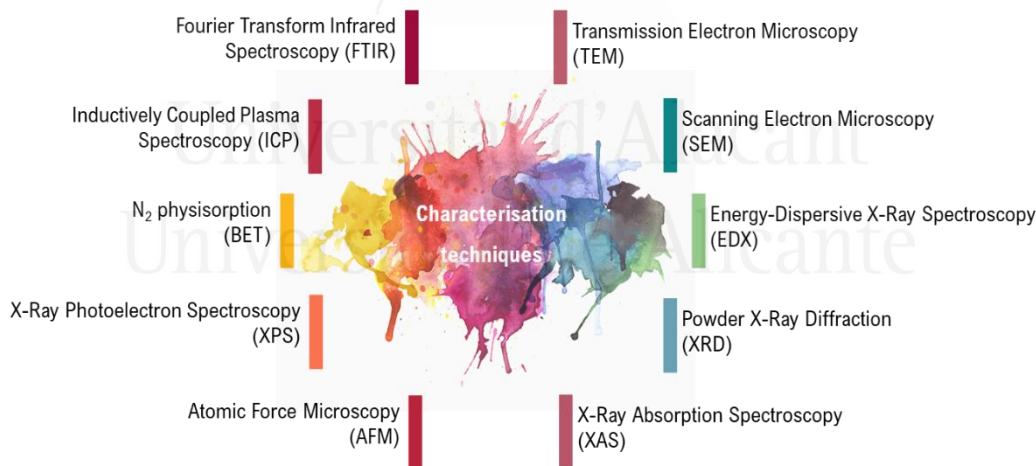
Figure 7. Characterisation techniques of supported MNPs.

---

[25] Review: Mourdikoudis, S.; Pallares, R. M.; Thanh, N. T. K. *Nanoscale*, **2018**, *10*, 12871-12934.

A.4.1. Transmission Electron Microscopy (TEM)[26]

In TEM, a thin sample is shot employing an incident beam of 120-200 keV and the transmission/scattering of the electrons is used to construct the images. The Selected Area Electron Diffraction (SAED) employs the diffraction of the electrons to elucidate the crystal structure, whereas Energy-Dispersive X-Ray Spectroscopy (EDX) allows to determine the composition distribution of the material by X-Ray emission.

Other variations of this technique are: (a) High-resolution TEM (HRTEM), that employs phase-contrast imaging for the construction of the image; (b) Cryo-Transmission Electron Microscopy (cryo-TEM), that allows the visualisation of unaltered samples in their frozen-native environment; (c) in the particular case of Scanning Transmission Electron Microscopy (STEM), the beam is focused just on a fine spot (in contrast to simple TEM); (d) High-Angle Annular Dark-Field Imaging (HAADF-STEM), where the image is formed by collecting scattered electrons with an annular dark-field detector; (e) Electron-Energy Loss Spectroscopy (STEM-EELS), based on the measurement of the kinetic energy variation of the electron after its interaction with the sample. This technique is commonly applied to identify the type and number of atoms present in the sample, their chemical state and their interactions.

A.4.2. Scanning Electron Microscopy (SEM)[27]

In SEM, an incident beam of 5-30 keV interacts with the sample across the surface in two directions (XY). Then, the secondary electrons or backscattered electrons (which depend directly on the atomic number) are scanned forming an image.

A.4.3. X-Ray Diffraction (XRD)[9a]

In XRD, the powder sample is bombarded with a monochromatic radiation, and when the beam crosses a split of similar thickness to that of the radiation wavelength, its optical interferences are analysed. These X-Rays are diffracted with angles that depend on the inter-atomic distances, giving information about the crystallographic structure, nature of the phase, lattice parameters and crystalline grain size.

[26] Tang, C. Y.; Yang, Z. in Hilal, N.; Ismail, A. F.; Matsuura, T.; Oatley-Radcliffe, D., Eds.; *Membrane Characterization. Part 2*; Elsevier: Amsterdam, 2017; pp. 145-159.
[27] Akhtar, K.; Khan, S.; Khan, S.; Asiri, A. M. in *Handbook of Materials Characterization*; Sharma, S. K., Ed.; Springer: New York (NY), 2018; pp. 113-145.

A.4.4. X-Ray Absorption Spectroscopy (XAS)[25]

This technique measures the X-Ray absorption coefficient of a material as a function of the energy. This technique can be used to identify elements because each element has its characteristic absorption corresponding to the different binding energies. X-Ray Absorption Fine Structure (EXAFS) is employed to study the size and the crystal structure. X-Ray Absorption Near Edge Structure (XANES) is useful to determine the oxidation state, vacant orbitals, electronic configuration, side symmetry of the absorbing atom of the species, and to study the ligand arrangement in the molecular shell of the MNPs.

A.4.5. Atomic Force Microscopy (AFM)[25]

AFM is based on measuring the interaction forces (attractive or repulsive) between a fine probe and the sample, forming three-dimensional images of surfaces.

A.4.6. X-Ray Photoelectron Spectroscopy (XPS)[28]

XPS is based on the photoelectric effect. This technique employs X-Rays (Mg-Kα = 1253.6 eV or Al-Kα = 1486.6 eV are the most common ones) to analyse the surface composition of materials. These photons interact with the atoms on the surface, triggering electrons to be emitted by photoelectric effect or just Auger electrons. Because each element has a unique variation of binding energies, this technique can be employed to identify and determine the concentration of each element on the catalyst's surface, as well as their oxidation state and chemical environment.

A.4.7. N_2 physisorption (BET)[25]

The textural characterisation of the nanomaterials is achieved by means of N_2 adsorption at low temperatures (-196 ºC), which provides information about surface area and porosity distribution of the corresponding nanomaterial. The mathematical determination of the surface area is performed by the application of the equation derived from the Brunauer-Emmett-Teller (BET) theory.[29]

A.4.8. Inductively Coupled Plasma (ICP) Spectroscopy[30]

In ICP, the liquid sample is injected into the instrument and is converted into an aerosol that reaches the plasma state (7727 ºC). Inside the plasma, atoms are excited and ionised,

---

[28] *Handbook of X-Ray Photoelectron Spectroscopy*; Chastain, J., Ed.; Perkin-Elmer Corporation; Physical Electronics Division: Minnesota, 1992.

[29] Brunauer, S.; Emmett, P. H.; Teller, E. *J. Am. Chem. Soc.* **1938**, *60*, 309-319.

[30] Boss, C. B.; Fredeen, K. J. *Concepts, Instrumentation and Techniques in Inductively Coupled Plasma Optical Emission Spectroscopy*, 3rd Edn., Perkin-Elmer, Inc., USA, 2004.

and their decay emission is analysed by an optical system separating the radiation by its wavelength (OES) or by mass spectrometry (MS).

A.4.9. Fourier-Transform InfraRed Spectroscopy (FTIR)[25]

FTIR is based on the measurement of the absorption of electromagnetic radiation of wavenumbers within the range of 4000-400 cm^{-1}, which provides information of the molecular structure on the surface of the nanomaterials.

Based on the vast information that these techniques give about heterogeneous catalysts based on MNPs, scientists are able to better understand the behaviour of their corresponding catalytic systems.

B.   MNPs in organic synthesis

In general, MNPs are useful materials in catalysis due to the abundance of active catalytic sites, high efficiency and selectivity, that has made them capable of improving a large number of transformations.[9,31] Some reactions promoted by MNPs are aminations, carbonylations, hydrogenations, oxidations, cycloadditions and a huge amount of homo and hetero-couplings, among many others.[9c]

Noble metals are the most popular metals to carry out these transformations due to their unique reactivity patterns. Nevertheless, their little abundance in Earth, makes them extremely expensive when compared to other metals. In this sense, other transition metals emerged as a practical alternative to the precious metals. Ti, V, Cr, Mn, Fe, Co, Ni and Cu show similar behaviour to noble ones in some transformations, with the additional benefits of global availability.[32]

---

[31] Reviews: (a) Ranu, B. C.; Chattopadhyay, K.; Adak, L.; Saha, A.; Bhadra, S.; Dey, R.; Saha, D. *Pure Appl. Chem.* **2009**, *81*, 2337-2354. (b) Yan, N.; Xiao, C.; Kou, Y. *Coord. Chem. Rev.* **2010**, *254*, 1179-1218. (c) Somorjai, G. A.; Li, Y. *Top Catal.* **2010**, *53*, 832-847.

[32] (a) Zhou, W.; Guo, L. *Chem. Soc. Rev.* **2015**, *44*, 6697-6707. (b) Ludwig, J. R.; Schindler, C. S. *Chem* **2017**, *2*, 313-316.

B.1. Copper nanoparticles (CuNPs)

In the past few years, the use of CuNPs in catalysis has emerged as a competitive alternative to the rare and expensive precious metals due to several reasons,[33] with cost being one of them.

Copper, together with iron, is about 800 times cheaper than the cheapest noble metal, palladium, referred to the price of the corresponding metal chlorides (Table 3, entries 5 and 7-8).

Table 3. Price/mmol ratio of metal chlorides from Sigma-Aldrich in 2019.

Entry	Metal chloride	€/mmol
1	Ir	66.00
2	Rh	45.00
3	Au	26.00
4	Ru	9.50
5	**Pd**	**8.50**
6	Ni	0.11
7	**Cu**	**0.01**
8	**Fe**	**0.008**

Another advantage is its low toxicity: Cu is an essential trace element for human metabolism, which deficiency is more a potential problem than its toxicity.[34a] The U.S. National Research Council currently recommends that adults receive 1.5-3.0 mg of copper daily to prevent deficiencies. The World Health Organisation (WHO) establishes a safe limit of 2.0 mg/L of copper in drinking water.[34b] Moreover, copper has been used in medicine due to the anti-inflammatory, anticancer, and anticonvulsant activities.[34]

Among the benefits that copper presents for catalysis, its readiness for alloying with other metals (such as Zn, Sn, Al and Ni, among others) and its different catalytically active species [Cu(0), Cu(I) and Cu(II)] are of interest.[35]

---

[33] Reviews: (a) Ranu, B. C.; Dey, R.; Chatterjee, T.; Ahammed, S. *ChemSusChem* **2012**, *5*, 22-44. (b) Zaera, F. *Chem. Soc. Rev.* **2013**, *42*, 2746-2762. (c) Ojha, N. K.; Zyryanov, G. V.; Majee, A.; Charushin, V. N.; Chupakhin, O. N.; Santra, S. *Coord. Chem. Rev.* **2017**, *353*, 1-57. (d) Powar, N. S.; Patel, V. J.; Pagare, P. K.; Pandav, R. S. *Chem. Methodol.* **2019**, *3*, 457-480. (e) Deka, P.; Borah, B. J.; Saikia, H.; Bharali, P. *Chem. Rec.* **2019**, *19*, 462-473.

[34] (a) Othmer, K. *Concise Encyclopedia of Chemical Technology*; John Wiley & Sons: Hoboken (NJ), 2007; Vol. 1, pp. 672-685. (b) Araya, M.; Olivares, M.; Pizarro, F.; Llanos, A.; Figueroa, G.; Uauy, R. *Environ. Health Perspect.* **2004**, *112*, 1068-1073.

[35] Gawande, M. B.; Goswami, A.; Felpin, F.-X.; Asefa, T.; Huang, X.; Silva, R.; Zou, X.; Zboril, R.; Varma, R. S. *Chem. Rev.* **2016**, *116*, 3722-3781.

Considering all these advantages, CuNPs are highly attractive for catalysis, because they are capable to promote organic transformations in a sustainable way compared to other metals or conventional catalysts. Some examples of their catalytic application in organic chemistry include coupling, cycloaddition, reduction, oxidations, multicomponent and photocatalytic reactions, among others.[35]

B.2. Supported CuNPs

In recent years, our research group has developed several catalytic systems based on supported copper nanoparticles according to the following principles: ease of preparation, air stable, low metal loading, involvement of benign solvents or solvent-free conditions, reusability and higher catalytic activity than the commercial catalysts. The latter is an important point as we believe that every laboratory-made catalyst should be more efficient than the commercial catalysts used for the same purpose in order to justify the time, materials and human resources employed during its preparation.

Our research group has prepared MNPs, such as NiNPs,[36] CuNPs,[37] and FeNPs[38] by the chemical reduction of metal salts, which show high reactivity and selectivity. More recently, this group has focused its attention on the immobilisation of CuNPs on different inorganic supports. Some applications of these catalysts based on supported CuNPs are:

1) Alkyne homocoupling[39]

$$R-\!\!\!\equiv\!\!\! \xrightarrow[\substack{\text{THF or neat} \\ 65\,^\circ\text{C}, 2\text{-}24\,\text{h}}]{\substack{1\,\text{mol}\%\,\text{CuNPs/TiO}_2 \\ 30\,\text{mol}\%\,\text{piperidine}}} R-\!\!\!\equiv\!\!\!-\!\!\!\equiv\!\!\!-R \quad 50\text{-}97\%$$
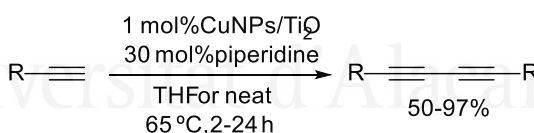
Scheme 1. Homocoupling of terminal alkynes catalysed by CuNPs/TiO$_2$.

[36] Reviews: (a) Alonso, F.; Yus, M. *Chem. Soc. Rev.* **2004**, *33*, 284-293. (b) Alonso, F.; Yus, M. *Pure Appl. Chem.* **2008**, *80*, 1005-1012. (c) Alonso, F.; Riente, P.; Yus, M. *Acc. Chem. Res.* **2011**, *44*, 379-391. (d) Yus, M.; Alonso, F. *e-EROS Encyclopedia of Reagents for Organic Synthesis [Online]*, 27 May 2014.

[37] (a) Alonso, F.; Vitale, C.; Radivoy, G.; Yus, M. *Synthesis* **2003**, 443-447. (b) Alonso, F.; Moglie, Y.; Radivoy, G.; Vitale, C.; Yus, M. *Appl. Catal. A: Gen.* **2004**, *271*, 171-176. (c) Radivoy, G.; Alonso, F.; Moglie, Y.; Vitale, C.; Yus, M. *Tetrahedron* **2005**, *61*, 3859-3864.

[38] (a) Alonso, F.; Moglie, Y.; Radivoy, G.; Vitale, C.; Yus, M. *Tetrahedron* **2006**, *62*, 2812-2819. (b) Moglie, Y.; Alonso, F.; Vitale, C.; Yus, M.; Radivoy, G. *Appl. Catal. A: Gen.* **2006**, *313*, 94-100. (c) Moglie, Y.; Radivoy, G.; Vitale, C. *Tetrahedron Lett.* **2008**, *49*, 1828-1831.

[39] Alonso, F.; Melkonian, T.; Moglie, Y.; Yus M. *Eur. J. Org. Chem.* **2011**, 2524-2530.

2) Click chemistry[40]
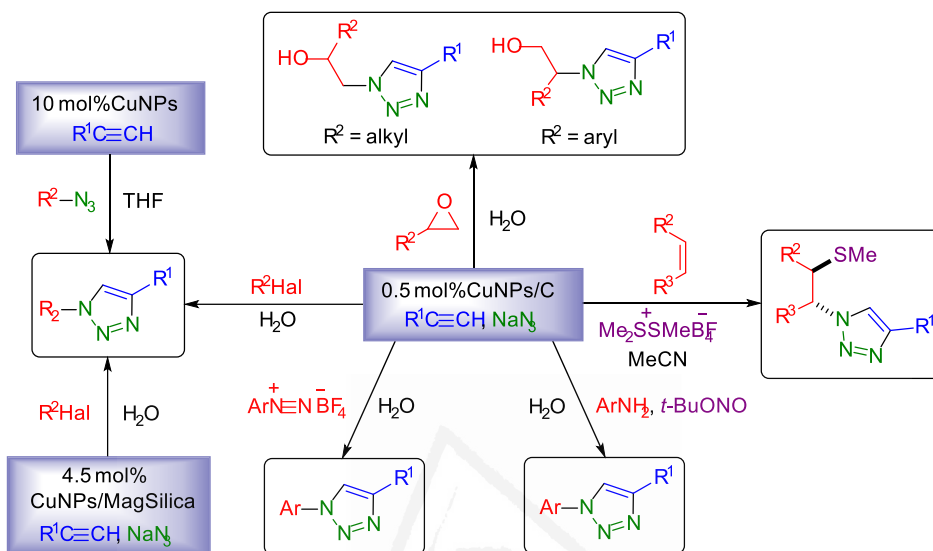
Scheme 2. Click chemistry from organic azides and from different azido precursors catalysed by unsupported and supported CuNPs, respectively. Scheme reproduced with permission from ref. 40. Copyright 2015 American Chemical Society.

3) Synthesis of indolizines and chalcones[41]
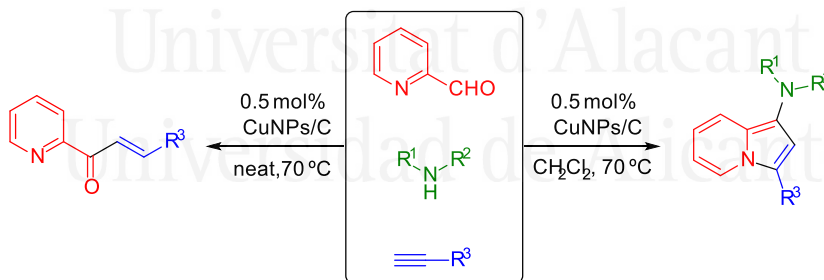
Scheme 3. Multicomponent synthesis of indolizines and synthesis of chalcones catalysed by CuNPs/C. Scheme reproduced with permission from ref. 41. Copyright 2015 American Chemical Society.

---

[40] Alonso, F.; Moglie, Y.; Radivoy, G. *Acc. Chem. Res.* **2015**, *48*, 2516-2528.

[41] (a) Albaladejo, M. J.; Alonso, F.; Yus, M. *Chem. Eur. J.* **2013**, *19*, 5242-5245. (b) Albaladejo, M. J.; Alonso, F.; González-Soria, M. J. *ACS Catal.* **2015**, *5*, 3446-3456.

General Objectives

General Objectives

Considering the previously mentioned benefits of heterogeneous nanocatalysis and the experience of our research group in this field, the main goals of this thesis were the following ones:

o   To prepare and characterise new catalysts based on supported copper nanoparticles.

o   To explore the biotoxicity of the catalysts.

o   To assess the activity of the catalysts in cross-coupling, cross-dehydrogenative coupling and some oxidation reactions.

o   To compare the catalytic activity of the catalysts with that of commercial ones.

o   To study the recyclability of the catalysts.

o   To determine the nature of the catalysis.

o   To study the corresponding reaction mechanisms.

Chapter 1. Synthesis, characterisation and biotoxicity of CuNPs

1.1. Antecedents

As previously mentioned, nanocatalysis can be considered as a competitive and sustainable alternative to conventional catalysis because of the high surface-to-volume ratio of the nanoparticles, which confers them high activity and selectivity. In particular, the immobilisation of metal nanoparticles allows a higher stability and dispersion of the NPs, with the possibility of catalyst recovery and reuse.

1.1.1. Riecke's method of synthesis

The most common method for the synthesis of MNPs is the chemical reduction of metal salts (see section A.2, p. 28).[10] In our particular case, the reduction step is based on the use of active alkali metals (Rieke's metals).[15]

This protocol involves the reduction of an anhydrous transition metal salt with the alkali metal and a catalytic amount of an arene, which acts as an electron carrier agent. The first step is an electronic transfer from the alkali metal to the arene, generating a radical anion (Ar$^{\bullet-}$) and/or dianion (Ar^{2-}). The following step is a fast-electron transfer from these species to the metal salt, forming MNPs in low-valence state.

Alkalimetal → Ar → M(0)NPs+ LiX

Alkalimetal^{+} → Ar$^{\bullet-}$ (Ar^{2-}) → MX$_n$
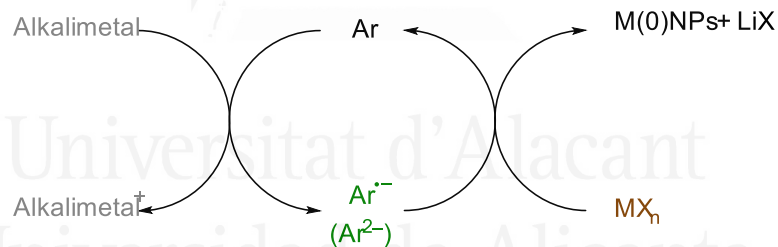
Scheme 4. Synthesis of MNPs by chemical reduction with Rieke's metals.

One of the main advantages of this methodology is that MNPs can be formed without the requirement of stabilising agents, at room temperature and in short reaction times.

1.1.2. Characterisation of supported CuNPs

As commented above, the proper characterisation of the catalyst is crucial in order to understand its activity. In this context, a plethora of techniques emerged for the characterisation of heterogeneous catalysts (see Section A.4, p. 32). The techniques that have been applied in this thesis and their main purpose are summarised in Table 4.

Table 4. Different techniques applied in this thesis.

Technique	Information provided
ICP-OES	Metal content of the bulk catalyst
N_2 physisorption	Surface area (BET)
XPS	Chemical composition and oxidation states of the different species on the catalyst surface
EDX	Chemical composition on the catalyst surface
TEM	Distribution, size and morphology of MNPs on the catalyst surface
XRD	Crystallographic structure and composition of the bulk catalyst

1.1.3. Biotoxicity of CuNPs

As previously discussed, MNPs have exceptional properties in catalysis compared with the bulk, but these properties can act as a double-edged sword. The same powerful properties of the MNPs can also influence their ability to induce biotoxicity. The general toxicity level for CuNPs has been ranked 3 (moderately toxic),[42] being the toxic dose of CuNPs ten times lower than that of ionic Cu to some organisms.[43]

Some researchers described that CuNPs have the capacity to produce damage in multiple locations, such as in the nuclear membranes, Ca^{2+} channels, NFkB inflammatory transcription factor and mitogen-activated protein kinase.[44] Moreover, CuNPs can easily form reactive oxygen species, which can produce nuclear and cytoplasmic apoptosis.[45] Additionally, both CuNPs and ionic Cu can negatively affect reproduction.[45a]

---

[42] Review: Hejazy, M.; Koohy, M. K.; Pour, A. B. M.; Najafi, D. *Nanomed. Res. J.* **2018**, *3*, 1-9.

[43] Review: Ameh, T.; Sayes, C. M. *Environ. Toxicol. Pharmacol.* **2019**, *71*, 103220.

[44] Hou, J.; Wang, X.; Hayat, T.; Wang, X. *Environ. Pollut.* **2017**, *221*, 209-217.

[45] (a) Roychoudhury, S.; Nath, S.; Massanyi, P.; Stawarz, R.; Kacaniova, M.; Kolesarova, A. *Physiol. Res.* **2016**, *65*, 11-22. (b) Review: Pohanka, M. *Bratisl. Lek. Listy.* **2019**, *120*, 397-409.

Nevertheless, some studies reported the stimulatory role of Cu on the ovulation rate,[46] gonadotropin secretion,[45a] release of insulin-like growth factor I and progesterone in cultured granulosa cells.[45a,47]

Thus, the preparation and application of safe CuNPs require the previous knowledge about the factors that can lead CuNPs to affect some physiological processes. In this sense, our research group, in collaboration with Sirotkin's group (Constantine the Philosopher University in Nitra, Slovakia), considered an attractive idea to study the effect of unsupported and supported CuNPs on reproduction, employing cultured porcine ovarian granulosa cells as target cells.

---

[46] Fevold, H. L.; Hisaw, F. L.; Greep. R. *Am. J. Physiol.* **1936**, *117*, 68-74.

[47] Roychoudhury, S.; Bulla, J.; Sirotkin, A. V.; Kolesarova, A. *J. Environ. Sci. Health A Tox. Hazard. Subst. Environ. Eng.* **2014**, *49*, 625-633.

1.2. Objectives

Based on this background, the following aims were set:

o To synthesise new catalytic systems based on CuNPs supported on inorganic solids such as active carbon (C), sodium zeolite-Y (ZY) and titanium dioxide (TiO_2), among others.

o To characterise the catalysts that show the best performance in certain organic reactions.

o To study the biotoxicity of unsupported and supported CuNPs of different morphologies on reproduction, through their effect on basic ovarian cell functions. (In collaboration with Sirotkin's group).

Universitat d'Alacant
Universidad de Alicante

1.3. Results and discussion

1.3.1. Synthesis of supported CuNPs

The preparation of our catalytic systems based on supported CuNPs follows the previously described Rieke's method, combined with the impregnation methodology. In this sense, three methods were implemented: impregnation (**A**), reduction-supporting (**B**) and impregnation-reduction (**C**).

1.3.1.1. Impregnation (A)

This technique is the most used for the synthesis of supported catalysts due to the ease of preparation and its low cost. In this strategy, the porous support is in contact with a solution of the corresponding metallic species, in our case, $CuCl_2$ in tetrahydrofuran (THF). Then, the catalyst is dried under vacuum.

1.3.1.2. Reduction-supporting (B)

Rieke's method was followed for the reduction step. In our particular case, we employed lithium powder as an alkali metal and 4,4'-di-*tert*-butylbiphenyl (DTBB) as an electron carrier. DTBB is one of the most widely used electron carriers because its radical anion and dianion are very potent reducing agents ($E_{1/2}$ = -2.14 V).[48] In this sense, $CuCl_2$ is reduced by metallic lithium powder in the presence of a catalytic amount of DTBB, in dry THF at room temperature under an inert atmosphere (Ar). In this protocol, it is important to avoid the presence of water in the reaction medium. The system can be described as shown in Scheme 5. First, lithium powder and DTBB react to generate Li-arene species, observing a change in colour to dark-green. The next step is the quick electron transfer ($10^6 - 10^9$ M^{-1} s^{-1}) from this system to anhydrous $CuCl_2$, generating a black suspension of reduced Cu(0)NPs. As already mentioned, CuNPs tend to aggregate in liquids but, in this case, electrosteric and electrostatic interactions of LiCl (generated *in situ*) and THF lead to a stable suspension. Finally, the inorganic support is added to this black mixture followed by filtration and drying in air.

---

[48] Curtis, M. D.; Allred, A. L. *J. Am. Chem. Soc.* **1965**, *87*, 2554-2563.
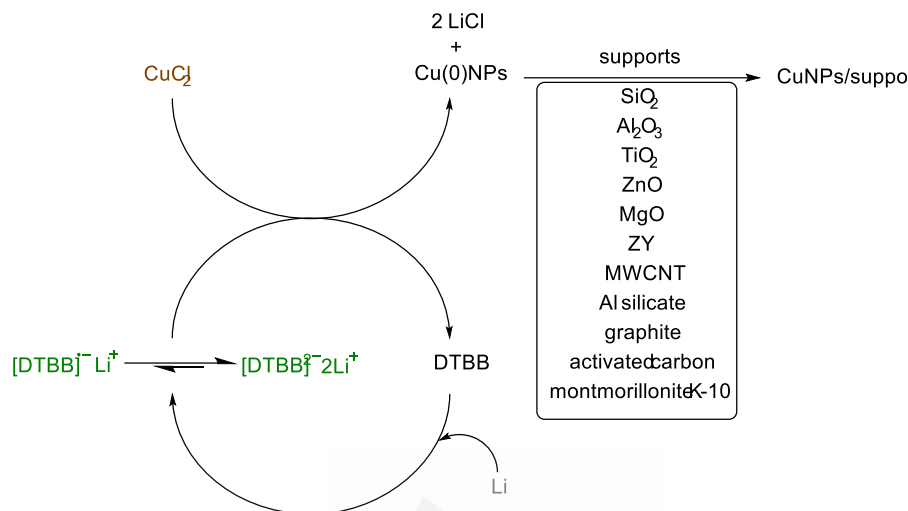
Scheme 5. General scheme for the synthesis of supported CuNPs by the reduction-supporting method.

1.3.1.3. Impregnation-reduction (C)

This strategy is a combination of methods **A** and **B**. In this case, a solution of the metallic precursor is brought into contact with the support (**A**) followed by the generation of the catalytic species through a reduction step as in (**B**).

Among the different methods, the reduction-supporting one (**B**) has been the most widely used in the present work.

1.3.2. Characterisation of supported CuNPs

With method **B** in hand, a plethora of catalysts was prepared employing a large variety of supports. Among these, inorganic oxides such as SiO_2, TiO_2, Al_2O_3, ZnO, MgO, CeO_2 or CeO_2 nanorods were used, as well as carbonaceous materials like activated carbon, graphite and carbon nanotubes (MWCNT). In addition, other inorganic and organic materials such as Al silicates, zeolites, montmorillonite K-10, 4 Å molecular sieves, sulphur, $K_2S_2O_8$, cellulose and chitosan were also employed.

We studied the performance of CuNPs supported on these materials in organic synthesis, with special attention to titanium dioxide (CuNPs/TiO_2), activated carbon (CuNPs/C) and sodium zeolite-Y (CuNPs/ZY). The characterisation of these three main catalysts follows:

Transmission Electron Microscopy (TEM) showed a good distribution of spherical NPs for CuNPs/TiO$_2$, CuNPs/C and CuNPs/ZY, with an average size of 0.98±0.42, 5.95±0.95 and 1.71±0.35 nm, respectively (Figures 8-A, 8-B, 9-A, 9-B, 10-A and 10-B).

Inductively Coupled Plasma Optical Emission Spectroscopy (ICP-OES) and Brunauer-Emmett-Teller (BET) analyses were employed to determine the copper content and the surface area, respectively, of each catalyst. The corresponding results are summarised in Table 5.

Table 5. ICP-OES and BET analyses of CuNPs.

Entry	Catalyst	wt% Cu	BET (m^2/g)
1	CuNPs/TiO$_2$	1.90	119
2	CuNPs/C	3.50	1224
3	CuNPs/ZY	3.00	621

X-Ray diffraction (XRD) analyses mainly showed peaks corresponding to the support, particularly for ZY, whereas Cu peaks were not observed probably due to the small crystal domains, low concentration and high dispersion of the copper species.[49]

As regards the selected area electron diffraction (SAED) patterns, CuNPs/ZY showed principally signals corresponding to zeolite-Y (Figure 9-D),[50] whereas CuNPs/C exposed to view the presence of Cu$_2$O and CuO species (Figure 10-D).

The presence of copper on the surface was confirmed by Energy-Dispersive X-Ray (EDX) and X-Ray Photoelectron Spectroscopy (XPS) experiments. EDX analyses, showed the characteristic lines of Cu at 8.04, 8.90 keV (K lines) and 0.92 keV (L lines) (Figures 8-C, 9-C and 10-C). XPS experiments revealed the presence of Cu(I) and Cu(II) oxides on the catalyst surface, in all cases. The results obtained are summarised in Table 6.

Table 6. XPS analyses of supported CuNPs.

Entry	Catalyst	Binding energy (eV) Cu 2$p_{3/2}$			ratio
		Cu$_2$O	CuO	Cu(II) satellites	
1	CuNPs/TiO$_2$	932.6	934.4	940.3/943.8	Cu$_2$O > CuO
2	CuNPs/C	931.7	934.0	943.3	Cu$_2$O = CuO
3	CuNPs/ZY	932.6	934.6	941.5/944.1	Cu$_2$O = CuO

[49] Huang, L.; Peng, F.; Wang, H.; Yu, H.; Li, Z. *Catal. Commun.* **2009**, *10*, 1839-1843.

[50] Kovo, A. S.; Hernández, O.; Holmes, S. M. *J. Mater. Chem.* **2009**, *19*, 6207-6212.

It is difficult to differentiate between Cu(0) and Cu(I) species only by the binding energy data due to their proximity (*ca.* 932.0-933.0 eV).[51] Auger analysis can discern between copper species employing kinetic energies. The corresponding values for copper species are 918.2, 916.0 and 917.6 eV for Cu(0), Cu(I) and Cu(II), respectively.[52] Taking these data into account, together with the observed Auger results (915-916 eV), it is possible to confirm the presence of Cu(I) species on the catalysts' surface.

According to the results summarised in Table 6, Cu(I) and (II) oxides were in an equal ratio for CuNPs/C and CuNPs/ZY, whereas CuNPs/TiO$_2$ showed mainly Cu(I) oxide. As a result, it can be concluded that the redox state of the CuNPs is affected by the support, what is attributed to different interfacial interactions. Thus, TiO$_2$ provides stabilisation for a more reduced state of copper, probably ascribed to a labile redox interplay between the pairs Cu(I)/Cu(II) ↔ Ti(III)/Ti(IV).[53]

---

[51] (a) Char, K. V. R.; Sagar, G. V.; Srikhanth, C. S.: Rao, V. V. *J. Phys. Chem. B* **2007**, *111*, 543-550. (b) Giménez-Mañogil, J.; Bueno-López, A.; García-García, A. *Appl. Catal. B: Environ.* **2014**, *152-153*, 99-107. (c) NIST X-Ray Photoelectron Spectroscopy Database, http://srda-ta.nist.gov/xps/.

[52] Briggs, D.; Seach, M. P. *Practical Surface Analysis by Auger and X-Ray Photoelectron Spectroscopy*; John Wiley & Sons: New York, 1983.

[53] (a) Wu, J. C. S.; Tseng, I.-H.; Chang, W.-C. *J. Nanopart. Res.* **2001**, *3*, 113-118. (b) Huang, L.; Peng, F.; Wang, H.; Yu, H.; Li, Z. *Catal. Commun.* **2009**, *10*, 1839-1843.

1.3.2.1. Characterisation of CuNPs/TiO$_2$
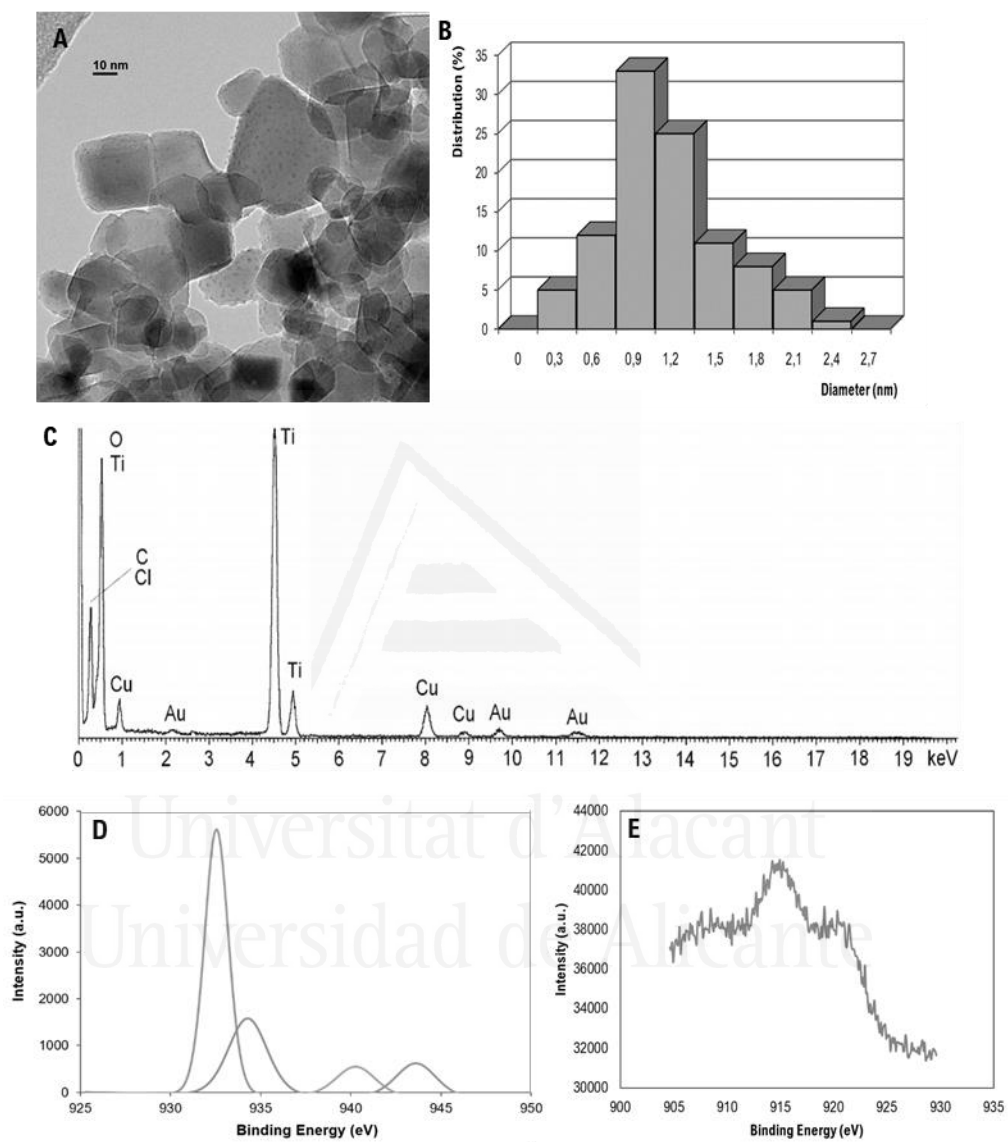
Figure 8. (A) TEM micrograph, (B) particle-size distribution, (C) EDX spectrum, (D) XPS spectrum and (E) Auger spectrum at the Cu 2$p_{3/2}$ level of CuNPs/TiO$_2$.

1.3.2.2. Characterisation of CuNPs/ZY

Figure 9. (A) TEM micrograph, (B) particle-size distribution, (C) EDX spectrum, (D) selected area electron diffraction (SAED) pattern, and (E) XPS spectrum at the Cu $2p_{3/2}$ level of CuNPs/ZY.

56

1.3.2.3. Characterisation of CuNPs/C

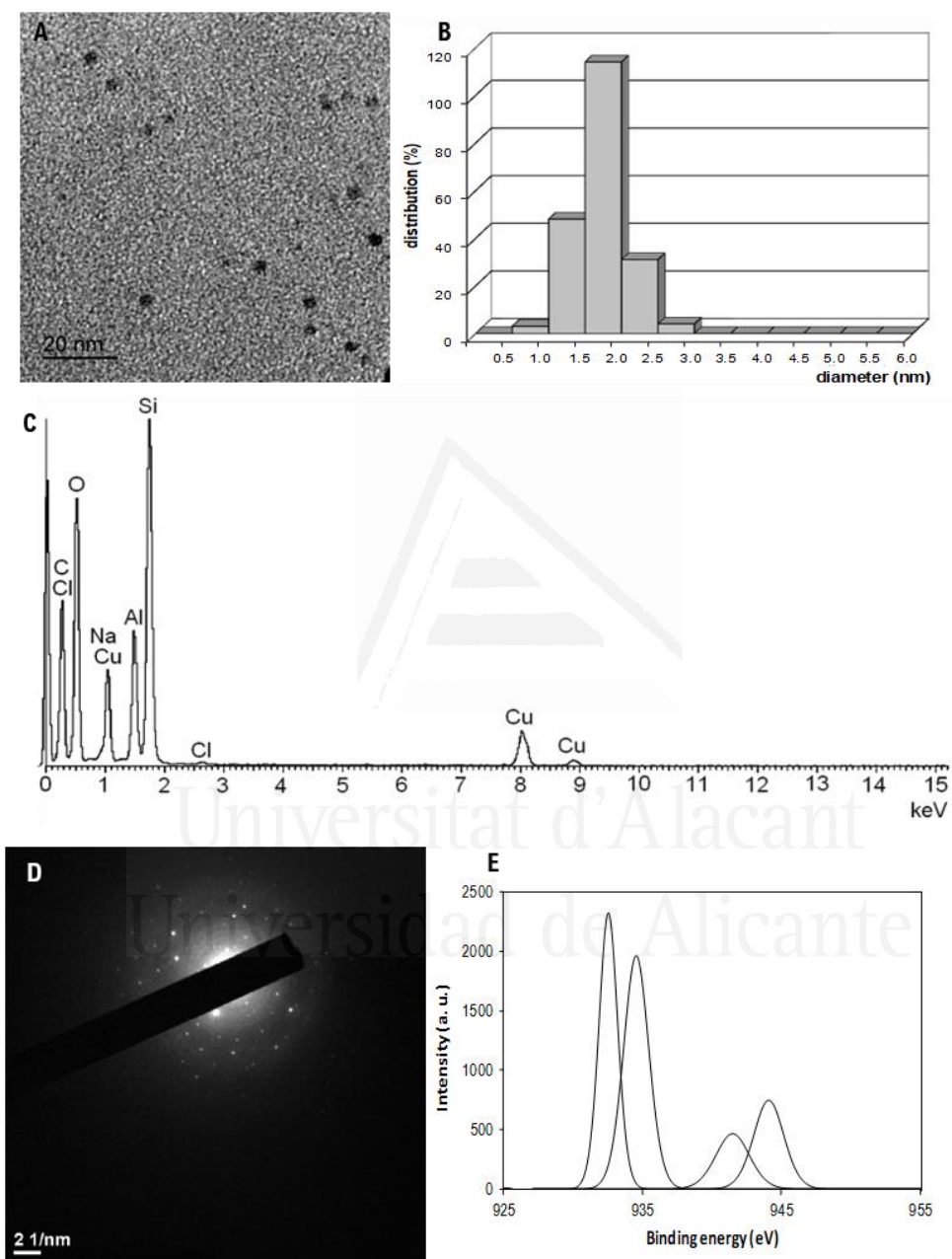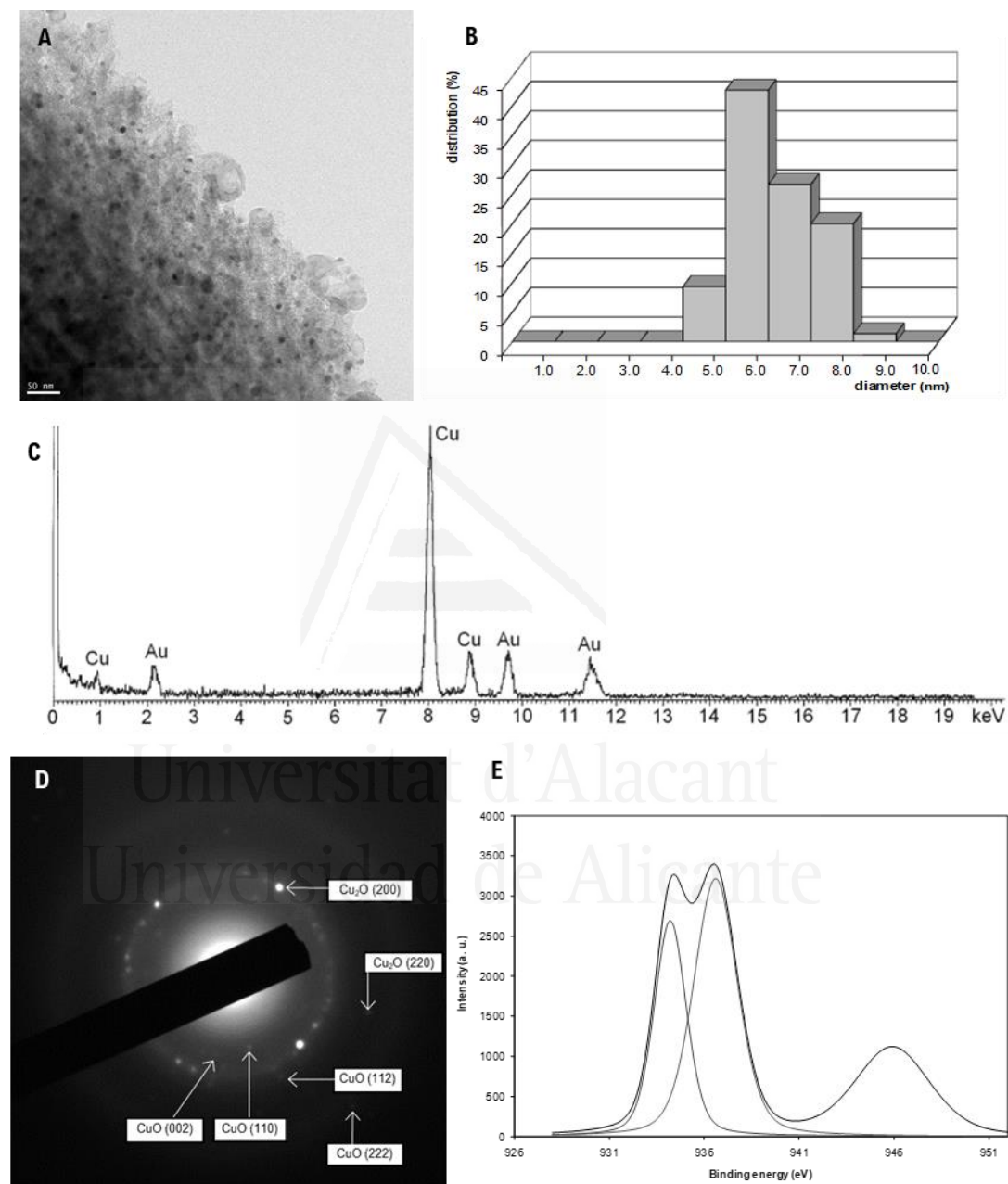**Figure 10**. (A) TEM micrograph, (B) particle-size distribution, (C) EDX spectrum, (D) selected area electron diffraction (SAED) pattern and (E) XPS spectrum at the Cu $2p_{3/2}$ level of CuNPs/C.

1.3.3. Biotoxicity of CuNPs

The biotoxicity study was focused on the effect of different types of CuNPs on basic ovarian cell functions. In particular, the cell viability, proliferation, apoptosis and the release of female (progestagens and oestrogens) and male (androgens) sexual hormones of cultured porcine ovarian granulosa cells were studied (Figure 11). For this purpose, the dose-dependent action (0, 1, 10 and 100 ng/mL) of CuNPs on the cell viability, the accumulation of the protein PCNA (Proliferating Cell Nuclear Antigen, proliferation marker)[54] and BAX (Bcl-2-Associated X protein, apoptosis marker) was evaluated.[55] Parallely, the release of progesterone, testosterone and 17β-oestradiol was analysed. These steroid hormones are involved in the adequate function of the reproductive system.[56]
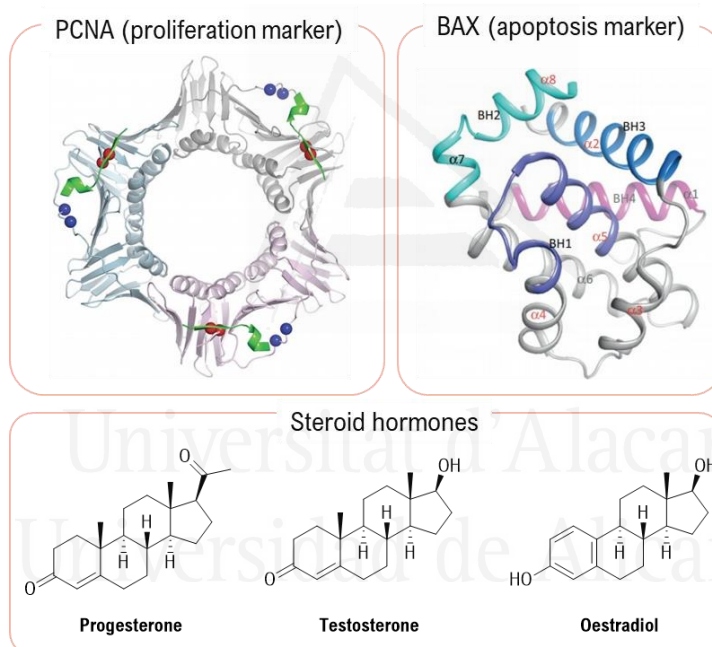
Figure 11. Structure of PCNA,[57] BAX[58] and some steroid hormones.

[54] Wang, S. C. *Trend Pharmacol. Sci.* **2014**, *35*, 178-186.

[55] Peña-Blanco, A.; García-Saéz, A. J. *FEBS J.* **2018**, *285*, 416-431.

[56] Sirotkin, A. V. *Regulators of Ovarian Functions*; Nova Publishers. Inc.: New York, 2014; p. 194.

[57] Vijayakumar, S.; Chapados, B. R.; Schmidt, K. H.; Kolodner, R. D.; Tainer, J. A.; Tomkinson, A. E. *Nucleic Acids Res.* **2007**, *35*, 1624-1637.

[58] Moldoveanu, T.; Follis, A. V.; Kriwacki, R. W.; Green, D. R. *Trends Biochem. Sci.* **2014**, *39*, 101-111.

Considering these markers, the impact on reproduction of unsupported and supported CuNPs was examined. Related to the supported ones, inorganic solids from different nature were employed as supports, obtaining spherical CuNPs supported on TiO_2, ZY and C. On the other hand, unsupported CuNPs with different morphologies were prepared, such as spherical, triangular and hexagonal CuNPs. The comparison of spherical CuNPs/TiO_2, CuNPs/ZY and CuNPs/C, and unsupported spherical, triangular and hexagonal CuNPs showed significant variations in their action on ovarian cell functions.

The polyol method described by Carpenter's group was followed for the preparation of unsupported triangular and hexagonal CuNPs,[59] whereas unsupported spherical CuNPs were synthesised using our general method (for further information, see the Experimental part, p. 209). The morphology and average size of the corresponding CuNPs were analysed by TEM [CuNPs/TiO_2 (Figure 8-A); CuNPs/ZY (Figure 9-A); CuNPs/C (Figure 10-A); unsupported CuNPs (Figure 12)].

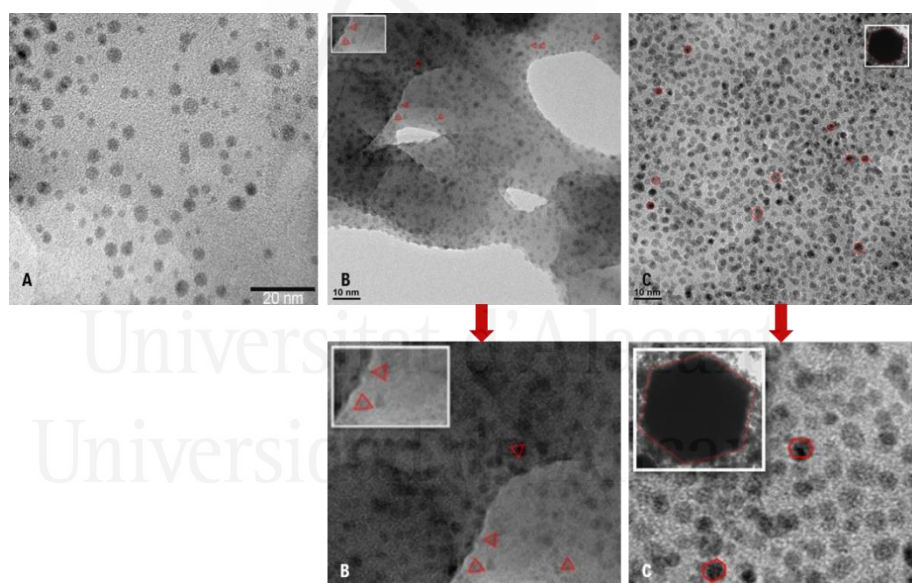**Figure 12.** TEM micrographs of unsupported spherical (**A**), triangular (**B**) and hexagonal (**C**) CuNPs.

A common behaviour of unsupported CuNPs was observed in the TEM experiments: after long exposure to TEM irradiation, CuNPs began to grow by coalescence. This effect was

[59] Carrol, K. J.; Reveles J. U.; Shultz, M. D.; Khanna, S. N.; Carpenter, E. E. *J. Phys. Chem.* **2011**, *115*, 2656-2664.

more dramatic in the case of unsupported triangular and hexagonal CuNPs, where the edges were rapidly distorted, and the original shape was harder to identify.

Table 7. Average size of unsupported and supported CuNPs.

Entry	CuNPs	Size (nm±median)
1	Spherical	2.88±0.94
2	Triangular	1.27±0.37
3	Hexagonal	1.81±0.52
4	TiO_2	0.98±0.42
5	ZY	1.71±0.35
6	C	5.95±0.95

Regarding the oxidation state of the CuNPs, it must be underlined that both unsupported and supported CuNPs were obtained as a mixture of copper oxides in all the cases.

1.3.3.1. Proliferation test (accumulation of PCNA)

In order to prove the presence of subcellular localisation of PCNA in cultured granulosa cells, fluorescence images were recorded (Figure 13).
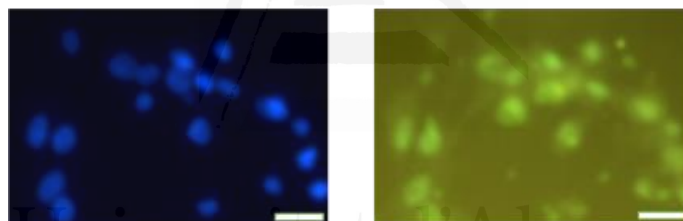
Figure 13. Fluorescent images of porcine granulosa cells containing PCNA. Immunocytochemistry images showing 4',6-diamidino-2-phenylindole dihydrochloride (DAPI, marker of nuclear DNA, blue) and fluorescein isothiocyanate (FITC, marker of PCNA antigen, green) staining in the same cells. Scale bars: 1 cm = 20 μm.

After confirming the presence of PCNA in the ovarian granulosa cells, some statistical studies were carried out evaluating the effect of the different CuNPs. Regarding unsupported CuNPs, spherical ones reduced the accumulation of the protein PCNA at doses of 1 or 10 ng/mL (Figure 14-A). On the contrary, triangular CuNPs (Figure 14-B) increased the proliferation in all the cases, whereas hexagonal CuNPs inhibited completely the PCNA accumulation (Figure 14-C).

Among the supported CuNPs, CuNPs/TiO_2 reduced the proliferation at doses of 10 and 100 ng/mL (Figure 14-D), while both, CuNPs/ZY (Figure 14-E) and CuNPs/C (Figure 14-F) increased PCNA accumulation. The same behaviour was observed for CuNPs/ZY in all cases, whereas CuNPs/C only did so at 100 ng/mL.
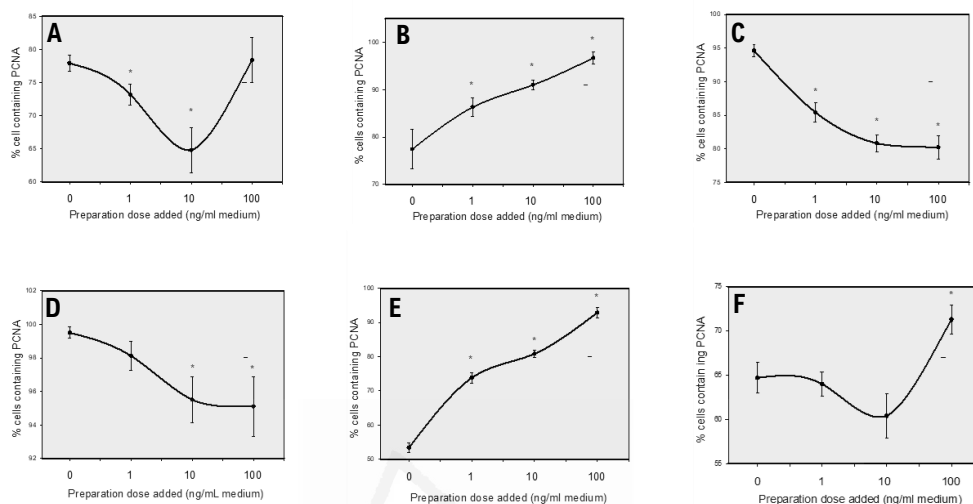
Figure 14. Comparison of the effect of spherical (**A**), triangular (**B**), hexagonal (**C**) CuNPs, and spherical CuNPs/TiO$_2$ (**D**), CuNPs/ZY (**E**) and CuNPs/C (**F**), added at the doses of 0, 1, 10 or 100 ng/mL medium, on the proliferation (accumulation of PCNA measured by quantitative immunocytochemistry) of cultured porcine ovarian granulosa cells. Each experiment was repeated three times using different animals. Each experimental group was represented by four chamber-slide wells (*n* = 12). The values are presented as mean ± SD; the asterisk indicates the effect of treatment – significant (P < 0.05) differences between cells treated *vs* untreated (dose 0 ng/mL) with nanoparticles.

1.3.3.2. Apoptosis test (accumulation of BAX)

As in the case of PCNA, the existence of subcellular localisation of BAX in cultured granulosa cells was confirmed by fluorescence images (Figure 15).
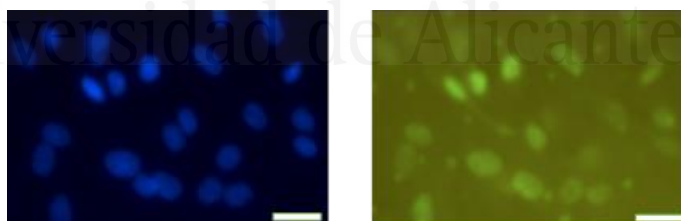
Figure 15. Fluorescent images of porcine granulosa cells containing BAX. Immunocytochemistry images showing DAPI (marker of nuclear DNA, blue) and FITC (marker of BAX antigen, green) staining in the same cells. Scale bars: 1 cm = 20 μm.

Concerning unsupported CuNPs, both spherical (Figure 16-A) and triangular NPs (Figure 16-B) suppressed cell apoptosis, in the case of spherical CuNPs at the doses of 10 or 100

ng/mL and only at 100 ng/mL for triangular ones. On the contrary, hexagonal CuNPs did not suppressed the BAX accumulation at all (Figure 16-C).

Supported CuNPs showed different behaviour. On one hand, CuNPs/TiO$_2$ (Figure 16-D) reduced BAX accumulation in all the cases, while CuNPs/C dropped its accumulation only at 100 ng/mL (Figure 16-F). On the other hand, CuNPs/ZY increased the apoptosis at 1 and 10 ng/mL (Figure 16-E).
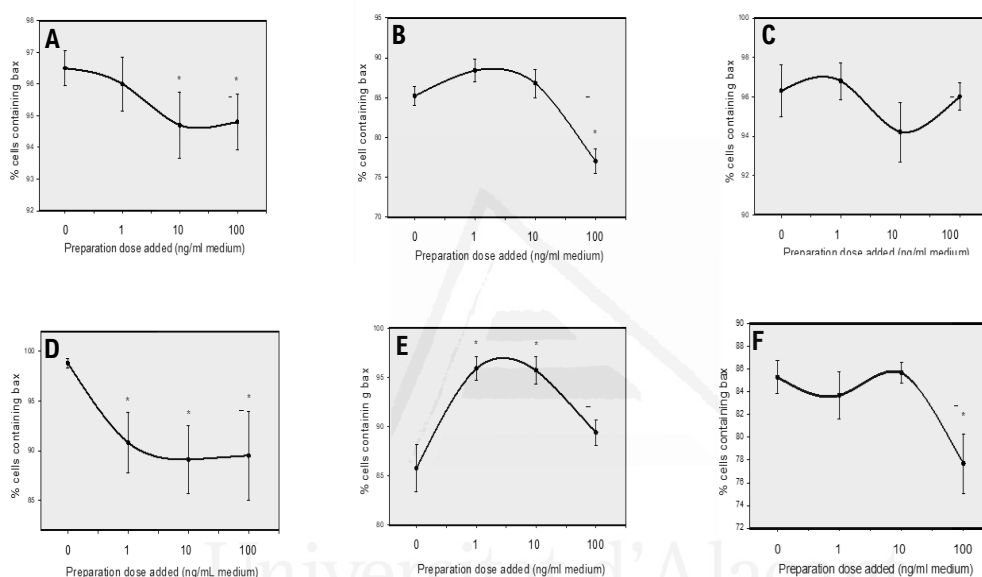

Figure 16. Comparison of the effect of spherical (**A**), triangular (**B**), hexagonal (**C**) CuNPs, and spherical CuNPs/TiO$_2$ (**D**), CuNPs/ZY (**E**) and CuNPs/C (**F**), added at the doses of 0, 1, 10 or 100 ng/mL medium on the apoptosis (accumulation of BAX measured by quantitative immunocytochemistry) of cultured porcine ovarian granulosa cells. Legends as in Figure 14.

1.3.3.3. Cell-viability test

Unsupported spherical (Figure 17-A) and triangular CuNPs (Figure 17-B) increased cell viability in all the cases, whereas hexagonal ones reduced the viability of cells when added at the doses of 10 and 100 ng/mL (Figure 17-C).

In the case of supported CuNPs, all of them favoured cell viability. CuNPs/TiO$_2$ (Figure 17-D) and CuNPs/ZY (Figure 17-E) promoted cell viability at the doses of 10 and 100 ng/mL whereas CuNPs/C (Figure 17-F) promoted cell viability only at the dose of 100 ng/mL.
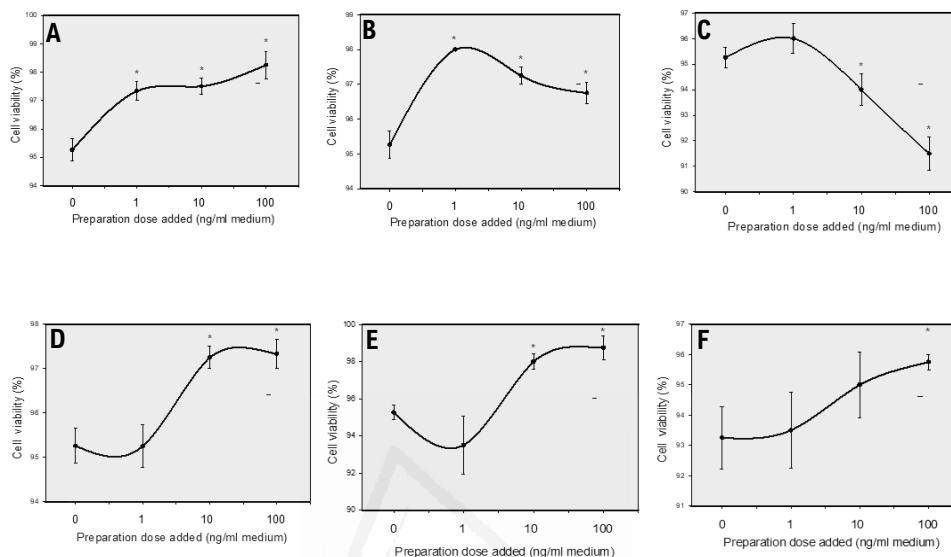
Figure 17. Comparison of the effect of spherical (**A**), triangular (**B**), hexagonal (**C**) CuNPs, and spherical CuNPs/TiO$_2$ (**D**), CuNPs/ZY (**E**) and CuNPs/C (**F**), added at the doses of 0, 1, 10 or 100 ng/mL medium, on the viability (measured by the Trypan blue extrusion test) of cultured porcine ovarian granulosa cells. Legends as in Figure 14.

1.3.3.4. Release of hormones by supported CuNPs

Only the catalysts based on supported CuNPs were evaluated, due to the nature of the procedures employed. Regarding the delivery of hormones, the nature of the support seems to be crucial.

CuNPs/TiO$_2$ supressed the release of progesterone at all the doses (Figure 18-A), whereas CuNPs/C favoured it at 1 and 10 ng/mL (Figure 18-C). The secretion of this female hormone was not affected by CuNPs/ZY (Figure 18-B).

The bell-shape effect of CuNPs/C (Figure 18-C) can be rationalised by the existence of adaptive negative response mechanisms preventing overstimulation of ovarian progesterone liberation, which could induce premature luteinisation and suppression of ovarian folliculogenesis.[56]

Figure 18. Comparison of the effect of spherical CuNPs/TiO$_2$ (**A**), CuNPs/ZY (**B**) and CuNPs/C (**C**), added at the doses of 0, 1, 10 or 100 ng/mL medium on the release of progesterone (measured by ELISA) by cultured porcine ovarian granulosa cells. Legends as in Figure 14.

Concerning testosterone, CuNPs/TiO$_2$ supressed the liberation of this hormone at all the doses (Figure 19-A). Opposite to this, CuNPs/ZY and CuNPs/C increased the accumulation of testosterone at the doses of 100 ng/mL (Figure 19-B) and 10 or 100 ng/mL (Figure 19-C), respectively.

Figure 19. Comparison of the effect of spherical CuNPs/TiO$_2$ (**A**), CuNPs/ZY (**B**) and CuNPs/C (**C**), added at the doses of 0, 1, 10 or 100 ng/mL medium on the release of testosterone (measured by ELISA) by cultured porcine ovarian granulosa cells. Legends as in Figure 14.

In the case of 17β-oestradiol, CuNPs/TiO$_2$ inhibited its release at the doses of 10 and 100 ng/mL (Figure 20-A), whereas CuNPs/ZY and CuNPs/C boosted its secretion at all the doses (Figures 20-B and 20-C).
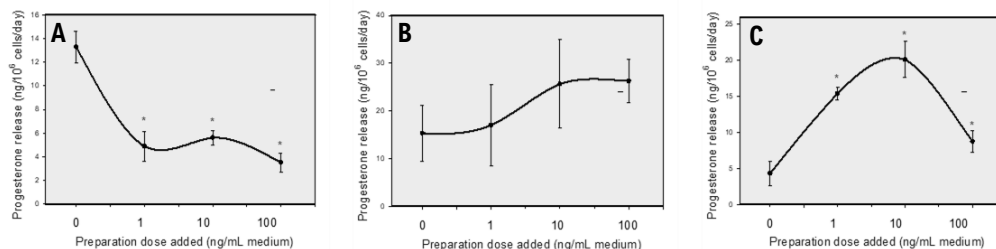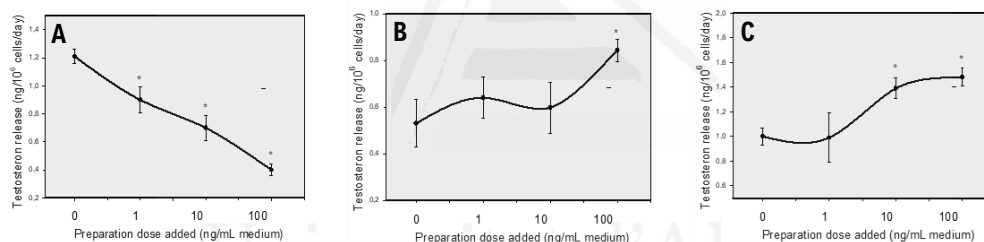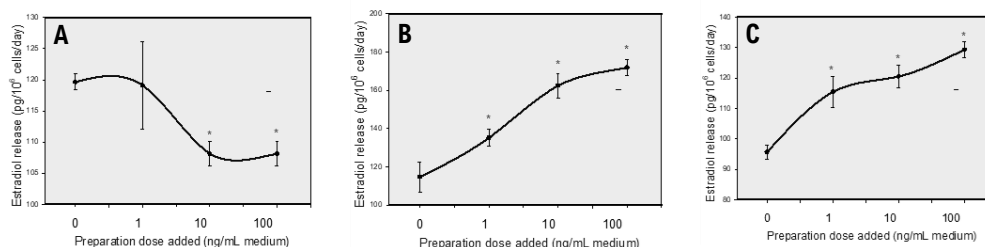
Figure 20. Comparison of the effect of spherical CuNPs/TiO$_2$ (**A**), CuNPs/ZY (**B**) and CuNPs/C (**C**), added at the doses of 0, 1, 10 or 100 ng/mL medium on the release of 17β-oestradiol (measured by ELISA) by cultured porcine ovarian granulosa cells. Legends as in Figure 14.

1.3.3.5. Summary of the biological experiments

All the information gathered from the experiments carried out confirms the direct impact of CuNPs on reproduction, affecting the basic functions of porcine granulosa ovarian cells. Simultaneously, this behaviour points out the different role and mechanisms of CuNPs on female reproduction. Gratifyingly, most of the CuNPs evaluated in our experiments are not toxic. On the contrary, they seem to enhance ovarian cell-viability, with the exception of the hexagonal ones (see Table 8). This could be due to the higher reactivity associated with vertices in MNPs. Moreover, we cannot ignore the fact that hexagonal CuNPs have been synthesised in the presence of toxic diethylene glycol.

Cell-viability can be defined by the balance between regulators of cell proliferation and death,[60] among which, PCNA and BAX can be found, respectively. Taking this into account, together with the results obtained in our experiments, cell-viability can be principally due to the suppression of BAX accumulation (Tables 8 and 9).

---

[60] (a) Pérez-Garijo, A.; Steller H. *Development* **2015**, *142*, 3253-3262. (b) Fritsch, J.; Zingler, P.; Sárchen, V.; Heck, A. L.; Schütze, S. *Biochim. Biophys. Acta, Mol. Cell Res.* **2017**, *864*, 2138-2146. (c) Gudipaty, S. A.; Conner, C. M.; Rosenblantt, J.; Montell D. J. *Annu. Rev. Cell Dev. Biol.* **2018**, *234*, 311-332.

Table 8. Effect of unsupported CuNPs on proliferation, apoptosis and cell-viability.

Test	Spherical CuNPs	Triangular CuNPs	Hexagonal CuNPs
proliferation	dropped at 1 and 10 ng/mL Figure 14-A	boosted at all doses Figure 14-B	dropped at all doses Figure 14-C
apoptosis	dropped at 10 and 100 ng/mL Figure 16-A	dropped at 100 ng/mL Figure 16-B	not affected at all doses Figure 16-C
cell-viability	boosted at all doses Figure 17-A	boosted at all doses Figure 17-B	dropped at 10 and 100 ng/mL Figure 17-C

Table 9. Effect of supported CuNPs on proliferation, apoptosis and cell-viability.

Test	CuNPs/TiO$_2$	CuNPs/ZY	CuNPs/C
proliferation	dropped at 10 and 100 ng/mL Figure 14-D	boosted at all doses Figure 14-E	boosted at 100 ng/mL Figure 14-F
apoptosis	dropped at all doses Figure 16-D	boosted at 1 and 10 ng/mL Figure 16-E	dropped at 100 ng/mL Figure 16-F
cell-viability	boosted at 10 and 100 ng/mL Figure 17-D	boosted at 10 and 100 ng/mL Figure 17-E	boosted at 100 ng/mL Figure 17-F

Related to the role of supported CuNPs in the release of sexual hormones, CuNPs/TiO$_2$ dropped the release of the three steroids (Table 10, column 2) whereas CuNPs/ZY and CuNPs/C favoured the secretion of these hormones in a dose-dependent manner (Table 10, columns 3 and 4).

Based on these results, the support seems to exert a significant role as only CuNPs/TiO$_2$ inhibits this function. Anatase TiO$_2$ is constituted by chains of distorted TiO$_6$ octahedra possessing undercoordinated atoms at the most abundant nanocrystal faces: i.e., 4- or 5-fold instead of 6-fold-coordinated Ti atoms, as well as 2-fold instead of 3-fold-coordinated O atoms, making TiO$_2$ particularly reactive.[61] It is known that oxygen-containing molecules can bind 5-fold-coordinated Ti atoms and 2-fold-coordinated O atoms. Therefore, an interaction of TiO$_2$ with the oxygen atoms of the steroid hormones or their precursors (enhanced in the case of testosterone and 17β-oestradiol due to the presence of hydroxyl groups in their

---

[61] Bourikas, K.; Kordulis, C.; Lycourghiotis, A. *Chem. Rev.* **2014**, *114*, 9754-9823.

structures) cannot be ruled out and might account for the particular behaviour of CuNPs/TiO$_2$ on hormone liberation.

Table 10. Release of steroid hormones by supported CuNPs.

Hormone	CuNPs/TiO$_2$	CuNPs/ZY	CuNPs/C
progesterone	dropped at all doses Figure 18-A	not affected at all doses Figure 18-B	boosted except at 100 ng/mL Figure 18-C
testosterone	dropped all doses Figure 19-A	boosted at 100 ng/mL Figure 19-B	boosted at 10 and 100 ng/mL Figure 19-C
17β-oestradiol	dropped at 10 and 100 ng/mL Figure 20-A	boosted at all doses Figure 20-B	boosted at all doses Figure 20-C

The inhibition and stimulation of the oestrogen output can be explained by the corresponding changes in its precursors, progesterone and testosterone. Moreover, 17β-oestradiol can stimulate the ovarian cell proliferation and inhibition of cell apoptosis while promoting ovarian follicle growth and suppressing cell atresia.[56]

Then, the promotion of cell-viability and PCNA accumulation by CuNPs/ZY, and the suppression of BAX accumulation by CuNPs/C could be justified by their capability to foster ovarian steroidogenesis. On the other hand, the inhibition of cell proliferation (but not apoptosis and cell-viability) by CuNPs/TiO$_2$ can be explained by suppression of the steroid hormones release.

Taking all these results into account, together with the reported works,[45a,46,47,62] it can be concluded that there is a potential positive effect of CuNPs on female reproductive functions, including fecundity.

In a more recent and related study, it has been explored whether plant extracts and phytochemicals can or cannot affect the activity of CuNPs on basic ovarian cell functions. We must point up that this kind of interaction has not been reported so far. For this purpose, CuNPs/TiO$_2$ was combined with the plant extracts of buckwheat (*Fagopyrum Esculentum*), vitex (*Vitex Agnus-Castus*) and the polyphenolic flavonoids rutin and apigenin. Some preliminary results show the capacity of the plant extracts and their polyphenolic constituents to suppress the activity of CuNPs/TiO$_2$ on ovarian functions. Therefore, to take CuNPs and

---

[62] (a) Yang, J.; Hu, S.; Rao, M.; Hu, L.; Lei, H.; Wu, Y.; Wang, Y.; Ke, D.; Xia, W.; Zhu, C. H. *Int. J. Nanomedicine* **2017**, *12*, 5959-5971. (b) Zhang, C. H.; Wang, Y.; Sun, Q. Q.; Xia, L. L.; Hu, J. J.; Cheng, K.; Wang, X.; Fu, X. X.; Gu, H. *Int. J. Biol. Sci.* **2018**, *14*, 1834-1844.

these plants or plant components jointly seems unadvisable concerning the ovarian functions. However, this interaction can be beneficial to prevent the potential noxious effect, when accidentally exposed to CuNPs, on other types of cells or organs. Further research on this subject is under way.

1.4. Conclusions

As a conclusion, an array of heterogeneous catalysts based on supported copper nanoparticles have been synthesised employing different methods, with special attention to the reduction-supporting procedure (**B**).

In order to understand the reactivity and selectivity of our catalysts, the complete characterisation of the most active ones (CuNPs/TiO$_2$, CuNPs/ZY and CuNPs/C) was performed.

The biotoxicity of unsupported and supported CuNPs was evaluated, being the first evidence that the nature of the CuNPs' action on reproductive functions can be defined by the morphology and the support of the CuNPs.

The lack of toxicity of supported CuNPs indicates the safety in their potential application for reproductive health endeavours. In addition, the potential efficacy of the stimulatory properties of CuNPs in reproduction cannot be overruled. Nevertheless, it must be considered that the stimulatory properties of CuNPs resemble some signs of harmful transformation of ovarian granulosa cells. Consequently, the efficiency of CuNPs to promote these transformations must be thoroughly checked before application.

Our supported catalytic systems might be helpful for the preparation and application of CuNPs with some desirable biological effects in medicine and to produce safe CuNPs-containing products.

Finally, it can be said that CuNPs have a direct impact on ovarian granulosa cells and have the capability to affect their viability, proliferation, apoptosis and sexual hormones secretion. Then, CuNPs with proper chemical variation could be potentially effective to control reproductive processes and to treat reproductive disorders.

Chapter 2. Formation of C-C, C-S and C-N bonds through cross-coupling catalysed by supported CuNPs

2.1. Antecedents

The formation of C-Heteroatom (C-N, C-O, C-S, C-P, C-Se), C-C and C-metal bonds has attracted a great deal of attention during the last century due to their presence in nature.[63a] One of the most powerful tools for the construction of these bonds is the group of transformations known as cross-coupling reactions. There is a vast number of procedures for carrying out these couplings. Among these methods, the use of supported MNPs is advantageous due to the good performance that they show and their capability of working within the framework of green chemistry.

2.1.1. Cross-coupling reactions catalysed by CuNPs[63]

Concerning the history of cross-coupling reactions catalysed by Cu, the first examples were reported by Ullmann in 1903 and 1905 for the synthesis of diarylamines[64] and for the arylation of phenol (Scheme 6).[65]
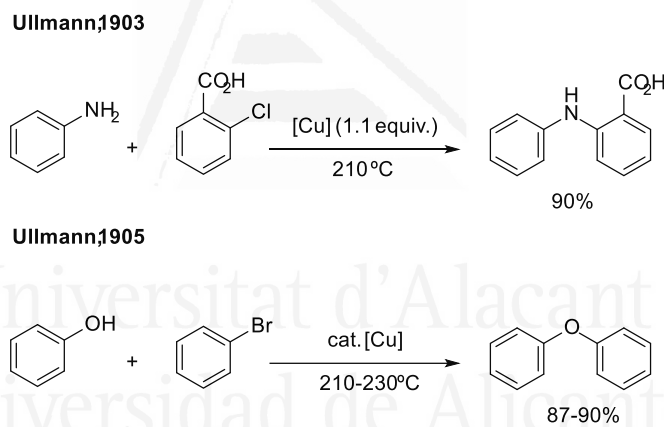
Scheme 6. First examples of cross-coupling reactions catalysed by Cu.

[63] Reviews: (a) Beletskaya, I. P.; Cheprakov, A. V. *Coord. Chem. Rev.* **2004**, *248*, 2337-2364. (b) Sambiago, C.; Marsden, S. P.; Blacker, A. J.; McGowan, P. C. *Chem. Soc. Rev.* **2014**, *43*, 3525-3550. (c) *Copper-Mediated Cross-Coupling Reactions*; Evano, G.; Blanchard, N. Eds.; Wiley-VCH: Weinheim, 2014. (c) Thapa, S.; Shrestha, B.; Gurung, S. K.; Giri, R. *Org. Biomol. Chem.* **2015**, *13*, 4816-4827. (d) Hirano, K.; Miura, M. *Chem. Lett.* **2015**, 868-873. (e) Beletskaya, I. P.; Alonso, F.; Tyurin, V. *Coord. Chem. Rev.* **2019**, *385*, 137-173.

[64] Ullmann, F. *Ber. Dtsch. Chem. Ges.* **1903**, *36*, 2382-2384.

[65] Ullmann, F.; Sponagel, P. *Ber. Dtsch. Chem. Ges.* **1905**, *38*, 2211-2212.

Based on Ullmann's studies, Goldberg reported the use of catalytic amounts of copper in the N-arylation of amides and anilines in 1906 (Scheme 7).[66]

Goldberg 1906
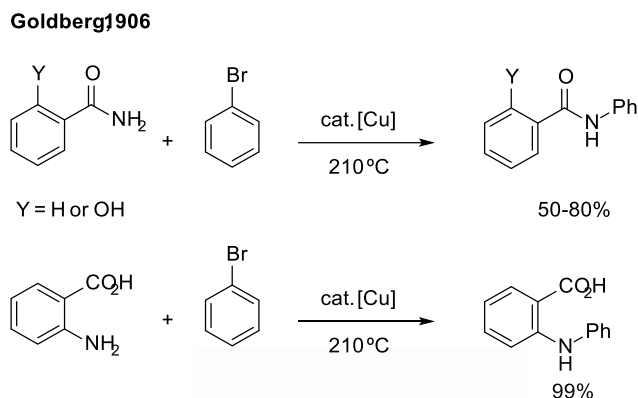
Scheme 7. Golberg's cross-coupling reactions catalysed by copper salts.

These transformations were the greatest breakthrough of the Ullmann-Goldberg married couple, who clearly set up the bases for the current cross-coupling reactions catalysed by copper. Afterwards, several studies emerged demonstrating the potential of copper catalysis in organic synthesis.

The formation of C-C, C-S and C-N bonds has attracted a great deal of attention during the last years, with the later being one the most widely studied, due to its importance in organic chemistry and in the development of novel drugs. In this sense, the use of supported CuNPs for cross-coupling reactions appears to be an attractive way to make C-C, C-S and C-N bonds.

Formation of C-C bonds[67]

The formation of C-C bonds is crucial for the synthesis of organic molecules. For this reason, a plethora of procedures have been developed during the last fifty years. Some of the most extensively used C-C bond construction procedures belong to the transformations known as cross-couplings reactions.[68] Some of the reactions that are included in this family

---

[66] Goldberg, I. *Ber. Dtsch. Chem. Ges.* **1906***, 39*, 1691-1692.

[67] (a) *Metal-Catalyzed Cross-Coupling Reactions, 2nd Edn.* Meijere, A.; Diederich, F. Eds.; Wiley-VCH: Weinheim, 2004. (b) Colacot, T. J. *New Trends in Cross-Coupling: Theory and Applications*; RSC: Cambridge, 2015.

[68] Moreno-Mañas, M.; Pleixats, R. *Acc. Chem. Res.* **2003**, *36*, 638-643.

are summarised below (Scheme 8). In this scenario, Pd has a leading position (59%) compared with other metals such as Cu (19%), Ni (11%), Fe (8%) and Co (3%).[69]

Mizoroki-Heck coupling, 1972

Sonogashira coupling, 1975

R^1-X + R^2-Y $\xrightarrow{\text{[Pd]}}$ R^1-R^2

X = Hal, OTf, etc
R^1 = aryl, vinyl
R^2 = aryl, alkyl
Y = MgX (Kumada-Corriu coupling, 1972)
    ZnX (Negishi coupling, 1977)
    SnR$^3_3$ (Stille coupling, 1977)
    B(OR^3)$_2$ (Suzuki-Miyaura coupling, 1979)
    SiR$^3_3$ (Hiyama coupling, 1988)
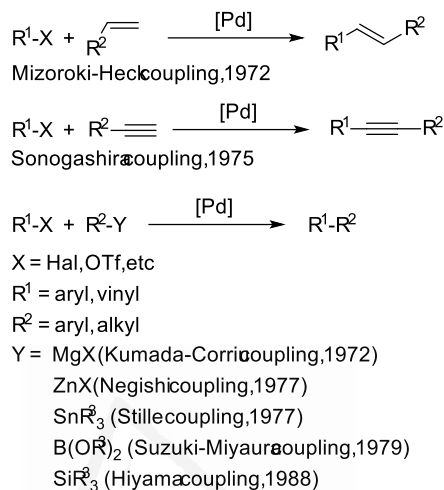
Scheme 8. Cross-coupling reactions catalysed by Pd.

The importance of these procedures in organic chemistry is supported by all the research works that have emerged since their discovery (Figure 21). Moreover, the high value of these coupling reactions was recognised with the 2010 Nobel Prize in Chemistry being awarded to Heck, Negishi and Suzuki.[70]
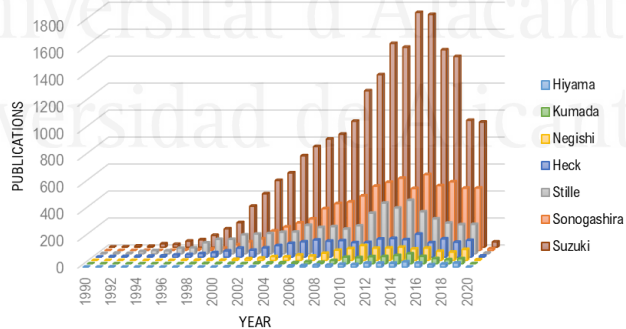

Figure 21. Number of publications on cross-coupling reactions (source: SciFinder-January 2020).

---

[69] (a) *Handbook of Organopalladium Chemistry for Organic Synthesis*; Negishi, E. Meijere, A. Eds.; John Wiley & Sons: New York (NY), 2002. (b) Molnár, A. *Palladium-Catalyzed Coupling Reactions: Practical Aspects and Future Developments*; Wiley-VCH: Weinheim, 2013.

[70] https://www.nobelprize.org/prizes/chemistry/2010/summary/.

Among these transformations, the Sonogashira coupling has emerged as a key strategy for the construction of C_{sp^2}-C_{sp} bonds.[71] This transformation typically involves a catalytic system based on Pd(0) in the presence of Cu(I) species and an amine or inorganic base (Scheme 9).

$$R^1\!\!-\!\!\equiv \;+\; X\text{-}R^2 \xrightarrow[\text{Cu(I)co-catalyst}]{\substack{\text{cat.[Pd(0)]}\\ \text{amineor inorganicbase}}} R^1\!\!-\!\!\equiv\!\!-\!\!R^2$$

R^1 = aryl, hetaryl, alkyl or SiR_3
R^2 = aryl, hetaryl or vinyl
X = Cl, Br, I or OTf
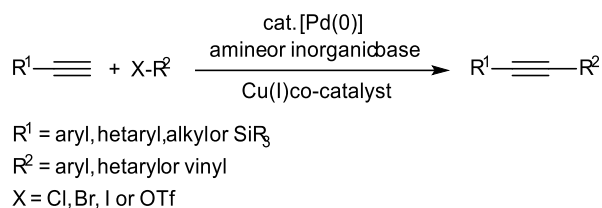
Scheme 9. General conditions for the Sonogashira cross-coupling reaction.

The mechanism of this transformation is based on six main steps (Scheme 10). The first step is the generation of the active catalytic Pd(0) species, followed by an oxidative addition of the organic halide, oxidising Pd(0) to Pd(II).
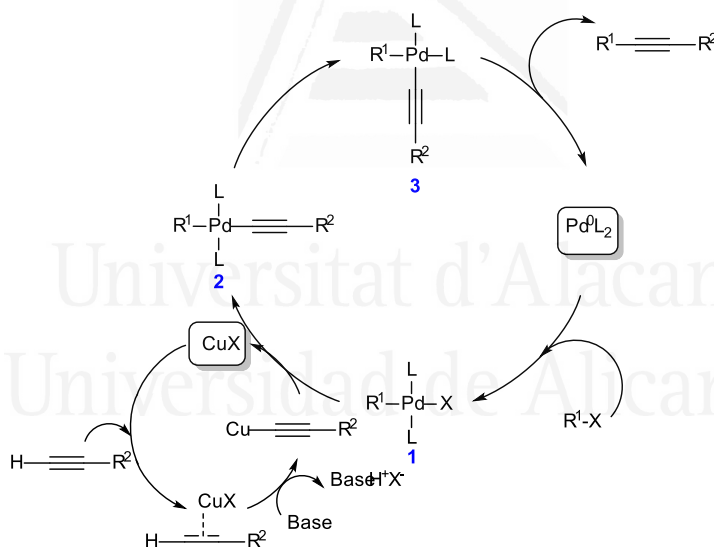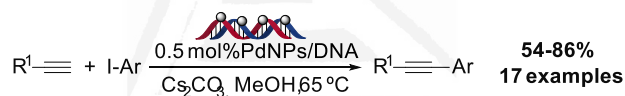

Scheme 10. Mechanism of the Sonogashira coupling.

[71] Reviews: (a) Chinchilla, R.; Najera, C. *Chem. Rev.* **2007**, *40*, 874-922. (b) Doucet, H.; Hierso, J.-C. *Angew. Chem. Int. Ed.* **2007**, *46*, 834-871. (c) Yin, L.; Liebscher, J. *Chem. Rev.* **2007**, *107*, 133-173. (d) Heravi, M. D.; Sadjadi, S. *Tetrahedron* **2009**, *65*, 7761-7775. (e) Pal, M. *Synlett* **2009**, 2896-2912. (f) Chinchilla, R.; Najera, C. *Chem. Soc. Rev.* **2011**, *40*, 5084-5121. (g) Bakherad, M. *Appl. Organomet. Chem.* **2013**, *27*, 125-140. (h) Wang, D.; Gao, S. *Org. Chem. Front.* **2014**, *1*, 556-566. (i) Karak, M.; Barbosa, L. C. A.; Hargaden, G. C. *RSC Adv.* **2014**, *4*, 53442-53466.

Parallel to this, Cu(I) in the presence of a base generates the corresponding Cu acetylide, which undergoes a transmetallation with the species **1** to form intermediate **2**. This intermediate suffers a *trans-cis* isomerisation followed by a reductive elimination that yields the final product and regenerates the active Pd(0) species.

During the last twenty years, this coupling has been widely studied, employing a huge number of Pd-based catalytic systems, such as unsupported and supported Pd-phosphorus complexes, Pd-nitrogen complexes, N-heterocyclic carbene (NHC) palladium complexes, palladacycles, ligand-free Pd species and PdNPs, among others.[71]

In this sense, our research group, in collaboration with Chacón-García's group, at the Universidad Michoacana of San Nicolás de Hidalgo (Mexico), has developed a new catalytic system for the copper- and ligand-free Sonogashira coupling based on PdNPs (PdO and PdO_2 species) supported on DNA (Scheme 11).[72] This system showed good performance in the coupling of aromatic halides with aliphatic and aromatic alkynes, employing 0.5 mol% Pd. The catalyst was recovered by centrifugation and reused for, at least, five cycles without losing any catalytic activity.

$$R^1 \!\!-\!\!\equiv \ + \ I\text{-}Ar \ \xrightarrow[\text{Cs}_2\text{CO}_3,\ \text{MeOH}, 65\ °\text{C}]{0.5\ \text{mol}\%\,\text{PdNPs/DNA}} \ R^1\!\!-\!\!\equiv\!\!-\!\!Ar \qquad \begin{array}{c}\textbf{54-86\%}\\ \textbf{17 examples}\end{array}$$

R^1 = Ph, 4-$NH_2C_6H_4$, 2-ClC_6H_4, C_6H_{13}, C_6H_{11}, C_7H_{11}, CH_2OH, $(CH_2)_2OH$, CH_2NMe_2
Ar = Ph, 4-$NO_2C_6H_4$, 4-$MeCOC_6H_4$, 4-$MeOC_6H_4$, 4-$NH_2C_6H_4$, 4-IC_6H_4, 2-IC_6H_4, 1-naphthy

Scheme 11. Sonogashira coupling catalysed by PdNPs supported on salmon-sperm DNA.

The affinity of DNA for PdNPs had not been previously described. Some XPS experiments were carried out in order to establish the interactions between PdNPs and DNA, observing a main interaction with the nitrogens of the nucleobases and a secondary interaction with the phosphate units, as shown in Figure 22.

[72] Camacho, A. S.; Martín-García, I.; Contreras-Celedón, C.; Chacón-García, L.; Alonso, F. *Catal. Sci. Technol.* **2017**, *7*, 2262-2273.
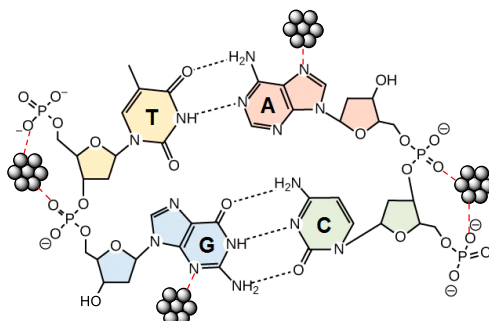
Figure 22. Proposed interactions of PdNPs with the DNA structure.

Regarding the mechanism of this copper- and ligand-free protocol, some control experiments were carried out, such as D labelling, effect of additives, etc. In addition, XPS experiments of the fresh and recycled catalysts revealed an obvious trend to accumulate Pd(0) after the reaction. These results point to a Pd(0)/Pd(II) catalytic system rather than a Pd(II)/Pd(IV) one. Based on the results obtained in the different experiments, the following mechanism was proposed (Scheme 12):
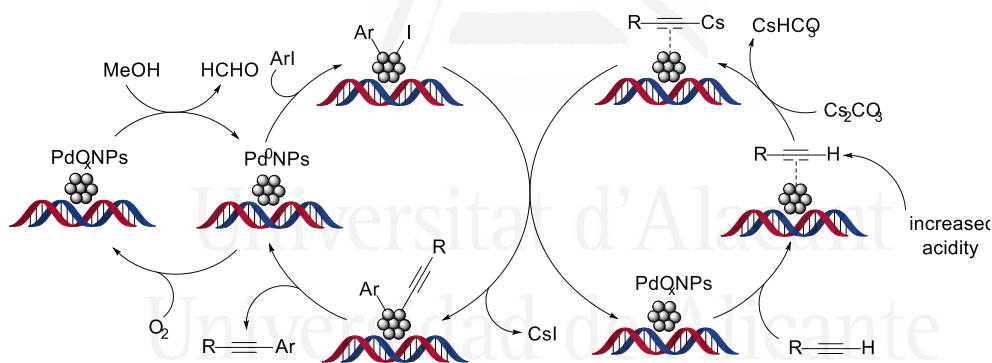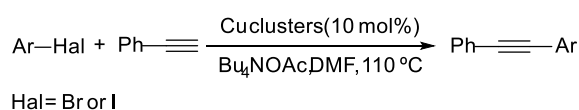

Scheme 12. Mechanism proposed for the Sonogashira coupling catalysed by PdNPs/DNA.

This palladium-based catalytic system has several benefits in comparison with others previously reported. Among them, we can mention: (a) simple preparation of the catalyst, involving a biodegradable support; (b) coupling under relatively mild conditions (MeOH, 65 ºC in air), with a good functional group tolerance; (c) the use of low metal loading (0.5 mol%) in the absence of copper salts and ligands; (d) alkyne homocoupling is minimised; (e) the catalyst is recyclable and (f) this system is superior to commercial (homogeneous and heterogeneous) Pd catalysts.

As previously mentioned, Pd is, by far, the most used transition metal in the Sonogashira coupling. During the last years, however, copper has emerged as a cheaper and sustainable alternative,[73] showing similar behaviour in this transformation (Section B.1., p. 36).

In this sense, the first example of CuNPs catalysing this coupling was reported by Rothenberg and co-workers in 2004 (Scheme 13).[74] In their studies, an efficient and air-stable catalyst was developed with the possibility of being reused, at least, three times without losing any catalytic activity.

$$Ar\text{—}Hal + Ph\text{—}\!\!\equiv\!\!\xrightarrow[\text{Bu}_4\text{NOAc,DMF,110 °C}]{\text{Cu clusters (10 mol\%)}} Ph\text{—}\!\!\equiv\!\!\text{—}Ar$$

$$Hal = Br\ or\ I$$

Scheme 13. First example of Sonogashira cross-coupling catalysed by Cu-nanoclusters.

Since the publication of this finding, a wide variety of studies related to the Sonogashira coupling based on supported Cu catalysts has been reported, employing silica,[75] alumina,[76] hydroxyapatite,[77] polystyrene,[78] titania[79] and boehmite,[80] among other supports. Concerning supported CuNPs, a few examples were described, some of which are summarised in Scheme 14. In general, the preparation of the catalysts implies more than one step, increasing the cost of these protocols.[81]

The development of sustainable catalytic systems for this coupling continues to be topical. More recently, two works reported the Sonogashira coupling catalysed by CuNPs/PANI-MWCNT[82a] and the multifunctional Lewis/Brønsted acid nanocatalyst

[73] Review: Murashkina, A. V.; Mitrofanov, A. Y.; Beletskaya, I. P. *Russ. J. Org. Chem.* **2019**, *55*, 1483-1497.

[74] Thathagar, M.; Beckers, J.; Rothenberg, G. *Green Chem.* **2004**, *6*, 215-218.

[75] (a) Zhang, L.; Li, P.; Wang, L. *Lett. Org. Chem.* **2006**, *3*, 282-285. (b) Wang, Z.; Wang, L.; Li, P. *Synthesis* **2008**, *9*, 1367-1372.

[76] Biffis, A.; Scattolin, E.; Ravasio, N.; Zaccheria, F. *Tetrahedron Lett.* **2007**, *48*, 8761-8764.

[77] Saha, D.; Chatterjee, T.; Mukherjee, M.; Ranu, B. C. *J. Org. Chem.* **2012**, *77*, 9379-9383.

[78] Kodicherla, B.; Perumgani, C. P.; Mandapati, M. R. *Appl. Catal. A: Gen.* **2014**, *483*, 110-115.

[79] Mitrofanov, A.; Brandés, S.; Herbst, F.; Rigolet, S.; Bessmertnykh-Lemeune, A. Beletskaya, I. P. *J. Mater. Chem. A* **2017**, *5*, 12216-12235.

[80] Bakherad, M.; Doosti, R.; Mirzaee, M.; Jadidi, K.; Amin, A. H.; Amiri, O. *Res. Chem. Intermed.* **2017**, *43*, 7347-7363.

[81] (a) Arundhathi. R.; Damodara, D.; Mohan, K. V.; Kantam, M. L.; Likhar, P. R. *Adv. Synth. Catal.* **2013**, *355*, 751-756. (b) Hajipour, A. R.; Hosseini, S. M.; Mohammadsaleh, F. *New J. Chem.* **2016**, *40*, 6939-6945. (c) Gholinejad, M.; Ahmadi, J.; Nájera, C. *ChemistrySelect* **2016**, *3*, 384-390. (d) Keypour, H.; Balali, M.; Nejat, R.; Bagherzadeh, M. *Appl. Organomet. Chem.* **2017**, *31*, e3691. (e) Wang, B.; Wang, Y.; Guo, X.; Jiao, Z.; Jin, G.; Guo, X. *Catal. Commun.* **2017**, *101*, 36-39.

[82] (a) Hajipour, A. R.; Jajarmi, S. *Appl. Organomet. Chem.* **2018**, *32*, e3992. (b) Nasseri, M. A.; Alavi, S. A.; Kazemnejadi, M.; Allahrescani, A. *RSC Adv.* **2019**, *9*, 20749-20759.

$CuFe_2O_4NPs/SiO_2/ZrO_2/SO_4^{2-}/CuNPs$,[82b] in good-to-excellent yields in both cases (Scheme 14). These catalysts could be recycled up to six and nine cycles, respectively, retaining their catalytic performance in both cases.

Ar—Hal + R——— $\xrightarrow[\text{conditions}]{\text{CuNPs/support}}$ Ar———R
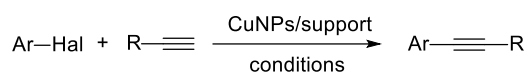
Hal = Br or I
R = aryl, alkyl

Kantam, 2013: CuO/Al$_2$O$_3$ (1 mol%), K$_2$CO$_3$, DMF, r.t., N$_2$
Mohammadsaleh, 2016: Cu(I)-DABCO/SiO$_2$ (10 mol%), KOH, DMF, 135-140°C, N$_2$
Gholinejad, 2016: CuAuFe$_2$O$_4$ (0.5 mol%), ^{t}BuOK, DMA, 115 °C
Bagherzadeh, 2017: Fe$_3$O$_4$/SiO$_2$/PP-Cu (1 mol%), DABCO, DMF/H$_2$O, 100 °C
Guo, 2017: Cu$_2$ONPs/RGO (2.5 mol%), KOH, DMF, 150 °C
Hajipour, 2018: Cu(I)-PANI/MWCNT (10 mol%), KOH, DMF, 135 °C
Nasseri, 2019: CuFe$_2$O$_4$NPs/SiO$_2$/ZrO$_2$/SO$_4^{2-}$/CuNPs (1 mol%), Et$_3$N, DMA, 80 °C

Scheme 14. Sonogashira coupling catalysed by supported CuNPs.

Formation of C-S bonds

As aforementioned, the construction of C-S bonds has attracted a huge interest during this century.[9d,83] Among the procedures for their formation in organic synthesis, the Ullmann-type C-S coupling is one of the most practiced.[84] In this regard, some examples of this transformation promoted by supported Cu-species have been reported.[63c] The first example was described by Ranu and co-workers in the reaction between aryl halides and thiols, catalysed by Cu(II) anchored to Al$_2$O$_3$ under ligand-free conditions.[85]

Concerning supported CuNPs, some of the catalytic systems used for this transformation involved porous inorganic and organic solids (Scheme 15) like microporous silicon,[86] maghemite[87] or chitosan.[88] In general, the use of electron-rich aryl iodides led to higher yields. In addition, the catalysts could be recycled, at least, three times in all cases.

[83] Reviews: (a) Beletskaya, I. P.; Ananikov, V. P. *Chem. Rev.* **2011**, *111*, 1596-1636. (b) Eichman, C. C.; Stambuli, J. P. *Molecules* **2011**, *16*, 590-608; (c) Lee, C.-F.; Liu, Y.-C. Badsara, S. S. *Chem. Asian J.* **2014**, *9*, 706-722; (d) Sujatha, A.; Thomas, A. M.; Amrutha, A. P.; Anilkumar, G. *Arkivoc* **2015**, *i*, 1-28.

[84] (a) Review: Murashkina, A. V.; Mitrofanov, A. Y.; Beletskaya, I. P. *Russ. J. Org. Chem.* **2019**, *55*, 1629-1641. (b) See, also: Panova, Y. S.; Kashin, A. S.; Vorobev, M. G.; Degtyareva, E. S.; Ananikov, V. P. *ACS Catal.* **2016**, *6*, 3637-3643.

[85] Bhadra, S.; Sreedhar, B.; Ranu, C. C. *Adv. Synth. Catal.* **2009**, *351*, 2369-2378.

[86] González-Arellano, C.; Luque, R.; Macquiarrie, D. J. *Chem. Commun.* **2009**, 1410-1412.

[87] Sharma, R. K.; Gaur, R.; Yadav, M.; Rathi, A. K.; Pechousek, J.; Petr, M.; Zboril, R.; Gawande, M. B. *ChemCatChem* **2015**, *7*, 3495-3502.

[88] Frindy, S.; Kadib, A.; Lahcini, M.; Primo, A.; García, H. *ChemCatChem* **2015**, *7*, 3307-3315.

Ar—Hal + RSH $\xrightarrow[\text{conditions}]{\text{CuNPs/support}}$ Ar—S—R
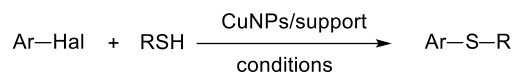
Hal = Cl, Br or I
R = aryl, alkyl

Luque, 2009: CuNPs/SMNP (0.8 mol%), K_2CO_3, CH_3CN, MW, <100 °C
Gawande, 2015: CuNPs/maghemite (3.7 mol%), Cs_2CO_3, DMF, 130 °C, N_2
García, 2015: CuNPs/chitosan (2 mol%), Et_3N, toluene, 130 °C

Scheme 15. C-S bond formation catalysed by supported CuNPs on porous solids.

The groups of Lee and Rajagopal described the thiolation of aryl halides employing CuONPs[89] and Cu(0)NPs[90] supported on silica (Scheme 16), respectively. In both cases, good-to-excellent yields were obtained. In addition, the catalysts could be reused up to four cycles for CuONPs and up to three for Cu(0)NPs, with insignificant loss of catalytic activity. In Rajagopal's work, the authors indicated that thiol arylation was performed in a totally heterogeneous way, *via* adsorption of the corresponding reagents on the CuNPs surface.
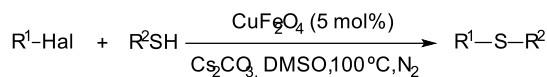
Ar—I + RSH $\xrightarrow[\text{conditions}]{\text{CuNPs/SiO}_2}$ Ar—S—R
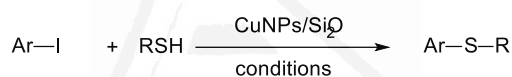
R = aryl, alkyl

Lee, 2010: CuONPs (1-5 mol%), Cs_2CO_3, DMSO or dioxane, 110 °C
Rajagopal, 2011: Cu(0)NPs (1.5 mol%), KOH, DMSO, 110 °C, N_2

Scheme 16. Thiolation of aryl iodides catalysed by CuNPs supported on SiO_2.

In 2011, Nageswar's group studied a heterogeneous catalyst based on $CuFe_2O_4$ for the arylation of thiols under ligand-free conditions (Scheme 17).[91] They achieved good results with aryl bromides and iodides under a nitrogen atmosphere, whereas, chlorides did not react under these conditions. Furthermore, the catalyst could be recycled three times without losing its activity.

[89] Chen, C. K.; Chen, Y. E.; Lin, C. H.; Lin, H. P.; Lee, C. F. *Chem. Commun.* **2010**, 282-284.
[90] Veerakumar, P.; Velayudham, M.; Lu, K.-L.; Rajagopal, S. *Catal. Sci. Technol.* **2011**, *1*, 1512-1525.
[91] Swapna, K.; Murthy, S. N.; Jyothi, M. T.; Nageswar, Y. V. D. *Org. Biomol. Chem.* **2011**, *9*, 5989-5996.
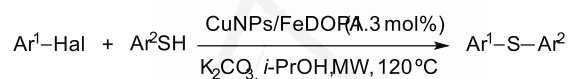
$$R^1\text{-Hal} \quad + \quad R^2SH \xrightarrow[\text{Cs}_2\text{CO}_3, \text{ DMSO}, 100\,^\circ\text{C}, \text{N}_2]{\text{CuFe}_2\text{O}_4 \text{ (5 mol\%)}} R^1\text{—S—}R^2$$

Hal = Br or I
R^1 = aryl, alkyl
R^2 = aryl, alkyl

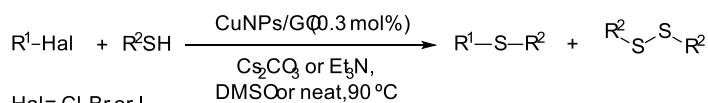**Scheme 17.** Thiolation of halides catalysed by NPs of $CuFe_2O_4$.

Another interesting approach to these transformations was described by Varma's group. in 2012.[92] This group designed a new catalytic system based on CuNPs supported on ferrite, which had been surface-modified with dopamine. Its catalytic performance was tested in two cross-coupling reactions: the thiol arylation with aryl iodides and the coupling of activated bromides with phenols, obtaining good yields in both cases. Moreover, the catalyst could be reused, at least three times, with the same catalytic activity.

$$Ar^1\text{-Hal} \quad + \quad Ar^2SH \xrightarrow[\text{K}_2\text{CO}_3, \text{ } i\text{-PrOH}, \text{MW}, 120\,^\circ\text{C}]{\text{CuNPs/FeDOPA (1.3 mol\%)}} Ar^1\text{—S—}Ar^2$$

Hal = Br or I

Scheme 18. Thioarylation of aryl halides catalysed by CuNPs supported on NPs of ferrite decorated with DOPA.

In 2013, Rao and co-workers demonstrated the good performance of CuNPs supported on graphene oxide (GO) in the thiolation reaction with organic halides, getting good-to-excellent yields (Scheme 19).[93] The reaction with aryl chlorides required the presence of solvents and stronger bases to achieve better results, with the drawback of increasing the yield of the diaryl disulphide from 5-10% (bromides and iodides) to 5-20% (chlorides). Concerning the recyclability, CuNPs/GO was recovered and reused, at least four times, showing the same performance.

$$R^1\text{-Hal} \quad + \quad R^2SH \xrightarrow[\substack{\text{Cs}_2\text{CO}_3 \text{ or Et}_3\text{N}, \\ \text{DMSO or neat}, 90\,^\circ\text{C}}]{\text{CuNPs/GO (0.3 mol\%)}} R^1\text{—S—}R^2 \quad + \quad R^2\text{}^{S}\text{}_{S}\text{}^{R^2}$$

Hal = Cl, Br or I
R^1 = aryl, alkyl
R^2 = aryl, alkyl

Scheme 19. Thiolation of halides catalysed by CuNPs supported on graphene oxide.

---

[92] Baig, R. B. N.; Varma, R. S. *Chem. Commun*. **2012**, *48*, 2582-2584.

[93] Kamal, A.; Srinivasulu, V.; Murty, J. N. S. R. C.; Shankaraiah, N.; Nagesh, N.; Reddy, T.; Subba Rao, A. V. *Adv. Synth. Catal*. **2013**, *355*, 2297-2307.

Additionally, transition-metal oxides have been employed as supports for newly designed heterogeneous catalytic systems in the arylation of thiols (Scheme 20). In this regard, Huang, Suib and co-workers reported the use of CuNPs supported on Cu_2O[94] and MnO_x,[95] respectively, obtaining good-to-excellent yields in both cases. In addition, the catalysts could be recycled up to five and four runs, respectively.

$$Ar\!-\!I \quad + \quad RSH \xrightarrow[\text{conditions}]{\text{CuNPs/support}} \quad Ar\!-\!S\!-\!R$$

R = aryl, alkyl
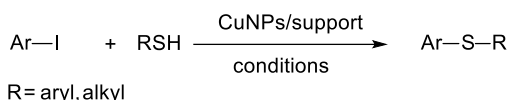
Huang, 2015: CuNPs/Cu_2O (0.7 mol%), Cs_2CO_3, DMSO, 110 °C
Suib, 2017: CuNPs/MnO_x (3 mol%), K_2CO_3, DMF, 140 °C

Scheme 20. Thiolation of aryl iodides catalysed by CuNPs supported on inorganic oxides.

Formation of C–N bonds[96]

Nitrogen-containing molecules are extremely important in organic chemistry due to their abundance in nature and their applications in medicine.[97] Among them, molecules containing *N*-aryl bonds are especially relevant and the most common methodology for their synthesis is the direct N-arylation of aryl halides with N-nucleophiles.

In this context, new catalytic systems based on supported Cu-complexes were described employing polymers,[98] ionic liquids[99] and inorganic compounds as supports.[100] Concerning supported CuNPs, only a few examples can be found in the literature. One of the first examples was an Ullmann-type reaction catalysed by CuNPs supported on carbon nanofibers (CNFs) under ligand-free conditions (Scheme 21), reported by Li and co-workers in 2014.[101] In this work, the authors described the first heterogeneous system based on supported CuNPs for the cross-coupling of phenols and nitrogen-containing heterocycles with aryl

[94] Chen, W.; Liu, X.; Li, H.; Fan, Z.; Zhen, B.; Weng, Z.; Lai, Z.; Huang, K.-W. *J. Mol. Engin. Mater.* **2015**, *3*, 1540001.

[95] Mullick, K.; Biswas, S.; Kim, C.; Ramprasad, R.; Ángeles-Boza, A.-M.; Suib, S. L. *Inorg. Chem*. **2017**, *56*, 10290-10297.

[96] Bariwal, J.; Eycken, E. V. *Chem. Soc. Rev.* **2013**, *42*, 9283-9303.

[97] (a) Cho, S. H.; Kim, J. Y.; Kwak, J.; Chang, S. *Chem. Soc. Rev.* **2011**, *40*, 5068-5083. (b) Hili, R.; Yudin, A. K. *Nat. Chem. Biol.* **2006**, *2*, 284-287.

[98] (a) Kantam, M. L.; Roy, M.; Roy, S.; Sreedhar, B.; Lal De, R. *Catal. Commun.* **2008**, *9*, 2226-2230. (b) Arundhati, R.; Kumar, D.; Sreedhar, B. *Eur. J. Org. Chem.* **2010**, 3621-3630. (c) Islam, M.; Mondal, S.; Mondal, P.; Roy, A. S.; Tuhina, K.; Mobarok, M.; Paul, S.; Salam, N.; Hossain, D. *Catal. Lett.* **2011**, *141*, 1171-1181. (d) Nasrollanzadeh, M.; Zahraei, A.; Pourbasheer, E. *Monatsh. Chem.* **2015**, *146*, 1329-1334.

[99] Li, H.; Can, J.; Weike, S. *Chin. J. Chem.* **2012**, *30*, 2394-2400.

[100] Patil, N. M.; Gupte, S. P. Chaudhari, R. V. *Appl. Catal. A: Gen.* **2010**, *372*, 73-81.

[101] Li, H.; Li, C.; Bai, J.; Zhang, C.; Sun, W. *RSC Adv.* **2014**, *4*, 48362-48367.

halides. The recyclability of the catalyst was not evaluated in the N-arylation but, was tested in the phenol arylation, reported in the same paper. In this case, the system was found to be active in up to five cycles, albeit with gradually decreasing conversions due to the Cu-leaching from the catalyst.
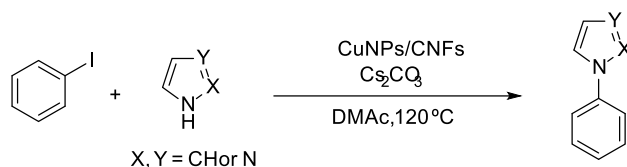

Scheme 21. Synthesis of *N*-aryl imidazoles catalysed by CuNPs/CNFs.

In the same year, Nador *et al.* described the arylation of imidazole catalysed by CuNPs supported on MagSilica (Scheme 22).[102] However, the reaction did not take place when tried to extrapolate this catalytic system to other azoles. In this study, the catalyst was successfully recycled up to three times without significant loss of catalytic activity.
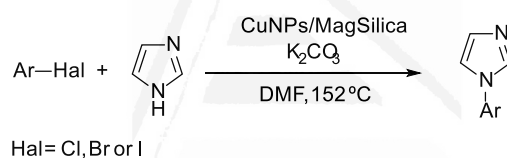
Scheme 22. Synthesis of *N*-aryl imidazoles catalysed by CuNPs/MagSilica.

In 2015, Corma's group described the cross-coupling reaction between iodides and some nitrogen-containing compounds catalysed by Cu clusters supported on polyvinylpyrrolidinone (PVP) or ethylene-vinyl alcohol copolymer (EVOH).[103] The stability of these catalysts was tested after four months, showing high activity and selectivity with TONs up to 10^4 (Scheme 23).
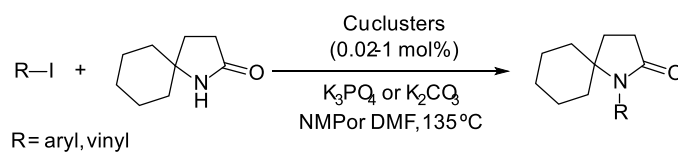
Scheme 23. Cross-coupling of iodides and a lactam catalysed by supported Cu clusters.

[102] Nador, F.; Volpe, M. A.; Alonso, F.; Radivoy, G. *Tetrahedron* **2014**, *70*, 6082-6087.

[103] Oliver-Messeguer, J.; Liu, L.; García-García, S.; Canós-Giménez, C.; Domínguez, I.; Gavara, R.; Doménech-Carbó, A.; Concepción, P.; Leyva-Pérez, A.; Corma, A. *J. Am. Chem. Soc.* **2015**, *137*, 3894-3900.

In 2017, Bakavoli and co-workers reported the N-arylation of aryl halides and N(H)-heterocycles catalysed by copper nanorods (CuNRs) supported on a polydentate ligand, built with three different polymers deposited on a mixture of inorganic oxides (Scheme 24).[104] This magnetic catalyst was recovered and recycled, at least, in five runs maintaining the same performance.
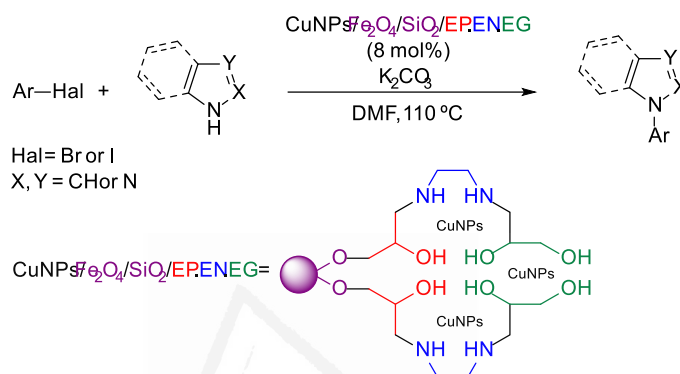
Scheme 24. Arylation of nitrogen-containig heterocycles catalysed by supported CuNPs.

Early this year, Ge and co-workers reported a new catalytic system based on CuNPs/HCS-MA-F127 for the arylation of amines, employing 8 mol% of copper loading.[105] This catalyst is based on CuNPs dispersed on hydrochar (HCS) by using Pluronic F127 as a surfactant. The hydrochar was synthesised from chitosan and decorated with maleic acid (MA). The catalyst was recycled up to five times, showing the same catalytic activity.
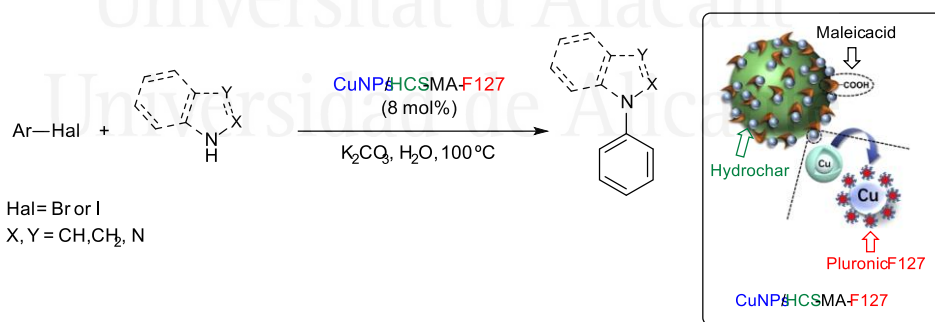
Scheme 25. Ullmann C–N coupling catalysed by supported copper. Figure on the right reproduced from ref. 105. Copyright 2020 Elsevier.

[104] Rajabzadeh, M.; Eshghi, H.; Khalifeh, R.; Bakavoli, M. *Appl. Organomet. Chem.* **2017**, *31*, e3647.

[105] Ge, X.; Ge, M.; Chen, X.; Qian, C.; Liu, X.; Zhou, S. *Mol. Catal.* **2020**, *484*, 110726.

In general, the reported protocols for the contruction of C-C, C-S and C-N bonds show high selectivity but involve rather complex catalytic systems. Moreover, in these methodologies, the use of chlorides and bromides is not efficient, and the scope of the reaction is limited due to their low functional-group tolerance.

Based on these antecedents, the development of new and efficient catalytic systems based on supported CuNPs for cross-coupling reactions is still challenging. In this sense, our research group, in collaboration with Prof. Beletskaya's group (Moscow State University, Russia), considered an attractive idea to study our catalytic systems based on supported CuNPs in cross-coupling reactions for the formation of C-C, C-S and C-N bonds.

2.2. Objectives

Taking into account the aforementioned background, the following objectives were pursued:

- o To study the catalytic activity of CuNPs supported on C, ZY, TiO_2 and MK-10 in the formation of C-C, C-S and C-N bonds through the Sonogashira cross-coupling, thiol and azole arylation reactions.
- o To study the recyclability of these catalysts in the different couplings.
- o To compare the catalytic activity of CuNPs/C, CuNPs/ZY and CuNPs/TiO_2 with that of some commercial copper catalysts.

Universitat d'Alacant
Universidad de Alicante

2.3. Results and discussion

2.3.1. Formation of C-C bonds: Sonogashira coupling

4-Iodoanisole (**1a**) and phenylacetylene (**2a**) were used as model substrates for this reaction. A preliminary screening of solvent, base, atmosphere, temperature and catalyst loading allowed us to conclude that the optimal conditions for the Sonogashira coupling were: 5 mol% copper loading and K_2CO_3 as a base in DMF at 120 ºC, under inert atmosphere. With these conditions in hand, four supported catalysts were tested (Table 11). As anticipated, the catalytic activity of CuNPs is strongly dependent on the nature of the support, with CuNPs/ZY (Table 11, entry 2) and CuNPs/C (Table 11, entry 3) exhibing the highest performance. These results might be related to the equal content of Cu_2O and CuO in these catalysts (see Section 1.3.2, pp. 56 and 57).

Table 11. Sonogashira coupling catalysed by supported CuNPs.[a]

MeO—⟨⟩—I + Ph≡≡ $\xrightarrow[\substack{K_2CO_3,\ DMF \\ 120\,ºC,\,8\ h,\ Ar}]{\substack{CuNPs/support \\ (5\ mol\%)}}$ MeO—⟨⟩—≡≡—Ph

1a   **2a**   **3aa**

Entry	CuNPs	3aa (%)[b]
1	TiO$_2$	19
2	**ZY**	**>99**
3	C	95
4	MK-10	79

[a] **1a** (0.25 mmol), **2a** (1.5 equiv.), CuNPs (5 mol%), K_2CO_3 (2 equiv.), DMF (1 mL), 120 ºC, 8 h, Ar. [b] ^{1}H NMR yield.

2.3.1.1. Scope

The best-performing catalyst (CuNPs/ZY) was employed for the coupling reaction between aryl halides and arylacetylenes (Table 12). Thus, an array of aryl iodides was tested. As expected, electron-poor iodides were more reactive than the electron-rich ones, generating the desired product in shorter reaction times (compare the reaction times of **1a** and **1b** with those of **1c**, **1d**, **1e** and **1k**). Regardless the presence of electron-donating or electron-withdrawing groups, **3aa**-**3ea** were obtained in excellent yields (Table 12, entries 1-5). Additionally, the selectivity of CuNPs/ZY towards the C-I bond was demonstrated with the formation of products **3fa**-**3ha** (Table 12, entries 6-8). The reaction with aryl bromides was less effective, even increasing the reaction temperature (Table 12, entries 9 and 10). Finally, the Sonogashira coupling of 4-iodobenzonitrile (**1c**) was tested with different arylacetylenes bearing electron-donating (Table 12, entries 12 and 13) and electron-withdrawing groups
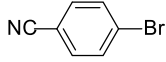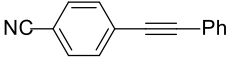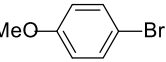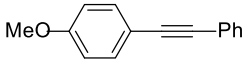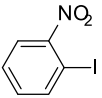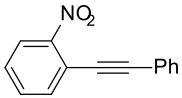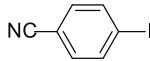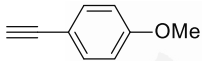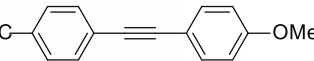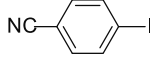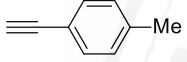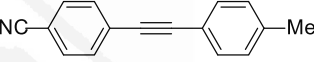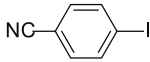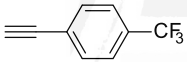
(Table 12, entry 14), obtaining the expected products in moderate and excellent yields, respectively.

Table 12. Scope of the Sonogashira coupling.[a]

Entry	Aryl halide	Alkyne	3	t (h)	Yield (%)[b]
1	MeO—⬡—I **1a**	≡—Ph **2a**	MeO—⬡—≡—Ph **3aa**	8	99
2	Me—⬡—I **1b**	≡—Ph **2a**	Me—⬡—≡—Ph **3ba**	8	99
3	NC—⬡—I **1c**	≡—Ph **2a**	NC—⬡—≡—Ph **3ca**	4	98
4	O₂N—⬡—I **1d**	≡—Ph **2a**	O₂N—⬡—≡—Ph **3da**	2	95
5	MeO₂C—⬡—I **1e**	≡—Ph **2a**	MeO₂C—⬡—≡—Ph **3ea**	2	98
6	F—⬡—I **1f**	≡—Ph **2a**	F—⬡—≡—Ph **3fa**	4	96
7	Cl—⬡—I **1g**	≡—Ph **2a**	Cl—⬡—≡—Ph **3ga**	4	98
8	Br—⬡—I **1h**	≡—Ph **2a**	Br—⬡—≡—Ph **3ha**	4	98

Table 12. Scope of the Sonogashira coupling (cont.).[a]

9	NC—⟨ ⟩—Br **1i**	≡—Ph **2a**	NC—⟨ ⟩—≡—Ph **3ca**	8 8[c]	25 60[c,d]
10	MeO—⟨ ⟩—Br **1j**	≡—Ph **2a**	MeO—⟨ ⟩—≡—Ph **3aa**	8	0
11	NO₂ ⟨ ⟩—I **1k**	≡—Ph **2a**	NO₂ ⟨ ⟩—≡—Ph **3ka**	2	99
12	NC—⟨ ⟩—I **1c**	≡—⟨ ⟩—OMe **2b**	NC—⟨ ⟩—≡—⟨ ⟩—OMe **3cb**	24[c]	40[d]
13	NC—⟨ ⟩—I **1c**	≡—⟨ ⟩—Me **2c**	NC—⟨ ⟩—≡—⟨ ⟩—Me **3cc**	24[c]	61[d]
14	NC—⟨ ⟩—I **1c**	≡—⟨ ⟩—CF₃ **2d**	NC—⟨ ⟩—≡—⟨ ⟩—CF₃ **3cd**	24[c]	90[d]

[a] **1** (0.25 mmol), **2** (1.5 equiv.), CuNPs/ZY (4 mol%), K_2CO_3 (2 equiv.), DMF (1 mL), 120 ºC, 8 h, Ar. [b] ^{1}H NMR yield. [c] Reaction at 150 ºC. [d] Isolated yield.

2.3.1.2. Catalyst recyclability and nature of the catalysis

CuNPs/ZY could be recovered by centrifugation and reused in four cycles without losing any catalytic activity (Figure 23). The catalyst was analysed by TEM after the fourth cycle and no perceptible alteration in the particle size was observed (Figure 24). The heterogeneous nature of the catalyst was analysed through the hot filtration test in combination with ICP-MS.[9a] After the first run, an inactive leaching of 0.14% was observed, whereas only 0.01% of copper was detected in the filtrate after the fourth cycle. The negative filtration test pointed to a process of heterogeneous nature.
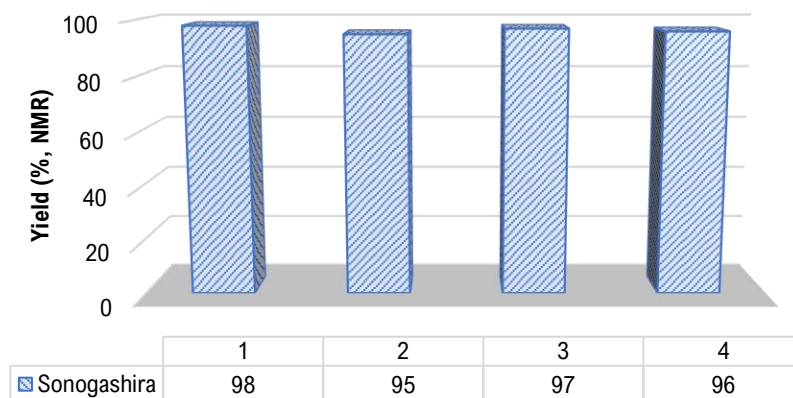
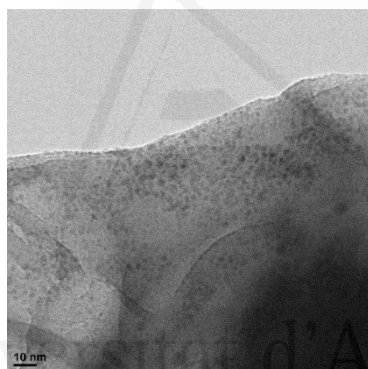**Figure 23.** Recycling of CuNPs/ZY in the synthesis of **3aa**.

Figure 24. TEM micrograph of CuNPs/ZY after four cycles in the Sonogashira coupling.

2.3.1.3. Comparison with other commercial Cu catalysts

The catalytic activity of CuNPs/ZY in the Sonogashira coupling between 4-iodoanisole (**1a**) and phenylacetylene (**2a**) was compared with that of an array of commercial copper catalysts (Table 13). Strikingly, CuNPs/ZY was superior to all the commercial catalysts tested (Table 13, entry 13). Only CuOTf and Cu(OTf)$_2$, the most expensive ones, furnished the desired product in moderate conversions (Table 13, entries 10 and 11).

Comparing our system with the previously reported ones, we can conclude that its catalytic activity is comparable with that of Rothenberg's system based on copper clusters.[74]

Commercial nano-CuO[106] showed less catalytic activity employing more drastic conditions than with our system based on CuNPs/ZY.

Table 13. Comparison of CuNPs/ZY with commercial copper catalysts in the Sonogashira coupling.[a]

Entry	Catalyst	Conversion (%)[b]
1	Cu(0)	0
2	Cu_2O	8
3	CuO	0
4	CuCl	5
5	$CuCl_2$	8
6	CuBr	0
7	CuI	4
8	CuOAc	9
9	$Cu(OAc)_2$	7
10	CuOTf	50[c]
11	$Cu(OTf)_2$	67[c]
12	$CuBr·SMe_2$	4
13	**CuNPs/ZY**	**>99**

[a] **1a** (0.25 mmol), **2a** (1.5 equiv.), Cu (4 mol%), K_2CO_3 (2 equiv.), DMF (1 mL), 120 ºC, 8 h, Ar. [b] Conversion into **3aa** determined by GLC based on **1a**.[c] The alkyne homocoupling side product 1,4-diphenylbuta-1,3-diyne and **3aa** were obtained in a *ca*. 1:2 ratio.

Nevertheless, our catalytic system was not so efficient in the Sonogashira coupling with aryl chlorides, whereas Cu(0)NPs/Al_2O_3 could catalyse this transformation at room temperature.[81a] Seemingly, the absence of an oxide film is crucial for its reactivity. In fact, CuO/Al_2O_3 showed lower activity in this transformation, and was not reused due to the high copper leaching observed after the first cycle (63%).[76]

Considering all these results, we can conclude that CuNPs/ZY can be a sustainable alternative to PdNPs for the Sonogashira coupling.

2.3.2. Formation of C-S bonds: thiol arylation

As with the Sonogashira coupling, a preliminary screening of solvent, base, atmosphere, temperature and catalyst was conducted using 4-iodobenzonitrile (**1c**) and thiophenol (**4a**) as

---

[106] Yuan, Y.; Zhu, H.; Zhao, D.; Zhang, L. *Synthesis* **2011**, 1792-1798.

model substrates. The optimal conditions involved the use of 1 mol% copper loading and K_2CO_3 as a base in DMF at 80 ºC, under an inert atmosphere. It must be underlined that the presence of air or the absence of solvent had a negative effect on the yield.

Four catalysts were tested in the thiol arylation of 4-iodobenzonitrile (**1c**) and thiophenol (**4a**) under the optimal conditions described above (Table 14). CuNPs/ZY proved to be the best choice, leading to **5ca** in 91% yield (Table 14, entry 2).

Table 14. Thiol arylation catalysed by supported CuNPs.[a]

NC—⟨ ⟩—I + PhSH $\xrightarrow[\text{80 ºC,4 h, Ar}]{\begin{array}{c}\text{CuNPs/support}\\(1\text{ mol\%})\\ \hline K_2CO_3\text{, DMF}\end{array}}$ NC—⟨ ⟩—SPh

1c   **4a**   **5ca**

Entry	CuNPs	5ca (%)[b]
1	TiO$_2$	79
2	**ZY**	**91**
3	C	77
4	MK-10	86

[a] **1c** (0.25 mmol), **4a** (1.5 equiv.), CuNPs (1 mol%), K_2CO_3 (2 equiv.), DMF (1 mL), 80 ºC, 4 h, Ar. [b] ^{1}H NMR yield.

2.3.2.1. Scope

Even though sufficiently high yields were obtained at 80 ºC (Table 14 entry 2), the substrate scope was also evaluated at 120 ºC in order to maximise the yield of the final product. First, the thioarylation of an array of aryl halides (**1**) was tested with thiophenol (**4a**) under the optimal conditions (Table 15). Regarding the substituents of the aryl iodides, the reaction yield seemed to increase with their power to deplete the electronic density of the aromatic ring (Table 15, entries 1-5). In the case of halogenated iodides, the same chemoselectivity as in the Sonogashira coupling was observed (Table 15, entries 4 and 5). Aryl bromides and chlorides bearing electron-donating groups were almost unreactive with this catalytic system (Table 15, entries 6-8). In general, the presence of electron-withdrawing groups in the aryl chlorides (Table 15, entries 9-13) led to the formation of the desired products, with the only exception of fluorine (Table 15, entry 9). Surprisingly, the products were formed in excellent yields after only 2 h (Table 15, entries 10-12), even for *ortho*-substituted aryl chlorides (Table 15, entry 13).

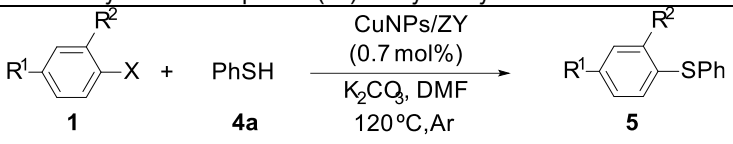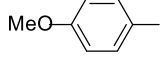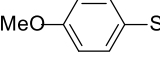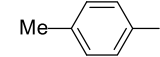**Table 15.** Arylation of thiophenol (**4a**) catalysed by CuNPs/ZY.[a]
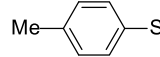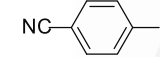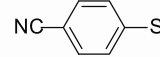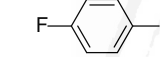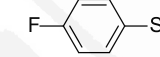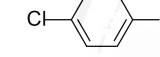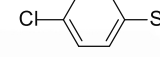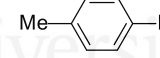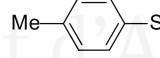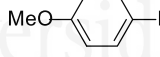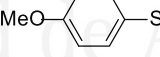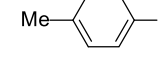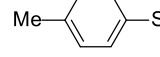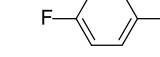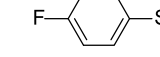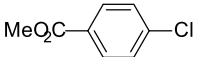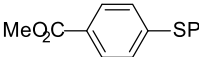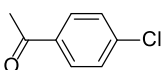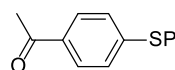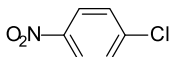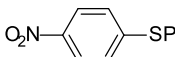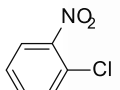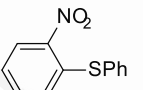
Entry	Aryl halide	5	t (h)	Yield(%)[b]
1	MeO——I **1a**	MeO——SPh **5aa**	16	60
2	Me——I **1b**	Me——SPh **5ba**	16	97
3	NC——I **1c**	NC——SPh **5ca**	2	99
4	F——I **1f**	F——SPh **5fa**	8	96
5	Cl——I **1g**	Cl——SPh **5ga**	8	96
6	Me——Br **1l**	Me——SPh **5ba**	16	15
7	MeO——Br **1j**	MeO——SPh **5aa**	16	0
8	Me——Cl **1m**	Me——SPh **5ba**	16	0
9	F——Cl **1n**	F——SPh **5fa**	16	0

Table 15. Arylation of thiophenol (**4a**) catalysed by CuNPs/ZY (cont.).[a]

10	MeO₂C—⬡—Cl	MeO₂C—⬡—SPh	2	95
	1o	**5oa**		
11	(acetyl)—⬡—Cl	(acetyl)—⬡—SPh	2	99
	1p	**5pa**		
12	O₂N—⬡—Cl	O₂N—⬡—SPh	2	95
	1q	**5qa**		
13	⬡(NO₂)—Cl	⬡(NO₂)—SPh	2	99
	1r	**5ra**		

[a] **1** (0.25 mmol), **4a** (1.5 equiv.), CuNPs/ZY (0.7 mol%), K₂CO₃ (2 equiv.), DMF (1 mL), 120 ºC, Ar. [b] ¹H NMR yield.

Following the same methodology as above but at 100 ºC, a large number of thiols were evaluated in the thiolation of 4-iodobenzonitrile (**1c**) (Table 16), including aromatic (Table 16, entries 1-3), heteroaromatic (Table 16, entries 4 and 5) and benzylic thiols (Table 16, entry 6). In the particular case of aliphatic substrates, KOH was used as a base in order to achieve better results (Table 16, entries 7-10). It must be underlined that thiol **4i** led to the corresponding nitrile or amide, by only changing the reaction temperature (Table 16, compare entries 8 and 9, footnotes c and d).

Table 16. Thiolation of 4-iodobenzonitrile (**1c**) catalysed by CuNPs/ZY.[a]
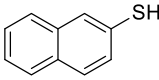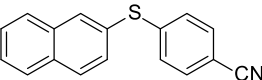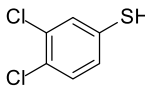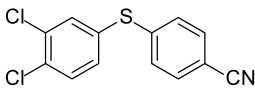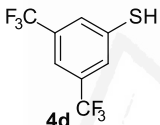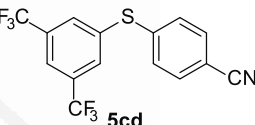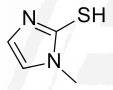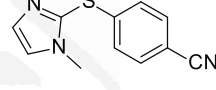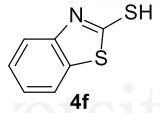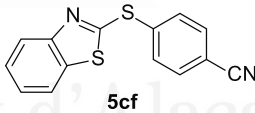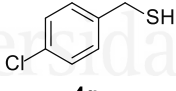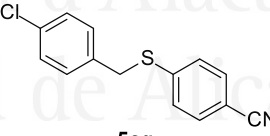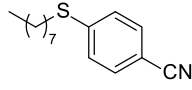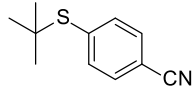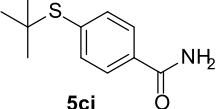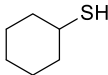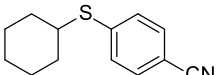
Entry	Thiol	5	Yield (%)[b]
1	4b	5cb	98
2	4c	5cc	45
3	4d	5cd	81
4	4e	5ce	52
5	4f	5cf	63
6	4g	5cg	92
7	4h	5ch	80[c]
8	4i	5ci	97[d]

Table 16. Thiolation of 4-iodobenzonitrile (**1c**) catalysed by CuNPs/ZY (cont.).[a]

| 9 | | 4i | | 5ci | | 60[c] |

| 10 | | 4j | | 5cj | | 87[c] |

[a] **1c** (0.25 mmol), **4** (1.5 equiv.), CuNPs/ZY (0.7 mol%), K_2CO_3 (2 equiv.), DMF (1 mL), 100 ºC, 4 h, Ar. [b] Isolated yield. [c] Reaction using KOH as a base (2 equiv.) at 120 ºC. [d] Reaction using KOH as a base (2 equiv.) at 70 ºC.

2.3.2.2. Catalyst recyclability and nature of the catalysis

CuNPs/ZY could be reused in four consecutive runs with insignificant and inert Cu leaching (Figure 25), in contrast with what observed by the group of Prof. Ananikov with unsupported copper oxide, where the reactions take place through leaching from the surface involving the formation of a copper thiolate (Scheme 26).[84b]

	1	2	3	4
Thioarylation	99	98	97	98
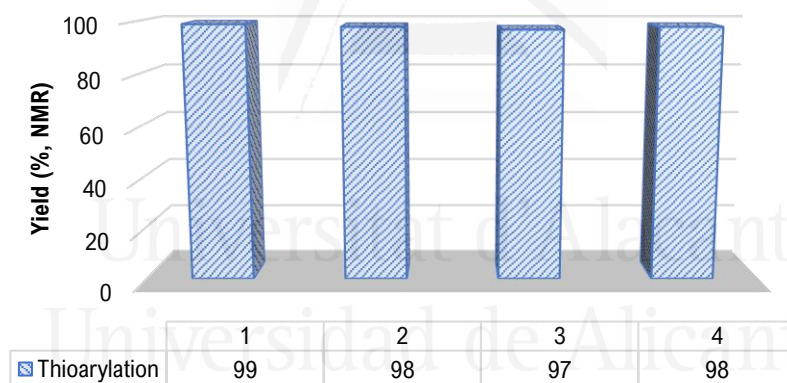
Figure 25. Recycling of CuNPs/ZY in the synthesis of **5ca**.
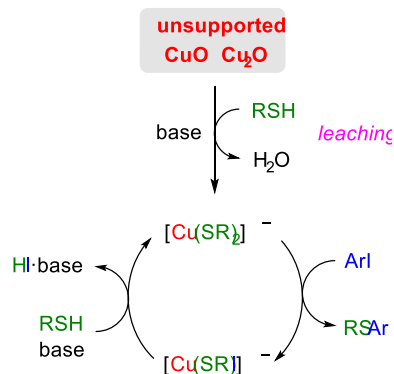
Scheme 26. Ananikov's mechanism of C–S cross-coupling reaction catalysed by copper oxide particles.

As in the previous coupling, the catalyst was analysed by TEM after the fourth run (Figure 26), without observing any agglomeration and any alteration of the particle size. The heterogeneous nature of the catalyst was analysed through the hot filtration test in combination with ICP-MS. After the first run, an inactive leaching of 0.12% was observed, whereas only 0.02% copper was detected in the filtrate after the fourth cycle. These results are very close to those observed in the Sonogashira coupling, demonstrating the heterogeneous nature of the catalyst.
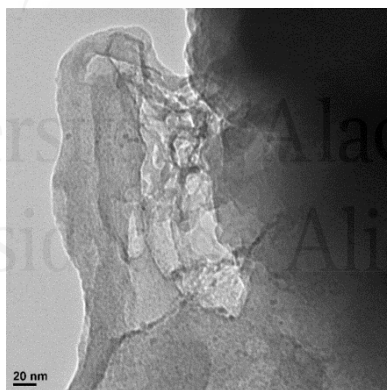
Figure 26. TEM micrograph of CuNPs/ZY after four cycles in the thiol arylation.

2.3.2.3. Comparison with other commercial Cu catalysts

The catalytic activity of CuNPs/ZY in the thiolation of 4-iodobenzonitrile (**1c**) with thiophenol (**4a**) was compared with that of a large variety of commercial copper catalysts (Table 17).

Table 17. Comparison of CuNPs/ZY with commercial copper catalysts in the thiol arylation.[a]

Entry	Catalyst	Conversion (%)[b]
1	Cu(0)	25
2	Cu_2O	23
3	CuO	32
4	CuCl	54
5	$CuCl_2$	64
6	CuBr	38
7	CuI	50
8	CuOAc	63
9	$Cu(OAc)_2$	91
10	CuOTf	77
11	$Cu(OTf)_2$	82
12	$CuBr \cdot SMe_2$	77
13	**CuNPs/ZY**	**94**

[a] **1c** (0.25 mmol), **4a** (1.5 equiv.), Cu (1 mol%), K_2CO_3 (2 equiv.), DMF (1 mL), 100 ºC, 4 h, Ar. [b] Conversion into **5ca** determined by GLC based on **1c**.

Analysing the results obtained, we observe that the lowest conversions were found for Cu(0), Cu_2O, CuO and CuBr (Table 17 entries 1, 2, 3 and 6), whereas $Cu(OAc)_2$ and CuNPs/ZY (Table 17, entries 9 and 13) gave the highest ones. Nevertheless, CuNPs/ZY was considered the best of the two latter catalysts due to its capability of being recycled.

Thiol arylation appears to be less dependent on the copper source, oxidation state and support, when compared to the results obtained in the Sonogashira coupling (compare Tables 14 and 17 with Tables 11 and 13).

2.3.3. Formation of C-N bonds: arylation of azoles

In this section, the four aforementioned catalysts were tested in the arylation of the azoles shown in Figure 27, and the effect of the support was evaluated.
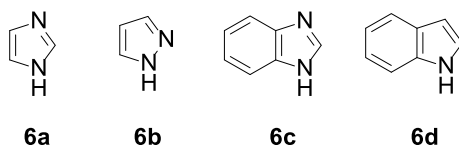
Figure 27. Azoles studied for the N-arylation with aryl halides catalysed by supported CuNPs.

2.3.3.1. Comparative study of the catalysts

4-Iodobenzonitrile was used as a model aryl halide for all the azoles. The four catalysts were active in promoting the azole arylation under the optimal conditions (Table 18). The best results were obtained by using CuNPs/TiO$_2$ as a catalyst (Table 18, column 3, entries 1, 2, 3 and 4), contrary to what observed in the Sonogashira coupling and thiol arylation. It is noteworthy that the reaction proceeded in a selective manner without the generation of any by-product. It is known that different copper oxidation states promoted this transformation [Cu(0)NPs,[107] CuINPs,[108] Cu$_2$ONPs,[109] CuONPs[110]]. Nevertheless, mechanistic studies (carried out by Franc and Jutand) point to the involvement of Cu(I) species in the first steps of the catalytic cycle.[111] These reports support the results described in Table 18 and justify the higher activity of CuNPs/TiO$_2$ in this reaction (principally composed of Cu$_2$O, see Section 1.3.2.1, p. 55).

Table 18. CuNPs-catalysed coupling of nitrogen-containing heterocycles with 4-iodobenzonitrile.[a]
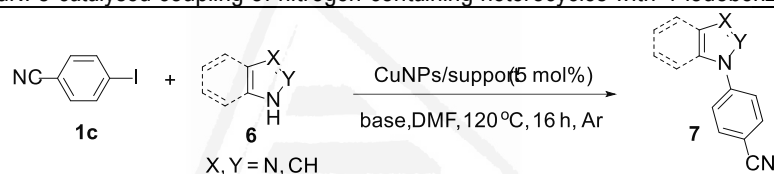
Entry	Azole	Base	TiO$_2$	ZY	MK-10	C
1	Imidazole (**6a**)	K$_2$CO$_3$	90 (**7ca**)	50 (**7ca**)	65(**7ca**)	71(**7ca**)
2	Pyrazole (**6b**)	K$_2$CO$_3$	82 (**7cb**)	75 (**7cb**)	75 (**7cb**)	80 (**7cb**)
3	Benzimidazole(**6c**)	K$_2$CO$_3$	72 (**7cc**)	49 (**7cc**)	68 (**7cc**)	61 (**7cc**)
4	Indole (**6d**)	K$_2$CO$_3$	59 (**7cd**)	36 (**7cd**)	41 (**7cd**)	59 (**7cd**)
5	Imidazole (**6a**)	Cs$_2$CO$_3$	>99 (**7ca**)	>99(**7ca**)	>99(**7ca**)	>99(**7ca**)

[a] **1c** (0.25 mmol), **6** (1.2 equiv.), CuNPs (5 mol%), base (2 equiv.), DMF (1 mL), 120 ºC, 16 h, Ar; ^{1}H NMR yield.

[107] (a) Kidwai, M.; Kumar-Mishra, N.; Bhardwaj, S.; Jahan, A.; Kumar, A.; Mozumdar, S. *ChemCatChem* **2010**, *2*, 1312-1317. (b) Huang, Z.; Li, F.; Chen, B.; Xue, F.; Chen, G.; Yuan, G. *Appl. Catal. A: Gen.* **2011**, *403*, 104-111. (c) Pai, G.; Chattopadhyay, P. *Tetrahedron Lett.* **2014**, *55*, 941-944. (d) Linga Reddy, P.; Arundhati, R.; Rawat, D. S. *RSC Adv.* **2015**, *5*, 92121-92127.

[108] Sreedhar, B.; Arundhathi, R.; Linga Reddy, P.; Lakshmi Katam, M. *J. Org. Chem.* **2009**, *74*, 7951-7954.

[109] (a) Son, S. U.; Park, I. K.; Park, J.; Hyeon, T. *Chem. Commun.* **2004**, 778-779. (b) Tang, B.-X.; Guo, S.-M.; Zhang, M.-B.; Li, J.-H. *Synthesis* **2008**, 1707-1716.

[110] (a) Rout, L.; Jammi, S.; Punniyamurthy, T. *Org. Lett.* **2007**, *9*, 3397-3399. (b) Lakshmi Kantam, M.; Yadav, J.; Laha, S.; Sreedhar, B.; Jha, S. *Adv. Synth. Catal.* **2007**, *349*, 1938-1942. (c) Jammi, S.; Sakthivel, S.; Rout, L.; Mukherjee, T.; Mandal, S.; Mitra, R.; Saha, P.; Punniyamurthy, T. *J. Org. Chem.* **2009**, *74*, 1917-1976. (d) Ganesh, S.; Karembu, R. *Ind. Eng. Chem. Res.* **2011**, *50*, 9594-9600. (e) Halder, M.; Islam, Md M.; Ansari, Z.; Ahammed, S.; Sen, K.; Islam, Sk M. *ACS Sustainable Chem. Eng.* **2017**, *5*, 648-657.

[111] Franc, G.; Jutand, A. *Dalton Trans.* **2010**, *39*, 7873-7875.

Regarding the azoles' reactivity, pyrazole (**6b**) was the most reactive with yields ranging from 75 to 82% (Table 18, entry 2), whereas indole (**6d**) was the least active, affording yields from 36 to 59% (Table 18, entry 4). It must be underlined that the use of Cs_2CO_3 as a base led to quantitative yields in the coupling of 4-iodobenzonitrile (**1c**) and imidazole (**6a**), regardless of the catalyst employed (Table 18, entry 5).

Therefore, the nature of the support has a direct effect not only in the activity of the CuNPs but also on the reactivity of the corresponding azoles.

2.3.3.2. Catalyst recyclability and nature of the catalysis

The recyclability of the catalyst was studied employing the optimal conditions found and Cs_2CO_3 as a base, unless otherwise stated. CuNPs/TiO$_2$ could be recovered by centrifugation and reused only twice before losing too much activity, whereas CuNPs/C could be recycled up to four cycles (Figure 28).

	1	2	3	4
TiO$_2$_K$_2$CO$_3$	90	70		
TiO$_2$_Cs$_2$CO$_3$	99	83		
ZY_Cs$_2$CO$_3$	99	65		
MK-10_Cs$_2$CO$_3$	99	78		
C_Cs$_2$CO$_3$	99	99	99	61
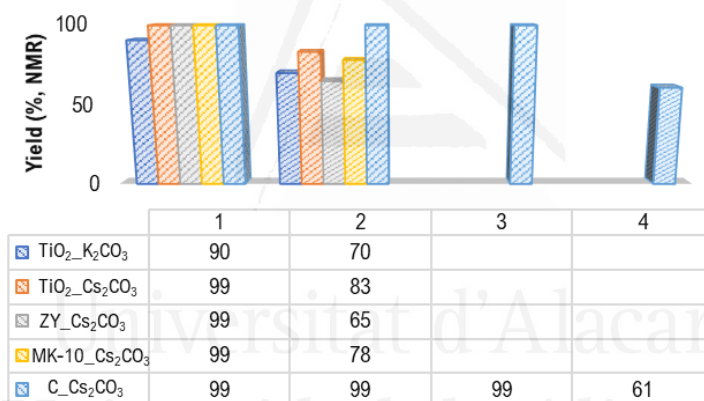
Figure 28. Recycling of CuNPs/support in the synthesis of **7ca**.

As in the previous couplings, the catalyst CuNPs/TiO$_2$ was analysed by TEM after the second run (Figure 29); however, the image is not clear enough to conclude any possible variation in the particle size. The heterogeneous nature of this catalyst was analysed through the hot filtration test in combination with ICP-MS. After the first run, an inactive leaching of 0.02% of copper was observed. In the case of CuNPs/C, an inactive copper leaching of 0.005% was observed in the first run and of 0.05% in the fourth run.
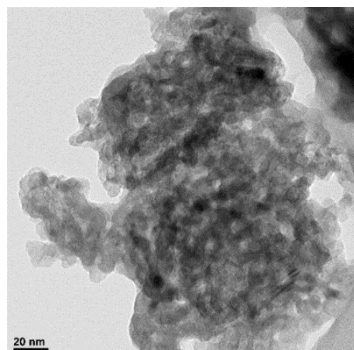
Figure 29. TEM micrograph of CuNPs/TiO$_2$ after two runs in the arylation of azoles.

The negligible inactive leaching detected with CuNPs/TiO$_2$ implies a strong metal-support interaction in the catalyst. This fact points to a catalyst poisoning effect as the possible phenomenon causing the perceived loss of catalytic activity after recycling. In order to confirm this hypothesis, XPS analyses were carried out.
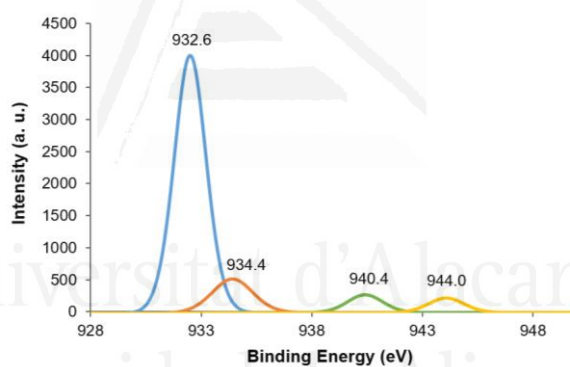
Figure 30. XPS spectrum at the Cu 2$p_{3/2}$ level of reused CuNPs/TiO$_2$.
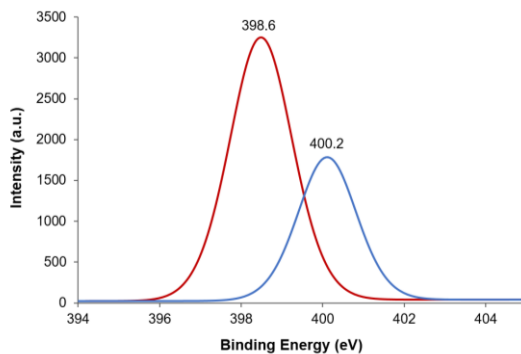
Figure 31. XPS spectrum at the N 1s level of reused CuNPs/TiO$_2$.
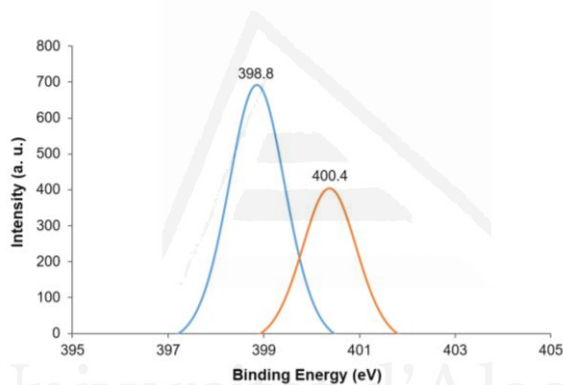
Figure 32. XPS spectrum at the N 1s level of fresh CuNPs/TiO$_2$ impregnated with 4-iodobenzonitrile (**1c**).

The XPS spectrum at the Cu 2$p_{3/2}$ level of the reused catalyst (Figure 30) did not change when compared with that of the fresh one (see Section 1.3.2.1, p. 55). XPS analysis at the N 1s level (Figure 31) showed two peaks, at 398.6 and 400.2 eV. These results were consistent with those displayed by fresh CuNPs/TiO$_2$ impregnated with 4-iodobenzonitrile (**1c**), which brought into view peaks at 398.8 and 400.4 eV (Figure 32), and with that of the described value for imidazole (400.2 eV).[112] Therefore, a poisoning effect by 4-iodobenzonitrile could account for the activity decrease observed upon reclycling.

---

[112] Singh, A.; Ansari, K. R.; Kumar, A.; Liu, W.; Songsong, C.; Lin, Y. *J. Alloys Compd.* **2017**, *712*, 121-123.

2.3.3.3. Comparison with other commercial Cu catalysts

As done in the couplings previously discussed, the catalytic activity of CuNPs/TiO$_2$ was compared with that of commercial copper catalysts in the arylation of imidazole (**6a**) with 4-iodobenzonitrile (**1c**), under the optimal reaction conditions (Table 19). It must be underlined that, while Cu$_2$O, CuO and CuOTf gave the desired product in good conversions (Table 19, entries 2, 3 and 10), they did not reach the performance of CuNPs/TiO$_2$, which yielded the product in quantitative conversion (Table 19, entry 13). Once again, the nanostructured catalyst showed better performance than the commercial ones.

Table 19. Comparison of CuNPs/TiO$_2$ with some commercial copper catalysts in the arylation of imidazole.[a]

Entry	Catalyst	Conversion (%)[b]
1	Cu(0)	28
2	Cu$_2$O	74
3	CuO	78
4	CuCl	44
5	CuCl$_2$	46
6	CuBr	18
7	CuI	62
8	CuOAc	25
9	Cu(OAc)$_2$	52
10	CuOTf	78
11	Cu(OTf)$_2$	67
12	CuBr·SMe$_2$	55
13	**CuNPs/TiO$_2$**	**99**

[a] **1c** (0.25 mmol), **6a** (1.5 equiv.), Cu (1.6 mol%), Cs$_2$CO$_3$ (2 equiv.), DMF (1 mL), 120 ºC, 16 h, Ar. [b] Conversion into **7ca** determined by GLC based on **1c**.

2.4. Conclusions

In this chapter, a comparative study on the activity of four catalytic systems based on supported CuNPs has been described in three types of cross-coupling reactions: the Sonogashira coupling, the thiol and azole arylation.

o   Sonogashira coupling (C-C bonds):

Among the four catalysts, CuNPs/ZY was the most effective for the formation of C-C bonds through the Sonogashira cross-coupling reaction. The optimal conditions found were: 4 mol% catalyst loading and K_2CO_3 as a base in DMF at 120 ºC, under an inert atmosphere. This catalytic system was effective for the coupling of arylacetylenes with aryl iodides, which took place in good-to-excellent yields, regardless of the electronic nature of the substituents, whereas poor-to-moderate yields were obtained with aryl bromides.

o   Thiol arylation (C-S bonds):

Like in the Sonogashira coupling, CuNPs/ZY was the best catalyst for the arylation of thiols, employing 0.7 mol% catalyst loading in DMF under an inert atmosphere. Regarding the temperature, the arylation of thiophenol (**4a**) was carried out at 120 ºC, whereas a temperature of 100 ºC was selected for other thiols. Concerning the base, K_2CO_3 was the best one for aromatic thiols and KOH for aliphatic ones, obtaining good-to-excellent yields in all the cases.

o   Arylation of azoles (C-N bonds):

Last but not least, the best results for the azole arylation were observed with CuNPs/TiO$_2$, using 1.6 mol% copper loading with Cs_2CO_3 as a base in DMF at 120 ºC, under inert atmosphere.

This comparative study was extended to twelve commercial copper catalysts. Among them, our nanoparticulate systems were superior in all the cases. On the other hand, only our catalysts had the capability to be successfully recycled, in up to four (Sonogashira coupling and thiol arylation) and three (arylation of azoles) cycles, retainig their high performance. A negligible inactive leaching was detected in all cases, confirming the heterogeneous nature of our catalysts. Thus, we can conclude that these protocols are an attractive alternative to those based on palladium catalysts for the construction of C-C, C-S and C-N bonds.

Chapter 3. CDC of tertiary amines and terminal alkynes catalysed by CuNPs/ZY. Synthesis of propargylamines

3.1. Antecedents

3.1.1. Introduction

There is in nature a great structural diversity of organic compounds showing bioactivity. That is why, one of the main goals in organic chemistry is the development of new synthetic methodologies that allow their preparation in an efficient, versatile and greener way.

These methodologies can be, in some cases, extrapolated to the synthesis of bioactive molecules. In this sense, the family of propargylamines has attracted a great deal of attention due to its synthetic versatility[113] and bioactivity.[114]
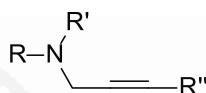
Figure 33. General structure of propargylamines.

Regarding the bioactivity of these compounds, some of them have been proved to be effective in targets related to neurodegenerative illnesses.[115] As an example, selegiline (Anipril®) and rasagiline (Azilect®) are used for combating the symptoms of Parkinson's disease. These compounds act as monoamine oxidase B (MAO-B) inhibitors, preventing neurological degeneration. These propargylamines are the main therapy in patients with an early stage of the disease or an adjunctive therapy in patients with advanced Parkinson's disease. Pargyline (Eutonyl®), interacts with MAO-B in the same way that selegiline, while at the same time interacting with MAO-A generating an antihypertensive effect. Another example of the use of propargylamines in medicine is clorgyline, which acts as a MAO-A inhibitor,

---

[113] Review: Nakamura, H. *Synlett* **2015**, *26*, 1649-1664.

[114] (a) Bar-Am, O.; Amit, T.; Weinreb, O.; Youdim, M. B. H.; Mandel, S. *J. Alzheimers Dis.* **2010**, *21*, 361-371. (b) Bolea, I.; Gella, A.; Unzeta, M. *J. Neural Transm.* **2013**, *120*, 893-902. (c) Louvel, J.; Carvalho, J. F. S.; Yu, Z.; Soethoudt, M.; Lenselink, E. B.; Klasasse, E.; Brusse, J.; Ijzerman, A. P. *J. Med. Chem.* **2013***, 56*, 9427-9440.

[115] (a) Murphy, D. L.; Karoum, F.; Pickar, D.; Cohen, R. M.; Lipper, S.; Mellow, A. M.; Tariot, P. N.; Sunderland, T. *J. Neural Transm. Suppl.* **1998**, *52*, 39-48. (b) Olanow, C. W. *Neurology* **2006**, *66*, S69-S79. (c) Naoi, W.; Maruyama, H.; Yi, Y.; Akao, Y.; Yamaoka, M.; Shamoto-Nagai *J. Neural Transm.* **2007**, *72*, 121-131. (d) Review: Oldfield, V.; Keating, G. M.; Perry, C. M *Drugs* **2007**, *67*, 1725-1747. (e) Baranyi, M.; Porceddu, P. F.; Gölöncsér, F.; Kulcsar, S.; Otrokocsi, L.; Kittel, A.; Pinna, A.; Frau, L.; Huleatt, P. B.; Khoo, M.-L.; Chai, C. L. L.; Duckel, P.; Mátyus, P.; Morelli, M.; Sperlágh, B. *Mol. Neurodegener*. **2016**, *11*, 1-21.

producing antidepressant and antianxiety effects (Figure 34). More recently, clorgyline was found active in the treatment of resistant prostate cancer.[116]

selegiline
(Anipril®)
MAO-B

rasagiline
(Azilect®)
MAO-B

pargyline
(Eutonyl®)
MAO-A/MAO-B

clorgyline
MAO-A
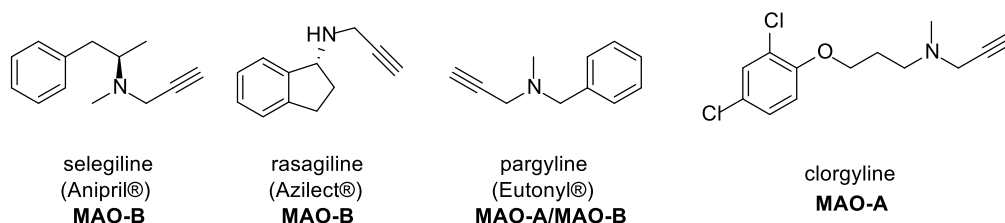
Figure 34. Propargylamines with therapeutic applications as MAO inhibitors.

Traditional methods for the synthesis of propargylamines involve the amination of halides,[117a] triflates,[117b] phosphates or propargyl acetates (Scheme 27-1).[117c] Another synthetic approach is the reaction of lithium acetylides or the Grignard's counterparts with imines (Scheme 27-2). The main drawback of this method is the use of stoichiometric amounts of organometallic compounds, the need for strictly controlling the reaction conditions and the low tolerance of these reagents towards some functional groups, often requiring additional protection and deprotection steps, among others. In this sense, some alternative procedures have been reported. The coupling of aldehydes, amines and alkynes (A³ coupling, Scheme 27-3)[118] and the nucleophilic substitution of chloromethyl amines (Scheme 27-4)[119] appeared, among them, as efficient routes for the construction of these compounds under mild conditions and with high atom-economy.

---

[116] Wang, K.; Luo, J.; Yeh, S.; You, B.; Meng, J.; Chang, P.; Niu, Y.; Li, G.; Lu, C.; Zhu, Y.; Antonarakis, E. S.; Luo, J.; Huang, C.-P.; Xu, W.; Chang, C. *Nat. Commun.* **2020**, *11*, 2889.

[117] (a) Kopka, I. E.; Fataftah, Z. A.; Rathke, M. W. *J. Org. Chem.* **1980***, 45*, 4616-4622. (b) Czernecki, S.; Valery, J.-M. *J. Carbohydr. Chem.* **1990**, *9*, 767-770. (c) Imada, I.; Yuasa, M.; Nakamura, I.; Murahashi, S.-I. *J. Org. Chem.* **1994**, *59*, 2282-2284.

[118] (a) Yoo, W.-J.; Zhao, L.; Li, C.-J. *Aldrichim. Acta.* **2011**, *44*, 43-51. (b) Yoo, W.-J.; Zhao, L.; Li, C.-J. In: *Science of Synthesis*; Mueller, T. J., Ed.; Thieme: Stuttgart, 2014; 1, pp. 189-217.

[119] (a) Xu, X.; Ge, Z.; Cheng, D.; Li, X. *Arkivoc* **2012**, *viii*, 107-118. (b) Chen, X.; Chen, T.; Zhou, Y.; Au, C.-T.; Han, C.-B.; Yin, S.-F. *Org. Biomol. Chem.* **2014**, *12*, 247-250.

$$R^1\text{-}C\equiv C\text{-}CH_2\text{-}LG \;+\; R^2{}_2NH \;\longrightarrow\; R^1\text{-}C\equiv C\text{-}CH_2\text{-}NR^2{}_2 \quad (1)$$

LG = Hal, OTf, OP(O)(OR^3)$_2$, OAc

$$R^1\text{-}C\equiv C\text{-}M \;+\; R^2CH{=}N\text{-}R^3 \;\longrightarrow\; R^1\text{-}C\equiv C\text{-}CH(R^2)\text{-}NR^3{}_2 \quad (2)$$

M = Li, MgHal

$$R^1\text{-}C\equiv C\text{-}H \;+\; R^2CHO \;+\; R^3{}_2NH \;\xrightarrow{\text{cat.}}\; R^1\text{-}C\equiv C\text{-}CH(R^2)\text{-}NR^3{}_2 \quad (3)$$

$$R^1\text{-}C\equiv C\text{-}H \;+\; CH_2Cl_2 \;+\; R^3{}_2NR^2 \;\xrightarrow{\text{cat.}}\; R^1\text{-}C\equiv C\text{-}CH_2\text{-}NR^3{}_2 \quad (4)$$
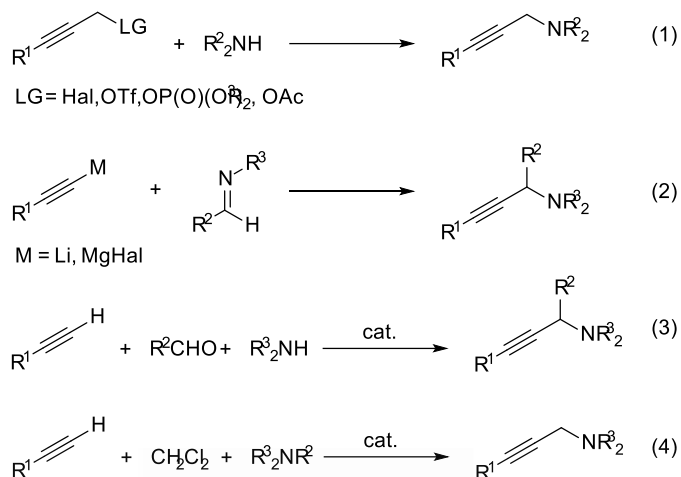
Scheme 27. General approaches for the synthesis of propargylamines.

3.1.2. Cross-dehydrogenative coupling (CDC)

Preferably, C–C bonds should be formed by the activation of only two C–H bonds. In this regard, the cross-dehydrogenative coupling (CDC, Scheme 28)[120] emerged as an interesting alternative to the methods previously mentioned. The interest on CDC is backed up by the number of reviews (more than 1960) that have appeared during the last years in the literature related to this transformation.

$$\equiv C{-}H \;+\; H{-}C\equiv \;\xrightarrow[\text{oxidant}]{[M]}\; \equiv C{-}C\equiv$$

C–H	C–C		
sp^3	sp^3 sp^3	sp^3 sp^2	sp^3 sp
sp^2	sp^2 sp^2	sp^2 sp	
sp	sp sp		
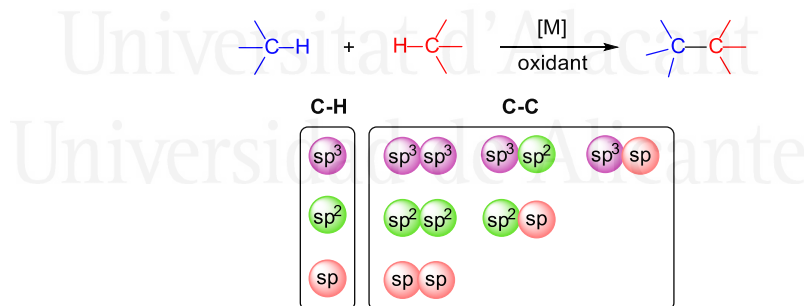
Scheme 28. General cross-dehydrogenative coupling (CDC) reactions.

Historically, the first cross-dehydrogenative coupling was reported by Glaser in 1869, for the homocoupling of alkynes catalysed by CuCl in the presence of ammonia under an oxygen atmosphere.[121] Later on, Glaser's reaction was modified by Eglinton (1956) and Hay

---

[120] *From C-H to C-C bonds: Cross-Dehydrogenative-Couplings;* Li, C.-J. Ed.; RSC Publising: Cambridge (UK), 2015.

[121] Glaser, C. *Ber. Dtsch. Chem. Ges.* **1869**, *2*, 422-424.

(1960) employing Cu(II) species and pyridine as a base,[122] 40 mol% of CuCl and pyridine or TMEDA,[123] respectively.

$$2 \ R\!\!-\!\!\!\equiv\!\!\!-H \xrightarrow{\text{conditions}} R\!\!-\!\!\!\equiv\!\!\!-\!\!\!\equiv\!\!\!-R$$
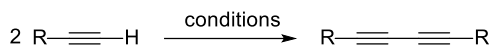
Glaser, 1869: CuCl, NH$_3$, EtOH, O$_2$
Eglinton, 1956: Cu(OAc)$_2$, MeOH, pyridine
Hay, 1960: CuCl, pyridine, O$_2$

Scheme 29. Alkyne homocoupling catalysed by copper.

Despite the fact that these works were the first examples of cross-dehydrogenative coupling, the concept of CDC would not be formally established until 2004, by Li and co-workers.[124] Since then, CDC is conceived as a powerful and atom-economy tool for the design of new organic molecules through the activation of two different C-H bonds as a means to create a new C-C bond.[125]

3.1.3. CDC of amines and alkynes

One of the reasons to synthesise propargylamines through CDC is that the α C-H (sp^3) bond of the corresponding amine can be easily activated by single-electron-transfer (SET) processes[126] or by transition metals,[127] forming the iminium intermediate **B**. This intermediate is exactly the same that would be formed in the A^3 coupling (Scheme 30).

---

[122] Eglinton, G.; Galbraith, A. R. *Chem. Ind.* **1956**, 737-738.

[123] Hay, A. S. *J. Org. Chem.* **1962**, *27*, 3320-3321.

[124] Li, Z.; Li, C.-J. *J. Am. Chem. Soc.* **2004**, *126*, 11810-11811.

[125] Selected reviews: (a) Li, C.-J. *Acc. Chem. Res.* **2009**, *42*, 335-344. (b) Scheuermann, C. J. *Chem. Asian J.* **2010**, *5*, 436-451. (c) Yeung, C. S.; Dong, V. M. *Chem. Rev.* **2011**, *111*, 1215-1292. (d) Girard, S. A.; Knauber, T.; Li, C.-J. *Angew. Chem. Int. Ed.* **2014**, *53*, 74-100. (e) Varun, B. V.; Dhineshkumar, J.; Bettadapur, K. R.; Siddaraju, Y.; Alagiri, K.; Prabhu, K. R. *Tetrahedron Lett.* **2017**, *58*, 803-824. (f) Wang, J.; Su, P.; Abdolmohammadi, S.; Vessally, E. *RSC Adv.* **2019**, *9*, 41684-41702. (g) Huang, C.-Y.; Kang, H.; Li, J.; Li, C.-J. *J. Org. Chem.* **2019**, *84*, 12705-12721. (h) Faisca Philips, A. M.; C. Guedes da Silva, M. F.; Pompeiro, A. J. L. *Catalysts* **2020**, *10*, 529. (i) Almasalma, A. A.; Mejía, E. *Synthesis* **2020**, DOI: 10.1055/s-0040-1707815.

[126] Leonard, N. J.; Leubner, G. W. *J. Am. Chem. Soc.* **1949**, *71*, 3408-3411.

[127] Murahashi, S.-I.; Komiya, N.; Terai, H. *Angew. Chem. Int. Ed.* **2005**, *44*, 6931-6933.
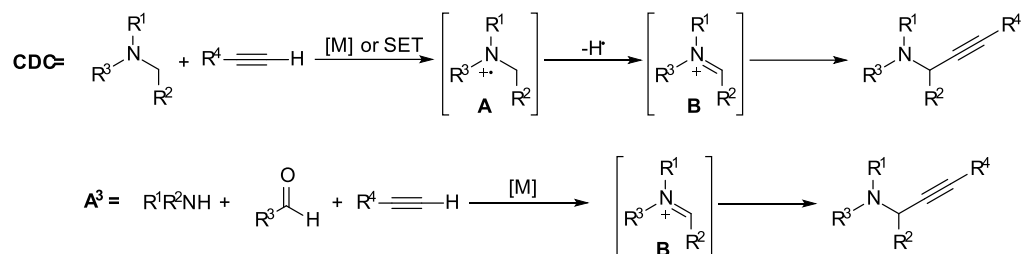
Scheme 30. Formation of the iminium intermediate in CDC and A^3 coupling reactions.

The CDC between the α C(sp^3)-H of amines and the C(sp)-H of alkynes to form propargylamines is one of the most widely studied CDC reactions.[128] These compounds are versatile intermediates for the construction of nitrogen-containing heterocycles,[129a] such as phenanthrolines,[129b] quinolines,[129c] pyrroles,[129d] pyrrolidines,[129e] indolizines[129f] and oxazolidones.[129g]

The synthesis of propargylamines through CDC usually involves the use of metal catalysts and oxidising agents. In recent years, some researchers have studied the use of Fe[130] and Zn[131] catalysts, but copper remains as the leading metal in this transformation. Alternatively, photoredox dual catalysis, employing Ru-complexes and copper, has emerged as an efficient method for the synthesis of propargylamine derivatives from tetrahydroisoquinolines (THIQs).[132]

[128] Review: Alonso, F.; Bosque, I.; Chinchilla, R.; Gonzalez-Gomez, J. C.; Guijarro, D. *Curr. Green. Chem.* **2019**, *6*, 105-126.

[129] (a) Nakamura, H.; Kamakura, T.; Ishikura, M.; Biellmann, J. F. *J. Am. Chem. Soc.* **2004**, *126*, 5958-5959. (b) Xiao, F.; Chen, T.; Liu, Y.; Whang, J. *Tetrahedron* **2008**, *64*, 2755-2761. (c) Shibata, D.; Okada, E.; Molette, J.; Médebielle, M. *Tetrahedron Lett.* **2008**, *49*, 7161-7164. (d) Yamamoto, Y.; Hayashi, H.; Saigoku, T.; Nishiyama, H. *J. Am. Chem. Soc.* **2005**, *127*, 10804-10805. (e) Harvey, D. F.; Sigano, D. M. *J. Org. Chem.* **1996**, *61*, 2268-2272. (f) Yan, B.; Liu, Y. *Org. Lett.* **2007**, *9*, 4323-4326. (g) Lee, E.-S.; Yeom, H.-S.; Hwang, J.-H.; Shin, S. *Eur. J. Org. Chem.* **2007**, 3503-3507.

[130] (a) Rao Volla, C. M.; Vogel, P. *Org. Lett.* **2009**, *11*, 1701-1704. (b) Liu, P.; Wang, Z.; Lin, J.; Hu, X. *Eur. J. Org. Chem.* **2012**, 1583-1589. (c) Shen, Q.; Zhang, L.; Zhou, Y.-R.; Li, J.-X. *Tetrahedron Lett.* **2013**, *54*, 6725-6728.

[131] (a) Sugiishi, T.; Nakamura, H. *J. Am. Chem. Soc.* **2012**, *134*, 2504-2507. (b) Jin, X.; Yamaguchi, K.; Mizuno, N. *RSC Adv.* **2014**, *4*, 34712-34715.

[132] (a) Rueping, M.; Koenigs, R. M.; Poscharny, K.; Fabry, D. C.; Leonori, D.; Vila, C. *Chem. Eur. J.* **2012**, *18*, 5170-5174. (b) Freeman, D. B.; Furst, L.; Condie, A. G.; Stephenson, C. R. J. *Org. Lett.* **2012**, *14*, 94-97. (c) Perepichka, I.; Kundu, S.; Hearne, Z.; Li, C.-J. *Org. Biomol. Chem.* **2015**, *13*, 447-451.

3.1.4. CDC catalysed by copper

Miura and co-workers reported the first example of the synthesis of propargylamines *via* CDC in 1993.[133] This group described the construction of these molecules in acetonitrile, employing CuCl$_2$ as catalyst under an oxygen atmosphere (Scheme 31).

R^1 = 4-Me, 4-OMe, 4-OEt, 3,4-Me$_2$
R^2 = Ph, 4-MeC$_6$H$_4$, 4-MeOC$_6$H$_4$, *n*-Pent
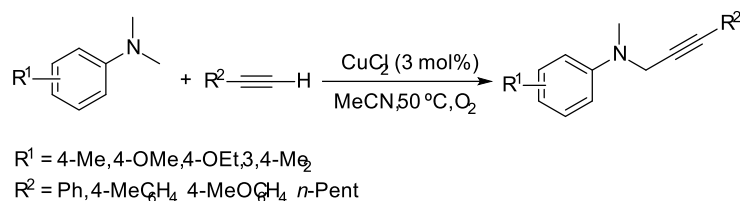
Scheme 31. Synthesis of propargylamines catalysed by CuCl$_2$.

In 2004, Li's group synthesised propargylamines through the CDC between tertiary amines and terminal alkynes, catalysed by CuBr in the presence of *tert*-butyl hydroperoxide (TBHP) as an oxidant and under an inert atmosphere (Scheme 32).[124] Moreover, they also reported the first enantioselective CDC[134] through the asymmetric alkynylation of *N*-aryl-1,2,3,4-tetrahydroisoquinolines catalysed by CuOTf in the presence of Pybox as a chiral ligand (Scheme 33).[135]

R^1 = Ph, 4-MeC$_6$H$_4$, 4-BrC$_6$H$_4$, Bn
R^2 = Ph, *n*-Bu, 4-MeC$_6$H$_4$, 4-MeOC$_6$H$_4$, 4-BrC$_6$H$_4$, 4-PhC$_6$H$_4$, 2-pyridyl, CH$_2$OH, CO$_2$CH$_3$, CH$_2$CO$_2$Et
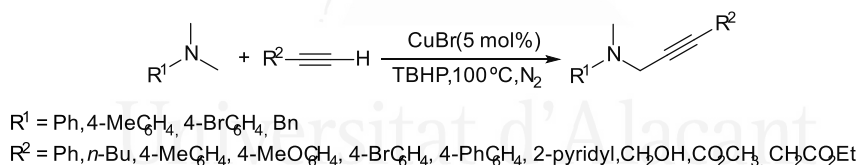
Scheme 32. CDC of tertiary amines and terminal alkynes catalysed by CuBr.

---

[133] Murata, S.; Teramoto, K.; Miura, M.; Nomura, M. *J. Chem. Res. (M)* **1993**, 2828-2836.

[134] Gandhi, S. *Org. Biomol. Chem.* **2019**, *17*, 9683-9692.

[135] (a) Li, Z.; Li, C.-J. *Org. Lett.* **2004**, *6*, 4997-4999. (b) Li, Z.; MacLeod, P. D.; Li, C.-J. *Tetrahedron: Asymmetry* **2006**, *17*, 590-597.
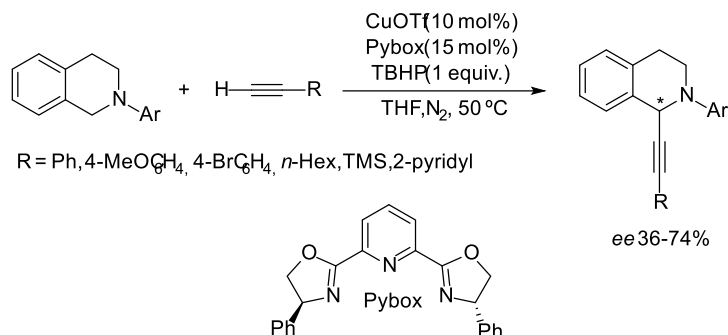
Scheme 33. Asymmetric CDC of *N*-aryl-1,2,3,4-tetrahydroisoquinolines and terminal alkynes catalysed by copper en presence of Pybox as a chiral ligand.

Numerous works about Cu-catalysed CDC between terminal alkynes and tertiary amines emerged since these results were published. The absence of heterogeneous catalytic systems for the synthesis of propargylamines through CDC reactions until 2012, motived our research group to study a new catalytic system based on supported copper nanoparticles for the CDC of tertiary amines and terminal alkynes.[136] During the development of this study, a few reports on this matter were published.

In 2013, Moores and co-workers described[137] the CDC between arylacetylenes and THIQs catalysed by magnetic copper ferrite nanoparticles. This catalyst was successfully recovered and reused up to ten times, showing the same performance every time (Scheme 34).
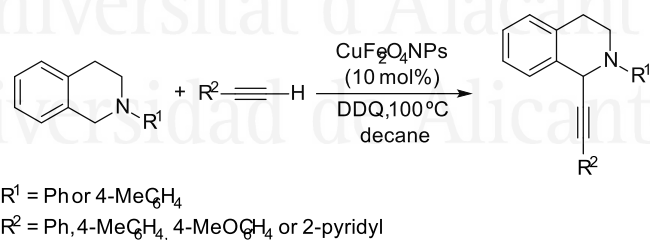
Scheme 34. CDC of THIQs and terminal alkynes catalysed by copper ferrite NPs.

In 2014, Dang *et al.* reported the use of the copper-based metal-organic frameworks MOF-199 (Scheme 35) and $Cu_2(BDC)_2(DABCO)_2$ (Scheme 36) for the CDC of acetylenes with

[136] Arroyo, A. *Acoplamiento de aminas y alquinos catalizado por nanopartículas de cobre soportadas*; Trabajo Fin de Máster, Universidad de Alicante, 2012-2013.
[137] Hudson, R.; Ishikawa, S.; Moores, A. *Synlett* **2013**, *24,* 1637-1642.

tertiary[138] and secondary[139] amines, respectively. Both MOFs were recycled, at least ten times, without losing any catalytic activity and with negligible leaching.

R[1] = H, Me or Br
R[2] = Ph, 4-MeC$_6$H$_4$, 4-MeOC$_6$H$_4$, n-Hex
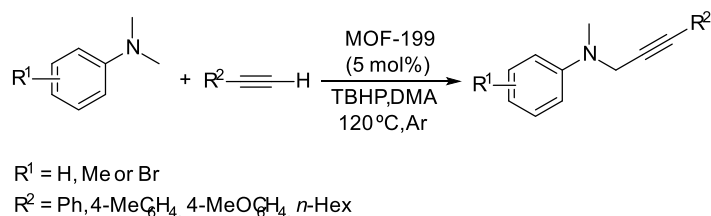
Scheme 35. Synthesis of propargylamines catalysed by a Cu-metal organic framework.

R[1] = H, Me or Cl
R[2] = Ph, 4-MeC$_6$H$_4$, 4-MeOC$_6$H$_4$, n-Hex
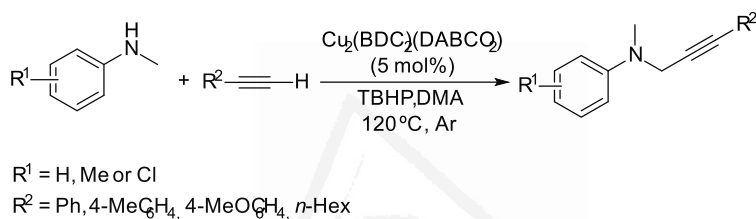
Scheme 36. CDC of secondary amines and terminal alkynes catalysed by a Cu-metal organic framework.

The same year, these authors also reported the alkynylation of secondary amines catalysed by copper ferrite NPs, observing the same kind of methylations as those promoted by Cu$_2$(BDC)$_2$(DABCO)$_2$.[139] After some control experiments, it was concluded that this reaction occurs due to the presence of methyl radicals (from TBHP) in the reaction medium (Scheme 37).[140]

R[1] = H, Me, Cl
R[2] = Ph, 4-MeC$_6$H$_4$, 4-MeOC$_6$H$_4$, n-Hex
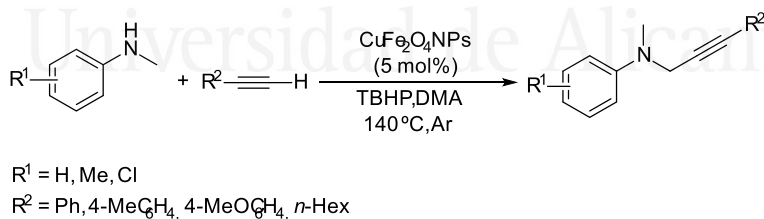
Scheme 37. CDC of secondary amines and terminal alkynes catalysed by magnetic copper ferrite NPs.

[138] Dang, G. H.; Hguyen, D. T.; Le, D. T.; Phan, N. T. S.; Truong, T. *J. Mol. Catal.* **2014**, *395*, 300-306.

[139] Dang, G. H.; Dang, T. T.; Le, D. T.; Truong, T.; Phan, N. *J. Catal.* **2014**, *319*, 258-264.

[140] Nguyen, A. T.; Pham, L. T.; Phan, N. T. S.; Truong, T. *Catal. Sci. Technol.* **2014**, *4*, 4281-4288.

In 2016, Gupta *et al.*[141] described the use of Cu₆Se₄.₅NPs for this type of coupling, reusing the catalyst in, at least, four cycles with only a slight descrease in the yield, what was attributed to some Cu leaching. The transformation took place in the presence of TBHP under a nitrogen atmosphere in poor-to-good yields.

n = 0, 1
R¹ = H, 4-Cl, 4-Br, 4-MeO, 2-Cl, 3-Cl
R² = Ph, 4-MeC₆H₄, 4-MeOC₆H₄, 4-CF₃, 2-pyridyl, *n*-Pent
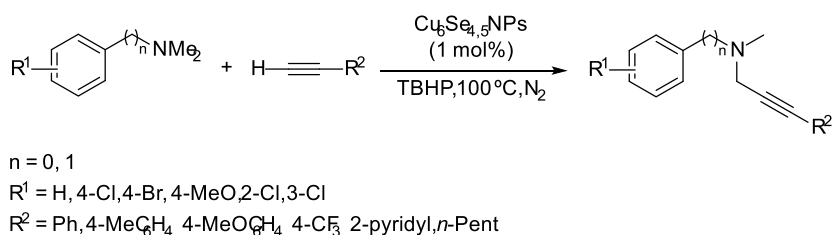
Scheme 38. Synthesis of propargylamines catalysed by Cu₆Se₄.₅NPs.

More recently, in 2017, Gómez and Favier and co-workers[142] showed the first application of zero-valent CuNPs on PVP in this transformation. The reaction was carried out in glycerol and in the presence of TBHP, under a hydrogen atmosphere (Scheme 39). The recyclability of this catalytic system was not studied in this reaction, but it was found to be successful in the amination of iodobenzene, included in the same publication.

n = 0, 1
R¹ = H, 4-Br, 3-Me
R² = H, Me
R³ = Ph, 4-MeC₆H₄, 4-MeOC₆H₄, *n*-Pent
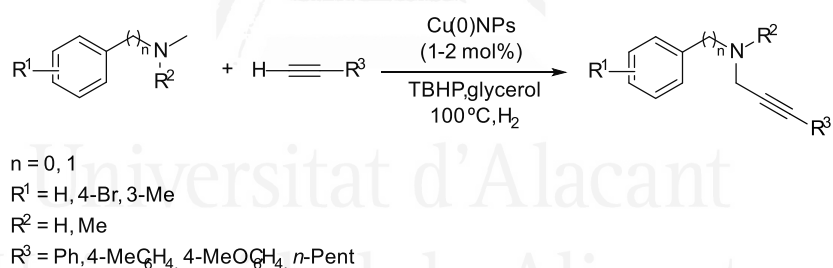
Scheme 39. CDC of tertiary amines and terminal alkynes catalysed by Cu(0)NPs.

In general, the methodologies reported in the literature involve high temperatures, inert atmosphere and exhibit low functional-group tolerance. Due to this fact, the development of new catalytic systems that avoid these drawbacks and allow the use of solvent-free and mild conditions is welcome.

---

[141] Gupta, S.; Joshi, H.; Jain, N.; Singh, A. K. *J. Mol. Catal. A: Chem.* **2016**, *423*, 135-142.

[142] Dang-Bao, T.; Pradel, C.; Favier, T.; Gómez, M. *Adv. Synth. Catal.* **2017**, *359*, 2832-2846.

3.2. Objectives

Based on this background, the following aims were settled:

- o To study the catalytic activity of supported CuNPs in the CDC of tertiary amines and terminal alkynes.
- o To analyse the optimal conditions and the scope of the reaction.
- o To study the recyclability of the catalyst.
- o To scale-up the process.
- o To study the reaction mechanism.
- o To compare the catalytic activity of our catalyst with that of some commercial copper catalysts.
- o To study the bioactivity of some propargylamines in partnership with Eli Lilly & Co.

3.3. Results and discussion

3.3.1. Optimisation of the catalytic system and reaction conditions

First, several catalysts, supports and solvents were screened for the CDC of *N,N*-dimethylaniline (**8a**) and phenylacetylene (**2a**) in the presence of *tert*-butylhydroperoxide (TBHP) as an oxidant agent (Table 20).

Some control experiments were carried out to demonstrate that our supported CuNPs were the actual promoters of this reaction (Table 20, entries 1 and 22), observing that the final product was not formed in the absence of catalyst. Then, the solvent was optimised (Table 20, entries 2-9), concluding that either the use of CH_3CN or neat conditions gave higher conversions (Table 20, entries 2 and 9). The effect of the atmosphere was also studied: the presence of argon had a positive effect on the conversion. On the other hand, inorganic supports such as TiO_2, MK-10 and ZY showed better performance that C or MgO (Table 20, compare entries 12, 14 and 18 with 10 and 16). The use of TBHP-H_2O instead of TBHP-decane led to better conversions (Table 20, entries 19-21). Nevertheless, only the catalyst based on CuNPs/ZY could be efficiently recycled (Table 20, entries 19-21, parentheses).

Table 20. Optimisation of the type of support.[a]

Entry	Catalyst	Solvent/Atmosphere	Conversion (%)[b] 9aa
1	-	-	0
2	CuNPs/C (1.4 mol%)	CH_3CN	23
3	CuNPs/C (1.4 mol%)	CH_2Cl_2	0
4	CuNPs/C (1.4 mol%)	MeOH	0
5	CuNPs/C (1.4 mol%)	H_2O	0
6	CuNPs/C (1.4 mol%)	*i*-PrOH	16
7	CuNPs/C (1.4 mol%)	PhMe	0
8	CuNPs/C (1.4 mol%)	THF	0
9	CuNPs/C (1.4 mol%)	-	24
10	CuNPs/C (1.4 mol%)	-/Ar	33

Table 20. Optimisation of the type of support (cont.).[a]

11	CuNPs/TiO$_2$ (3 mol%)	-	63
12	CuNPs/TiO$_2$ (3 mol%)	-/Ar	53
13	CuNPs/MK-10 (1.8 mol%)	-	62
14	CuNPs/MK-10 (1.8 mol%)	-/Ar	67
15	CuNPs/MgO (1.5 mol%)	-	43
16	CuNPs/MgO (1.5 mol%)	-/Ar	9
17	CuNPs/ZY (3 mol%)	-	62
18	CuNPs/ZY (3 mol%)	-/Ar	67
19	CuNPs/TiO$_2$ (3 mol%)[c]	-/Ar	88 (0)[d]
20	CuNPs/MK-10 (1.8 mol%)[c]	-/Ar	92 (63)[d] (0)[e]
21	CuNPs/ZY (3 mol%)[c]	-/Ar	89 (91)[d] (93)[e]
22	ZY	-/Ar	0

[a] **8a** (0.5 mmol), **2a** (1 equiv.), CuNPs/support (20 mg), TBHP-decane (1 equiv.), solvent (1 mL), 70 ºC, 24 h, in air, unless otherwise stated. [b] Conversion determined by GLC. [c] **8a** (1 mmol), **2a** (1.2 mmol), CuNPs/support (50 mg), TBHP-H$_2$O (1.2 equiv.), 70 ºC, 24 h in air. [d] Second cycle. [e] Third cycle.

In order to study the influence of the different methods used to prepare the catalysts in their activity, the CDC model reaction between *N,N*-dimethylaniline (**8a**) and phenylacetylene (**2a**), in presence of TBHP as an oxidant agent, was evaluated. For this purpose, three methods were analysed: impregnation (**A**), reduction-supporting (**B**) and impregnation-reduction (**C**), with or without thermal treatment (for further information see the section 1.3.1, p. 51).
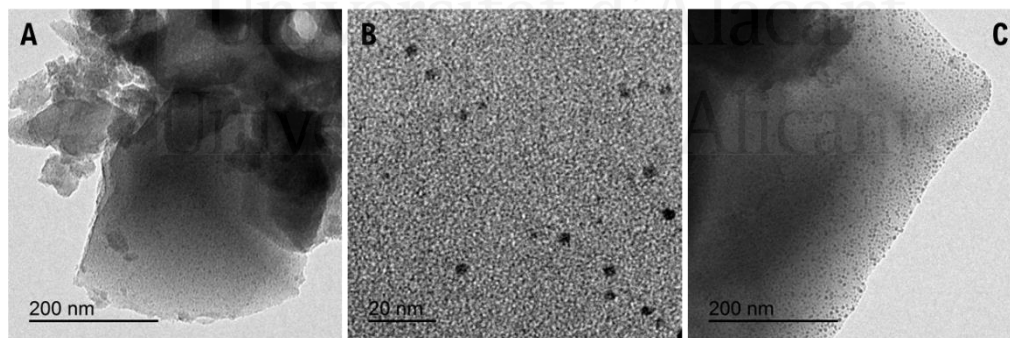
Figure 35. TEM micrographs of CuNPs/ZY synthesised by impregnation (**A**), reduction-supporting (**B**) and impregnation-reduction (**C**).

In general, the presence of water, regardless of its origin (naturally present in the zeolite or added in the preparation step), favoured the incorporation of Cu (Table 21, compare entries 1 and 2 with 3, and 6 with 7). Analysing the results summarised in Table 21, the catalyst with

the best performance was that synthesised by method **A**. However, only the catalysts prepared with method **B** could be efficiently recycled.

Table 21. Optimisation of the method for the catalyst preparation.[a]

Entry	Method[b]	wt% Cu	Conversion (%)[c] 9aa
1	**A**-THF/Ar	1.0	86
2	**A**-THF/Ar[d]	2.1	77
3	**A**-H_2O/air	4.4	65
4	**B**-THF/Ar	3.8	69
5	**B**-THF/Ar[d]	3.7	56
6	**C**-THF/Ar[d]	1.7	53
7	**C**-H_2O/air	3.6	48

[a] **8a** (1 mmol), **2a** (1.2 equiv.), CuNPs/ZY (1.5 mol%), TBHP-decane (1.2 equiv.), 70 ºC, 24 h, Ar. [b] Method of preparation of the catalyst: impregnation (**A**); reduction-supporting (**B**); impregnation-reduction (**C**). [c] Conversion determined by GLC. [d] ZY was previously dried at 100 ºC for 0.5 h.

With the catalyst prepared by method **B**, the optimisation of the catalyst loading and the amount of TBHP (in decane or H_2O) was carried out (Table 22). Interestingly, the reactions carried out under argon and TBHP-decane showed an increase in the conversion when the catalyst loading was reduced (Table 22, entries 1-4). This effect could point to a more effective interation between the catalyst and the reagents. Increasing the amount of TBHP-decane up to two equivalents only affected the conversion slightly (Table 22, entries 5 and 7), whereas high-to-quantitative conversion in the final product was obtained with TBHP-H_2O, independently of the catalyst loading (Table 22, entries 11 and 13-15). Analysing the results summarised in Table 22, the optimal conditions were considered those in entry 13.

Table 22. Optimisation of the conditions.[a]

Entry	Atmosphere	Catalyst (mg)[b]	TBHP (equiv.)[c]	Conversion (%)[d] 9aa
1	Ar	100	decane (1.20)	38
2	Ar	50	decane (1.20)	69
3	Ar	25	decane (1.20)	80
4	Ar	12.5	decane (1.20)	83
5	Ar	50	decane (2.00)	76
6	air	50	decane (1.20)	67
7	air	50	decane (2.00)	77
8	Ar	25	H_2O (1.20)	76
9	Ar	50	H_2O (1.20)	73
10	Ar	50	H_2O (1.50)	82
11	**Ar**	**50**	**H_2O (2.00)**	**>99**
12	air	50	H_2O (1.20)	84
13	**Air**	**50**	**H_2O (2.00)**	**>99**
14	air	25	H_2O (2.00)	91
15	air	12.5	H_2O (2.00)	90

[a] **8a** (1 mmol), **2a** (1.2 equiv.), CuNPs/ZY, TBHP, 70 ºC, 24 h, air. [b] Prepared by method **B** (Table 21, entry 4). [c] 6 M in decane or 80% in H_2O. [d] Conversion determined by GLC.

3.3.2. Scope

With the optimised conditions in hand, a wide variety of terminal alkynes (Table 23) and tertiary amines (Table 24) was tested. First, the CDC of *N,N*-dimethylaniline (**8a**) with terminal alkynes of different nature was evaluated. Aromatic alkynes with neutral (**9aa**), electron-donating (**9ab** and **9ac**) and electron-withdrawing groups (**9ae**) were tested, leading to the formation of the final product in good-to-excellent yields (Table 23, entries 1-4). The reaction showed good performance even with both open-chain (**9af**) and cyclic (**9ag**) aliphatic alkynes, as well as with functionalised ones (**9ah**, **9ai** and **9ja**) (see Table 23, entries 5-9).

Table 23. CDC of *N,N*-dimethylaniline with terminal alkynes catalysed by CuNPs/ZY.[a]
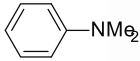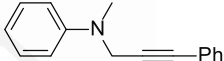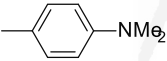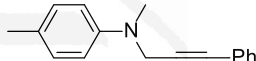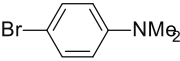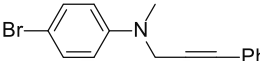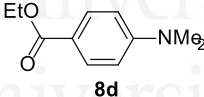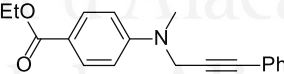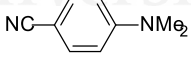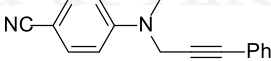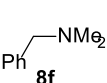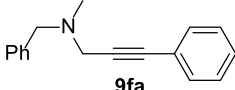
Entry	2	9	Yield (%)[b]
1	≡—Ph **2a**	Ph—N propargyl Ph **9aa**	98
2	≡—C6H4—OMe **2b**	Ph—N propargyl C6H4—OMe **9ab**	90
3	≡—C6H4—Me **2c**	Ph—N propargyl C6H4—Me **9ac**	87
4	≡—C6H4—CO2Me **2e**	Ph—N propargyl C6H4—CO2Me **9ae**	73
5	≡—(CH2)5CH3 **2f**	Ph—N propargyl (CH2)5CH3 **9af**	80
6	≡—cyclohexyl **2g**	Ph—N propargyl cyclohexyl **9ag**	95
7	≡—(CH2)4Cl **2h**	Ph—N propargyl (CH2)4Cl **9ah**	93
8	≡—CO2Et **2i**	Ph—N propargyl CO2Et **9ai**	86
9	≡—C6H10(OH) **2j**	Ph—N propargyl C6H10(OH) **9aj**	75

[a] **8a** (1 mmol), **2** (1.2 equiv.), CuNPs/ZY (1.5 mol%), TBHP-H_2O (2 equiv.), 70 ºC, 15-24 h, air.
[b] Isolated yield.

On the other hand, an array of anilines with different electronic nature was tested in the CDC with phenylacetylene (**2a**, Table 24). The presence of electron-donating groups at the *para* position facilitated the formation of the corresponding propargylamines **9ba** and **9ca** in
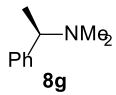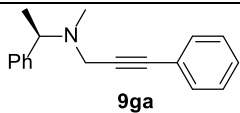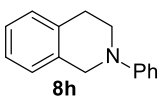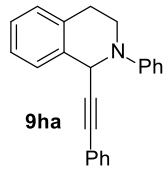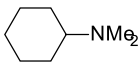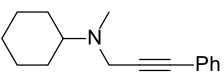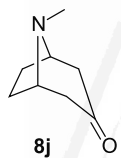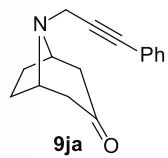
high yields (Table 24, entries 2 and 3), whereas electron-withdrawing groups (**9da** and **9ea**) led to lower yields independently of the temperature (Table 24, entries 4 and 5). These results were expected due to the inability of the latter groups to stabilise the iminium intermediate. Benzylic amines were also studied, showing a high regioselectivity at the methyl position (**9fa**, **9ga** and **9ha**) in moderate-to-good yields (Table 24, entries 6-8). Last but not least, aliphatic amines were successfully tested (Table 24, entries 9 and 10) in excellent (**9ia**) and moderate yields (**9ja**). It must be underlined that, aliphatic amines are very seldom explored substrates,[131b] and usually only poor yields have been reported.[143]

Table 24. CDC of tertiary amines and phenylacetylene (**2a**) catalysed by CuNPs/ZY.[a]

Entry	8	9	Yield (%)[b]
1	8a	9aa	98
2	8b	9ba	87[c]
3	8c	9ca	90
4	8d	9da	43[d]
5	8e	9ea	50[d,e]
6	8f	9fa	73

---

[143] Niu, M.; Yin, Z.; Fu, H.; Jiang, Y.; Zhao, Y. *J. Org. Chem.* **2008**, *73*, 3961-3963.

Table 24. CDC of tertiary amines and phenylacetylene (**2a**) catalysed by CuNPs/ZY (cont.).[a]

7	8g	9ga	70
8	8h	9ha	62
9	8i	9ia	95
10	8j	9ja	50

[a] **8** (1 mmol), **2a** (1.2 equiv.), CuNPs/ZY (1.5 mol%), TBHP-H$_2$O (2 equiv.), 70 ºC, 15-24 h, air. [b] Isolated yield. [c] Yield after distillation. [d] Reaction at 100 ºC. [e] ^{1}H NMR yield.

Although the synthesis of propargylamines through CDC usually involves tertiary amines, the optimal conditions were applied to the reaction between *N*-methylaniline (**8k**) and phenylacetylene (**2a**), affording the product **9aa** in quantitative conversion (Scheme 40). This methylation-alkynylation process was already observed by Truong, as previously mentioned in the introduction.[139,140]
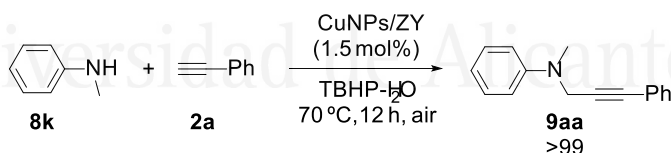
Scheme 40. CDC of **8k** and **2a** catalysed by CuNPs/ZY.

On the other hand, the CDC of TMEDA (**8l**) with phenylacetylene (**2a**), under the same conditions, led to the formation of monoalkylated **9la** and aminomethylated **10** (Scheme 41). This behaviour is consistent with Li's studies,[130c] where the use of TBHP was described to lead to the major formation of **10** instead of **9la**, whereas molecular oxygen favoured the formation of **9la**.
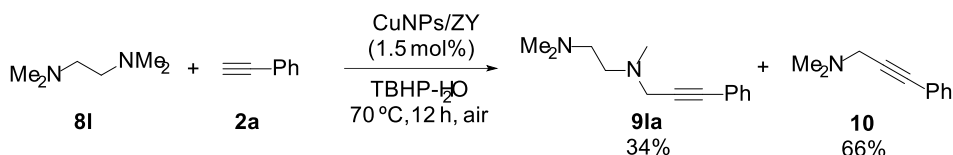
Scheme 41. CDC of **8l** and **2a** catalysed by CuNPs/ZY.

3.3.3. Catalyst recyclability, nature of the catalysis and reaction scale-up

It must be underlined that the catalyst CuNPs/ZY showed ease of manipulation and did not require an inert atmosphere. As an additional benefit, the catalyst could be recovered by centrifugation and reused, up to seven times, with only a slight loss of catalytic activity (Figure 36).

	1	2	3	4	5	6	7
CDC	93	91	89	91	88	82	80
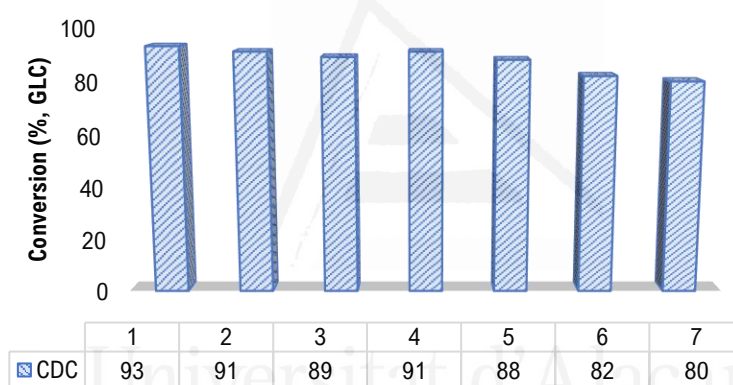
Figure 36. Recycling of CuNPs/ZY in the synthesis of **9aa**.

In order to demonstrate the heterogeneous nature of our catalyst, a hot filtration test[9a] was carried out. For this experiment, the CDC between *N,N*-dimethylaniline (**8a**) and phenylacetylene (**2a**) was performed under the optimal conditions. After 2 h, a sample of the reaction was analysed, giving 5% conversion of **9aa**. The catalyst was then removed from the reaction medium, while the filtrate remained under heating for 12 h; the conversion did not increase at all (5% of **9aa**). This experiment, in concordance with the negliglible amount of leached copper found in the filtrate by ICP-MS (0.78 ppb), confirms the heterogeneous nature of CuNPs/ZY.

Although these experiments seem to point to a heterogeneous process, we cannot refuse the fact that the catalyst could be act as reservoir for metal species that leach into solution and re-adsorb on the support after promoting the reaction. This kind of behaviour is

typical of suspensions of MNPs enclosed in group VIII.[144] Nevertheless, Scaiano and co-workers proved, by single-molecule spectroscopy, that the catalytic process that involves CuNPs and terminal alkynes (such as in Click chemistry) takes place on the surface of the CuNPs.[145]

In addition, the reaction was efficiently scaled up to 12 mmol, observing conversions of 93% and 67% (**9aa)**, employing a catalyst loading of 1.5 mol% and 0.4 mol%, respectively. The kinetic profile for the CDC between **8a** and **2a**, at this scale, seems to reveal an induction period of about 1 h (Figure 37).
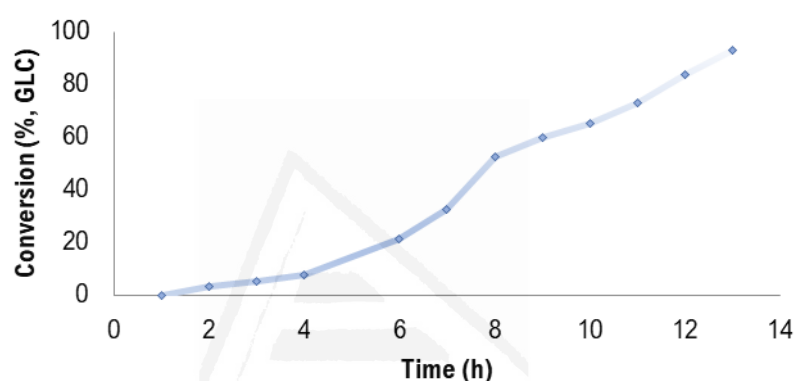
Figure 37. Plot showing the evolution of the formation of **9aa** under the standard CDC conditions at 12 mmol scale. Reaction conditions: **1a** (12 mmol), **2b** (1.2 equiv.), TBHP-H_2O (2 equiv.), CuNPs/ZY (1.5 mol%) at 70 ºC, air.

3.3.4. Comparison with other commercial Cu catalysts

The catalytic activity of CuNPs/ZY was compared with that of an array of commercial copper catalysts in the CDC between *N,N*-dimethylaniline (**8a**) and phenylacetylene (**2a**) (Table 25). Among them, the best results in the formation of **9aa** were obtained with CuCl (10 mol%), CuBr (10 mol%) and CuBr·SMe_2 (2 mol%) (see Table 25, entries 4, 6 and 14). However, the commercially available catalysts tested yielded significant amounts of the alkyne homocoupling product (1,4-diphenylbuta-1,3-diyne, **11a**), while our catalyst was very selective towards the formation of the propargylamine **9aa** and much more effective (Table 25, entry 16). Hence, the nanostructure of CuNPs/ZY seems to be crucial for its reactivity and selectivity.

[144] Review: Durán-Pachón, L.; Rothenberg, G. *Appl. Organomet. Chem.* **2008**, *22*, 288-299.

[145] Decan, M. R.; Impellizzeri, S.; Marin, M. L.; Scaiano, J. C. *Nat. Commun.* **2014**, *5*, 4612.
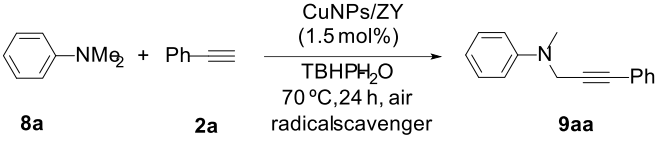
Table 25. CDC of **8a** and **2a** catalysed by commercial Cu catalysts.[a]

Entry	Catalyst	mol%	8a/9aa/11a (%)[b]
1	Cu(0)	10	37/50/13
2	Cu_2O	10	22/53/25
3	CuO	10	93/5/2
4	CuCl	10	11/74/15
5	$CuCl_2$	10	11/39/50
6	CuBr	10	14/79/7
7	CuI	10	12/68/20
8	$Cu(OAc)_2$	10	26/61/13
9	$CuBr·SMe_2$	10	27/67/6
10	$Cu(OTf)_2$	10	44/40/16
11	CuBr	1	50/42/8
12	CuI	1	24/62/14
13	$Cu(OAc)_2$	2	17/59/24
14	$CuBr·SMe_2$	2	20/75/5
15	$Cu(OTf)_2$	2	24/56/20
16	**CuNPs/ZY**	**1.5**	**0/>99/0**

[a] **8a** (1 mmol), **2a** (1.2 equiv.), Cu, $TBHP-H_2O$ (2 equiv.), 70 ºC, 24 h, air. [b] Conversion determined by GLC.

3.3.5. Reaction mechanism

Regarding the mechanism of this CDC reaction, a main point of discussion is whether the iminium ion is radically or ionically formed.[125] In order to clarify if this step involves radical processes, some control experiments with radical traps were carried out (Table 26).

Table 26. CDC of **8a** and **2a** in the presence of radical scavengers.[a]

Entry	Radical scavenger	9aa (%)[b]
1	norbornene	92
2	cumene	80
3	2,6-di-*tert*-butylphenol	65[c]
4	TEMPO[d]	10[e]

[a] **8a** (1 mmol), **2a** (1.2 equiv.), CuNPs/ZY (1.5 mol%), TBHP-H_2O (2 equiv.), 70 °C, 24 h, air. [b] Conversion determined by GLC. [c] 2,6-Di-*tert*-butylanisole was formed in *ca*. 40% conversion. [d] 2,2,6,6-Tetramethylpiperidine-1-oxyl. [e] 1-Methoxy-2,2,6,6-tetramethylpiperidine was formed in *ca*. 75% conversion.

The radical-scavenger derivatives observed in the cases of 2,6-di-*tert*-butylphenol (2,6-di-*tert*-butylanisole) and TEMPO (1-methoxy-2,2,6,6-tetramethylpiperidine) revealed the presence of methyl radicals in the reaction medium. These radicals could be obtained *via* a *β*-cleavage of TBHP followed by a homolytic C–C bond cleavage, forming acetone (Scheme 42).
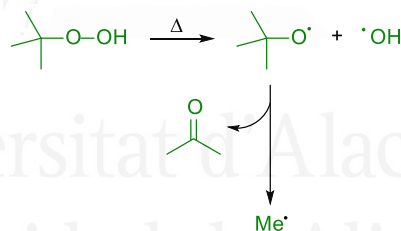
Scheme 42. Formation of methyl radicals from TBHP.

To further confirm this possibility, 2,4-dinitrophenylhydrazine (2,4-DNPH) was employed to trap the formed acetone, generating the corresponding hydrazone. For this purpose, 1.5 equiv. of 2,4-DNPH were added to the standard reaction, observing the formation of a white precipitate after 5 h, which was identified as acetone 2,4-dinitrophenylhydrazone (**12**); this experiment confirmed the formation of acetone in the reaction medium (Scheme 43).
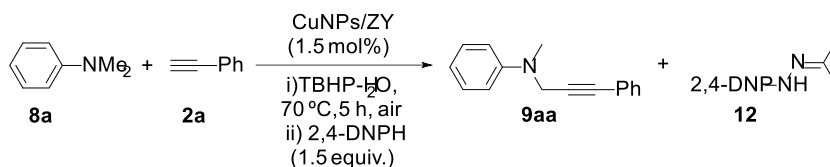
Scheme 43. Experiment demonstrating the generation of acetone in the CDC of **8a** and **2a**.

On the other hand, transition metals can promote the cleavage of TBHP into *tert*-butoxyl radicals.[146] Because of that, two control experiments were performed to prove that β-cleavage of TBHP readily occurs at the temperature used for the CDC even in the absence of the catalyst (Scheme 44).
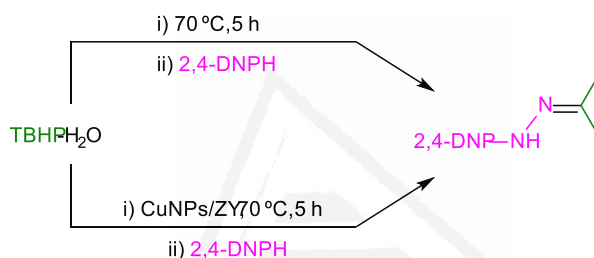
Scheme 44. Control experiments on the transformation of TBHP into acetone.

In addition, other oxidant agents were tested in order to confirm the requirement of methyl radicals in the reaction medium (Scheme 45). Benzoyl peroxide, which generates $PhCO_2^{\bullet}$ and $Ph^{\bullet}$, did not generate **9aa**. In contrast, di-*tert*-butyl peroxide (t-BuO$^{\bullet}$ and Me$^{\bullet}$) and acetyl peroxide ($MeCO_2^{\bullet}$ and Me$^{\bullet}$), two reagents capable to generate Me$^{\bullet}$, formed **9aa** in 10%. These results point to the methyl radicals having a crucial role in the reaction.
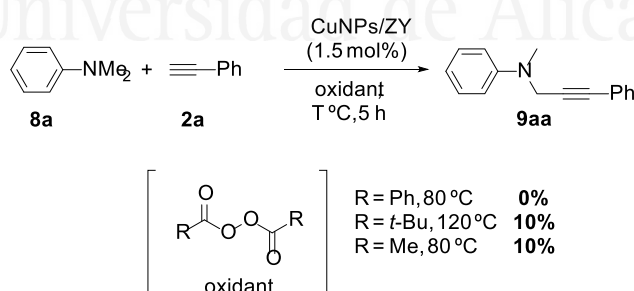
Scheme 45. CDC of **8a** and **2a** catalysed by CuNPs/ZY in the presence of different peroxides.

---

[146] Richardson, W. H. *J. Am. Chem. Soc.* **1965**, *87*, 247-253.

The role of the different copper species was also evaluated in the standard CDC reaction. Copper can participate in the formation of the nucleophile *in-situ* (copper acetylide) but also in the oxidation of the substrate (to the iminium ion). Keeping in mind these two possible roles, XPS analyses were performed in order to study the distribution of the oxidation states of copper. Fresh CuNPs/ZY presents Cu_2O and CuO species in a *ca.* 1:1 ratio (see 1.3.2.2., p. 56). However, the catalyst recovered after the reaction of **8a** and **2a** showed almost no signal for CuO (Figure 39, top), being Cu_2O the predominant species on the catalyst's surface (confirmed by the $CuL_3M_{45}M_{45}$ Auger peak at 571.0 eV, Figure 40).[147]

On the other hand, the recovered CuNPs/ZY (Figure 39, top) was treated with TBHP-H_2O at 70 ºC during 5 h, resulting in the regeneration of CuO species to almost the same proportion as in the fresh catalyst (Figure 38), as its XPS spectrum reveals (Figure 39, bottom). These results underline the crucial role of CuO in the CDC reactions. We believe that the success of this CDC catalysed by CuNPs resides in the combination of both CuO and Cu_2O and their redox activities.
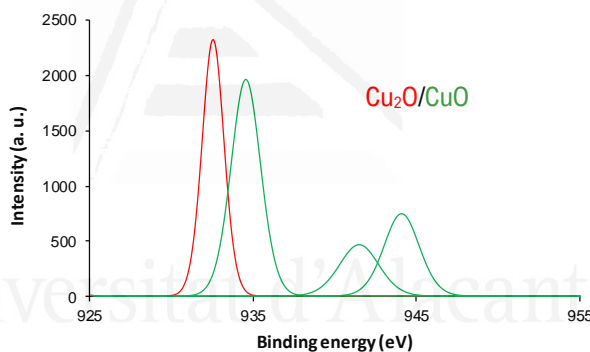
Figure 38. XPS spectrum of fresh CuNPs/ZY at the Cu 2$p_{3/2}$ level

---

[147] Diaz-Droguett, D. D.; Espinoza, R.; Fuenzalida, V. M. *Appl. Surf. Sci.* **2011**, *257*, 4597-4602.
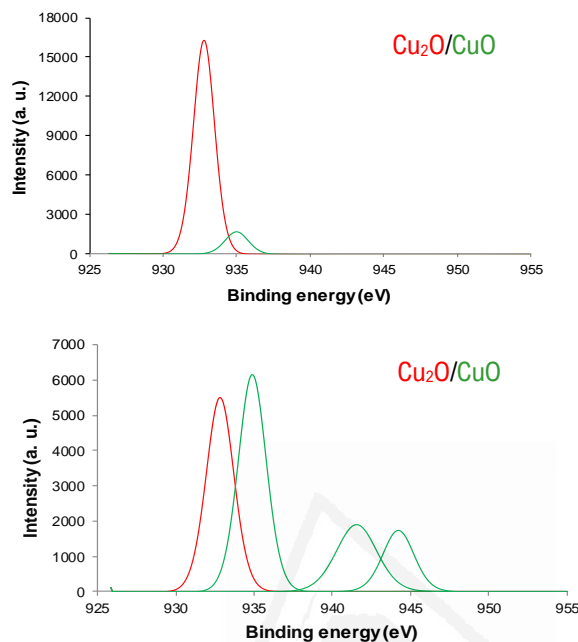
Figure 39. XPS spectrum of CuNPs/ZY at the Cu $2p_{3/2}$ level, recovered after the CDC reaction (top) and after re-oxidation (bottom).
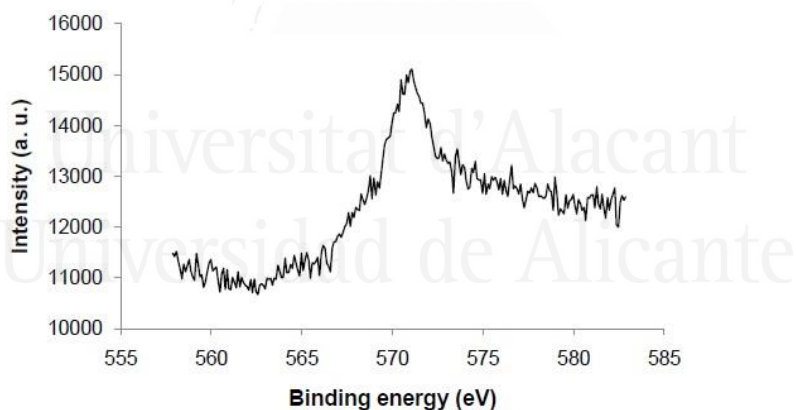
Figure 40. Auger spectrum of CuNPs/ZY recovered at the end of the CDC reaction.

With all these results in hand, the reaction mechanism below was proposed (Scheme 46). First, Cu$_2$ONPs interacts with the terminal alkyne to form the corresponding copper acetylide,[148] process that was found to be favoured in aqueous medium.[149] At the same time,

---

[148] Albadalejo, M. J.; Alonso, F.; Moglie, Y.; Yus, M. *Eur. J. Org. Chem.* **2012**, 3093-3104.

[149] Alonso, F.; Moglie, Y.; Radivoy, G.; Yus, M. *J. Org. Chem.* **2011**, *76*, 8394-8405.

thermal cleavage of TBHP occurs to form methyl radicals and acetone. On the other hand, CuO promotes the oxidation of the amine to the corresponding radical cation, although the direct oxidation by TBHP cannot be ruled out. The Cu_2O generated in this process (Figure 39, top) is re-oxidised to CuO by the action of TBHP (and/or O_2) which, in turn, generates more *tert*-butoxyl radical. The following step is the most controversial among the researchers, possibly consisting in a hydrogen-atom transfer (HAT) between the amine radical cation and the methyl radical, providing the iminium intermediate; the cooperation of other radical species cannot be disregarded, though the role of the methyl radical has been proven to be essential in this study. Whether the single-electron transfer (SET) comes before the HAT or *vice versa* is hard to ascertain;[150] we have proposed a SET-HAT process. The final step would be the addition of the copper acetylide to the iminium ion, leading to the formation of the corresponding propargylamine.
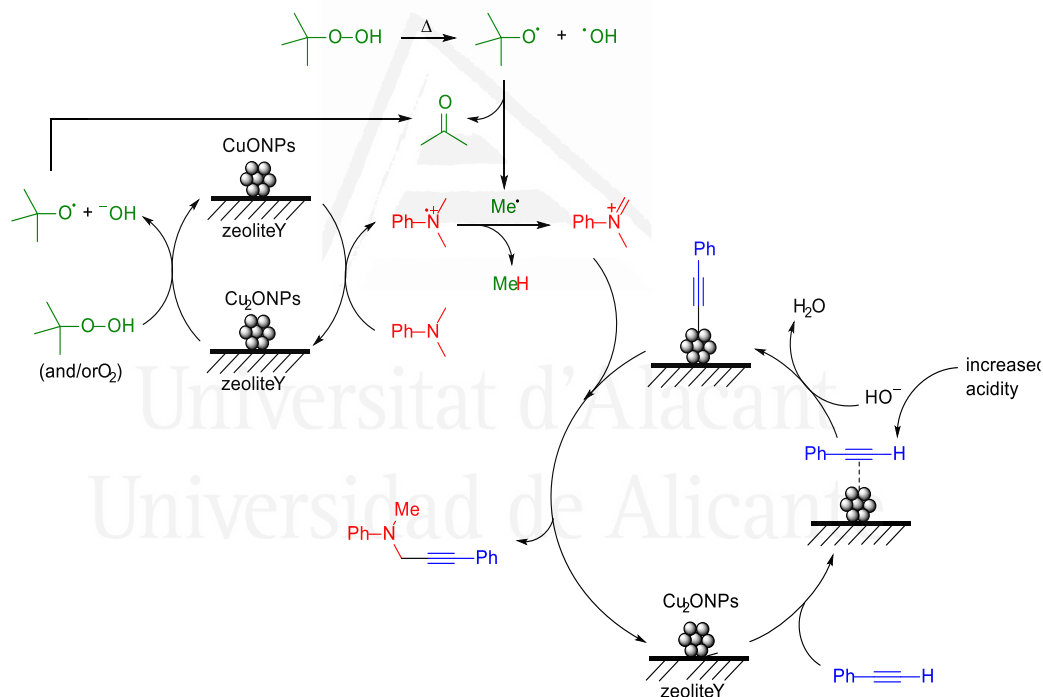
Scheme 46. Reaction mechanism proposed for the synthesis of propargylamines through the CDC of tertiary amines and terminal alkynes catalysed by CuNPs/ZY.

---

[150] Cheng, G.-J.; Song, L.-J.; Yang, Y.-F.; Zhang, X.; Wiest, O.; Wu, Y.-D. *ChemPlusChem* **2013**, *78*, 943-951.

3.3.6. Bioactivity

As previously mentioned, propargylamines show interesting biological activities. In this sense, we decided to evaluate the biological activity of our propargylamines in collaboration with Eli Lilly & Co's Open Innovation Drug Discovery (OIDD) program. Eli Lilly & Co carried out the *in silico* and *in vitro* screening of our compounds. While the common targets for propargylamines are related to neurodegeneration, we wanted to study their activity against other kind of ailments, with the hope to broaden the therapeutical scope of this family of compounds. Among the propargylamines tested, three of them (Figure 41) showed some bioactivity.
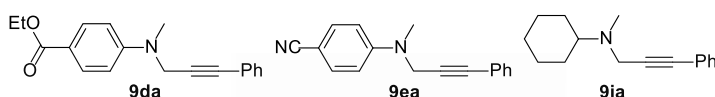
Figure 41. Bioactive propargylamines **9da**, **9ea** and **9ia**.

The results obtained in the different single point experiments are summarised in Table 27. Interesting results were observed in the Arginase inhibition (Entry 3).

Table 27. Bioactivity of compounds **9da**, **9ea** and **9ia**.

Entry	Target	X µM	% Inhibition		
			9da	9ea	9ia
1	PCSK9 Inhibition	40	-	10.24	4.02
2	NNMT inhibitor	10	-	-	4.49/6.73
3	Arginase (ARG-1)	100	25.01	44.50	31.28
4	IL-17 PPI	100	7.65	11.98	5.44
5	Tuberculosis	20	-	3.60	-
6	MTB	5	-	6.88	-
7	Leishmania	5	12.65	6.92	-
8	Chagas Disease	5	12.59	5.15	-

NNMT = Nicotinamide *N*-Methyltransferase; IL-17 = InterLeukin 17;
MTB = Mycrobacterium Tuberculosis.

Arginase (ARG-1) is an enzyme of the urea cycle found in liver that promotes the conversion of L-arginine into L-ornithine and urea. ARG-1 is a highly specific and sensitive biomarker of hepatotoxicity acting as detector of hepatocellular injury. Due to this, ARG-1 is now a key target for the differential diagnosis of hepatocellular carcinoma (HCC) from metastatic tumors to the liver.[151]

---

[151] (a) Yan, B. C.; Gong, C.; Song, J.; Krausz, T.; Tretiakova, M.; Hyjek, E.; Al-Ahmadie, H.; Alves, V.; Xiao, S. Y.; Anders, R. A.; Hart, J. A. *Am. J. Surg. Pathol.* **2010**, *34*, 1147-1154. (b) Timek, D. T.; Shi, J.; Liu, H.; Lin, F. *Am. J. Clin. Pathol.* **2012**, *138*, 203-210. (c) Fujiwara, M.; Kwok, S.; Yano, H.; Pai, R. K. *Cancer Cytopathol.* **2012**, *120*, 230-237.

3.4. Conclusions

As a summary of this chapter, we have developed a new heterogeneous catalyst based on CuNPs supported on zeolite Y for the CDC between tertiary amines and terminal alkynes, with different electronic nature in both substrates, in presence of a slight excess of TBHP-H_2O. This catalytic system has been applied to the synthesis of propargylamines in moderate-to-excellent yields. Contrary to other reports, the CDC reaction takes place efficiently without the requirement of solvents or an inert atmosphere and under milder reaction conditions.

Regarding the recyclability of the catalyst, CuNPs/ZY has been recovered and reused, at least, in seven cycles, maintaining a good catalytic activity, and the reaction has been scaled up to 12 mmol with a similar performance.

In addition, this catalyst has shown better results than those of some commercially available copper sources, while avoiding the formation of homocoupling products. This fact demonstrates the crucial role of the nanostructured morphology of our catalyst.

Based on control experiments, a plausible reaction mechanism has been proposed, paying special attention to the critical role of methyl radicals and that of the Cu_2O and CuO redox couple.

As such, the catalytic system based on CuNPs/ZY is an attractive alternative to other catalysts for the synthesis of propargylamines through the CDC reaction. In addition, the ease of preparation of the catalyst, low metal loadings employed, and the absence of both solvents and inert conditions, are some clear advantages over the previous reported systems.

Finally, the biological activity of some of the synthesised propargylamines has been evaluated in different targets, with propargylamines **9da**, **9ea** and **9ia** showing some activity, especially in the inhibition of Arginase.

Chapter 4. CDC of tetrahydroisoquinolines and nitroalkanes catalysed by CuNPs/TiO$_2$. Synthesis of dihydroindoloisoquinolines

4.1. Antecedents

4.1.1. Introduction

Amid the wide diversity of nitrogen-containing structures, 5,6-dihydroindolo[2,1-a]isoquinolines (the blue general structure in Figure 42) are of particular interest in medicine. Several molecules of this type have proven to be effective in the treatment of breast cancer (**13a-c**) due to their strong capability to inhibit tubulin polymerisation and their ability to slow down the growth of human cancer cells *in vitro*.[152] In addition, the dihydroindoloisoquinoline skeleton is present in some natural products such as cryptaustoline (**13e**) or derivatives,[153] which can act as antifungal (**13f**)[154] and melatonin agonists (**13d**).[155]
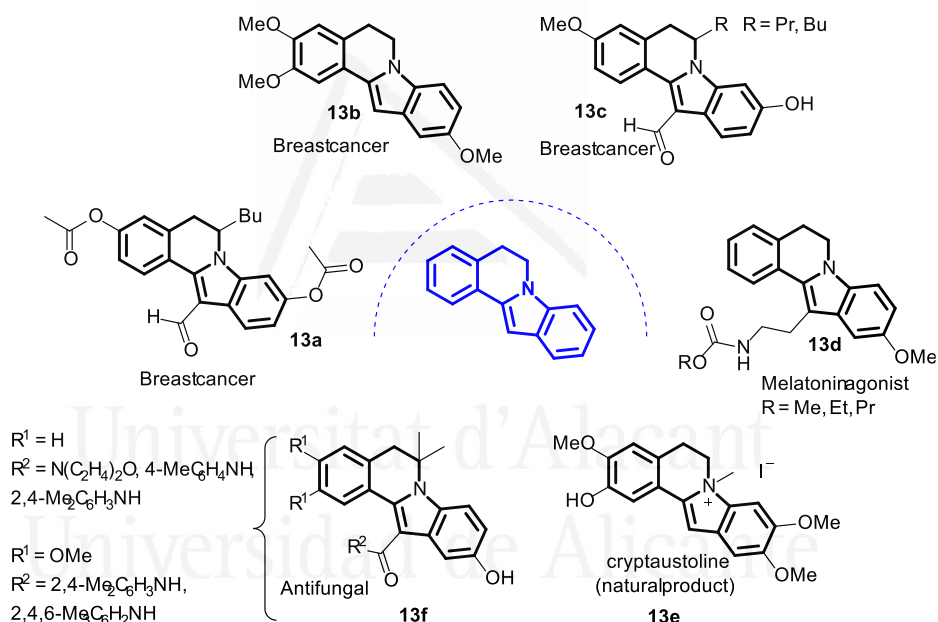
Figure 42. General structure of dihydroindoloisoquinolines (blue) and some bioactive examples.

[152] (a) Polossek, T.; Ambros, R.; von Angerer, S.; Brandl, G.; Mannschreck, A.; von Angerer, E. *J. Med. Chem.* **1992**, *35*, 3537-3547. (b) Goldbrunner, M.; Loidl, G.; Polossek, T.; Mansschreck, A.; von Angerer, E. *J. Med. Chem.* **1997**, *40*, 3524-3533.

[153] (a) Orito, K.; Harada, R.; Uchiito, S.; Tokuda, M. *Org. Lett.* **2000**, *2*, 1799-1801. (b) Philips, A. M. F.; Guedes da Silva, M. F. C.; Pombeiro, A. J- L. *Front. Chem.* **2020**, *8*, 30.

[154] Surikova, O. V.; Mikhailovskii, A. G.; Pershina, N. N.; Aleksandrova, G. A.; Semeriko, V. V.; Vakhrin. *Pharm. Chem. J.* **2010**, *44*, 296-298.

[155] Faust, R.; Garratt, P. J.; Jones, R.; Yeh, L.-K. *J. Med. Chem.* **2000**, *43*, 1050-1061.

In general, the synthesis of these compounds involves the intramolecular cyclisation of *N*-aryl-1,2,3,4-tetrahydroisoquinolines (Schemes 46 and 47).[156] Nevertheless, this protocol requires the presence of a suitable group at the *ortho* position on the *N*-aryl moiety.[156] This transformation has been carried out catalysed by niobium(V) chloride (Scheme 47),[156a] using stoichiometric amounts of base,[156b] or employing iridium complexes under thermal[156c] or photoredox[156d-f] conditions (Scheme 48). More recently, Takai and co-workers described the use of Mo(CO)$_6$ to catalyse the intramolecular cyclisation of pre-funtionalised THIQs, in toluene at 135 °C, in poor-to-moderate yields.[157]
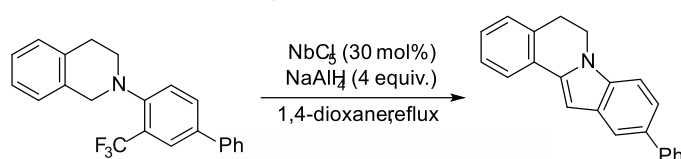
Scheme 47. Catalytic C-H carbenoid insertion approach towards 5,6-dihydroindolo[2,1-*a*]isoquinolines.
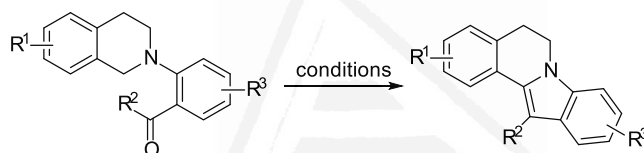
Yan, 2013: ^{t}BuOK, DMF, 90 °C, Ar
Xiao, 2013: [Ir(cod)Cl]$_2$, dppe, HOAc, reflux
Ye, 2016: [Ir(ppy)$_2$(dtbbpy)]PF$_6$, K$_2$HPO$_4$, methyl 2-mercaptoacetate, 5 W blue LED, r.t., MeCN, Ar
Zhu, 2016: Ir(ppy)$_2$(dtbbpy)PF$_6$, (PhO)$_2$PO$_2$H, 23 W CFL, r.t., DMF, N$_2$
Takai, 2019: Mo(CO)$_6$, 3,5-di-*tert*-butylcyclohexa-3,5-diene-1,2-dione, toluene, 135 °C

Scheme 48. Synthesis of 5,6-dihydroindoloisoquinolines from *N*-2-acylaryltetrahydroisoquinolines.

In the same year (2019), Zhang *et al.* studied the formation of this type of compounds throught the coupling of indolecarboxaldehydes and hypervalent diaryliodonium salts, employing Pd(OAc)$_2$ as a catalyst in DMF at 145 °C, reporting good-to-excellent yields.[158]

[156] (a) Fuchibe, K.; Kaneko, T.; Mori, K.; Akiyama, T. *Angew. Chem. Int. Ed.* **2009**, *48*, 8070-8073. (b) Wei, W.; Dong, X.; Nie, S.; Chen, Y.; Zhang, X.; Yan, M. *Org. Lett.* **2013**, *15*, 6018-6021. (c) Nie, S.; Sun, X.; Wei, W.; Zhang, X.; Xiao, J. *Org. Lett.* **2013**, *15*, 2394-2397. (d) Yuan, X.; Wu, X.; Dong, S.; Wu, G.; Ye, J. *Org. Biomol. Chem.* **2016**, *14*, 7447-7450. (e) Li, W.; Duan, Y.; Zhang, M.; Cheng, J.; Zhu, C. A. *Chem. Commun.* **2016**, *52*, 7596-7599. (f) Cheng, J.; Xie, J.; Zhu, C.; *Chem. Commun.* **2018**, *54*, 1655-1658.

[157] Asako, S.; Ishihara, S.; Hirata, K.; Takai, K. *J. Am. Chem. Soc.* **2019**, *141*, 9832-9836.

[158] Ye, Z.; Li, Y.; Xu, K.; Chen, N.; Zhang, F. *Org. Lett.* **2019**, *21*, 9869-9873.
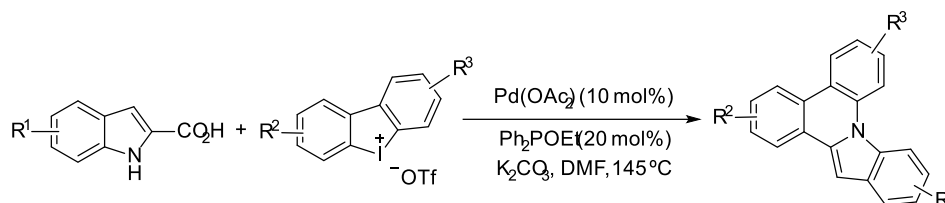
Scheme 49. Palladium-catalysed synthesis of dihydroindoloisoquinolines from indolecarboxaldehydes and hypervalent diaryliodonium salts.

Generally, the reported protocols from *N*-aryl-tetrahydroisoquinolines require the presence of an acyl *ortho* group on the *N*-aryl moiety. Moreover, in these methods, it is quite common the use of iridium catalysis, stoichiometric amounts of reagents, and/or incompatible conditions with sensitive groups. Therefore, the study of new strategies is essential to make the synthesis of dihydroindoloisoquinolines more efficient and sustainable. In this sense, we have found the CDC reaction between THIQs and nitroalkanes [159,125d] as a sustainable and alternative route towards dihydroindoloisoquinolines.

4.1.2. CDC of THIQs and nitroalkanes

As described in Chapter 3, the cross-dehydrogenative coupling is a powerful tool for the construction of new C-C bonds through the activation of two different C-H bonds. The CDC between *N*-aryl-1,2,3,4-tetrahydroisoquinolines and nitroalkanes was first described by Li and co-workers using copper(I) bromide as catalyst under oxidant conditions (Scheme 50).[160]
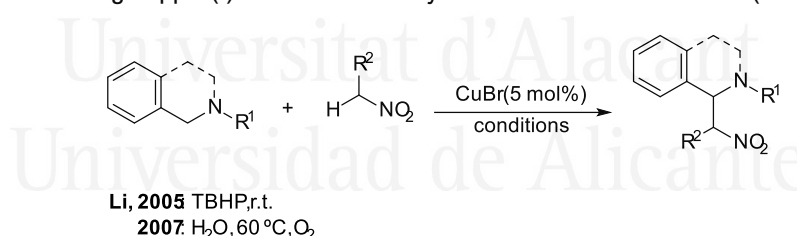
Scheme 50. CDC of benzylic amines and nitroalkanes reported by Li's group.

Since the first report on this transformation, a plethora of studies related to the CDC of THIQs and nitroalkanes was published. In them, parameters such as the activation mode (thermal, photochemical or electrochemical), catalyst type (organic or metallic) and external oxidant used were assessed for the formation of the corresponding 1-(nitroalkyl)-2-aryl-

---

[159] Reviews: Noble, A.; Anderson, J. C. *Chem. Rev.* **2013**, *113*, 2887-2939.

[160] (a) Li, Z.; Li, C.-J. *J. Am. Chem. Soc.* **2005**, *127*, 3672-3673. (b) Baslé, O.; Li, C.-J. *Green Chem.* **2007**, *9*, 1047-1050.

1,2,3,4-tetrahydroisoquinolines (Scheme 51).[125g,161] In general, this transformation requires the use of a huge excess of the nitrocompound which, in turn, acts as the solvent.[162]
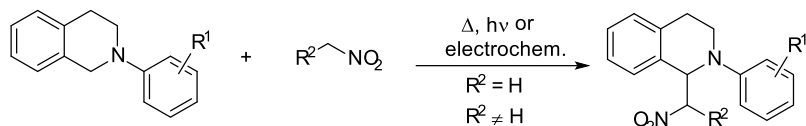
Scheme 51. Common CDC reaction of THIQs and nitroalkanes.

Related with this transformation, more than one hundred articles were published during the last sixteen years, with only one of them describing an outcome different to the formation of the corresponding *β*-nitroamine. In 2015, Rusch *et al.* reported the formation of 12-nitro-5,6-dihydroindolo[2,1-*a*]isoquinolines through the CDC of THIQs and nitroalkanes, photocatalysed by donor-substituted anthraquinones in the presence of stoichiometric amounts of a base, under an air atmosphere (Scheme 52).[163] Under the optimal conditions, 12-nitro-5,6-dihydroindolo[2,1-*a*]isoquinolines were obtained in poor-to-moderate yields (19-53%), together with small amounts (10-30%) of the corresponding 2-aryl-3,4-dihydroisoquinolin-1(2*H*)-ones and traces (<10%) of 5,6-dihydroindolo[2,1-*a*]isoquinolines.

[161] For leading and selected references, see: (a) Tsang, A. S.-K.; Todd, M. H. *Tetrahedron Lett.* **2009**, *50*, 1199-1202. (b) Yu, A.; Gu, Z.; Chen, D.; He, W.; Tan, P.; Xiang, J. *Catal. Commun.* **2009**, *11*, 162-166. (c) Su, X.-Z.; Xia, X.-F.; Yang, Y.-F.; Ji, K.-G.; Liu, X.-Y.; Liang, Y. M. *J. Org. Chem.* **2009**, *74*, 7464-7469. (d) Baslé, O.; Borduas, N.; Dubois, P.; Chapuzet, J. M.; Chan, T.-H.; Lessard, J.; Li, C.-J. *Chem. Eur. J.* **2010**, *16*, 8162-8166. (e) Condie, A. G.; González-Gómez, J. C.; Stephenson, C. R. J. *J. Am. Chem. Soc.* **2010**, *132*, 1464-1465. (f) Shu, X.-Z.; Yang, Y.-F.; Xia, X.-F.; Ji, K.-G.; Liu, X.-Y.; Liang, Y.-M. *Org. Biomol. Chem.* **2010**, *8*, 4077-4079. (g) Xie, Z.; Wang, C.; de Krafft, K. E.; Lin, W. *J. Am. Chem. Soc.* **2011**, *133*, 2056-2059. (h) Xie, J.; Li, H.; Zhou, J.; Cheng, Y.; Zhu, C. A. *Angew. Chem. Int. Ed.* **2012**, *51*, 1252-1255. (i) Rueping, M.; Zoller, J.; Fabry, D. C.; Poscharny, K.; Koenigs, R. M.; Weirich, T. E.; Mayer, J. *Chem. Eur. J.* **2012**, *18*, 3478-3481. (j) Ratnikov, M. O.; Xu, X.; Doyle, M. P. *J. Am. Chem. Soc.* **2013**, *135*, 9475-9479. (k) Ortiz Villamizar, M. C.; Galvin C. E. P.; Kouznetsov, V. V. in *Heterocycles via Cross Dehydrogenative Coupling*; Srivastava, A.; Jana, C. Eds.; Springer: Singapore, 2019; pp. 77-105. (i) Wen, X.; Duan, Z.; Liu, J.; Lu, W.; Lu, X. *Org. Lett.* **2020**, *22*, 5721-5725.

[162] See, for instance, the following recent reports: (a) Wang, J.; Ma, J.; Li, X.; Li, Y.; Zhang, G.; Zhang, F.; Fan, X. *Chem. Commun.* **2014**, *50*, 14237-14240. (b) Yang, X.-L.; Zou, C.; He, Y.; Zhao, M.; Chen, B.; Xiang, S.; O'Keeffe, M.; Wu, C.-D. *Chem. Eur. J.* **2014**, *20*, 1447-1452. (c) Wang, B.; Prakash Shelar, D.; Han, X.-Z.; Li, T.-T.; Guan, X.; Lu, W.; Liu, K.; Chen, Y.; Fu, W. F.; Che, C. M. *Chem. Eur. J.* **2015**, *21*, 1184-1190. (d) Wang, X.-Z.; Meng, Q.-Y.; Zhong, J. J.; Gao, X.-W.; Lei, T.; Zhao, L.-M.; Li, Z.-J.; Chen, B.; Tung, C. H.; Wu, L. Z. *Chem. Commun.* **2015**, *51*, 11256-11259. (e) Zhang, W.-Q.; Li, Q.-Y.; Zhang, Q.; Lu, Y.; Lu, H.; Wang, W.; Zhao, X.; Wang, X.-J. *Inorg. Chem.* **2016**, *55*, 1005-1007. (f) Yang, W.; Wei, L.; Yan, T.; Cai, M. *Catal. Sci. Technol.* **2017**, *7*, 1744-1755. (g) Liu, W.; Su, Q.; Ju, P.; Guo, B.; Zhou, H.; Li, G.; Wu, Q. *ChemSusChem* **2017**, *10*, 664-669.

[163] Rusch, F.; Unkel, L. N.; Alpers, D.; Hoffmann, F.; Brasholz, M. *Chem. Eur. J.* **2015**, *21*, 8336-8340.
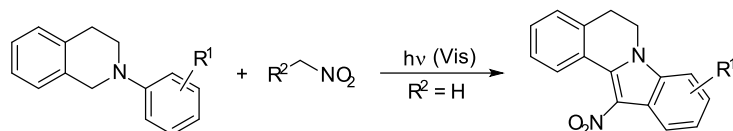
Scheme 52. Synthesis of 12-nitroindoloisoquinolines by Brasholz's group through a photocatalytic CDC/dehydrogenation/6π-cyclisation/oxidation cascade.

Based on this background and keeping in mind the principles of green chemistry, it can be said that the development of new environmentally friendly and economically affordable protocols for the synthesis of 5,6-dihydroindolo[2,1-*a*]isoquinolines is of a great interest.

4.2. Objectives

As a part of our fascination on the catalytic activity of supported CuNPs and based on the previous background, the following aims were set:

- o To study the catalytic activity of supported CuNPs in the CDC between tetrahydroisoquinolines and nitroalkanes.
- o To determine the optimal conditions and the scope of the reaction.
- o To study the recyclability of the catalyst.
- o To compare the catalytic activity of our catalyst with that of commercially available catalysts.
- o To study the reaction mechanism.

4.3. Results and discussion
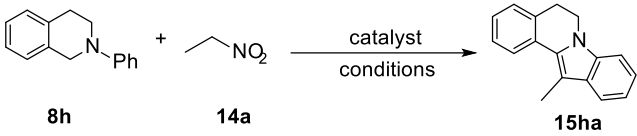
4.3.1. Optimisation of the catalytic system and reaction conditions

First, the catalyst support, solvent, temperature and atmosphere were optimised for the CDC model reaction of *N*-phenyl-1,2,3,4-tetrahydroisoquinoline (**8h**) and nitroethane (**14a**), obtaining the results summarised in Table 28. It is noteworthy that, contrary to what widely reported in the literature, 12-methyl-5,6-dihydroindolo[2,1-*a*]isoquinoline (**15ha**) was formed, instead of 1-(1-nitroethyl)-2-phenyl-1,2,3,4-tetrahydroisoquinoline.

In order to confirm that this coupling does actually require a metal catalyst, several control experiments were carried out, without observing the formation of the final product in any case (Table 28, entries 1 and 9). Then, different metals and supports were screened (Table 28, entries 2-8), obtaining the best performance with copper as a metal and TiO_2 as a support (Table 28, entry 8). Then, an array of different solvents was tested, with the best results being achieved under neat conditions (Table 28, entries 8 and 10-17). The catalyst loading was also varied, finding 1.5 mol% to be the optimal amount (Table 28, entries 8 and 18-21). The conversion was notably lower under microwave (MW) radiation (Table 28, entry 24), whereas light exposure did not affect the reaction (Table 28, entry 25). The temperature and atmosphere of the reaction were also optimised, being 70 ºC under air the best conditions (Table 28, entries 8 and 25-27).

Taking all these results in hand, the optimal conditions were considered to be 1.5 mol% of $CuNPs/TiO_2$ as catalyst under neat conditions, under an air atmosphere at 70 ºC and with an excess of the corresponding nitroalkane (2.4 equiv.) (Table 28, entry 8).

Table 28. Optimisation of the catalyst and conditions in the reaction of **8h** and **14a**.[a]

Entry	Catalysts (mol%)[b]	Solvent	T (ºC)	15ha (%)[c]
1	-	-	70	0
2	CuNPs/ZY	-	70	52
3	CuNPs/MK-10	-	70	43
4	CuNPs/C	-	70	32
5	CuNPs/CeO$_2$	-	70	31
6	CoNPs/ZY	-	70	24
7	MnNPs/TiO$_2$	-	70	8
8	**CuNPs/TiO$_2$**	**-**	**70**	**>99**
9	TiO$_2$	-	70	0
10	CuNPs/TiO$_2$	H$_2$O	70	17
11	CuNPs/TiO$_2$	MeOH	70	10
12	CuNPs/TiO$_2$	i-PrOH	70	39
13	CuNPs/TiO$_2$	DMF	70	85
14	CuNPs/TiO$_2$	CH$_3$CN	70	37
15	CuNPs/TiO$_2$	DMSO	70	71
16	CuNPs/TiO$_2$	PhMe	70	6
17	CuNPs/TiO$_2$	DCE	70	8
18	CuNPs/TiO$_2$ (0.15)	-	70	21
19	CuNPs/TiO$_2$ (0.38)	-	70	52
20	CuNPs/TiO$_2$ (0.75)	-	70	53
21	CuNPs/TiO$_2$ (2.25)	-	70	76
22	CuNPs/TiO$_2$	-	rt	3
23	CuNPs/TiO$_2$	-	100	71
24	CuNPs/TiO$_2$	-	70[d]	2
25	CuNPs/TiO$_2$	-	70[e]	93
26	CuNPs/TiO$_2$	-	70[f]	78
27	CuNPs/TiO$_2$	-	70[g]	80

[a] **8h** (0.1 mmol), **14a** (2.4 equiv.), catalyst, overnight, air. [b] Catalyst loading: 1.5 mol%, unless otherwise stated. [c] Conversion determined by GLC. [d] MW (100 W), 1 h. [e] Reaction protected from light. [f] Under an O$_2$ atmosphere. [g] Under an Ar atmosphere.

4.3.2. Scope

A collection of *N*-aryl-1,2,3,4-tetrahydroisoquinolines, of different electronic nature, was tested in the CDC with nitroethane (**14a**) under the optimal conditions. The dihydroindoloisoquinoline **15ha**, derived from the standard unsubstituted *N*-phenyltetrahydroisoquinoline, was obtained in almost quantitative yield (Table 29, entry 1). THIQs with substituents at the *para* position of the *N*-aryl ring were also tested, giving the corresponding products in moderate-to-good yields (Table 29, entries 2-4). Generally, the presence of electron-withdrawing groups led to lower yields, in direct relation with their ability to delocalise the negative charge, with this effect being dramatic in the case of the nitro group (Table 29, entries 5-7); excellent yield was obtained for fluorine (**15sa**, Table 29, entry 8).

On the other hand, the effect of the steric hindrance in the reaction outcome was evaluated employing 3,5-disubstituted *N*-aryl THIQs (Table 29, entries 9 and 10), recording poor-to-moderate yields of the products. These results could be explained by the non-bonding repulsive *peri*-type effect between the methyl group and the corresponding THIQs substituents.

The regioselectivity of the process was evaluated with *N*-(3,4-dimethylphenyl) and *N*-(3,4-dimethoxyphenyl) THIQs, observing a regioisomeric mixture (1:1) for the methyl-substituted substrate (Table 29, entry 11), whereas only one regioisomer was obtained with its methoxy-substituted homologue (Table 29, entry 12). These results suggest that the regiochemistry of the process could be controlled by means of the stetic demand of the substituents. Due to the importance of methoxy groups in the bioactivity of dihydroindoloisoquinolines (Figure 42), we attempted to apply our method to the synthesis of 2,3-dimethoxy-12-methyl-5,6-dihydroindolo[2,1-*a*]isoquinoline (**15xa**), which was obtained in good yield after 36 h of reaction (Table 29, entry 13). Finally, moderate-to-good yields were obtained with other nitroalkanes, albeit by increasing the temperature to 100 ºC (Table 29, entries 14-15).

Table 29. CDC of 1,2,3,4-tetrahydroisoquinolines and nitroalkanes catalysed by CuNPs/TiO$_2$.[a]

Entry	8	14	15	Yield (%)[b]
1	8h	14a	15ha	98
2	8m	14a	15ma	72
3	8n	14a	15na	72
4	8o	14a	15oa	62
5	8p	14a	15pa	70
6	8q	14a	15qa	57[c]
7	8r	14a	15ra	0

Table 29. CDC of 1,2,3,4-tetrahydroisoquinolines and nitroalkanes catalysed by CuNPs/TiO$_2$ (cont.).[a]
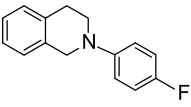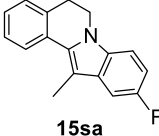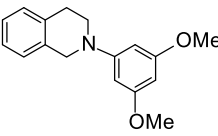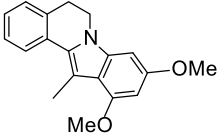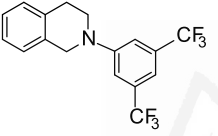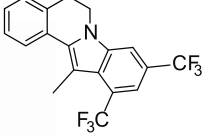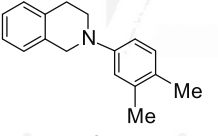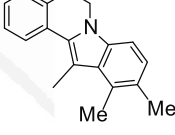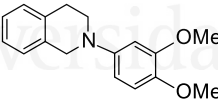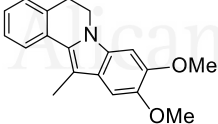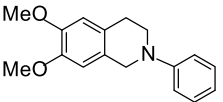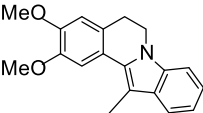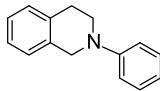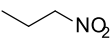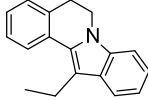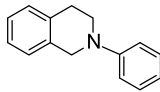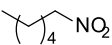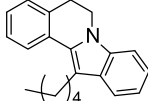
8	**8s**	**14a**	**15sa**	90
9	**8t**	**14a**	**15ta**	43[c]
10	**8u**	**14a**	**15ua**	36[d]
11	**8v**	**14a**	**15va** **15va'**	64[e]
12	**8w**	**14a**	**15wa**	91[f]
13	**8x**	**14a**	**15xa**	66[g]

Table 29. CDC of 1,2,3,4-tetrahydroisoquinolines and nitroalkanes catalysed by CuNPs/TiO$_2$ (cont.).[a]

14	**8h**	**14b**	**15hb**	86[h]
15	**8h**	**14c**	**15hc**	63[h]

[a] **8h** (0.5 mmol), **14a** (2.4 equiv.), CuNPs/TiO$_2$ (1.5 mol%), neat, 70 ºC, overnight, air. [b] Isolated yields. [c] ^{1}H NMR yield. [d] 30 h. [e] As an approximately 1:1 regioisomeric mixture. [f] 10 equiv. of EtNO$_2$. [g] 36 h. [h] Reaction at 100 ºC.

4.3.3. Catalyst recyclability and nature of the catalysis

CuNPs/TiO$_2$ showed an easy manipulation without the requirement of an inert atmosphere. As an additional benefit, the catalyst could be recovered by centrifugation. Unluckily, while the catalyst could be efficiently recovered, the maximum conversion achieved in a second run dropped to around 50%. In order to understand this behaviour, XPS experiments were carried out, revealing the presence of adsorbed nitrogen-containing molecules on the catalyst surface after the first run (Figure 43). Probably, these species act as catalyst poisoning agents, causing the passivation of its surface.

On the other hand, the XPS experiment on CuNPs/TiO$_2$ at the Cu 2$p_{3/2}$ level shows a substantial decrease in the Cu(I) content after the first run [compare Figure 8 (p. 55) and Figure 44] and only Cu(II) species were observed on the inactive catalyst surface (Figure 45).
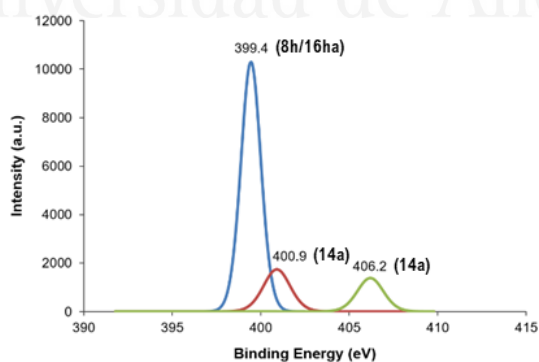
Figure 43. XPS analysis of CuNPs/TiO$_2$ (N 1s level) after the first run.
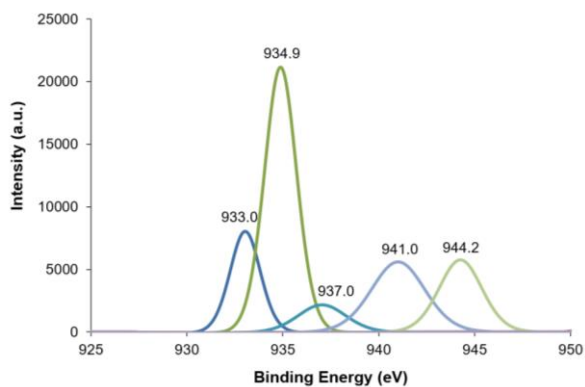
Figure 44. XPS analysis of CuNPs/TiO$_2$ (Cu 2$p_{3/2}$ level) after the first run.
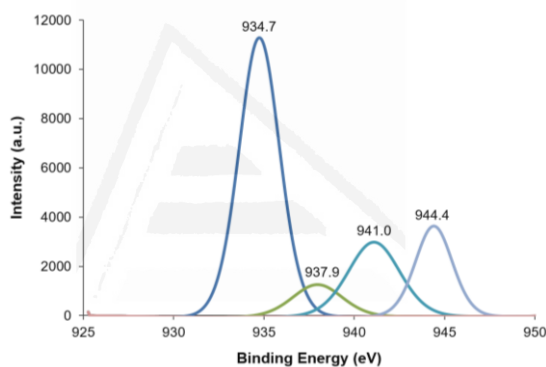
Figure 45. XPS analysis of inactive CuNPs/TiO$_2$ (Cu 2$p_{3/2}$ level).

Hence, the presence of adsorbed nitrogen species on the catalyst surface coupled with the ineffective regeneration of Cu(I) species, could be the reason behind the decrease in the catalytic activity of the recycled system.

Some control experiments were carried out in order to demonstrate the heterogeneous nature of our catalyst. [9a] The standard reaction was performed in presence of the various metal-poisoning agents under the optimal conditions, with the outcome summarised in Table 30.

Table 30. Poisoning tests.[a]
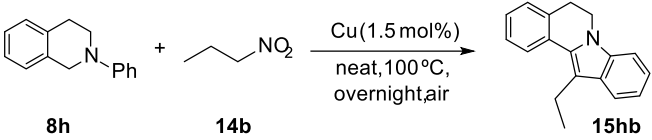
Entry	Additive[b]	Conversion (%)[c] 15ha
1	CS$_2$ (0.25 equiv.)	39
2	PPh$_3$ (0.25 equiv.)	0
3	Hg(0) (10 equiv.)	19

[a] **8h** (0.1 mmol), **14a** (2.4 equiv.), CuNPs/TiO$_2$ (1.5 mol%), additive, neat, 100 ºC, overnight, air. [c] Determined by GLC.

The above results point to a heterogeneous nature of our catalyst. Nonetheless, a hot filtration test was also carried out. For this experiment, the CDC reaction between *N*-phenyl-1,2,3,4-tetrahydroisoquinoline (**8h**) and nitroethane (**14a**) was performed under the optimal conditions. After 5 h, a sample of the reaction was analysed, observing a conversion of 30% for the synthesis of **15ha**. The catalyst was then removed from the reaction medium, while the filtrate remained under additional heating for 10 h. The small conversion increase recorded (to only 40%) might be probably due to the action of 6 wt% of leached copper found in the filtrate by ICP-MS. However, the Cu leaching cannot explain the quantitative conversion attained by the catalyst. That is why these experiments confirm the primarily heterogeneous nature of CuNPs/TiO$_2$.

4.3.4. Comparison with other commercial Cu catalysts

The catalytic activity of CuNPs/TiO$_2$ in the CDC between *N*-phenyl-1,2,3,4-tetrahydroisoquinoline (**8h**) and nitropropane (**14b**) was compared with that of an array of commercial copper catalysts (Table 31). Among them, CuCl gave the best results with 33% conversion into **15hb**. This is not even near the 86% conversion achieved with our system under the same conditions (Table 31, entry 15). Our catalyst was more selective and far more effective than any commercial copper catalyst tested, demonstrating the key role of its nanostructure.

Table 31. Comparison with commercial Cu catalysts.[a]

Entry	Catalyst	Conversion (%)[b]
1	Cu(0)	<5
2	Cu_2O	<5
3	CuO	<5
4	CuCl	33
5	$CuCl_2$	20
6	CuBr	<5
7	$CuBr_2$	19
8	CuI	19
9	CuOAc	<5
10	$Cu(OAc)_2$	<5
11	CuOTf	<5
12	$Cu(OTf)_2$	<5
13	$CuBr·SMe_2$	12
14	$CuNO_3·2.5H_2O$	19
15	**$CuNPs/TiO_2$**	**86[c]**

[a] **8h** (0.1 mmol), **14b** (2.4 equiv.), Cu (1.5 mol%), neat, 100 ºC, overnight, air.
[b] Conversion determined by GLC. [c] Isolated yield based on **8h**.

4.3.5. Mechanism

Considering the unpredictable behaviour of our catalytic system in the CDC between THIQs and nitroalkanes, we felt obliged to gain a comprehensive insight into the reaction mechanism. In this sense, control experiments with radical scavengers were performed in order to demonstrate the presence of radicals in the reaction medium (Table 32). The decrease in the conversion experienced when using radical traps suggests a radical mechanism. The presence of the radical promoter AIBN, however, led to the expected product in moderate conversion (Table 32, entry 4).

Table 32. Experiments with radical traps and AIBN.[a]

Entry	Additive[b]	Conversion (%)[c] 15ha
1	TEMPO	0[d]
2	norbornene	12
3	2,6-di-*tert*-butylphenol	0
4	AIBN	65
5	activated C[e]	15

[a] **8h** (0.1 mmol), **14a** (2.4 equiv.), CuNPs/TiO$_2$ (1.5 mol%), additive, neat, 100 ºC, overnight, air. [b] Additive loading: 0.1 equiv., unless otherwise stated. [c] Conversion determined by GLC. [d] 2-Phenyl-3,4-dihydroisoquinolin-1(2*H*)-one was quantitatively formed. [e] 10 mg.

In order to isolate the reaction intermediate, the optimal conditions were applied to *N*-pentasubstituted and bulky *N*-substituted THIQs. Due to the difficulty (**8z**) and impossibility (**8y**) for the cyclisation step to take place in these THIQs, the corresponding CDC adducts **16** were successfully isolated (Scheme 53).

As a final experiment, intermediate **16ha** was treated with nitroethane (**14a,** 1.4 equiv. added to facilitate stirring) in the presence of CuNPs/TiO$_2$, leading to the formation of the dihydroindoloisoquinoline **15ha** in excellent yield (93%, Scheme 53).

These results verified that the corresponding *β*-nitroamines (**16**) are indeed the precursors of the final 5,6-dihydroindolo[2,1-*a*]isoquinolines (**15**) and the unprecedented role of CuNPs in promoting a Friedel-Crafts type reaction in which the NO$_2$ group acts as leaving group.
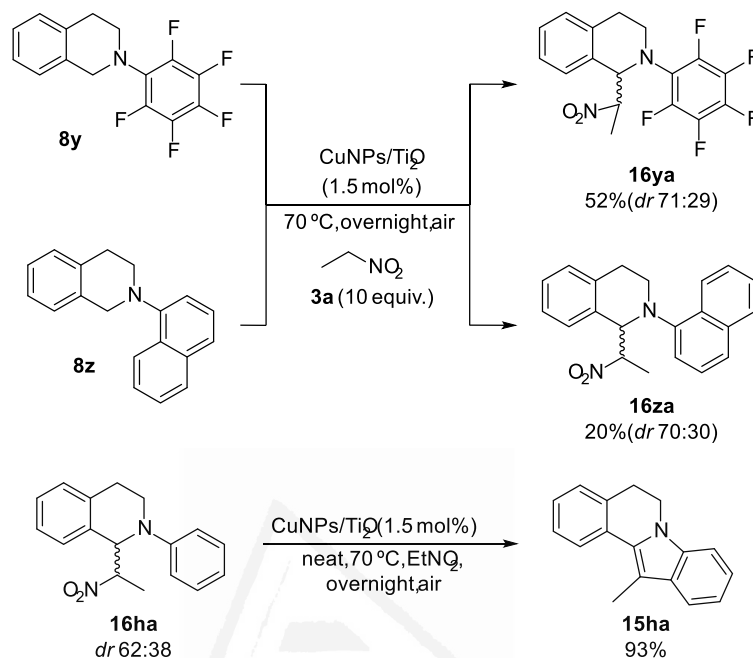
Scheme 53. Experiments designed to unveil the reaction pathway.

In addition, some XPS experiments were carried out in order to determine the pathway of this transformation. To evaluate the interaction between the different species and the catalyst, the Cu $2p_{3/2}$ and N $1s$ levels of CuNPs/TiO$_2$ impregnated with nitroethane (**14a,** Figure 47), *N*-phenyl-1,2,3,4-tetrahydroisoquinoline (**8h,** Figure 48) and 12-methyl-5,6-dihydroindolo[2,1-*a*]isoquinoline (**15ha,** Figure 49) were analysed. The XPS spectra at the Cu $2p_{3/2}$ level of fresh CuNPs/TiO$_2$ and N $1s$ level of TiO$_2$ impregnated with nitroethane (**14a**) were used as reference spectra (Figure 46).
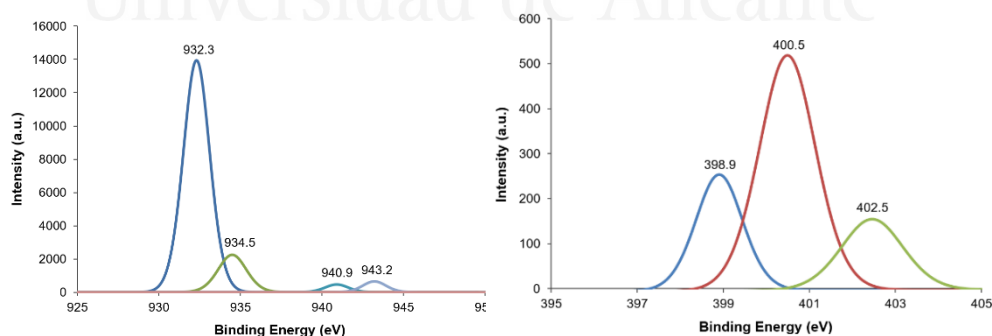
Figure 46. XPS spectra at the Cu $2p_{3/2}$ level of fresh CuNPs/TiO$_2$ (left) and N $1s$ level of TiO$_2$ impregnated with nitroethane (**14a**) (right).
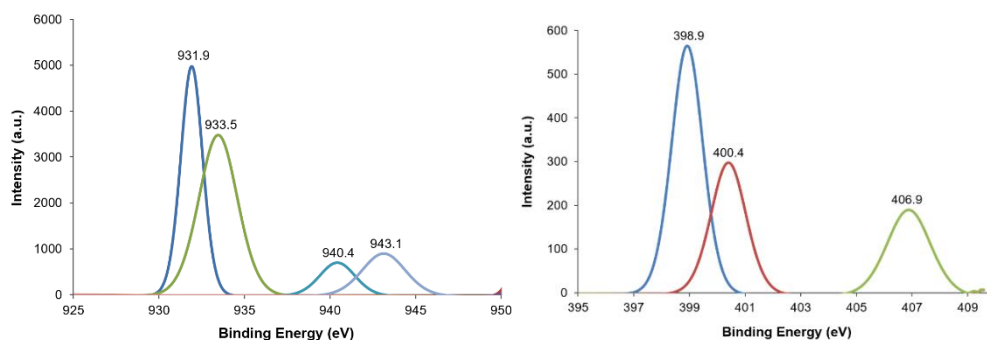
Figure 47. XPS spectra at the Cu $2p_{3/2}$ level (left) and N $1s$ level (right) of CuNPs/TiO$_2$ impregnated with nitroethane **14a**.
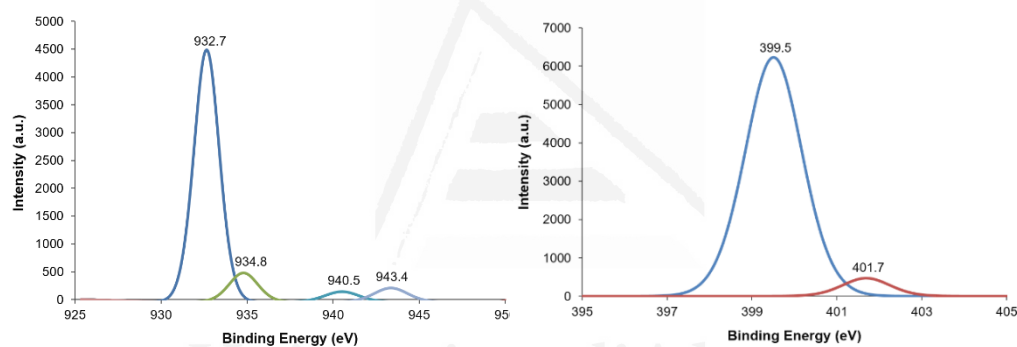
Figure 48. XPS spectra at the Cu $2p_{3/2}$ level (left) and N $1s$ level (right) of CuNPs/TiO$_2$ impregnated with THIQ **8h**.
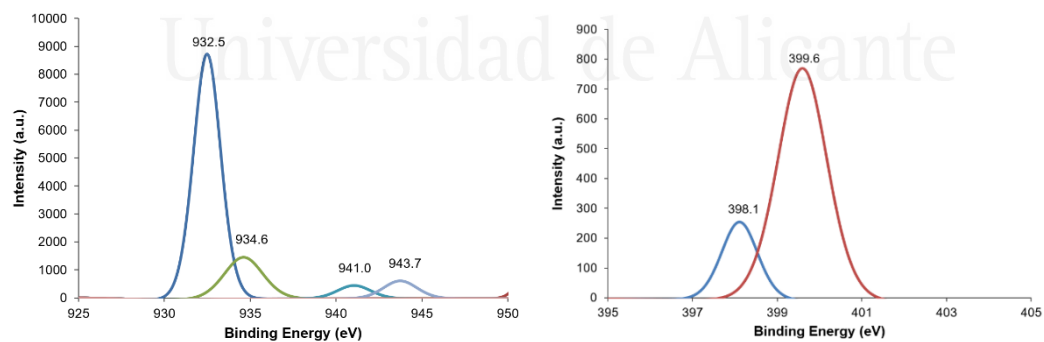
Figure 49. XPS spectra at the Cu $2p_{3/2}$ level (left) and N $1s$ level (right) of CuNPs/TiO$_2$ impregnated with 12-methyl-5,6-dihydroindolo[2,1-*a*]isoquinoline (**15ha**).

The XPS spectrum at the Cu $2p_{3/2}$ level of CuNPs/TiO$_2$ impregnated with nitroethane suggests a strong interaction of the CuNPs with the nitro group [Figures 46 (left) and 47 (left)]. When comparing the spectrum of the fresh catalyst with that of the impregnated one, a shift to lower binding energies was observed in the latter [from 932.3 to 931.9 eV for Cu(I) and from 934.5 to 933.5 eV for Cu(II)]. Moreover, the nitro group seems to oxidise the present Cu(I) species, as the intensity of the Cu(II) band increases significantly [compare Figures 46 (left) and 47(left)]. On the other hand, CuNPs/TiO$_2$ impregnated with THIQ **8h** [Figure 48 (left)] and 12-methyl-5,6-dihydroindolo[2,1-*a*]isoquinoline [**15ha**, Figure 49 (left)] suffered no alteration at all in its Cu $2p_{3/2}$ spectra [compare Figure 46 (left) with Figures 48 (left) and 49 (left)].

As regards the XPS spectra at the N 1*s* level, the presence of interactions between the nitrogen-containing molecules and both, support [Figure 46 (right)] and CuNPs, was confirmed [Figures 47 (right), 48 (right) and 49 (right)]. Once again, nitroethane and CuNPs showed the strongest interaction, shifting the binding energy of neat TiO$_2$ from 402.eV [Figure 46 (right)] to 406.9 eV [Figure 47 (right)].

Considering these results, it can be concluded that the nitro group oxidises Cu$_2$ONPs to CuONPs, inhibiting the catalytic activity of our system upon reuse, because Cu$_2$ONPs cannot be sufficiently regenerated; in addition, other nitrogen-containing molecules (**8h** and **15ha**) can act as surface poisoning agents, also affecting the catalytic activity.

A mechanism pathway was proposed based on the previously mentioned experiments. First, Cu$_2$ONPs reduce the nitro group through a SET, followed by hydrogen abstraction, generating CuONPs and the corresponding nitronate anion. At the same time, CuONPs oxidise the THIQ to form a radical cation. Then, the TiO$_2$ lattice oxygen generates the counterpart cation (iminium ion) through hydrogen abstraction. The next step is the addition of the nitronate anion to the corresponding iminium ion to form the CDC adduct (*β*-nitroamine). This intermediate undergoes an intramolecular cyclisation through a Friedel-Crafts type reaction, liberating nitrous acid which, under the reaction conditions, decomposes into NO$_2$ and NO. The deep red colour of the reaction medium and negligible amount of nitrites and nitrates observed by ionic chromatography (20 and 55 ng, respectively) allow to discard the presence of nitrogen salts in that medium. Finally, the re-aromatisation of the tetrahydro-5*H*-indolo[2,1-*a*]isoquinolon-7-ium ion and the final oxidation of this intermediate, mediated by the action of CuONPs, gives the corresponding dihydroindoloisoquinolines.

In addition, this reaction mechanism explains the lack of reactivity of the nitro substituted THIQ **15ra**; the lone electron pair on nitrogen may take part in a resonant structure in which

the negative charge is strongly stabilised by the nitro group and inaccessible to promote the intramolecular reaction.
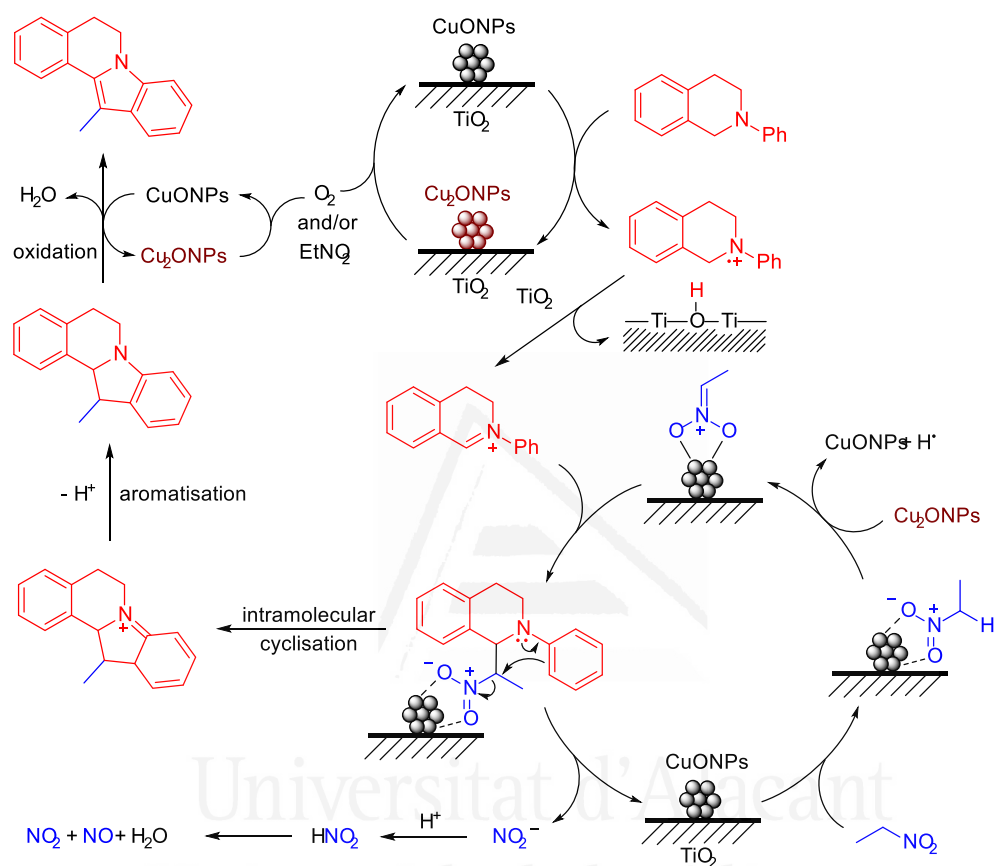
Scheme 54. Reaction mechanism proposed for the synthesis of dihydroindoloisoquinolines through the CDC of tetrahydroisoquinolines and nitroalkanes catalysed by CuNPs/TiO$_2$.

4.3.6. Late-stage functionalisation

Nowadays, unconventional disconnections, C-H activations and late-stage functionalisation have been attracting a great deal of attention in organic synthesis.[164] In this sense, the functionalisation of 12-methyl-5,6-dihydroindolo[2,1-*a*]isoquinolines was studied. Due to the apparent importance of the carbaldehyde moiety in the bioactivity of the THIQs (**13d** and **13f**, Figure 42, p. 143), we resolved to perform the oxidation of the methyl group attached to the dihydroindoloisoquinoline skeleton.

Several oxidasing systems were tested for this purpose, such as MnO_2, Mn_3O_4, I_2, $CuBr \cdot SMe_2$/DABCO/O_2, DDQ and CuCl/TEMPO. The best results were obtained using MnO_2 (3 equiv.) at 110 ºC, achieving quantitative conversion into **15ha** in 1.5 h (Scheme 55). Although a thorough optimisation of this reaction was not studied, we observed that a good conversion could be attained using 10 mol% MnO_2 instead of an excess.
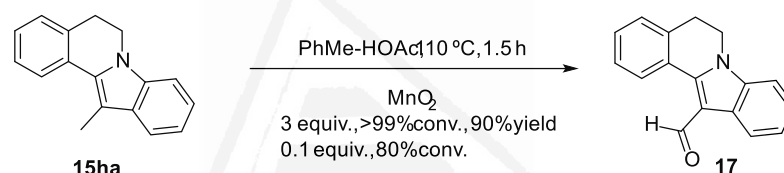
Scheme 55. Oxidation of **15ha** to **17**.

---

[164] Perspective: Blackmore, D. C.; Castro, L.; Churcher, I.; Rees, D. C.; Thomas, A. W.; Wilson, D. M.; Wood, A. *Nat. Chem.* **2018**, *10*, 383-394.

4.4. Conclusions

As a summary, a domino CDC-cyclisation reaction between THIQs and nitroalkanes has been discovered, enabling the direct formation of dihydroindoloisoquinolines instead of the typical β-nitroamines. This process allows the formation of two C-C bonds from three C-H bonds in one step.

The synthesis of these compounds has been achieved employing CuNPs/TiO$_2$ under neat conditions at 70 or 100 ºC, avoiding the addition of both ligands and oxidants. THIQs of different electronic nature were tested, achieving moderate-to-excellent yields of the products.

Regarding the recyclability of the system, CuNPs/TiO$_2$ cannot be reused due to two main reasons: the oxidation of the catalytically active Cu(I) species to Cu(II) by the nitroalkane and the poisoning effect of nitrogen-containing species adsorbed on the surface of the catalyst.

Nevertheless, our catalyst has shown better results than the commercial ones while avoiding the formation of by-products at the same time, what demonstrates the crucial role of the nanostructured catalyst.

Based on control experiments, a plausible reaction mechanism has been proposed, which highlights the critical role of the nitroalkane in the Cu$_2$O and CuO redox couple.

This protocol uses a relatively cheap and easy-to-handle catalyst under mild and solventless conditions. These are great advantages over other existing methodologies that use expensive iridium catalysts, organic solvents and/or harsh conditions, factors that limit their scope.

Chapter 5. Dehydrogenation of amines employing heterogeneous photocatalysis

5.1. Antecedents

Introduction

Imines, also known as Schiff bases, are a remarkable group of nitrogen-containing molecules (Figure 50). These compounds are especially useful as building blocks, as intermediates in the synthesis of bioactive heterocyclic compounds and for the synthesis of fine chemicals.[165]

$R^1, R^3 = aryl\ or\ alkyl$
$R^2 = H, aryl\ or\ alkyl$
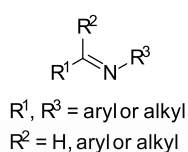
Figure 50. General structure of imines.

Concerning synthetic approaches for the preparation of imines, the following strategies are the most common ones: (a) the condensation reaction of carbonyl compounds and amines (Schiff's condensation);[166] (b) the oxidative dehydrogenation of alcohols in the presence of amines;[167] (c) the oxidative dehydrogenation of secondary amines;[167] and (d) the coupling of primary amines.[167,168] These transformations can be performed either *via* conventional catalysis[167] or photocatalysis.[169]

Among these methodologies, the coupling of primary amines is one of the most widely studied nowadays, employing different types of catalysts.[167,168] Despite the generally good performance ot these systems, some protocols contain rather expensive metals, stoichiometric amounts of chemical oxidants and most of them use thermal activation.

In this sense, our research group has developed a new catalytic system based on sulfur-stabilised copper nanoparticles, capable of performing this transformation under mild conditions (Scheme 56).[170] This system was tested for benzylamines, obtaining the imines in good-to-excellent yields, and proved to be superior to an array of commercially available copper catalysts. In addition, the catalyst was recycled twice without losing any catalytic

---

[165] Martin, S. F. *Pure Appl. Chem.* **2009**, *81*, 195-204.

[166] Schiff, H. *Ann. Chem.* **1864**, *131*, 118-119.

[167] Review: Chen, B.; Wang, L.; Gao, S. *ACS Catal.* **2015**, *5*, 5851-5876.

[168] Review: Largeron, M. *J. Org. Chem.* **2013**, 5225-5235.

[169] Review: Zhang, X.; Rakesh, K. P.; Ravindar, L.; Qin, H.-L. *Green Chem.* **2018**, *20*, 4790-4833.

[170] Díaz, G. *Oxidation of amines to imines catalysed by supported metal nanoparticles*; Master's report, University of Alicante, 2016.

activity. Further attempts to reuse the catalyst were, however, unsuccessful, probably due to surface poisoning phenomena. Nonetheless, the low metal loading employed (0.3 mol%) together with the superior activity when compared with commercial catalysts, makes CuNPs/S_8 an interesting alternative to noble metal-based catalysts for this oxidative coupling.

$R^1 = R^2 = H; R^3 = H, Me, MeO, CO_2Me, Cl, CF_3$
$R^1 = Me, Cl, Br; R^2 = R^3 = H$
$R^1 = H; R^2 = R^3 = MeO$
$R^1 = CF_3; R^2 = H; R^3 = F$

11 examples
40-97%
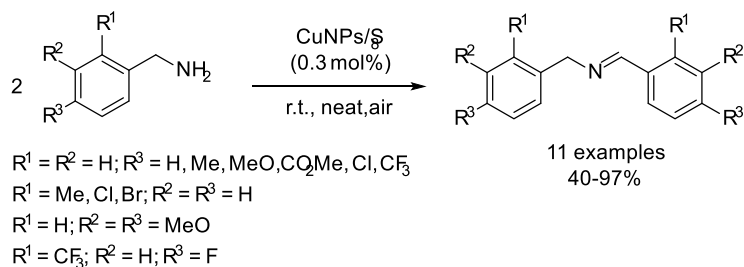
Scheme 56. Oxidation of amines to imines catalysed by CuNPs/S_8.

More recently, our research group decided to study the oxidation of secondary amines for the construction of bioactive cyclic imines.[171,172] Amid the diversity of cyclic amines, 1,2,3,4-tetrahydroisoquinolines (THIQs) attracted our attention because are considered privileged structures in drug discovery, with several therapeutic applications.[173]

For example, THIQs were found to be active in cardiovascular, central nervous system, infectious, inflammatory, metabolic and oncology diseases, among others. Some marketed drugs which contain the THIQ scaffold (Figure 51) are: Accupril™, used to treat hypertension;[174] Vesicare™, which is a muscarinic receptor antagonist effective against

[171] Vilariño, N.; Ferreiro, S. F.; Crespo, A.; Gil, J. in *Phycotoxins: Chemistry and Biochemistry, 2nd Edn;* Botana, L. M.; Alfonso, A. Eds.; Jonh Wiley & Sons: Chichester (UK), 2015; pp. 343-360.

[172] Reviews: (a) Otero, A.; Chapela, M.-J.; Atanassova, M.; Vieites, J. M.; Cabado, A. G. *Chem. Res. Toxicol.* **2011**, *24*, 1817-1829. (b) Davidson, K.; Baker, C.; Higgins, C.; Higman, W.; Swan, S.; Veszelovszki, A.; Turner, A. D. *Mar. Drugs* **2015**, *13*, 7087-7112. (c) Molgó, J.; Marchot, P.; Aráoz, R.; Benoit, E.; Iorga, B. I.; Zakarian, A.; Taylor, P.; Bourne, Y.; Servent, D. *J. Neurochem.* **2017**, *142*, 41-51. (d) Saha, D.; Bagchi, S.; Sharma, A. *J. Heterocycl. Commun.* **2018**, *54*, 302-313. (e) Iwanejko, J.; Wojaczyńska, E. *Org. Biomol. Chem.* **2018**, *16*, 7296-7314.

[173] Yet, L. *Privileged Structures in Drug Discovery: Medicinal Chemistry and Synthesis, 1st Edn.;* John Wiley & Sons: Hoboken (NJ), 2018; pp. 356-413.

[174] Klutchlo, S.; Blanklet, C. J.; Fleming, R. W.; Hinkley, J. M.; Werner, A. E.; Nordin, I.; Holmes, A.; Hoefle, M. L.; Cohen, D. M.; Essenburg, A. D.; Kaplan, H. R. *J. Med. Chem.* **1986**, *26*, 1953-1961.

overactive bladder disorders;[175] Merital/Alival[TM] prescribed as antidepressant;[176] Yondelis[TM], a chemotherapeutic agent against soft-tissue sarcoma and ovarian cancer;[177] and Xiidra[TM], used for the treatment of dry-eye syndrome.[178]

quinapril
Accupril[TM]

solifenacin
Vesicare[TM]

nomifensine
Merital/Alival[TM]

trabectedim
Yondelis[TM]

lifitegrast
Xiidra[TM]
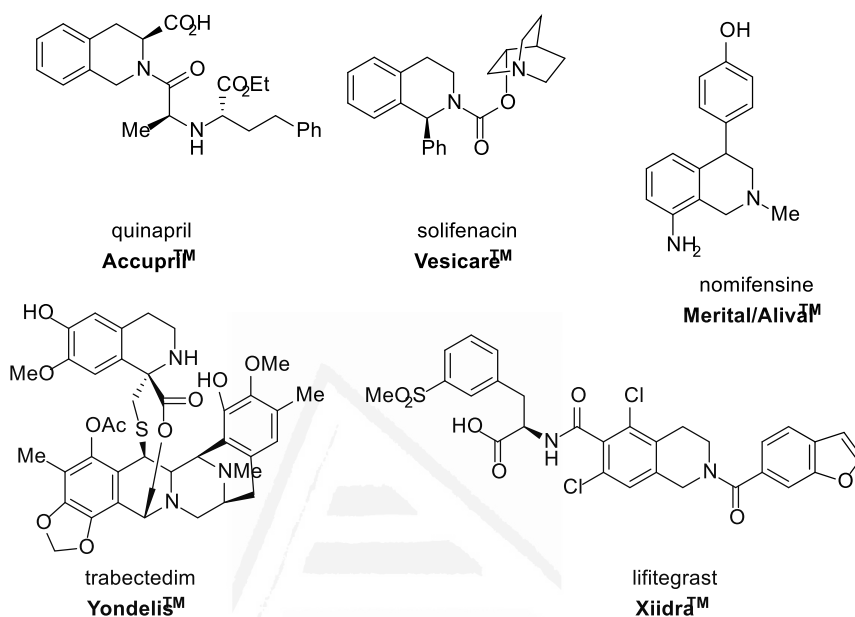
Figure 51. Drugs containing the THIQ scaffold.

Taking this background into consideration, our research group decided to study (a) the dehydrogenative oxidation of 1,2,3,4-tetrahydroisoquinolines, (b) the potential application of the resulting dihydroisoquinolines in medicinal chemistry (as some of them, such as ancistrocladidine, depicted in Figure 52, show remarkable bioactivity),[172e] and (c) their role as intermediates in the functionalisation of THIQs, as they are able to undergo several types of interesting reactions through the iminic double bond (Scheme 57) [172e,179]

[175] (a) Uchida, T.; Krauwinkel, W. J.; Mulder, H.; Smulders, R. *Br. J. Clin. Pharmacol.* **1996**, *4*, 877-885. (b) Mitch, C. H.; Brown, T. J.; Bymaster, F. P.; Calligaro, D. O.; Dieckman, D.; Merrit, L.; Peters, S. C.; Quimby, S. J.; Shannon, H. E.; Shipley, L. A.; Ward, J. S.; Hansen, K.; Olesen P. H.; Sauerberg, P.; Sheardown, M. J.; Swedberg, M. D.; Sizdak, P.; Greenwooed, B. *J. Med. Chem.* **1997**, *40*, 538-546. (c) Robinson, D.; Cardozo, L. *Expert Opin. Investig. Drugs* **2004**, *12*, 1339-1348. (d) Smulders, R.; Krauwinkel, W. J.; Swart, P. J.; Huang, M. *J. Clin. Pharmacol.* **2004**, *58*, 4-7.

[176] Brogden, R. N.; Heel, R. C.; Speight, T. M.; Avery G. S. *Drugs* **1979**, *18*, 1-24.

[177] Cassier, P. A.; Dufresne, A.; Blay, J.-Y.; Fayette, J. *Ther. Clin. Risk Manag.* **2008**, *4*, 109-116.

[178] (a) Semba, C. P.; Gadek, T. R. *Clin. Ophthalmol.* **2016**, *10*, 1083-1094. (b) Donnenfeld, E. D.; Karpecki, P. M.; Majmudar, P. A.; Kelly, K.; Raychaudhuri, A.; Roy, M.; Semba, C. P. *Cornea* **2016**, *35*, 741-748.

[179] Yang, L.; Zhu, J.; Sun, C.; Deng, Z. Qu, X. *Chem. Sci.* **2020**, *11*, 364-371.

ancistrocladidine
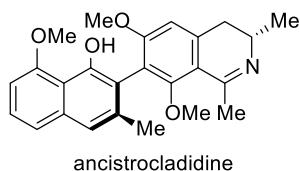
Figure 52. THIQ imine derivative with antimalarial activity.
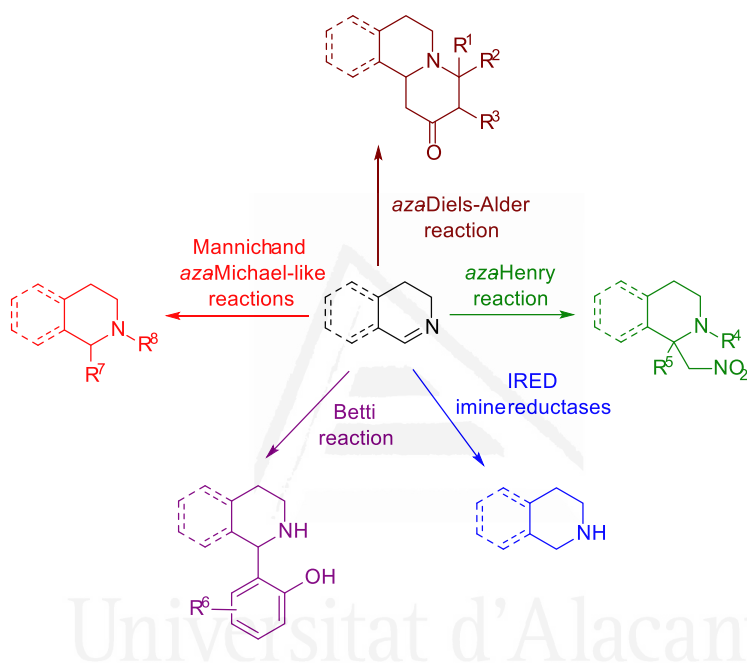
Scheme 57. Synthetic applications of imines derived from THIQs.

Due to the versatility of 3,4-dihydroisoquinolines (DHIQs), the development of new catalytic systems to promote the formation of these compounds has attracted a great deal of attention over the last few years.[180] Nonetheless, the photocatalytic approaches from tetrahydroisoquinolines (THIQs) have not been studied in depth.

5.1.1. Photocatalysis: oxidation of THIQs

As stated earlier, only a few examples were found in the literature related to the dehydrogenative oxidation of THIQs to DHIQs promoted by photocatalysis (Scheme 58).[181] In these works, photocatalytic systems based on tetraphenylporphyrin (H$_2$TPP) and singlet

---

[180] Review: Hati, S.; Holzgrade, U.; Sen, S. *Beilstein J. Org. Chem.* **2017**, *13*, 1670-1692.

oxygen,[181a] semiconductors (Nb_2O_5),[181b] graphene oxide (GO),[181c] cross-linked polymers (CF-HCP),[181d] metal organic frameworks (PCN-222)[181e] and ruthenium salts,[181f] can be found. All the catalysts showed good-to-excellent yields in this transformation but, in general, recyclability studies of the heterogeneous systems were not performed.
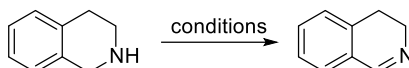
Chen, 2009: Tungsten lamp (300 W), H_2TPP, EtOAc, 4 Å MS, $^1O_2$
Tanaka, 2011: λ > 300 nm, Nb_2O_5, benzene, air
Yamakoshi, 2016: Tungsten lamp (200 W), GO, $CHCl_3$, 4 Å MS, O_2
Liu, 2017: green LED (30 W), CF-HCP, CH_3CN, O_2
Jiang, 2018: Xe lamp (100 mW/cm^2), PCN-222, CH_3CN, air
Stodulski, 2020: CFL (23 W), [Ru(bpy)$_3$](PF$_6$)$_2$, CH_3CN, Na_3PO_4, O_2

Scheme 58. Reported semidehydrogenation of THIQ employing photocatalysis.

Among the diverse types of catalytic systems, we decided to focus on heterogeneous photocatalysts based on semiconductors,[182] modified or not with CuNPs. This type of reaction promoters has grown immensely in the last decades because it shows analogy with the photosynthesis, the most essential chemical process in nature.

5.1.2. Heterogeneous photocatalysis: semiconductors

A proper semiconductor photocatalyst must have as low values of electron-hole recombination and band gap energy as possible, in order to adequately promote organic transformations. In addition, the structure of these catalysts can be modified in order to improve both, their catalytic activity and spectral range.

The most common procedures to improve their properties are: (a) doping with metal ions, non-metals (N, S, etc.) or sensitizers (organic dyes); (b) bulk modifications; and (c) surface modifications (grafting), among others.[183]

---

[181] (a) Jiang, G.; Chen, J.; Huang, J.-S.; Che, C.-M. *Org. Lett.* **2009**, *11*, 4568-4571. (b) Furukawa, S.; Ohno, Y.; Shishido, T.; Teramura, K.; Tanaka, T. *ACS Catal.* **2011**, *1*, 1150-1153. (c) Kumar, R.; Gleißner, E. H.; Tiu, E. G. V.; Yamakoshi, Y. *Org. Lett.* **2016**, *18*, 184-187. (d) Zhi, Y.; Li, K.; Xia, H.; Xue, M.; Mu, Y.; Liu, X. *J. Mater. Chem. A* **2017**, *5*, 8697-8704. (e) Xu, C.; Liu, H.; Li, D.; Su, J.-H.; Jiang, H.-L. *Chem. Sci.* **2018**, *9*, 3152-3158. (f) Stanek, F.; Pawlowski, R.; Morawska, P.; Bujok, R.; Stodulski, M. *Org. Biomol. Chem.* **2020**, *18*, 2103-2112.

[182] Review: Xu, C.; Anusuyadevi, P. R.; Aymonier, C.; Luque, R.; Marre, S. *Chem. Soc. Rev.* **2019**, *48*, 3868-3902.

[183] (a) Kisch, H. *Semiconductor Photocatalysis: Principles and Applications*; Wiley-VCH: Weinheim, 2015. (b) Lee, S.-K.; Mills, A.; O'Rourke, C. *Chem. Soc. Rev.* **2017**, *46*, 4877-4894.

As well as in conventional heterogeneous catalysis, the characterisation of the heterogeneous photocatalyst is necessary to understand its behaviour. The most commonly employed techniques for the characterisation of these kind of catalysts are: (a) Elemental Analysis (especially useful when doping with non-metals); (b) Diffuse Reflectance Spectroscopy (for the measurement of band gaps); (c) Photocurrent and Photovoltage measurements (for the value of the quasi-Fermi levels); (d) N_2 physisorption (to determine the surface area); (e) TEM (to study particle size and distribution); (f) Differential Titration (for zero zeta potential point determination); and (g) Time-resolved Emission and Photovoltage (to determine charge carrier lifetimes).[183]

In general, these catalysts are easy to prepare by precipitation and subsequent calcination. In the case of doping and surface modification, the common methodologies are: co-precipitation, impregnation, supporting, ion implantation and ligand-exchange reactions. There is a great variety of semiconductor photocatalysts, some of which, along their relevant properties, have been compiled in Figure 53.
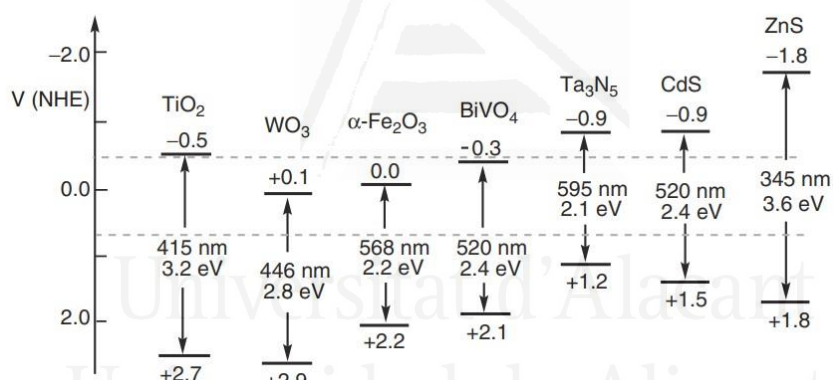
Figure 53. Band edge positions (as powder in water), light absorption onsets and band gap energies of several representative semiconductors. Figure reproduced from ref. 183. Copyright 2015 Wiley-VCH.

Amid these photocatalysts, our research group has been focused on systems based on MNPs supported on titanium dioxide, also known as titania (TiO_2).

5.1.3. Titania (TiO₂) in photocatalysis

Titania is one of the cheapest and most important semiconductor photocatalysts employed in organic chemisty.[184,185] TiO_2 has three different photocatalytically active structures; rutile, anatase and brookite (Figure 54).[186] Typically, anatase, the most active phase, is the one used in organic transformations together with TiO_2 P25, which is a mixture of rutile and anatase in a 25/75 ratio, respectively.
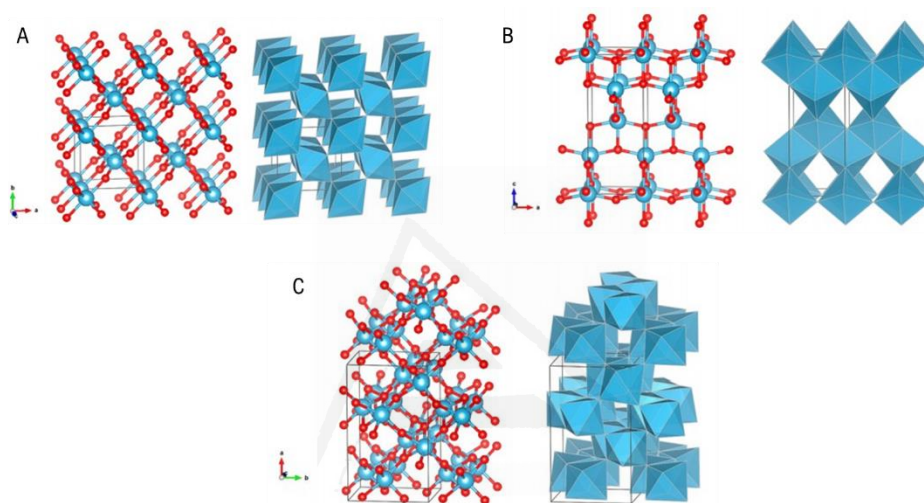
Figure 54. Structures of TiO_2: rutile (A), anatase (B) and brookite (C). Figure reproduced from ref. 186. Copyright 2014 American Chemical Society.

The principal reason behind the interest on TiO_2 P25 resides in its interface between structures. The conduction potential of the rutile phase is more positive than that of the anatase. Thus, rutile can act as an electron acceptor, increasing the separation between hole (h^+) and electron (e^-), decreasing the rate of the electron-hole recombination, one of the main problems in photocatalysis.[187]

---

[184] Reviews: (a) Guo, Q.; Zhou, C.-Y.; Ma, Z.-B.; Ren Z.-F.; Fan, H.-J.; Yang, X.-M. *Acta Phys.-Chim. Sin.* **2016**, *32*, 28-47. (b) Guo, Q.; Zhou, C.; Ma, Z.; Ren, Z.; Fan, H.; Yang, X. *Chem. Soc. Rev.* **2016**, *45*, 3701-3730. (c) Noman, M. T.; Ashraf, M. A.; Ali, A. *Environ. Sci. Pollut. Res.* **2019**, *26*, 3262-3291. (d) Riente, P.; Noël, T. *Catal. Sci. Technol*. **2019**, *9*, 5186-5232.

[185] (a) Lang, X.; Chen, C.; Ma, W.; Ji, H.; Zhao, J. in *Photochemistry*; Albini, A.; Fasani, E.; Protti, S. Eds.; The Royal Society of Chemistry: Cambridge (UK), 2017; Vol. 44, pp. 364-383. (b) Review: Cheng, H.; Xu, W. *Org. Biomol. Chem.* **2019**, *17*, 9977-9989.

[186] Zhang, H.; Banfield, J. F. *Chem. Rev.* **2014**, *114*, 9613-9644.

[187] (a) Mi, Y.; Weng, T. *Sci. Rep.* **2015**, *5*, 11482. (b) Maheu, C.; Cardenas, L.; Puzenat, E.; Afanasiev, P.; Geantet, C. *Phys. Chem. Chem. Phys.* **2018**, *20*, 25629-25637.
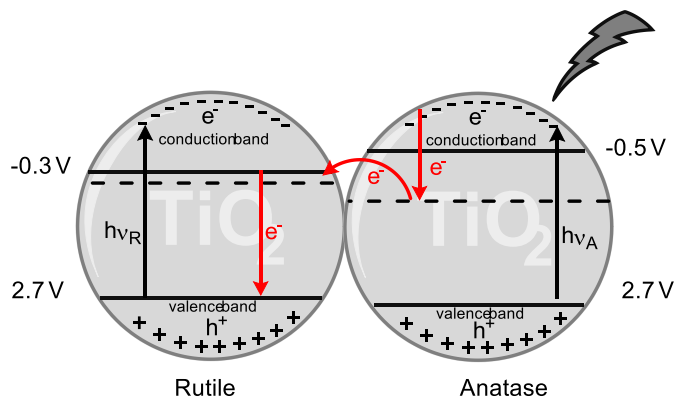
Figure 55. TiO$_2$ P25 interface.

Among the possibilities for modifying the semiconductor's surface, we decided to concentrate our attention on doping with metals, applying impregnation and supporting protocols for the photocatalyst preparation. The main benefits of this type of modification are: (a) an increase in the surface area, (b) a decrease in the band gap energy, (c) enhanced charge separation and (d) increased absorption of visible light (due to the surface plasmon resonance of the corresponding metal), among others (Figure 56).[188]
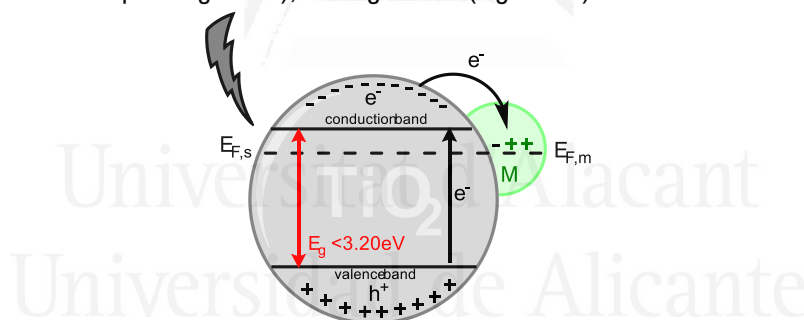
Figure 56. Semiconductor photocatalyst doped with metals.

Typically, a semiconductor photocatalyst is excited under irradiation (wavelenght depending on its band gap energy) to promote an electron from the valence band to the conduction band. When doped with metals, irradiation can also excite the system in such a manner that an electron from the metal is promoted to the semiconductor's conduction band. This process has its own energetic gap, independent of the band gap energy of the

[188] Reviews: (a) Bärtsch, M.; Niederberger, M. *ChemPlusChem* **2017**, *82*, 42-59. (b) Ma, L.; Chen, S.; Shao, Y.; Chen, Y.-L.; Liu, M.-X.; Li, H.-X.; Mao, Y.-L.; Ding, S.-J. *Catalysts* **2018**, *8*, 634. (c) Fu, Y.-S.; Li, J.; Li, J. *Nanomaterials* **2019**, *9*, 359.

semiconductor. Thus, the amount of wavelenghts able to excite the system is expanded (Table 33).

Table 33. Photon absorption energy values of visible light.

Light	λ (nm)	Photon Energy (eV)
Violet	380-450	2.75-3.26
Blue	450-495	2.50-2.75
Green	495-570	2.17-2.50
Yellow	570-590	2.10-2.17
Orange	590-620	2.00-2.10
Red	620-750	1.65-2.00

This combination results in an increase of the action spectrum of the doped photocatalyst. Nonetheless, the metal can act also as an electron scavenger promoting undesired electron-hole recombinations and, in some cases, decreasing the photoactive points of the system.

Thus, a careful balance between the light, metal and the corresponding semiconductor must be achieved to carry out the desired transformations. Therefore, depending on the nature of the organic reaction, the presence of metals could be counterproductive even if it does decrease the band gap energy.

In general, the most studied metallic elements for semiconductor photocatalyst doping are noble metals. Therefore, it is of extreme importance to develop novel catalytic systems which avoid their use, substituing them for non-noble metals or alloys.

In this sense, our research group, in collaboration with Prof. Scaiano's group (University of Ottawa, Canada), considered an attractive idea to study our CuNPs supported on TiO_2 as photocatalysts in the dehydrogenative oxidation of THIQs.

5.2. Objectives

Taking into consideration the aforementioned background, the following objectives were set:

- o To measure the band gap energies of our photocatalytic systems.
- o To study the photocatalytic activity of CuNPs supported on TiO_2 in the dehydrogenative oxidation of 1,2,3,4-tetrahydroisoquinolines.
- o To study the photophysical properties of transient species.

5.3. Results and discussion

5.3.1. Band gap energy measurements

To begin our study, we determined the band gap energy of our catalytic systems *via* Diffuse Reflectance (DR) Spectroscopy. In this technique, only the part of the beam that is scattered within a solid sample and returned to the surface was considered.

In this technique, the powdered sample is irradiated with a light beam at a certain angle. Part of the inciding beam is reflected symmetrically, causing specular reflection, while the rest of the beam scatters within the surface of the sample, causing reflection in all directions, which is known as diffuse reflection/reflectance.

DR is dependent on the wavelength of the inciding beam; therefore, reflectance F(R) *vs* wavelength (nm) plots can be recorded with a suitable UV-Vis spectrophotometer. For studies with our catalysts, we set the system to measure DR only, ignoring specular reflection. The F(R) *vs* wavelenght plots are depicted in Figure 57.
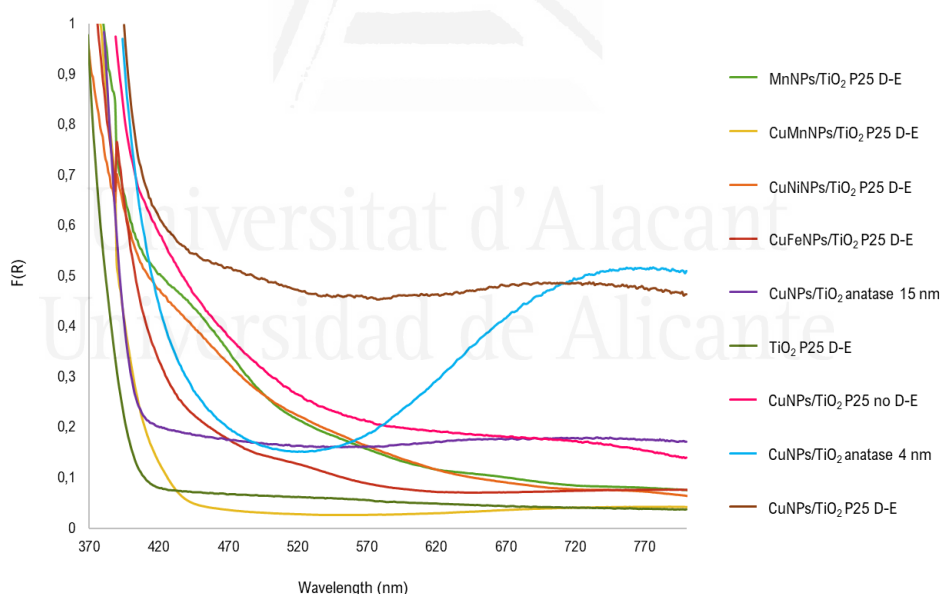
Figure 57. Diffuse reflectance graphs of supported MNPs on TiO_2 (D-E = Degussa-Evonik).

Employing this technique, the band gap energies can be calculated using the relation between the energy and the wavelength ($E_g = hc/\lambda$) or the Kubelka-Munk equation.[189]

$$F(R) = \frac{(1-R)^2}{2R} ; R = \text{Reflectance}$$

$$[F(R)h\upsilon]^{1/n} = A(h\upsilon - E_g)$$

$$[F(R)h\upsilon]^{1/n} \rightarrow 0$$

The plot of $[F(R)h\upsilon]^{1/n}$ *vs* energy (E_g, in eV) gives the band gap energy of the corresponding semiconductor when extrapolated to zero. The value of *n* is ½ or 2 for direct and indirect transitions, respectively. Nonetheless, the graphic representation of the reflectance function F(R) *vs* energy (eV), without considering any type of transitions, fits well with our experimental data.

In order to determine which representation is more appropriate for our photocatalytic systems, we carried out the DR experiment with TiO_2 (P25 D-E) and plotted F(R) *vs* E_g, $[F(R)h\upsilon]^2$ *vs* E_g and $[F(R)h\upsilon]^{1/2}$ *vs* E_g, obtaining band gap energies of 3.20, 3.55 and 3.01 eV, respectively. With these results, and seeing that the closest to the reported E_g value of TiO_2 (P25 D-E) was obtained using the F(R) *vs* E_g plot, we decided to use this representation, as it is a good enough approximation for the measurement of the corresponding band gap energies.

All the results obtained by DR experiments are summarised in Table 34. First, the systems based on CuNPs supported on different types of TiO_2 were examined, observing slight differences between them (Table 34, entries 2-5). Consequently, the structure and particle size of the TiO_2 used seem not to affect the band gap energy values significantly. Hereafter, the catalysts based on manganese (Table 34, entry 6) and bimetallic systems were studied (Table 34, entries 7-9). Among them, the lowest E_g value was observed in the case of $CuNiNPs/TiO_2$ (Table 34, entry 8).

[189] (a) Valencia, S.; Marin, J. M.; Restrepo, G. *Open Mater. Sci. J.* **2010**, *4*, 9-14. (b) López, R.; Gómez, R. *J. Sol-Gel Sci. Technol.* **2012**, *61*, 1-7.

Table 34. Band gap energy of MNPs supported on TiO_2.

Entry	Catalyst	λ (nm)	E_g (eV)
1	TiO_2 (P25 D-E)	397	3.20
2	CuNPs/TiO_2 (P25 D-E)	441	2.88
3	CuNPs/TiO_2 (P25 no D-E)	460	2.76
4	CuNPs/TiO_2 (anatase 15 nm)	412	3.08
5	CuNPs/TiO_2 (anatase 4 nm)	445	2.85
6	MnNPs/TiO_2 (P25 D-E)	441	2.88
7	CuMnNPs/TiO_2 (P25 D-E)	400	3.17
8	CuNiNPs/TiO_2 (P25 D-E)	475	2.67
9	CuFeNPs/TiO_2 (P25 D-E)	420	3.02

D-E = Degussa-Evonik.

5.3.2. Optimisation of the catalytic system and reaction conditions

Having determined the band gap energies of our catalysts, we decided to use near-UV light (λ = 369 nm) and blue visible light (λ = 450 nm) for their activation in the semidehydrogenation of 1,2,3,4-tetrahydroisoquinoline (**18a**).

First, we screened several catalysts based on CuNPs, supported on different types of TiO_2, for the synthesis of the dihydroisoquinoline **19a** under oxygen and UV activation (Table 35, entries 1-4), showing TiO_2 P25 Degussa-Evonik the best performance after 3 h (Table 35, entry 1). Thus, the structure and particle size seem to be important for this transformation.

Catalysts based on other metals were evaluated as well (Table 35, entries 5-8) but, in all the cases, lower conversions were obtained. Nonetheless, it must be underlined that MnNPs/TiO_2 (P25 D-E) led to a good conversion towards the formation of the corresponding DHIQ (**19a**).

The standard reaction catalysed by CuNPs/TiO_2 (P25 D-E) was also carried under visible light irradiation (blue LED, λ = 450 nm), leading to only traces of the product (Table 35, entry 9).

Some control experiments were performed in order to confirm whether the presence of MNPs was or was not necessary for the transformation to take place. On one hand, the reaction in the absence of catalyst did not take place at all (Table 35, entry 10). On the other hand, only the neat support TiO_2 P25 D-E promoted this transformation in comparable conversions to those obtained with CuNPs/TiO_2 (Table 35, compare entries 1 and 11). The same conversion was obtained after 3 h, 82 and 81% of **19a**, for CuNPs/TiO_2 and TiO_2, respectively. After 23 h of reaction, the conversion into **19a** dropped to 12 and 15%,

respectively, whereas 40 and 72% conversions into **20a** were recorded for CuNPs/TiO$_2$ and TiO$_2$, respectively (Table 35, entries 1 and 11). With these results in hand, the reaction carried out with TiO$_2$ seemed to proceed more cleanly, avoiding the formation of by-products while maintaining the same performance as the CuNPs/TiO$_2$ system. For this reason, TiO$_2$ (P25 D-E) was selected as the optimum catalyst to this transformation.

The following step was the optimisation of the reaction atmosphere (Table 35, entries 11-13), observing good conversions into **19a** under oxygen after 3 h and under air after 23 h. The control of the degree of oxidation of **18a** towards **19a** was easier under air (Table 35, compare entries 11 and 13).

The catalyst loading and beam power density were also studied. The best result was obtained at a concentration of 0.06 M of TiO$_2$ in acetonitrile (Table 35, compare entry 11 with entries 14-16) and a beam power density of 0.14 W/cm^2 (Table 35, compare entry 11 with entries 17-23).

Table 35. Optimisation of the dehydrogenative oxidation of **18a**.[a]

Entry	Catalyst[b]	Atm.	λ (nm)	Power density (W/cm^2)	Conv.(%)[c] 19a/20a[d]	Conv.(%)[c] 19a/20a[e]
1	CuNPs/TiO$_2$ (P25 D-E)	O$_2$	369	0.14	82/8	12/40
2	CuNPs/TiO$_2$ (P25 no D-E)	O$_2$	369	0.14	53/7	11/25
3	CuNPs/TiO$_2$ (anatase 4 nm)	O$_2$	369	0.14	71/7	45/5
4	CuNPs/TiO$_2$ (anatase 15 nm)	O$_2$	369	0.14	56/9	7/49
5	MnNPs/TiO$_2$ (P25 D-E)	O$_2$	369	0.14	71/13	11/5
6	CuMnNPs/TiO$_2$ (P25 D-E)	O$_2$	369	0.14	32/3	29/17
7	CuNiNPs/TiO$_2$ (P25 D-E)	O$_2$	369	0.14	20/3	10/29
8	CuFeNPs/TiO$_2$ (P25 D-E)	O$_2$	369	0.14	21/2	42/21

Table 35. Optimisation of the dehydrogenative oxidation of **18a** (cont.).[a]

9	CuNPs/TiO$_2$ (P25 D-E)	O$_2$	450	0.14	0/0	2/14
10	-	O$_2$	369	0.14	0/0	0/0
11	**TiO$_2$ (P25 D-E)**	**O$_2$**	**369**	**0.14**	**81/16**	**15/72**
12	TiO$_2$ (P25 D-E)	Ar	369	0.14	0/0	0/0
13	**TiO$_2$ (P25 D-E)**	**air**	**369**	**0.14**	**19/8**	**70/30**
14	TiO$_2$ (P25 D-E)	O$_2$	369	0.14	61/17	10/7[f]
15	TiO$_2$ (P25 D-E)	O$_2$	369	0.14	46/32	0/2[g]
16	TiO$_2$ (P25 D-E)	O$_2$	369	0.14	75/14	43/37[h]
17	TiO$_2$ (P25 D-E)	O$_2$	369	0.005	-	66/16
18	TiO$_2$ (P25 D-E)	air	369	0.005	-	49/41
19	TiO$_2$ (P25 D-E)	O$_2$	369	0.07	-	66/16
20	TiO$_2$ (P25 D-E)	air	369	0.07	-	61/18
21	TiO$_2$ (P25 D-E)	O$_2$	369	0.20	11/31	Decomp.
22	TiO$_2$ (P25 D-E)	air	369	0.20	10/15	Decomp.
23	TiO$_2$ (P25 D-E)	O$_2$	369	0.28	5/39	Decomp.

[a] **18a** (0.5 mmol), catalyst (10 mg), CH$_3$CN (2 mL). [b] Catalyst concentration: 0.06 M, unless otherwise stated. [c] Conversion determined by GLC (no by-products were observed). [d] Reaction time: 3 h. [e] Reaction time: 23 h. [f] Catalyst concentration: 0.01 M. [g] Catalyst concentration: 0.03 M. [h] Catalyst concentration: 0.12 M.

The evolution of the dehydrogenative oxidation of **18a** was monitored under oxygen (Figure 58) and under air (Figure 59). Analysing the plots, the reaction under oxygen peaked in conversion after 3 h (81% of **19a**), while in air, it did so after 6 h, albeit with similar values (80% of **19a**). At that point, the amount of **19a** started to decrease, as a precursor of isoquinoline (IQ, **20a**). The latter transformation was favoured under oxygen, furnishing 15% of DHIQ (**19a**) and 82% of IQ (**20a**) after 23 h. Surprisingly, 70% of DHIQ (**19a**) and 30% of IQ (**20a**) were obtained under air after the same reaction time (Figures 58 and 59). Therefore, a higher concentration of oxygen seems to be detrimental to the selective formation of **19a** for longer reactions times, whereas an almost steady good ratio of **19a/20a** is maintained in the lower concentration of oxygen in air after 8 h.
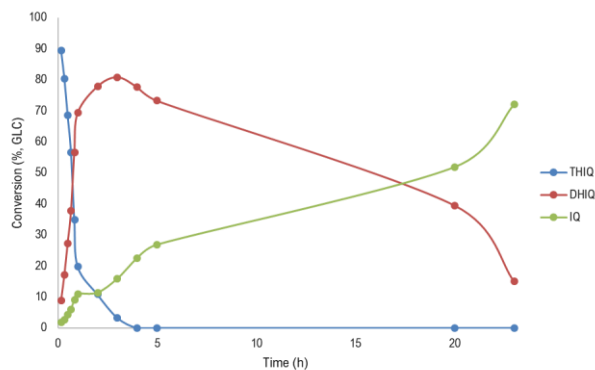
Figure 58. Reaction profile for the dehydrogenative oxidation of **18a** in CH$_3$CN under oxygen.
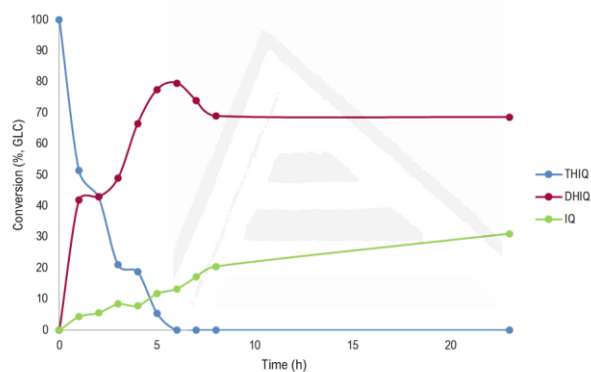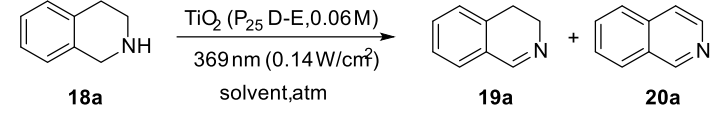
Figure 59. Reaction profile for the dehydrogenative oxidation of **18a** in CH$_3$CN under air.

With the catalyst loading and power density optimised, the effect of the solvent polarity was evaluated next, with the results obtained being summarised in Table 36. When comparing these results at 3 h with those obtained in CH$_3$CN under oxygen (Table 35, entry 11), similar conversions were obtained with CH$_3$CN:H$_2$O, *i*-PrOH and DMSO after 3 h of reaction (Table 36, entries 1, 8 and 10). Nevertheless, the formation of by-products seems to be favoured in these cases, especially for longer reaction times. In water, both under air and argon, the behaviour of the system was similar to that in CH$_3$CN under air after 23 h, favouring the formation of **19a** over **20a** (compare entry 13 in Table 35 with entries 4 and 5 in Table 36).
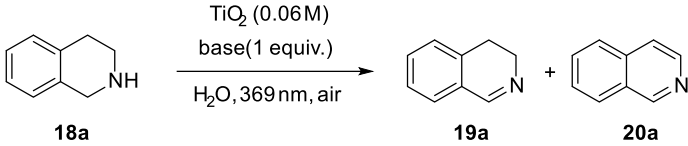
Table 36. Effect of the solvent polarity in the dehydrogenative oxidation of **18a**.[a]

Entry	Solvent	Atm.	Conv. (%)[b] 19/20[c]	Conv. (%)[b] 19/20[d]
1	$CH_3CN:H_2O$	O_2	67/10	15/55
2	$CH_3CN:H_2O$	air	59/9	48/30
3	H_2O	O_2	49/15	66/34
4	**H_2O**	**air**	**30/9**	**69/31**
5	**H_2O**	**Ar**	**23/6**	**73/27**
6	H_2O[e]	Ar	35/5	63/23
7	H_2O_2	air	0/0	0/0
8	*i*-PrOH	O_2	75/13	5/24
9	MeOH	O_2	19/20	0/24
10	DMSO	O_2	62/19	0/16
11	toluene	O_2	59/6	26/53
12	toluene	air	-	66/28
13	$CHCl_3$	O_2	56/14	0/19
14	$CHCl_3$	air	-	63/18
15	THF	O_2	41/20	3/21

[a] **18a** (0.5 mmol), catalyst (10 mg), solvent (2 mL). Catalyst concentration: 0.06 M, unless otherwise stated. [b] Conversion determined by GLC (the rest of the percentage corresponds to **18a** and/or by-products). [c] Reaction time: 3 h. [d] Reaction time: 23 h. [e] Deoxygenated H_2O.

In an attempt to increase the rate of the reaction, the effect of the presence of 1 equiv. of base in the conversion after 3 h was evaluated, generating the results summarised in Table 37.

Analysing these results, we could observe that the presence of a base had no significant effect on the reaction rate. While NaHCO₃, Cs₂CO₃ and *t*BuOK showed the best results in the conversion to **19a** (Table 37, entries 3, 5 and 7), it was not enough to offset the technical and environmental inconveniences derived from their use and, thus, we decide not to employ any bases in this transformation.

Table 37. Effect of the base.[a]

TiO$_2$ (0.06 M)
base (1 equiv.)
$\xrightarrow{\text{H}_2\text{O, 369 nm, air}}$

18a → **19a** + **20a**

Entry	Base	Conversion (%)[b] 19a/20a
1	KOH	24/5
2	K$_3$PO$_4$	24/5
3	NaHCO$_3$	47/6
4	K$_2$CO$_3$	17/3
5	**Cs$_2$CO$_3$**	**54/6**
6	Ba(OH)$_2$·8H$_2$O	9/3
7	^{t}BuOK	46/6

[a] **18** (0.5 mmol), TiO$_2$ (10 mg), H$_2$O (2 mL), 369 nm (0.14 W/cm^2), 3 h, air. [b] Conversion determined by GLC.

Although the reaction proceeds faster in acetonitrile, we would better use water as a solvent for further studies on this transformation. Thus, we established the following optimal conditions for this reaction: 0.06 M TiO$_2$ (P25 D-E) as photocatalyst, in water under air, irradiating the reaction medium with a power density of 0.14 W/cm^2 from UV LEDs (λ = 369 nm), in the absence of base.

5.3.3. Study of the THIQ and TiO$_2$ interaction

Taking all these results into account, the interaction between 1,2,3,4-tetrahydroisoquinoline (**18a**) and TiO$_2$ seems to be stronger than the corresponding interaction with the homologous metal-TiO$_2$ system. We decided to carry out a series of experiments in order to understand this behaviour.

First, DR experiments were performed to observe the corresponding interaction between TiO$_2$ and THIQ. In this sense, TiO$_2$ (P25 D-E) was impregnated with **18a** and analysed.

The results obtained in the DR analysis of the impregnated TiO$_2$ are depicted in Figure 60. The F(R) *vs* the wavelength function corresponding to TiO$_2$ impregnated with THIQ (**18a**) was shifted to higher wavelengths, into the visible region of the spectrum. This behaviour was somewhat expected due to the yellowish colour of the impregnated TiO$_2$.
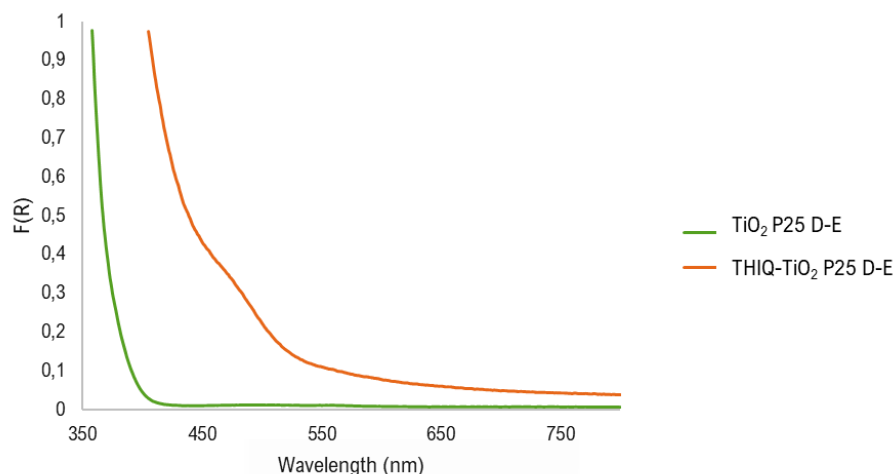
Figure 60. Reflectance function *vs* wavelength graph of TiO_2 (P25 D-E) impregnated with THIQ (**18a**).

The value of the band gap energy was obtained (λ = 502 nm, E_g = 2.53 eV), from the corresponding F(R) *vs* E_g plot, as aforementioned. This value is smaller than that of the supported metallic systems (Table 34).

Due to the dissociative behaviour of amines, they can associate with the TiO_2 surface, facilitating their oxidation *via* single electron transfer and generating an electron charge-transfer complex. This type of interactions were previously reported by Scaiano's group in the case of TiO_2 impregnated with indole.[190]

Continuing with the study of THIQ-TiO_2 interactions, an attenuated total reflectance Fourier-transform infrared spectroscopy (ATR-FTIR) experiment was performed, confirming the attachment of the organic molecule to the TiO_2 surface (purple line, Figure 61).

---

[190] Pitre, S. P.; Yoon, T. P.; Scaiano, J. C. *Chem. Commun.* **2017**, *53*, 4335-4338.
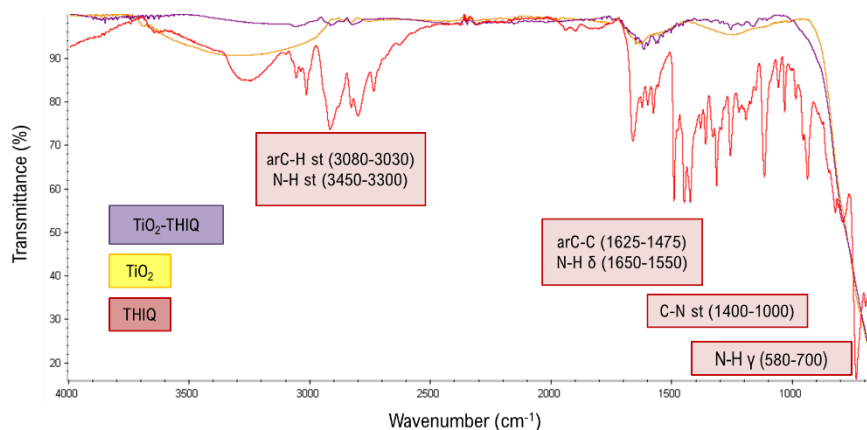
Figure 61. ATR-FTIR spectra of **18a**, TiO_2 (P25 D-E) and TiO_2 (P25 D-E) impregnated with **18a**.

Analysing the resulting spectra and focusing our attention on the region around 3300 cm^{-1}, we can see that the peak related to the NH bond of THIQ (compare red and purple lines) and the broad OH signal of the TiO_2 (compare orange and purple lines) have dissapeared in the TiO_2-THIQ system. These results point to a possible interaction between the NH bond of the THIQ (**18a**) and the OH present on the TiO_2 surface.

Next, the adsorption of THIQ on TiO_2 was studied by UV-Vis spectroscopy. First, the absorption spectrum of 1,2,3,4-tetrahydroisoquinoline (**18a**) was acquired at a known concentration of 0.32 mM in acetonitrile, resulting in the plot represented in Figure 62.
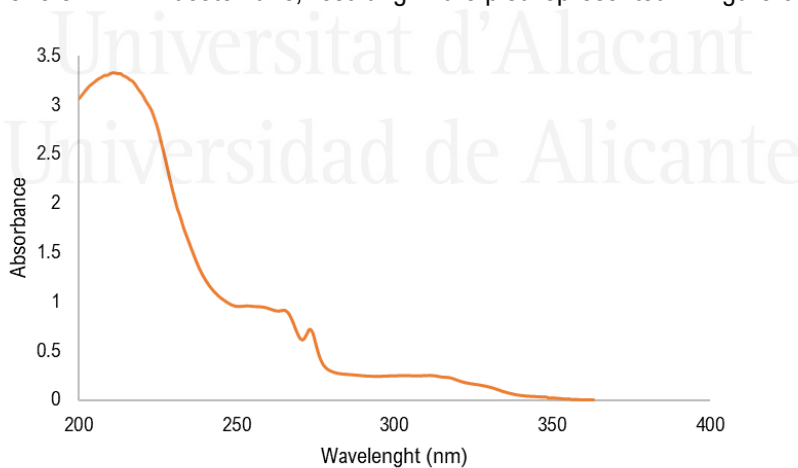
Figure 62. Absorption spectrum of 0.32 mM 1,2,3,4-tetrahydroisoquinoline (**18a**) in CH_3CN.

A maximum absorbance was recorded at 215 nm. With this value in hand, an absorbance *vs* concentration plot was elaborated. Then, the Lambert-Beer's law, which stablishes a linear relationship between absorbance and concentration, was used to determine the amount of **18a** attached on the TiO$_2$ surface.
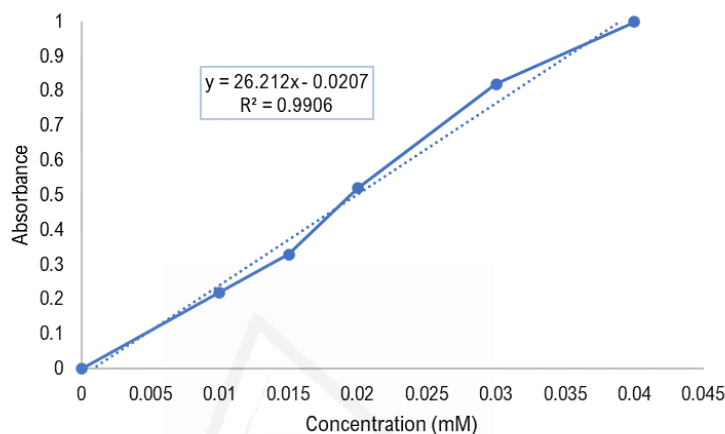
Figure 63. Lambert-Beer representation of 1,2,3,4-tetrahydroisoquinoline (**18a**) in CH$_3$CN.

With the plot constructed, the suspension generated in the standard reaction (in CH$_3$CN) was analysed, which, after interpolation with this plot, gave 0.009 mmol of **18a** adsorbed on the TiO$_2$ (P25 D-E) surface. In order to determine if the attached THIQ could be removed unaltered from the catalyst's surface, the TiO$_2$ impregnated with **18a** was irradiated under UV light in the absence and presence of Cs$_2$CO$_3$. The reaction extract was analysed by GLC, but no peak was observed, confirming the strong interaction between **18a** and the titania.
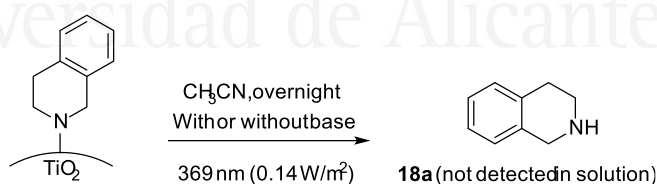
Scheme 59. Control experiment with impregnated TiO$_2$.

5.3.4. Time-resolved experiments

In order to gain insight into the reaction mechanism some time-resolved experiments with Laser Flash Photolysis (FLP) were performed. LFP is a pump-probe technique used to examine the dynamic behaviour of reactive intermediates and excited states of photochemical

processes (Figure 64). The pump (laser) is a short excitation pulse (in the order of nanoseconds) that generates the transcient species, and the probe (continuous light beam) is the technical resource that allows the monitoring of the species of interest.[191]
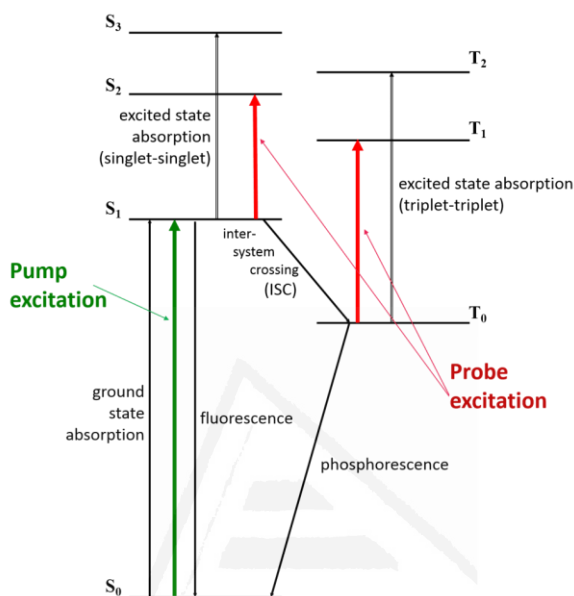
Figure 64. Energy diagram for transient absorption of a excited state employing Laser Flash Photolysis (Figure reproduced from Edinburgh Instruments Ltd.).

LFP monitors the change in absorption (ΔOD) as a function of time, which depends on the energy of the laser pulses and is independent of the monitoring light. In our case, the experiment was performed employing the 355 nm harmonic (Nd/YAG) as pump at 30 mJ of energy to generate the transient species.

First, we carried out some fluorescence experiments in order to deepen our knowledge about the photophysical behaviour of **18a**. In the emission spectrum (using 350 nm as excitation wavelength) two peaks were observed at around 280 and 330 nm, whereas only one peak, at around 380 nm, was registered in the excitation experiment (employing 350 nm as the emission wavelength). The two peaks observed in the emission spectrum correspond to the two possible conformers of **18a** [hydrogen (NH) in axial or equatorial position].[192]

---

[191] (a) Scaiano, J. C. in *Reactive Intermediate Chemistry*; Moss, R. A.; Platz, M. S.; Jones, M. Jr., Eds.; John Wiley & Sons: Hoboken (NJ), 2004; pp. 847-872. (b) Review: Cosa, G.; Scaiano, J. C. *Photochem. Photobiol.* **2004**, *80*, 159-174.
[192] Kanamaru, N.; Tanaka, J. *J. Phys. Chem.* **1991**, *95*, 6441-6446.
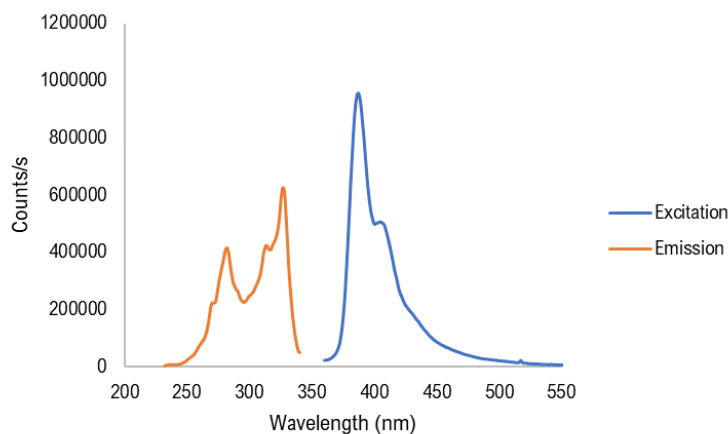
Figure 65. Excitation and emission spectra of fluorescence experiments with 1,2,3,4-tetrahydroisoquinoline (**18a**) in CH_3CN, employing λ = 350 nm as monitoring wavelength.

With all the information gathered from this series of analysis, along with the absorption data, we proceeded with the LPF experiments. In order to avoid second order interferences (self-reactions), the concentration of the samples was limited to that corresponding to a maximum absorbance value of 0.3-0.4.

The instrument was calibrated with 1-azaxantone, both in air and argon (Figures 66 and 67), obtaining time constants of $7.96 \cdot 10^6$ and $1.15 \cdot 10^6$ s^{-1} and mean lifetimes of 126 and 869 ns, respectively. These results are in agreement with those reported in the literature, confirming the adequate alignment and status of the system.
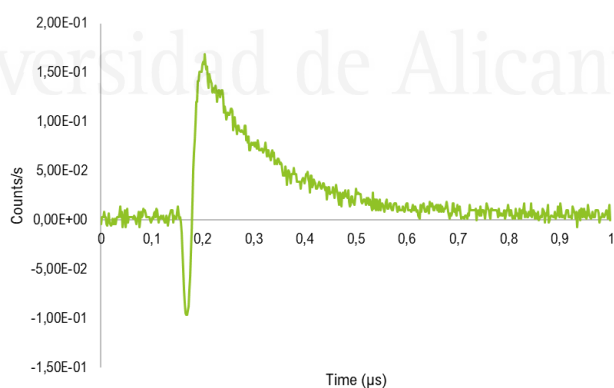
Figure 66. LFP trace of 1-azaxanthone in CH_3CN under air. Monitoring wavelength of 600 nm (without fluorescence correction), $\lambda_{exc.}$ = 355 nm, 15 mJ of power pulse; Abs. = 0.15.
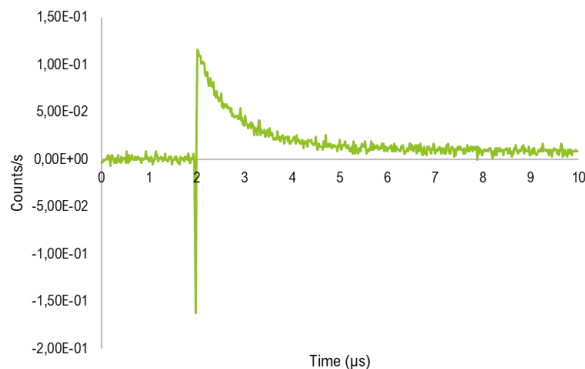
Figure 67. LFP trace of 1-azaxanthone in CH$_3$CN under argon. Monitoring wavelength of 600 nm (without fluorescence correction), $\lambda_{exc.}$ = 355 nm, 15 mJ of power pulse; Abs. = 0.15.

With the LFP-system in good running condition, the experiments with THIQ (**18a**) were carried out. First, its kinetic spectrum was recorded in order to determine the wavelength of the maximum absorption, being this 380 nm. On the other hand, the LFP emission spectrum was also registered, showing two different peaks which, as in the case of fluorimetry experiments, correspond to both conformers of THIQ (**18a**). Then, we studied the triplet decay of **18a**, obtaining the trace depicted in Figure 68.
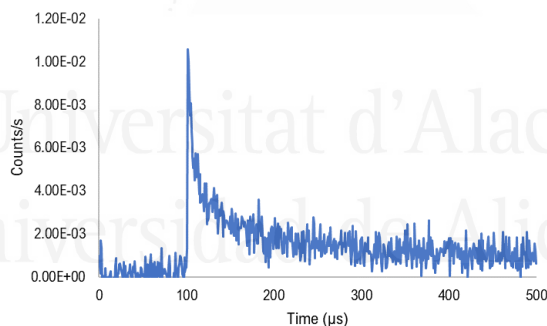
Figure 68. LFP trace of 1,2,3,4-tetrahydroisoquinoline (**18a**) in CH$_3$CN under argon. Monitoring wavelength of 380 nm (without fluorescence correction), $\lambda_{exc.}$ = 355 nm, 30 mJ of power pulse, [THIQ, **18a**] = 0.032 M; Abs. = 0.3.

This trace seems to fit quite well to a pseudo-first order kinetics, with a rate constant of $1.03 \cdot 10^5$ s^{-1} and an excited state lifetime (**18a***) of 9730.1 ns. Nonetheless, these results are not in compliance with those reported in the literature for this molecule.[193] In addition,

---

[193] (a) Bera, P. K.; Chakraborty, A.; Chowdhury, M. *Chem. Phys. Lett.* **1997**, *277*, 57-64. (b) Kanamaru, N. *J. Lumin.* **2002**, *96*, 5-35.

recording the spectrum at 10 or 20 mJ of energy did not lead to any trace at all. These variations in the traces depending on the power of the laser pulse suggested that the trace obtained at 30 mJ may not correspond to the triplet of **18a**. Further experiments will be carried out in order to demonstrate this hypothesis.

5.4. Conclusions

As a conclusion of this chapter, the band gap energies of an array of heterogeneous catalysts based on metal nanoparticles supported on titania were determined. These catalysts were tested in the selected-photocatalysed semidehydrogenative oxidation of 1,2,3,4-tetrahydroisoquinoline (**18a**). However, the presence of the MNPs seemed to be detrimental to the catalytic activity of the system, with the best conversions into 3,4-dihydroisoquinoline being attained with neat TiO_2 (P25 D-E).

In order to understand the reactivity and selectivity of titania, some experiments were performed related to the interaction between THIQ and TiO_2. The results of these experiments point to the possible formation of an electron charge transfer complex between the starting material and the photocatalyst.

To gain further knowledge about this process, LFP experiments were carried out. While some results were obtained, they were not in compliance with the reported literature, thus needing further studies to fully comprehend the mechanism of this process.

Despite the good selectivity for the synthesis of 3,4-dihydroisoquinolines, further experiments are required. Then, the scope of the reaction, recyclability of the catalyst and mechanistic studies will be assesed in future studies.

General Conclusions

General Conclusions

Concluding this thesis, a variety of catalysts based on supported CuNPs have been prepared, have been fully characterised and their catalytic activity has been tested in different organic reactions. In general, these catalysts have demonstrated to be efficient heterogeneous catalysts in the formation of C-C, C-S and C-N bonds through cross-coupling reactions, and in the synthesis of propargylamines and dihydroindoloisoquinolines through cross-dehydrogenative coupling reactions.

The supported copper catalysts are easily prepared, active at low metal loadings, generally reusable, air tolerant, able to work under solvent-free conditions, and show higher performance than commercial copper catalysts. Concerning the latter issue, this study also supports the prominent catalytic activity of the nanosized metallic species when compared with the bulk counterparts.

When supported on titania, the selective oxidation of tetrahydroisoquinoline to dihydroisoquinoline has been attained under photochemical activation. However, in this case a major role seems to be played by the titania itself. Further work is needed to assess the applicability of the supported CuNPs as heterogeneous photocatalysts in organic synthesis.

In addition, the supported nanosized metals have been shown to be powerful tools for the modulation of basic ovarian functions, with potential application in the treatment of reproduction disorders.

Finally, it has been 61 years since Feynman presented his talk and I concur with him: *There's plenty of room at the bottom.*

Experimental Part

General

Reagents and solvents

Anhydrous copper(II) chloride (97%, Aldrich), lithium powder (MEDALCHEMY S. L.), DTBB (4,4'-di-*tert*-butylbiphenyl, Aldrich), sodium zeolite-Y (Aldrich), TiO_2 (anatasa nanopowder, 15 nm; Alfa Aesar), activated carbon (Norit CA1, Sigma-Aldrich), montmorillonite K-10 (Sigma-Aldrich) and all other reagents (Aldrich, Acros, Alfa Aesar, Flurochem) were commercially available of the best grade and were used without further purification. THF was dried in a Sharlab PS-400-3MD solvent purification system using an alumina column.

Instruments

The TEM images were recorded with a JEOLJEMM2010 microscope, equipped with a lanthanum hexaboride filament operated at an acceleration voltage of 200 kV. For their observations, the as-prepared samples were mounted on holey-carbon coated gold grids. The size distribution of the CuNPs was determined by TEM. EDX analyses were carried out with an Oxford Inca Energy TEM100 attachment.

The XPS spectra were measured with a VG-Microtech Multilab 3000 electron spectrometer using a non-monochromatised Mg-Kα (1253.6 eV, for CuNPs/C) and Al-Kα (1486.6 eV, for CuNPs supported on ZY, TiO_2 and MK-10) radiation source of 300 W and a hemispheric electron analyser equipped with 9 channeltron electron multipliers. The pressure inside the analysis chamber during the scans was about $5 \cdot 10^{-7}$ $N \cdot m^{-2}$. Higher resolution survey scans were performed at a pass energy of 50 eV. The intensities of the different contributions were obtained by means of the calculation of the integral of each peak, after having eliminated the baseline with S form and adjusting the experimental curves to a combination of Lorentz (30%) and Gaussian (70%) lines. All the bond energies were referred to the line of the C 1*s* to 284.4 eV, obtaining values with a precision of ± 0.2 eV.

Diffuse Reflectance (DR) measurements were performed with a Agilent Cary 7000 UV-Vis-NIR Universal Measurement Spectrophotometer coupled with an Agilent praying Mantis accessory (Scaiano's laboratory).

ICP-OES analyses were performed with a Perkin Elmer Optima 4300 DV (dual vision) apparatus and ICP-MS analyses were carried out with Thermo Elemental VG PQ-ExCell instrument, using in both cases the Cetac model U5000AT+ as an ultrasonic nebuliser.

All reactions were carried out on a multireactor apparatus using the corresponding reactor tubes. Melting points were obtained with a Reichert Thermovar apparatus and are uncorrected.

Infrared analysis was performed with a Jasco 4100LE (Pike MIRacle ATR) spectrophotometer; wavenumbers ($\tilde{v}$) are given in cm^{-1}.

NMR spectra were recorded on Bruker Avance 300 and 400 spectrometers (300 and 400 MHz for ^{1}H NMR; 75 and 101 MHz for ^{13}C NMR); chemical shifts are given in (δ) parts per million and coupling constants (J) in Hertz. The ^{1}H NMR yields were determined from the reaction crudes using mesitylene as the internal standard or the signal of the limiting reagent.

Mass spectra (EI) were obtained at 70 eV on Agilent 5763 (GC) and Agilent 5973 (DIP) spectrometers; fragment ions in *m/z* with relative intensities (%) in parentheses. HRMS analyses (EI) were also carried out at 70 eV on an Agilent 7200 (Q-TOF) spectrometer. The purity of volatile compounds and the chromatographic analyses (GLC) were determined with a Youling 6100 instrument equipped with a flame ionisation detector and a HP-5MS 30 m capillary column (0.25 mm diameter, 0.25 µm film thickness), using nitrogen (1 mL/min) as carrier gas, $T_{injector}$ = 270 ºC, T_{column} = 60 ºC (3 min) and 60–270 ºC (15 ºC/min); retention times (t_R) are given in min.

Analytical thin-layer chromatography (TLC) was carried out on TLC plastic sheets with silica gel 60 F$_{254}$ (Merck). Column and preparative chromatography were performed using silica gel 60 of 40–60 microns and P/UV254, respectively (hexane/EtOAc as eluent).

The light power was measured using the StellarNet BLUE-wave UV-Vis spectrometer (300-1100 nm wavelength range) equipped with a USB-2 interface with a snapshot memory to provide instantaneous spectral images from a hight sensitive CCD detector with 2048 elements. A single strand fiber optic cable (diameter = 600 µm, length = 200 m) delivers input *via* a standard SMA 905 fiber optic connector. The information was analysed employing the Spectrawiz software included in the USB 2.0.

LFP experiments were carried out employing a Nd/YAG laser (532) in a LFP-111 laser flash photolysis system (Luzchem Research Inc., Ottawa, Canada) and 1 × 1 cm^2 quartz cuvettes. Samples were degassed and prepared with a total volume of 3 mL and an absorbance of 0.3 at the excitation wavelenght. The fluorescence emission measurements were performed in a Photon Technology International (PTI) spectrofluorimeter at room temperature using 1 × 1 cm^2 quartz cuvettes. The lifetimes were measured with an Easy-Life (PTI) system and calculated using the integrates Esay-Life software. (Scaiano's Laser laboratory).

Experimental part of Chapter 1

1.1. Preparation of copper nanoparticles

1.1.1. Synthesis of unsupported CuNPs

The syntheses of triangular and hexagonal CuNPs were carried out following the general procedure described by Carpenter's group.[59] This procedure involves the preparation of 0.1 M $CuCl_2$ in the corresponding polyol (propylene glycol for triangular and diethylene glycol for hexagonal CuNPs), followed by the addition of NaOH (0.3 M) and reflux for 2 h.

Spherical CuNPs were prepared following the methodology of our research group (1.3.1, p. 51).[36b] In a typical procedure, anhydrous copper(II) chloride (1 mmol) was added to a suspension of lithium (2 mmol) and 4,4'-di-*tert*-butylbiphenyl (DTBB, 0.1 mmol) in dry THF (2 mL) at room temperature under an argon atmosphere. The reaction mixture, which was initially dark green, rapidly changed to black, indicating that the suspension of copper nanoparticles was formed.

1.1.2. Synthesis of supported CuNPs

The supported CuNPs were synthesised following the same methodology as above but, in this case, the black suspension was diluted with dry THF (18 mL) followed by the addition of the corresponding inorganic support (1.28 g): sodium zeolite-Y (Sigma-Aldrich), activated carbon (Norit CA1, Sigma-Aldrich) or TiO_2 (anatasa nanopowder, Alfa Aesar). Then, the resulting mixture was stirred for 1 h at room temperature, filtered, and the solid was successively washed with MeOH (5 mL) and THF (20 mL), and dried in air during 24 h.

1.2. Biological experiments

1.2.1. Isolation and culture of granulosa cells

Ovaries at the follicular phase of the ovarian cycle of non-cycling pubertal gilts, approximately 180 days age, were obtained after slaughter at a local slaughterhouse and processed as described previously elsewhere.[47,194] The collected granulosa cells at a final concentration of 10^6 cells/mL were cultured in sterile DMEM/F12 1:1 medium supplemented with 10% fetal calf serum (both from BioWhittakerTM) and 1% antibiotic-antimycotic solution (Sigma-Aldrich) in 16-well (200 μL/well) chamber slides (Nunc Inc., International). After 3-4 days pre-culture, the medium (of the same composition as above) was renewed, and the

---

[194] Sirotkin, A. V.; Alexa, R.; Dekanova, P.; Kadasi, A.; Stochmalova, A.; Grossmann, R.; Alwasel, S. H; Harrath, A. H. *Int. J. Pharmacol.* **2015**, *11*, 570-578.

cells were cultured for 2 days in the medium with and without the CuNPs mentioned above at the concentrations of 0, 1, 10 or 100 ng/mL. These are the typical CuNPs concentrations that have been tested in previous animal in-vivo and in-vitro experiments.[195] After two days of culture, the cells were washed with ice-cold PBS (pH = 7.5), fixed in paraformaldehyde (4% in PBS, pH = 7.2–7.4; 60 min) and kept at 4 °C until immunocytochemical analysis. The culture medium was frozen at –17 °C to await RIA. The NPs were dispersed by gentle pipetting in the culture medium during 1 min, up to a concentration of 100 ng/mL, immediately before the addition to the cells.

1.2.2. Cell-viability test

Cell viability was evaluated by using the Trypan blue exclusion test, according to Strober.[196] Briefly, the medium from the culture plates was removed after incubation of the granulosa cells. Subsequently, the cell monolayer was subjected to Trypan blue staining (Sigma-Aldrich) for 15 min. Following removal of this dye, the plates were washed twice with physiological solution and subjected to microscopic inspection (magnification: 400×). The ratio of dead (stained) cells to total cell count was calculated.

1.2.3. Immunocytochemical analysis of proliferation and apoptosis markers

The presence of PCNA and BAX in the cells was detected by immunocytochemistry, as described previously elsewhere,[47,194] by using primary monoclonal antibodies against these molecules (all from Santa Cruz Biotechnology, Inc.). They were placed in either, a dilution of 1:500 in PBS secondary swine antibodies against mouse IgG labeled with horseradish peroxidase (Servac, dilution of 1:1000) and visualised by staining with DAB-substrate (Roche Diagnostics GmbH), or by secondary polyclonal goat antibodies against mouse IgGs labeled with the fluorescent marker fluorescein isothiocyanate (FITC; dilution 1:1000). The presence of molecules in the cells was determined using a light and fluorescence microscope (Leica GmbH). Cells processed without the primary or secondary antibody were used as the negative controls. The cells expressing a signal greater than the background negative control levels were considered positive. The proportion of cells containing visible molecules relative to the total cell number was calculated.

---

[195] (a) Liu, Y.; Liang, J.; Wang, Q.; He, Y.; Chen, Y. *J. Appl. Toxicol.* **2016**, *36*, 454-463. (b) Ashajyothi, C.; Handral, H. K.: Kelmani, R. C. *Nanoscale Res. Lett.* **2018**, *13*, 93. (c) Noureen, A.; Jabeen, F.; Tabish, T. A.; Zahoor, M. K.; Ali, M.; Isbal, R.; Yaqub, S.; Chaudhry, A. S. *Nanotechnology* **2018**, *29*, 464003. (d) Sutunkova, M. P.; Privalova, L. I.; Minigalieva, I. A.; Gurvich, V. B.; Panov, V. G.; Katsnelson, B. A. *Toxicol. Rep.* **2018**, *5*, 363-376.

[196] Strober, W. *Curr. Protoc. Immunol.* **2001**, Appendix 3B.

1.2.4. Immunoassay of hormones

Concentrations of progesterone, testosterone and *17β*-oestradiol were determined in 25 μL aliquots of incubation medium by the enzyme-linked immunosorbent assay (ELISA). Hormones were assayed using ELISA's kits according to the manufacturer's instructions (LDN Immunoassays and Services).

Antiserum against progesterone cross-reacted ≤1.1% with 11-desoxycorticosterone, ≤0.35% with pregnenolone, ≤0.3% with 17*α*-hydroxyprogesterone, ≤0.2% with corticosterone, <0.1% with oestriol, 17*β*-oestradiol, testosterone, cortisone and 11-desoxycortisol, <0.02% with DHEA-S and cortisol. The sensitivity of the assay was 0.045 ng/mL. Intra- and inter-assay coefficients of variation did not exceed 5.40% and 5.59%, respectively.

The cross-reactivity of antiserum against testosterone was ≤3.3% with 11*β*-hydroxytestosterone and 19-nortestosterone, ≤0.9% with androstenedione, ≤0.8% with 5*α*-dihydrotestosterone, <0.1% with 17*α*-methyltestosterone, epitestosterone, 17*β*-oestradiol, progesterone, cortisol, oestrone and danazol. The maximal intra- and inter-assay coefficients of variation were 4.16% and 4.73%, respectively. Sensitivity of the assay was 0.083 ng/mL.

The sensitivity of the 17*β*-oestradiol assay was 6.2 pg/mL. Intra- and inter-assay coefficients of variation did not exceed 6.4% and 4.5%, respectively. The cross-reactivity of antiserum against 17*β*-oestradiol was ≤9.5% with fulvestrant, ≤4.2% with estrone, ≤3.8% with E2-3-glucuronide, ≤3.6% with E2-3-sulphate, ≤0.4% with estriol, <0.1% with androstenedione, 17*α*-hydroxyprogesterone, corticosterone, pregnenolone, E2-17-glucuronide, progesterone and testosterone.

All ELISA assays were validated for culture medium samples by dilution tests.

1.2.5. Statistical analysis

Each experiment was repeated three times using different animals (10–15 gilts per experiment). Each experimental group was represented by four chamber-slide wells. By RIA, blank control values were subtracted from the value determined in cell-conditioned serum-supplemented medium to exclude any non-specific background (less than 13% of the total values). Secretion rates were calculated per 10^6 cells/day or mg tissue/day. Differences between groups were evaluated using the Shapiro-Wilk's normality and Student's t-tests and Sigma Plot 11.0 (Systat Software, GmbH). Values were presented as the mean ± SD. Differences were compared for statistical significance at P-levels less than 0.05 (P < 0.05).

Experimental part of Chapter 2

2.1. General procedure for cross-coupling reactions

2.1.1. Sonogashira coupling (Table 12)

The aryl halide (**1**, 0.25 mmol), arylacetylene (**2**, 1.5 equiv.), CuNPs/ZY (4 mol%), K_2CO_3 (2 equiv.) and DMF (1 mL) were added to a reactor tube. The mixture was warmed to 120 ºC under argon and stirred for the specified time in Table 12. The reaction crude was diluted with EtOAc (3 mL) and filtered through a pad with Celite, followed by extraction of the filtrate with water (3 × 3 mL) to remove the DMF, washing with brine (4 mL) and drying with anhydrous $MgSO_4$. The resulting organic phase was subjected to solvent evaporation under vacuum and to ^{1}H NMR analysis (mesitylene as the internal standard).

2.1.2. Arylation of thiophenol (Table 15)

The aryl halide (**1**, 0.25 mmol), thiophenol (**4a**, 1.5 equiv.), CuNPs/ZY (0.7 mol%), K_2CO_3 (2 equiv.) and DMF (1 mL) were added to a reactor tube. The mixture was warmed to 120 ºC under argon and stirred for the specified time in Table 15. The reaction crude was diluted with EtOAc (3 mL) and filtered through a pad with Celite, followed by extraction of the filtrate with water (3 × 3 mL) to remove the DMF, washing with brine (4 mL) and drying with anhydrous $MgSO_4$. The resulting organic phase was subjected to solvent evaporation under vacuum and ^{1}H NMR analysis (mesitylene as the internal standard).

2.1.3. Arylation of thiols (Table 16)

4-Iodobenzonitrile (**1c**, 0.5 mmol), the thiol (**4**, 1.5 equiv.), CuNPs/ZY (0.7 mol%), K_2CO_3 (2 equiv.) or KOH (2 equiv.) and DMF (2 mL) were added to a reactor tube. The mixture was warmed to 70 or 100 ºC under argon and stirred for 4 h. The reaction crude was diluted with EtOAc (6 mL) and filtered through a pad with Celite, followed by extraction of the filtrate with water (3 × 6 mL) to remove the DMF and washing with brine (8 mL). The resulting organic phase was subjected to solvent evaporation under vacuum and purification by column chromatography (silica gel, hexane/EtOAc).

2.1.4. Arylation of azoles (Table 18)

4-Iodobenzonitrile (**1c**, 0.25 mmol), the corresponding azole (**6**, 1.2 equiv.), CuNPs catalyst (5 mol% Cu), K_2CO_3 (2 equiv.) and DMF (1 mL) were added to a reactor tube. The mixture was warmed to 120 ºC under argon and stirred for 16 h. The reaction crude was diluted with EtOAc (3 mL) and filtered through a pad with Celite, followed by extraction of the filtrate with water (3 × 3 mL) to remove the DMF, washing with brine (4 mL) and drying with

anhydrous $MgSO_4$. The resulting organic phase was subjected to solvent evaporation under vacuum and ^1H NMR analysis (mesitylene as the internal standard).

2.2. Physical and spectroscopic data

2.2.1. Sonogashira coupling

All compounds **3** were characterised by comparison of their physical and spectroscopic data with those described in the literature: **3aa**,[197] **3ba**,[198] **3ca**,[199] **3da**,[200] **3ea**,[201] **3fa**,[202] **3ga**,[200] **3ha**,[203] **3ka**,[200] **3cb**,[204] **3cc**[205] and **3cd**.[206]

2.2.2. Arylation of thiophenol

Compounds **5aa**-**5ra** were characterised by comparison of their physical and spectroscopic data with those described in the literature: **5aa**,[207] **5ba**,[208] **5ca**,[209] **5fa**,[209] **5ga**,[210] **5oa**,[211] **5pa**,[209] **5qa**[208] and **5ra**.[208]

[197] Mouriès, V.; Waschbüsch, R.; Carran, J.; Savignac, P. *Synthesis* **1998**, 271-274.

[198] Nájera, C.; Gil-Moltó, J.; Karlström, S.; Falvello, L. R. *Org. Lett.* **2003**, *5*, 1451-1454.

[199] Huang, H.; Liu, H.; Jiang, H.; Chen, K. *J. Org. Chem.* **2008**, *73*, 6037-6040.

[200] Okuro, K.; Furuune, M.; Enna, M.; Miura, M.; Nomura, M. *J. Org. Chem.* **1993**, *58*, 4716-4721.

[201] Suzuka, T.; Okada, Y.; Ooshiro, K.; Uozumi, Y. *Tetrahedron* **2000**, *66*, 1064-1069.

[202] Kakusawa, N.; Yamaguchi, K.; Kurita, J. *J. Organomet. Chem.* **2005**, *690*, 2956-2966.

[203] Karastatiris, P.; Mikroyannidis, J. A.; Spiliopoulos, I. K.; Kulkarni, A. P.; Jenekhe, S. A. *Macromolecules* **2004**, *37*, 7867-7878.

[204] Bernini, R.; Cacchi, S.; Fabrizi, G.; Forte, G.; Petrucci, F.; Prastaro, A.; Niembro, S.; Shafir, A.; Vallribera, A. *Org. Biomol. Chem.* **2009**, *7*, 2270-2273.

[205] Tlahuext-Aca, A.; Hopkinson, M. N.; Sahoo, B.; Glorius, F. *Chem. Sci.* **2016**, *7*, 89-93.

[206] Nishihara, Y.; Inoue, E.; Noyori, S.; Ogawa, D.; Okada, Y.; Iwasaki, M.; Takagi, K. *Tetrahedron* **2012**, *68*, 4869-4881.

[207] Schopfer, U.; Schlapbach, A. *Tetrahedron* **2001**, *57*, 3069-3073.

[208] Kornblum, N.; Cheng, L.; Kerber, R. C.; Kestner, M. M.; Newton, B. N.; Pinnick, H. W.; Smith, R. G.; Wade, P.A. *J. Org. Chem.* **1976**, *41*, 1560-1564.

[209] Wong, Y.-C.; Jayanth, T. T.; Cheng, C.-H. *Org. Lett.* **2006**, *8*, 5613-5616.

[210] Fernández-Rodríguez, M. A.; Hartwig, J. F. *J. Org. Chem.* **2009**, *74*, 1663-1672.

[211] Bates, C. G.; Gujadhur, R. K.; Venkataraman, D. *Org. Lett.* **2002**, *4*, 2803-2806.

2.2.3. Arylation of thiols

Compounds **5cb**,[212] **5cg**,[213] **5ch**,[214] **5ci**[215] and **5cj**,[216] were characterised by comparison of their physical and spectroscopic data with those described in the literature. Data for the new compounds **5** follows:

4-[(3,4-Dichlorophenyl)thio]benzonitrile (5cc): Yellow solid (63 mg, 45%); R_f 0.83 (hexane/EtOAc, 1:1); m.p. 108.6–109.0 ºC; t_R 16.99 min; IR (neat) $\tilde{u}$ = 3035, 2925, 2225, 869, 629, 615 cm^{-1}; ^{1}H NMR (400 MHz, CDCl$_3$): δ = 7.24, 7.54 (AA'XX' system, J = 8.6 Hz, 4H), 7.30 (dd, J = 8.2, 2.1 Hz, 1H), 7.48 (d, J = 8.3 Hz, 1H), 7.56 (d, J = 2.1 Hz, 1H); ^{13}C NMR (101 MHz, CDCl$_3$) δ = 109.9, 118.4, 128.4, 131.6, 131.7, 132.6, 132.7, 133.7, 133.8, 135.0, 143.4. GC-MS (EI): m/z (%) = 283 (M$^+$+4, 15), 282 (M$^+$+3, 11), 281 (M$^+$+2, 71, 280 (M$^+$+1, 18), 279 (M$^+$, 100), 243 (18), 210 (11), 209 (68), 208 (13), 142 (11). HRMS (EI): m/z calcd. for C$_{13}$H$_7$Cl$_2$N$_2$ 278.9676, found 278.9671.
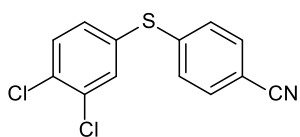
4-{[3,5-Bis(trifluoromethyl)phenyl]thio}benzonitrile (5cd): Yellow oil; (141 mg, 81%); R_f 0.54 (hexane/EtOAc, 9:1); t_R 13.09 min; IR (neat) $\tilde{u}$ = 3104, 3030, 2230, 1592, 1486, 1350, 1275, 1130, 822, 681 cm^{-1}. ^{1}H NMR (300 MHz, CD$_3$OD) δ = 7.49, 7.74 (AA'XX' system, J = 8.3 Hz, 4H), 7.73–7.97 (m, 3H). ^{13}C NMR (75 MHz, CD$_3$OD) δ = 111.1, 117.7, 118.8, 121.5, 122.9 (q, $^1J_{C-F}$ = 272.3 Hz), 130.5, 131.6 (q, $^3J_{C-F}$ = 2.9 Hz), 132.6 (q, $^2J_{C-F}$ = 33.6 Hz), 132.9, 137.5, 140.8. GC-MS (EI) m/z (%) = 348 (M$^+$+1, 16), 347 (M$^+$, 100), 328 (11), 326 (13), 258 (22). HRMS (EI): m/z calcd. for C$_{15}$H$_7$F$_6$NS 347.0203, found 347.0205.
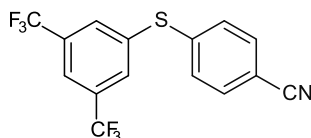
4-[(1-Methyl-1H-imidazol-2-yl)thio]benzonitrile (5ce): Yellow solid; (56 mg, 52%); R_f 0.25 (hexane/EtOAc, 1:1); m.p. 104.0–104.6 ºC; t_R 15.49 min; IR (neat) $\tilde{u}$ = 3045, 3194, 2761, 2223, 658, 618 cm^{-1}. ^{1}H NMR (300 MHz, CDCl$_3$) δ = 3.68 (s, 3H), 7.11, 7.51 (AA'XX' system, J = 8.5 Hz, 4H), 7.17 (s, 1H), 7.27 (s, 1H). ^{13}C NMR (75 MHz, CDCl$_3$) δ = 33.9, 109.7, 118.4, 124.6, 126.8, 127.6, 130.9, 132.7, 142.7 ppm. GC-MS (EI) m/z (%) =
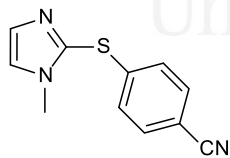
[212] Zhang, J.; Medley, C. M.; Krause, J. A.; Guan, H. *Organometallics* **2010**, *29*, 6393-6401.

[213] Van der Walt, M. M.; Terre'Blanche, G.; Lourens, A. C. U.; Petzer, A.; Petzer, J. P. *Bioorg. Med. Chem. Lett.* **2012**, *22*, 7367-7370.
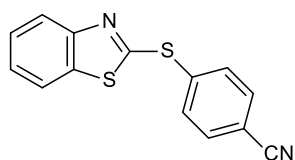
[214] Okauchi, T.; Kuramoto, K.; Kitamura, M. *Synlett* **2010**, 2891-2894.

[215] Jouffroy, M.; Kelly, C. B.; Molander, G. A. *Org. Lett.* **2016**, *18*, 876-879.

[216] Fernández-Rodríguez, M. A.; Shen, Q.; Hartwig, J. F. *Chem. Eur. J.* **2006**, *12*, 7782-7796.
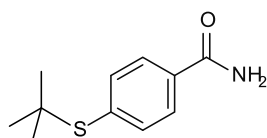
216 (M$^+$+1, 13), 215 (M$^+$, 63), 214 (100), 208 (10), 207 (34), 182 (12), 116 (11), 72 (10). HRMS (EI): *m/z* calcd. for $C_{11}H_9N_3S$ 215.0517, found 215.0501.

4-(Benzo[*d*]thiazol-2-ylthio)benzonitrile (5cf): Yellow solid; (85 mg, 63%); R_f 0.82 (hexane/EtOAc, 1:1); m.p. 91.3–91.8 ºC; t_R 18.13 min; IR (neat) $\tilde{\upsilon}$ = 3070, 2917, 2850, 2225, 1455, 1423, 1006, 829, 758, 727 cm^{-1}. ^{1}H NMR (300 MHz, CDCl$_3$): *δ* = 7.34–7.39 (m, 1H), 7.44–7.49 (m, 1H), 7.67–7.78 (m, 5H), 7.94–7.96 (d, *J* = 8.2 Hz, 1H). ^{13}C NMR (75 MHz, CDCl$_3$) *δ* = 112.9, 118.0, 121.1, 122.7, 125.4, 126.6, 133.0, 133.1, 136.0, 137.6, 153.4, 163.6. GC-MS (EI) *m/z* (%) = 269 (M$^+$+1, 21), 268 (M$^+$, 67), 267 (100), 208 (12), 207 (35). HRMS (EI): *m/z* calcd. for $C_{14}H_8N_2S_2$ 268.0129, found 268.0153.

4-(*tert*-Butylthio)benzamide (5si): Yellow solid; (63 mg, 60%); R_f 0.25 (hexane/EtOAc, 1:1); m.p. 138.9–139.1 ºC; t_R 14.49 min; IR (neat) $\tilde{\upsilon}$ = 3398, 3199, 2922, 2854, 1645, 1612, 1456, 1400, 1361, 1300, 1149, 1086, 848, 781 cm^{-1}. ^{1}H NMR (300 MHz, (CD$_3$)$_2$SO) *δ* = 1.20 (s, 9H), 7.38 (s, 1H), 7.50, 7.80 (AA'XX' system, *J* = 8.3 Hz, 4H), 7.98 (s, 1H). ^{13}C NMR [75 MHz, (CD$_3$)$_2$SO] *δ* = 30.2, 45.7, 127.3, 134.0, 135.3, 135.8, 166.9. GC-MS (EI) *m/z* (%) = 209 (M$^+$, 15), 153 (100), 137 (41), 136 (15), 57 (41). HRMS (EI) *m/z*: calcd. for $C_{11}H_{15}NOS$ 209.0874, found 209.0870.

2.2.4. Arylation of azoles

All compounds **7** were characterised by comparison of their physical and spectroscopic data with those described in the literature: **7ca**,[217] **7cb**,[217] **7cc**,[218] and **7cd**.[219]

[217] Choudary, B. M.; Sridhar, C.; Kantam, M. L.; Venkanna, G. T.; Sreedhar, B. *J. Am. Chem. Soc.* **2005**, *127*, 9948-9949.

[218] Zhang, H.; Cai, Q.; Ma, D. *J. Org. Chem.* **2005**, *70*, 5164-5173.

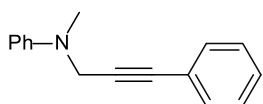[219] Lane, B. S.; Sames, D. *Org. Lett.* **2004**, *6*, 2897-2900.

Experimental part of Chapter 3

3.1. General procedure for the CDC of tertiary amines and terminal alkynes catalysed by CuNPs/ZY (Tables 23 and 24)

The tertiary amine (**8**, 1 mmol), the alkyne (**2**, 1 equiv.) and t-BuOOH-H_2O (2 equiv.) were added to a reactor tube containing CuNPs/ZY (1.5 mol%) under air. The reaction mixture was warmed to 70 °C and stirred at that temperature for 20 h. The resulting mixture was diluted with EtOAc (15 mL), filtered through Celite and subjected to column chromatography (silica gel, hexane-ethyl acetate) to give the pure propargylamines **9**. The catalyst could be recovered by diluting the reaction crude with EtOAc (15 mL), followed by centrifugation (2500 rpm, 15 min), catalyst separation and washing (EtOAc), and final drying under vacuum.
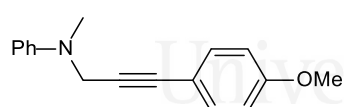
3.2. Physical and spectroscopic data

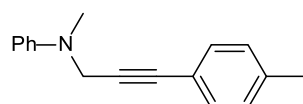**N-Methyl-N-(3-phenylprop-2-yn-1-yl)aniline (9aa)**.[124] Yellow oil (217 mg, 98%); R_f 0.63 (hexane/EtOAc, 9:1); t_R 15.05 min; IR (neat) $\tilde{v}$ = 3068, 3026, 2883, 2808, 1598, 1577, 1503, 1489, 1453, 1442, 1359, 1335, 1240, 1196, 1112, 1030, 995, 922, 750, 715, 688 cm^{-1}. ^{1}H RMN (300 MHz, CDCl$_3$) δ = 7.38–7.26 (m, 7H), 6.93–6.90 (m, 2H), 6.81 (tt, J = 7.4, 1.0 Hz, 1H), 4.26 (s, 2H), 3.03 (s, 3H); ^{13}C NMR (75 MHz, CDCl$_3$) δ = 149.3, 131.7, 129.1, 128.2, 128.1, 123.2, 118.2, 114.4, 85.0, 84.1, 43.3, 38.7; GC-MS (EI) m/z (%) = 222 (M$^+$+1, 16), 221 (M$^+$, 99), 220 (91), 144 (19), 116 (11), 115 (100), 104 (14), 89 (11), 77 (23).

N-[3-(4-Methoxyphenyl)prop-2-yn-1-yl]-N-methylaniline (9ab).[124] Yellow solid (226 mg, 90%); R_f 0.51 (hexane/EtOAc, 9:1); m.p. 68–69 °C; t_R 16.84 min; IR (neat) $\tilde{v}$ = 3068, 3042, 3009, 2958, 2824, 2224, 1598, 1570, 1505, 1495, 1462, 1452, 1439, 1368, 1319, 1291, 1267, 1246, 1234, 1204, 1194, 1183, 1168, 1105, 1029, 1012, 999, 984, 974, 960, 916, 872, 834, 815, 801, 753, 692, 678, 642 cm^{-1}. ^{1}H NMR (400 MHz, CDCl$_3$) δ = 7.31–7.26 (m, 4H), 6.91 (d, J = 8.0 Hz, 2H), 6.82–6.78 (m, 3H), 4.24 (s, 2H), 3.78 (s, 3H), 3.03 (s, 3H); ^{13}C NMR (101 MHZ, CDCl$_3$) δ = 159.5, 149.5, 133.3, 129.2, 118.2, 115.2, 114.5, 113.9, 84.1, 83.6, 55.4, 43.5, 38.8; GC-MS (EI) m/z (%) = 251 (M$^+$, 28), 250 (13), 146 (12), 145 (100), 102 (12), 77 (12).
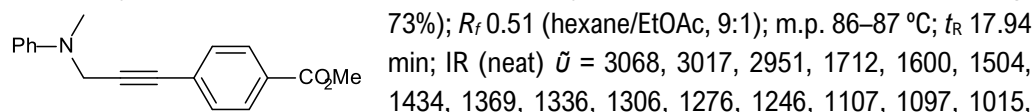
N-Methyl-N-[3-(p-tolyl)prop-2-yn-1-yl]aniline (9ac).[124] Orange solid (205 mg, 87%); R_f 0.66 (hexane/EtOAc, 9:1); m.p. 91–92 °C; t_R 15.81 min; IR (neat) $\tilde{v}$ = 3063, 3030, 2921, 2870, 2812, 2228, 1598, 1504, 1453, 1334, 1238, 1199, 1010, 1034, 995, 922, 815, 750, 689, 664 cm^{-1}.
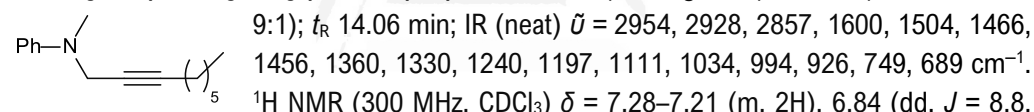
^{1}H NMR (400 MHZ, CDCl$_3$) δ = 7.29–7.25 (m, 4H), 7.06 (d, J = 7.9 Hz, 2H), 6.91 (dd, J = 8.8, 0.9 Hz, 2H), 6.82–6.78 (m, 1H), 4.25 (s, 2H), 3.02 (s, 3H), 2.31 (s, 3H); ^{13}C NMR (101 MHz, CDCl$_3$) δ = 149.5, 138.3, 132.5, 131.8, 129.2, 129.1, 120.1, 118.2, 114.5, 84.3, 43.5, 38.8, 21.6; GC-MS (EI) m/z (%) = 236 (M$^+$+1, 11), 235 (M$^+$, 65), 234 (52), 144 (10), 129 (100), 128 (27), 127 (12), 77(19).

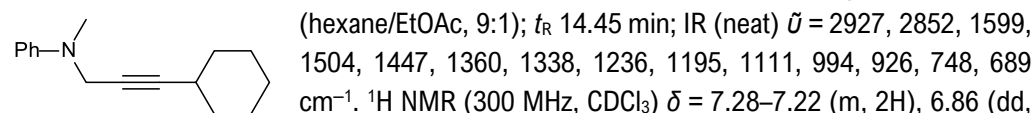**Methyl 4-{3-[methyl(phenyl)amino]prop-1-yn-1-yl}benzoate (9ae).** Yellow solid (204 mg, 73%); R_f 0.51 (hexane/EtOAc, 9:1); m.p. 86–87 ºC; t_R 17.94 min; IR (neat) $\tilde{u}$ = 3068, 3017, 2951, 1712, 1600, 1504, 1434, 1369, 1336, 1306, 1276, 1246, 1107, 1097, 1015, 995, 924, 863, 768, 751, 733, 690, 611 cm^{-1}. ^{1}H NMR (300 MHz, CDCl$_3$) δ = 7.95–7.91 (m, 2H), 7.43–7.39 (m, 2H), 7.31–7.25 (m, 2H), 6.92–6.89 (m, 2H), 6.82 (tt, J = 7.5, 1.0 Hz, 1H), 4.28 (s, 2H), 3.90 (s, 3H), 3.04 (s, 3H); ^{13}C NMR (75 MHz, CDCl$_3$) δ = 166.7, 149.3, 131.8, 129.6, 129.5, 129.3, 127.9, 118.4, 114.5, 88.4, 83.6, 52.3, 43.5, 38.9; GC-MS (EI) m/z (%) = 280 (M$^+$+1, 18), 279 (M$^+$, 100), 278 (90), 219 (10), 173 (48), 144 (18), 114 (17), 77 (14); elemental analysis calcd for C$_{18}$H$_{17}$NO$_2$: C 77.40, H 6.13, N 5.01, found: C 77.06, H 5.93, N 4.86.

N-Methyl-N-(non-2-yn-1-yl)aniline (9af).[139] Brown oil (183 mg, 80%); R_f 0.77 (hexane/EtOAc, 9:1); t_R 14.06 min; IR (neat) $\tilde{u}$ = 2954, 2928, 2857, 1600, 1504, 1466, 1456, 1360, 1330, 1240, 1197, 1111, 1034, 994, 926, 749, 689 cm^{-1}. ^{1}H NMR (300 MHz, CDCl$_3$) δ = 7.28–7.21 (m, 2H), 6.84 (dd, J = 8.8, 1.0 Hz, 2H), 6.78–6.75 (m, 1H), 4.00 (t, J = 2.1 Hz, 2H), 2.94 (s, 3H), 2.16–2.10 (m, 2H), 1.46–1.39 (m, 2H), 1.34–1.23 (m, 6H), 0.87 (t, J = 6.9 Hz, 3H); ^{13}C NMR (75 MHz, CDCl$_3$) δ = 149.6, 129.1, 118.0, 114.4, 84.6, 75.4, 43.0, 38.6, 31.4, 28.9, 28.6, 22.7, 18.8, 14.2; GC-MS (EI) m/z (%) = 229 (M$^+$, 64), 228 (100), 172 (19), 170 (12), 159 (11), 158 (62), 157 (17), 156 (12), 145 (11), 144 (90), 143 (15), 132 (76), 131 (11), 120 (17), 107 (20), 106 (26), 103 (12), 104 (21), 91 (10), 79 (12), 77 (40), 51 (10).

N-(3-Cyclohexylprop-2-yn-1-yl)-N-methylaniline (9ag). Yellow oil (216 mg, 95%); R_f 0.77 (hexane/EtOAc, 9:1); t_R 14.45 min; IR (neat) $\tilde{u}$ = 2927, 2852, 1599, 1504, 1447, 1360, 1338, 1236, 1195, 1111, 994, 926, 748, 689 cm^{-1}. ^{1}H NMR (300 MHz, CDCl$_3$) δ = 7.28–7.22 (m, 2H), 6.86 (dd, J = 8.8, 1.0 Hz, 2H), 6.81–6.76 (m, 1H), 4.02 (d, J = 2.1 Hz, 2H,), 2.95 (s, 3H), 2.36–2.30 (m, 1H), 1.74–1.56 (m, 5H), 1.45–1.27 (m, 5H); ^{13}C NMR (75 MHz, CDCl$_3$) δ = 149.9, 129.1, 118.1, 114.6, 88.8, 74.1, 43.1, 38.6, 32.9, 29.1, 26.0, 24.9; GC-MS (EI) m/z (%) = 228 (M$^+$+1, 75), 227 (M$^+$, 75), 226 (100), 170 (10), 144 (51), 132 (19), 120 (12), 106 (13), 104 (11), 91 (11), 79 (12), 77 (28); HRMS (EI) m/z calcd for C$_{16}$H$_{21}$N 227.1614, found 227.1654.

N-(7-Chlorohept-2-yn-1-yl)-N-methylaniline (9ah). Orange oil (219 mg, 93%); R_f 0.60 (hexane/EtOAc, 9:1); t_R 14.60 min; IR (neat) $\tilde{u}$ = 3021, 2945, 2861, 1599, 1504, 1454, 1428, 1361, 1331, 1301, 1240, 1197, 1110, 1033, 994, 925, 751, 690, 669, 649 cm^{-1}. ^{1}H NMR (300 MHz, CDCl$_3$) δ = 7.28–7.22 (m, 2H), 6.86–6.76 (m, 3H), 4.00 (t, J = 2.1 Hz, 2H), 3.48 (t, J = 6.5 Hz, 2H), 2.94 (s, 3H), 2.20–2.16 (m, 2H), 1.83–1.74 (m, 2H), 1.63–1.53 (m, 2H); ^{13}C NMR (75 MHz, CDCl$_3$) δ = 149.5, 129.1, 118.1, 114.5, 83.6, 76.3, 44.7, 43.0, 38.7, 31.5, 26.0, 18.1; GC-MS (EI) m/z (%) = 237 (M$^+$+2, 23), 236 (M$^+$+1, 39), 235 (M$^+$, 70), 234 (91), 200 (26), 198 (23), 172 (11), 170 (13), 159 (13), 158 (50), 157 (36), 156 (20), 145 (11), 144 (77), 143 (19), 133 (11), 132 (100), 131 (10), 120 (13), 117 (13), 107 (11), 106 (31), 105 (14), 104 (27), 91 (19), 79 (16), 78 (13), 77 (63), 65 (11), 51 (16); HRMS (EI) m/z calcd for C$_{14}$H$_{18}$ClN 235.1128, found 235.1122.
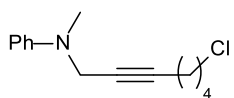
Ethyl 4-[methyl(phenyl)amino]but-2-ynoate (9ai). Brown oil (187 mg, 86%); R_f 0.43 (hexane/EtOAc, 9:1); t_R 13.60 min; IR (neat) $\tilde{u}$ = 2996, 2957, 2927, 2224, 1707, 1600, 1504, 1364, 1237, 1114, 1054, 1034, 995, 923, 749, 690 cm^{-1}. ^{1}H NMR (300 MHz, CDCl$_3$) δ = 7.30–7.25 (m, 2H), 6.85–6.81 (m, 3H), 4.19 (q, J = 7.1 Hz, 2H), 4.18 (s, 2H), 2.99 (s, 3H), 1.27 (t, J = 7.1 Hz, 3H); ^{13}C NMR (75 MHz, CDCl$_3$) δ = 153.4, 148.7, 129.3, 118.8, 114.4, 83.5, 76.2, 62.1, 42.7, 38.9, 14.1; GC-MS (EI) m/z (%) = 217 (M$^+$, 32), 188 (14), 172 (33), 145 (62), 144 (100), 120 (28), 106 (15), 105 (11), 104 (18), 77 (42), 51 (10); HRMS (EI) m/z calcd for C$_{13}$H$_{15}$NO$_2$ 217.1103, found 217.1099.

1-{3-[Methyl(phenyl)amino]prop-1-yn-1-yl}cyclohexanol (9aj). Orange oil (183 mg, 75%); R_f 0.46 (hexane/EtOAc, 7:3); t_R 15.29 min; IR (neat) $\tilde{u}$ = 3390, 2931, 1599, 1502, 1442, 1331, 1069, 1057, 963, 752, 690 cm^{-1}. ^{1}H NMR (300 MHz, CDCl$_3$) δ = 7.28–7.21 (m, 2H), 6.87–6.84 (m, 2H), 6.79 (ddd, J = 8.3, 2.0, 1.0 Hz, 1H), 4.07 (s, 2H), 2.95 (s, 3H), 1.84–1.79 (m, 2H), 1.62–1.33 (m, 9H); ^{13}C NMR (75 MHz, CDCl$_3$) δ = 149.4, 129.1, 118.4, 114.7, 87.9, 79.8, 68.9, 43.1, 40.2, 38.8, 25.2, 23.4; GC-MS (EI) m/z (%) = 244 (M$^+$+1, 14), 243 (M$^+$, 89), 242 (100), 186 (13), 172 (11), 146 (30), 145 (16), 144 (83), 132 (57), 131 (16), 120 (32), 107 (26), 106 (33), 105 (14), 104 (18), 91 (13), 79 (16), 77 (43), 55 (15); HRMS (EI) m/z calcd for C$_{16}$H$_{21}$NO 243.1623, found 243.1610.
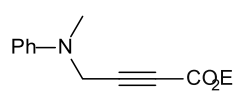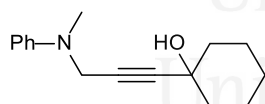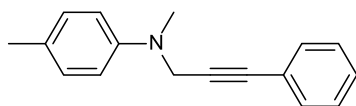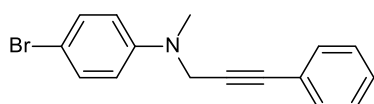
N,4-Dimethyl-N-(3-phenylprop-2-yn-1-yl)aniline (9ba).[124] Yellow oil (205 mg, 87%); R_f 0.54 (hexane/EtOAc, 9:1); t_R 15.95 min; IR (neat) $\tilde{u}$ = 3026, 2918, 2868, 1615, 1518, 1489, 1333, 1239, 1191, 921, 804, 755, 690 cm^{-1}. ^{1}H NMR (300 MHz, CDCl$_3$) δ = 7.38–
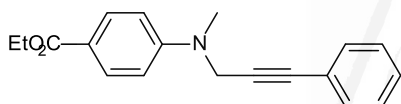
7.35 (m, 3H), 7.27–7.25 (m, 2H), 7.08, 6.84 (AA'XX' system, 4H), 4.22 (s, 2H), 2.99 (s, 3H), 2.27 (s, 3H); ^{13}C NMR (75 MHz, CDCl$_3$) δ = 147.3, 131.7, 129.6, 128.2, 123.1, 115.0, 85.1, 84.2, 43.8, 39.0, 20.3; GC-MS (EI) m/z (%) = 236 (M$^+$+1, 19), 235 (M$^+$, 100), 243 (70), 220 (12), 158 (13), 120 (25), 118 (18), 91 (27), 65 (12).

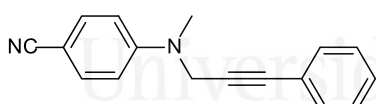**4-Bromo-*N*-methyl-*N*-(3-phenylprop-2-yn-1-yl)aniline (9ca)**.[124] Yellow oil (270 mg, 90%); R_f 0.37 (hexane/EtOAc, 9:1); t_R 17.45 min; IR (neat) ũ = 3013, 2954, 2879, 2820, 2235, 1593, 1493, 1362, 1338, 1259, 1196, 1111, 1017, 921, 808, 756, 690 cm^{-1}; ^{1}H NMR (300 MHz, CDCl$_3$) δ = 7.37–7.35 (m, 5H), 7.28, 6.76 (AA'XX' system, 4H), 7.27 (m, 1H), 4.23 (s, 2H), 3.01 (s, 3H); ^{13}C NMR (75 MHz, CDCl$_3$) δ = 148.2, 131.8, 131.7, 128.2, 122.8, 115.9, 110.2, 84.4, 84.3, 43.3, 38.8; GC-MS (EI) m/z (%) = 301 (M$^+$+1, 34), 300 (M$^+$, 27), 299 (37), 298 (22), 220 (11), 184 (13), 116 (15), 115 (100), 89 (10).

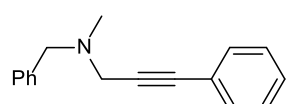**Ethyl 4-[methyl(3-phenylprop-2-yn-1-yl)amino]benzoate (9da)**. Yellow oil (126 mg, 43%); R_f 0.63 (hexane/EtOAc, 7:3); t_R 19.69 min; IR (neat) ũ = 3011, 2991, 2908, 1698, 1602, 1522, 1276, 1182, 1103, 769, 757, 693 cm^{-1}; ^{1}H NMR (300 MHz, CDCl$_3$) δ = 7.95, 6.83 (AA'XX' system, 4H), 7.35–7.28 (m, 2H), 7.27–7.25 (m, 3H), 4.36–4.29 (q, J = 7.1 Hz, 4H), 3.12 (s, 3H), 1.37 (t, J = 7.1 Hz, 3H); ^{13}C NMR (75 MHz, CDCl$_3$) δ = 166.9, 152.2, 131.7, 131.2, 128.2, 122.6, 118.9, 84.3, 84.1, 60.2, 42.7, 38.4, 14.5; GC-MS (EI) m/z (%) = 294 (M$^+$+1, 15), 293 (M$^+$, 72), 292 (19), 264 (31), 248 (16), 116 (11), 115 (100); HRMS (EI) m/z calcd for C$_{19}$H$_{19}$NO$_2$ 293.1416, found 293.1417.

4-[Methyl(3-phenylprop-2-yn-1-yl)amino]benzonitrile (9ea). Yellow oil (123 mg, 50%); R_f 0.47 (hexane/EtOAc, 7:3); t_R 18.42 min; IR (neat) ũ = 3063, 2908, 2211, 1604, 1520, 1372, 1177, 920, 826, 757 cm^{-1}; ^{1}H NMR (300 MHz, CDCl$_3$) δ = 7.52, 6.82 (AA'XX' system, 4H), 7.39–7.30 (m, 5H), 4.32 (s, 2H), 3.13 (s, 3H); ^{13}C NMR (75 MHz, CDCl$_3$) δ = 151.5, 133.5, 133.4, 131.7, 128.5, 128.3, 122.4, 112.8, 99.1, 84.5, 83.5, 42.6, 38.4; GC-MS (EI) m/z (%) = 246 (M$^+$, 50), 116 (11), 115 (100), 102 (10); HRMS (EI) m/z calcd for C$_{17}$H$_{14}$N$_2$ 246.1157, found 246.1140.

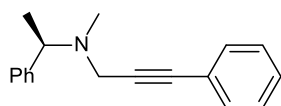**_N_-Benzyl-*N*-methyl-3-phenylprop-2-yn-1-amine (9fa)**.[124] Orange oil (173 mg, 73%); R_f 0.60 (hexane/EtOAc, 7:3); t_R 14.99 min; IR (neat) ũ = 3026, 2927, 2829, 2782, 1599, 1489, 1453, 1442, 1364, 1324, 1123, 1072, 1026, 912, 826, 755, 738, 690 cm^{-1}; ^{1}H NMR (300 MHz, CDCl$_3$) δ = 7.49–7.45 (m, 2H), 7.36–7.35 (m, 2H), 7.33–7.24 (m, 6H), 3.64 (s, 2H), 3.52 (s, 2H), 2.41 (s, 3H); ^{13}C NMR (75 MHz, CDCl$_3$) δ = 138.4, 131.8, 129.3, 128.3, 128.3, 128.0, 127.2,
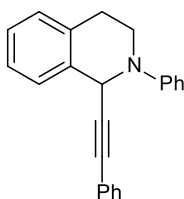
123.3, 85.7, 84.4, 60.3, 45.8, 42.0; GC-MS (EI) m/z (%) = 235 (M⁺, 23), 234 (31), 158 (37), 144 (24), 132 (10), 118 (13), 116 (16), 115 (100), 92 (11), 91 (64).

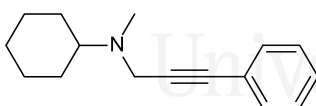**(R)-N-Methyl-3-phenyl-N-(1-phenylethyl)prop-2-yn-1-amine (9ga)**. Orange oil (175 mg, 70%); R_f 0.63 (hexane/EtOAc, 7:3); t_R 15.24 min; $[α]^{25}$ + 203º (CHCl₃, c 1.00); IR (neat) $ũ$ = 3056, 3035, 2967, 2794, 1604, 1489, 1448, 1322, 1070, 1028, 754, 699, 690 cm⁻¹; ¹H NMR (300 MHz, CDCl₃) $δ$ = 7.52–7.47 (m, 2H), 7.42–7.28 (m, 8H), 3.69, 3.46 (AB system, J = 17.4 Hz, 2H), 3.68 (d, J = 6.6 Hz, 1H), 2.42 (s, 3H), 1.45 (d, J = 6.6 Hz, 3H); ¹³C NMR (75 MHz, CDCl₃) $δ$ = 144.6, 131.9, 128.5, 128.4, 128.1, 127.6, 127.2, 123.5, 85.6, 84.8, 62.6, 44.9, 40.1, 21.3; GC-MS (EI) m/z (%) = 249 (M⁺, 7), 235 (16), 234 (87), 172 (13), 144 (11), 118 (13), 115 (100), 105 (20), 77 (12); HRMS (EI) m/z calcd for C₁₈H₁₉N 249.1517, found 249.1510.

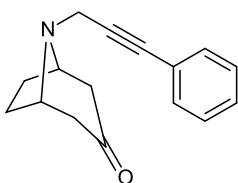**2-Phenyl-1-(phenylethynyl)-1,2,3,4-tetrahydroisoquinoline (9ha)**.[135a] Yellow oil (192 mg, 62%); R_f 0.56 (hexane/EtOAc, 9:1); t_R 21.69 min; IR (neat) $ũ$ = 3059, 3024, 2957, 2922, 1659, 1596, 1502, 1489, 1451, 1376, 1338, 1260, 1224, 1199, 1026, 937, 922, 754, 747, 731, 710, 689 cm⁻¹; ¹H NMR (300 MHz, CDCl₃) $δ$ = 7.26–7.02 (m, 14H), 5.56 (s, 1H), 3.63–3.58 (m, 2H), 3.08–2.87 (m, 2H);¹³C NMR (75 MHz, CDCl₃) $δ$ = 148.5, 134.3, 133.3, 130.7, 128.1, 127.9, 127.0, 126.9, 126.4, 126.2, 125.2, 121.9, 118.6, 115.6, 87.5, 83.7, 51.3, 42.4, 27.9; GC-MS (EI) m/z (%) = 310 (M⁺+1, 14), 309 (M⁺, 61), 308 (100), 206 (14), 204 (36), 203 (28), 202 (39), 77 (16).

N-Methyl-N-(3-phenylprop-2-yn-1-yl)cyclohexanamine (9ia).[131b] Yellow oil (216 mg, 95%); R_f 0.37 (hexane/EtOAc, 9:1); t_R 14.82 min; IR (neat) $ũ$ = 3009, 2926, 2852, 1489, 1448, 1324, 1041, 754, 690 cm⁻¹; ¹H NMR (300 MHz, CDCl₃) $δ$ = 7.44–7.42 (m, 2H), 7.30–7.28 (m, 3H), 3.64 (s, 2H), 2.44 (m, 1H), 2.43 (s, 3H), 1.99–1.95 (m, 2H), 1.82–1.77 (m, 2H), 1.64–1.61 (m, 2H), 1.31–1.19 (m, 4H);¹³C NMR (75 MHz, CDCl₃) $δ$ = 131.7, 128.2, 127.9, 123.4, 85.6, 84.8, 61.1, 43.7, 38.6, 29.8, 26.1, 25.5; GC-MS (EI) m/z (%) = 227 (M⁺, 15), 184 (27), 171 (39), 170 (51), 116 (30), 115 (100), 94 (32), 68 (15).

8-(3-Phenylprop-2-yn-1-yl)-8-azabicyclo[3.2.1]octan-3-one (9ja). Yellow oil (120 mg, 50%); R_f 0.55 (hexane/EtOAc, 1:1); t_R 16.40 min; IR (neat) $ũ$ = 3025, 2991, 2957, 2924, 2848, 1715, 1638, 1444, 1421, 1197, 1002, 759, 717 cm⁻¹; ¹H NMR (300 MHz, CDCl₃) $δ$ = 7.47–7.44 (m, 2H), 7.32–7.30 (m, 3H), 3.76 (m, 2H), 3.62 (s, 2H), 2.75 (dd, J = 16.8, 4.4 Hz, 2H), 2.28 (dd, J = 16.8, 1.7 Hz, 2H), 2.17–2.13 (m, 2H), 1.68 (m, 2H); ¹³C

NMR (75 MHz, CDCl$_3$) δ = 209.5, 131.8, 128.3, 122.9, 85.8, 84.0, 58.9, 48.5, 41.5, 27.6; GC-MS (EI) m/z (%) = 239 (M$^+$, 9), 238 (11), 210 (11), 197 (42), 196 (12), 182 (18), 181 (23), 180 (14), 128 (26), 116 (10), 115 (100), 89 (11), 82 (17); HRMS (EI) m/z calcd. for C$_{16}$H$_{17}$NO 239.1310, found 239.1305.

Experimental part of Chapter 4

4.1. General procedure for the synthesis of 1,2,3,4-tetrahydroisoquinolines 8

4.1.1. From aryl iodides (8h, 8k, 8n, 8q and 8w)[135b]

1,2,3,4-Tetrahydroisoquinoline (**18a**, 3 mmol) and the aryl iodide (2.5 mmol) were added to a suspension of CuI (0.2 mmol) and K$_3$PO$_4$ (4 mmol) in 2-propanol (2 mL) and ethylene glycol (0.22 mL). The reaction mixture was heated at 90 ºC under an argon atmosphere for 24 h. The reaction crude was diluted with Et$_2$O (3 × 5 mL) followed by extraction with water (3 × 5 mL). The combined organic phases were washed with brine and dried with anhydrous MgSO$_4$. The solvent was removed by rotatory evaporation and the residue was purified by column chromatography (hexane/EtOAc).

4.1.2. From aryl bromides (8l, 8m, 8o, 8r, 8t, 8u, 8v and 8x)[220]

1,2,3,4-Tetrahydroisoquinoline (**18a**, 3 mmol) and the aryl bromide (2.5 mmol) were added to a suspension of Pd(OAc)$_2$ (0.13 mmol), (±)-BINAP (0.14 mmol) and ^{t}BuOK (3.5 mmol) in dry toluene (4 mL). The reaction mixture was heated at 100 ºC under an argon atmosphere for 24 h. The reaction was quenched with water and extracted with CH$_2$Cl$_2$ (3 × 5 mL). The combined organic phases were washed with brine and dried with anhydrous MgSO$_4$. The solvent was removed by rotatory evaporation and purified by column chromatography (hexane/EtOAc).

4.1.3. From aryl fluorides (8p)[221]

1,2,3,4-Tetrahydroisoquinoline (**18a**, 3 mmol) and the 4-fluorobenzonitrile (2.5 mmol) were added to a suspension of Cs$_2$CO$_3$ (6 mmol) in DMSO (6 mL). The reaction mixture was heated at 50 ºC for 1 h. The reaction was quenched with water and extracted with EtOAc (3 × 5 mL). The combined organic phases were washed with brine and dried with anhydrous MgSO$_4$. The solvent was removed by rotatory evaporation and purified by column chromatography (hexane/EtOAc).

[220] Wu, X.; Chen, D.-F.; Chen, S.-S.; Zhu, Y.-F. *Eur. J. Org. Chem.* **2015**, 468-473.

[221] Zhang, W.; Yang, S.; Shen, Z. *Adv. Synth. Catal.* **2016**, *358*, 2392-2397.

4.2. Physical and spectroscopic data

Compounds **8h**,[222] **8m**,[223] **8n**,[163] **8o**,[223] **8p**,[224] **8q**,[163] **8r**,[225] **8s**,[226] **8u**,[226] **8v**,[226] **8x**,[223] **8y**[227] and **8z**[228] were characterised by comparison of their physical and spectroscopic data with those reported in the literature. The characterisation of the new compounds **8t** and **8w** follows:

Characterisation of the new 1,2,3,4-tetrahydroisoquinolines 8

2-(3,5-Dimethoxyphenyl)-1,2,3,4-tetrahydroisoquinoline (8t). Light yellow oil (427 mg, 53%); R_f 0.65 (hexane/EtOAc, 8:2); t_R 17.51 min; IR (neat) $\tilde{v}$ = 3002, 2837, 1583, 1458, 1201, 1149, 1067, 806, 746 cm^{-1}; ^{1}H NMR (400 MHz, CDCl$_3$) δ = 7.29–7.24 (m, 4H; 4 × ArH), 6.27 (d, J = 1.9 Hz, 2H; 2 × ArH), 6.13 (s, 1H; ArH), 4.49 (s, 2H; CH$_2$N), 3.89 (s, 6H; 2 × CH$_3$O), 3.63 (t, J = 5.8 Hz, 2H; CH$_2$C*H*$_2$N), 3.06 (t, J = 5.8 Hz, 2H; C*H*$_2$CH$_2$N); ^{13}C NMR (101 MHz, CDCl$_3$) δ = 161.7, 152.4, 135.0, 134.4 (5 × ArC), 128.5, 126.6, 126.5, 126.2, 94.1, 90.5 (7 × CH), 55.3 (2 × CH$_3$O), 50.3, 50.6, 29.2 (3 × CH$_2$); GC-MS (EI) *m/z* (%) = 270 (M$^+$+1, 16), 269 (M$^+$, 94), 268 (100), 254 (24), 207 (11), 104 (20); HRMS (EI) *m/z* calcd. for C$_{17}$H$_{19}$NO$_2$ 269,1416, found 269.1405.
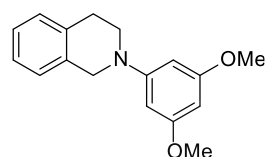
2-(3,4-Dimethoxyphenyl)-1,2,3,4-tetrahydroisoquinoline (8w). White solid (246 mg, 30%); R_f 0.47 (hexane/EtOAc, 8:2); m.p. 86.0–86.9 ºC; t_R 17.01 min; IR (neat) $\tilde{v}$ = 2996, 2828, 1584, 1520, 1243, 1151, 1029, 812, 762 cm^{-1}; ^{1}H NMR (400 MHz, CDCl$_3$) δ = 7.10–7.05 (m, 4H; 4 × ArH), 6.73 (d, J = 8.7 Hz, 1H; ArH), 6.58 (d, J = 2.7 Hz, 1H; ArH), 6.45 (dd, J = 8.7, 2.7 Hz, 1H; ArH), 4.23 (s, 2H; CH$_2$N), 3.81, 3.76 (2s, 6H; 2 × CH$_3$O), 3.38 (t, J = 5.9 Hz, 2H; CH$_2$C*H*$_2$N), 3.92 (t, J = 5.9 Hz, 2H; C*H*$_2$CH$_2$N); ^{13}C NMR (101 MHz, CDCl$_3$) δ = 149.6, 145.8, 143.2, 134.5 (5 × ArC), 128.7, 126.5, 126.3, 126.0, 112.2, 107.8, 102.7 (7 × CH), 56.4, 55.9 (2 × CH$_3$O) 52.3, 48.5, 29.2 (3 × CH$_2$); GC-MS (EI) *m/z* (%) = 270 (M$^+$+1, 16), 269 (M$^+$, 100), 268 (30), 255 (15), 254 (77), 165 (13), 150 (13); HRMS (EI) *m/z* calcd. for C$_{17}$H$_{19}$NO$_2$ 269,1416, found 269.1409.
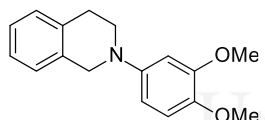
[222] Gajare, A. S.; Toyota, K.; Yoshifuji, M.; Ozawa, F. *J. Org. Chem*. **2004**, *69*, 6504-6506.

[223] Nauth, A. M.; Otto, N.; Opatz, T. *Adv. Synth. Catal*. **2015**, *357*, 3424-3428.

[224] Zhong, J.-J.; Meng, Q.-Y.; Wang, G.-X.; Liu, Q.; Chen, B.; Feng, K.; Tung, C.-H.; Wu, L.-Z. *Chem. Eur. J*. **2013**, *19,* 6443-6450.

[225] Toma, G.; Yamaguchi, R. *Eur. J. Org. Chem*. **2010**, 6404-6408.

[226] Sharma, K.; Borah, A.; Neog, K.; Gogoi, P. *ChemistrySelect* **2016**, *1*, 4620-4623.

[227] Korbad, B. L.; Lee, S.-H. *Chem. Commun.* **2014**, *50*, 8985-8988.

[228] Brzozowski, M.; Forni, J. A.; Savage, P.; Polyzos, A. *Chem. Commun.* **2015**, *51*, 334-337.

4.3. General procedure for the CDC of tetrahydroisoquinolines and nitroalkanes catalysed by CuNPs/TiO$_2$ (Table 29)

The starting tetrahydroisoquinoline (**8**, 0.5 mmol), the nitro compound (**14**, 2.4 or 10 equiv.) and CuNPs/TiO$_2$ (1.5 mol%) were added to a reactor tube under neat conditions. The mixture was warmed to 70 or 100 ºC in air and stirred overnight (*ca*. 15 h). The reaction crude was diluted with EtOAc (3 mL) and filtered through a pad with Celite and MgSO$_4$. The resulting organic phase was subjected to solvent evaporation under vacuum and purification by column chromatography (silica gel, hexane/EtOAc).

4.4. Physical and spectroscopic data

12-Methyl-5,6-dihydroindolo[2,1-*a*]isoquinoline (15ha).[156c] White solid (114 mg, 98%); R_f 0.75 (hexane/EtOAc, 8:2); m.p. 149.0–152.1 ºC [lit.[156c] 148.1–151.8 ºC]; t_R 17.28 min; IR (neat) $\tilde{v}$ = 3042, 2917, 2846, 1604, 1572, 1459, 1355, 1341, 1127, 830, 766, 730 cm^{-1}; ^{1}H NMR (400 MHz, CDCl$_3$) δ = 7.85 (d, J = 7.8 Hz, 1H; ArH), 7.61 (d, J = 7.8 Hz, 1H; ArH), 7.34 (t, J = 7.2 Hz, 1H; ArH), 7.30–7.27 (m, 2H; 2 × ArH), 7.23–7.19 (m, 2H; 2 × ArH), 7.10 (t, J = 7.2 Hz, 1H; ArH), 4.20 (t, J = 6.1 Hz, 2H; CH$_2$N), 3.12 (t, J = 6.1 Hz, 2H; C*H*$_2$CH$_2$N), 2.63 (s, 3H, CH$_3$); ^{13}C NMR (101 MHz, CDCl$_3$) δ = 135.4, 133.6, 130.8, 130.4, 129.5, 107.3 (6 × ArC), 128.5, 127.2, 126.7, 125.7, 122.0, 119.1, 119.0, 108.7 (8 × CH), 40.2, 30.3 (2 × CH$_2$), 10.9 (CH$_3$); GC-MS (EI) *m/z* (%) = 234 (M$^+$+1, 17), 233 (M$^+$, 97), 232 (100), 230 (18), 217 (27), 109 (15).
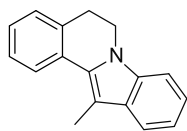
10,12-Dimethyl-5,6-dihydroindolo[2,1-*a*]isoquinoline (15ma). Yellow solid (89 mg, 72%); R_f 0.77 (hexane/EtOAc, 8:2); m.p. 105.2–105.8 ºC; t_R 18.36 min; IR (neat) $\tilde{v}$ = 3011, 2923, 2856, 1596, 1547, 1455, 1340, 1259, 1037, 1030, 797, 764, 739, 669 cm^{-1}; ^{1}H NMR (300 MHz, CDCl$_3$) δ = 7.84 (d, J = 7.8 Hz, 1H; ArH), 7.39–7.18 (m, 5H; 5 × ArH), 7.05–7.03 (m, 1H; ArH), 4.19 (t, J = 6.3 Hz, 2H; CH$_2$N), 3.12 (t, J = 6.3 Hz, 2H; C*H*$_2$CH$_2$N), 2.60, 2.48 (2s, 6H; 2 × CH$_3$); ^{13}C NMR (75 MHz, CDCl$_3$) δ = 133.9, 133.5, 130.9, 130.6, 129.6, 128.3, 106.8 (7 × C), 128.4, 127.2, 126.5, 125.6, 123.7, 118.6, 108.4 (7 × CHAr), 40.2, 30.4 (2 × CH$_2$), 21.7, 10.9 (2 × CH$_3$); GC-MS (EI) *m/z* (%)= 247 (M$^+$, 100), 246 (90), 245 (13), 244 (15), 231 (15), 207 (11). HRMS (EI) *m/z* calcd. for C$_{18}$H$_{17}$N 247.1361, found 247.1349.
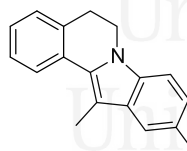
12-Methyl-10-phenyl-5,6-dihydroindolo[2,1-*a*]isoquinoline (15na). Yellow solid (111 mg, 72%); R_f 0.63 (hexane/EtOAc, 8:2); m.p. 121.7–122.8 ºC; t_R 24.20 min; IR (neat) $\tilde{v}$ = 3055, 3035, 2922, 2854, 1597, 1551, 1457, 1262, 798, 754, 744, 735, 693, 669 cm^{-1}; ^{1}H NMR (300 MHz, CDCl$_3$) δ = 7.93 (d, J = 7.8 Hz, 1H; ArH), 7.89 (s, 1H; ArH), 7.76 (d, J = 7.8 Hz, 2H; ArH), 7.54–7.50 (m, 3H; 3 × ArH), 7.45–7.29 (m, 5H; 5 × ArH), 4.26 (t, J = 6.2 Hz, 2H; C*H$_2$*N), 3.17 (t, J = 6.2 Hz, 2H; C*H$_2$*CH$_2$N), 2.74 (s, 3H; CH$_3$); ^{13}C NMR (101 MHz, CDCl$_3$) δ = 142.8, 134.9, 133.5, 132.6, 131.4, 130.3, 129.9, 107.6 (8 × ArC), 128.7, 128.4, 127.4, 127.2, 126.7, 126.3, 125.6, 121.8, 117.4, 108.9 (12 × CH), 40.3, 30.2 (2 × CH$_2$), 10.8 (CH$_3$); GC-MS (EI) *m/z* (%) = 310 (M$^+$+1, 24), 309 (M$^+$, 100), 308 (75), 306 (10), 293 (18), 155 (11), 146 (15), 77 (14). HRMS (EI) *m/z* calcd. for C$_{23}$H$_{19}$N 309.1508, found 309.1502.
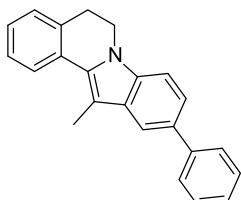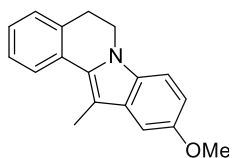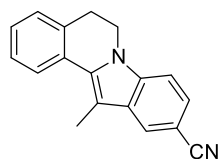
10-Methoxy-12-methyl-5,6-dihydroindolo[2,1-*a*]isoquinoline (15oa). Light orange solid (82 mg, 62%); R_f 0.65 (hexane/EtOAc, 8:2); m.p. 93.7–94.8 ºC; t_R 19.05 min; IR (neat) $\tilde{v}$ = 3000, 2922, 1603, 1491, 1455, 1265, 1219, 1173, 1036, 894, 834, 803, 771 cm^{-1}; ^{1}H NMR (300 MHz, CDCl$_3$) δ = 7.84 (d, J = 7.8 Hz; 1H, ArH), 7.37–7.18 (m, 4H; 4 × ArH), 7.05–7.04 (m, 1H; ArH), 6.90–6.86 (m, 1H; ArH), 4.18 (t, J = 6.2 Hz, 2H; CH$_2$N), 3.89 (s, 3H; CH$_3$O), 3.12 (t, J = 6.2 Hz, 2H; C*H$_2$*CH$_2$N), 2.60 (s, 3H; CH$_3$O); ^{13}C NMR (75 MHz, CDCl$_3$) δ = 133.2, 131.3, 130.7, 130.3, 129.5, 106.7, 127.7 (7 × C), 128.3, 127.0, 126.5, 125.4, 112.2, 109.3, 100.6 (7 × CH), 56.0 (CH$_3$O), 40.2, 30.2 (2 × CH$_2$), 10.9 (CH$_3$); GC-MS (EI) *m/z* (%) = 264 (M$^+$+1, 19), 263 (M$^+$, 100), 262 (32), 248 (13), 220 (52), 218 (13), 204 (18), 132 (11), 108 (11), 102 (22). HRMS (EI) *m/z* calcd. for C$_{18}$H$_{17}$NO 263.1310, found 263.1303.

12-Methyl-5,6-dihydroindolo[2,1-*a*]isoquinoline-10-carbonitrile (15pa). Yellow solid (90 mg, 70%); R_f 0.25 (hexane/EtOAc, 8:2); m.p. 126.7–127.7 ºC; t_R 22.64 min; IR (neat) $\tilde{v}$ = 3000, 2922, 2852, 2217, 1608, 1460, 1339, 877, 805, 775, 767 cm^{-1}; ^{1}H NMR (300 MHz, CDCl$_3$) δ = 7.94 (s, 1H; ArH), 7.85 (d, J = 7.8 Hz, 1H; ArH), 7.44–7.26 (m, 5H; 5 × ArH), 4.25 (t, J = 6.1 Hz, 2H; CH$_2$N), 3.17 (t, J = 6.1 Hz, 2H; C*H$_2$*CH$_2$N), 2.62 (s, 3H; CH$_3$); ^{13}C NMR (75 MHz, CDCl$_3$) δ = 136.8, 133.6, 129.4, 118.6, 108.0, 101.9 (7 × ArC), 132.8 (CN), 128.6, 127.7, 127.5, 126.0, 124.8, 124.5, 121.2, 109.4 (7 × CH), 40.6, 30.0 (2 × CH$_2$), 10.7 (CH$_3$); GC-MS (EI) *m/z* (%) = 259 (M$^+$+1, 15), 258 (M$^+$, 100), 257 (90), 256 (6), 255 (14), 242 (31). HRMS (EI) *m/z* calcd. for C$_{18}$H$_{14}$N$_2$ 258.1157, found 258.1143.

1-(12-Methyl-5,6-dihydroindolo[2,1-*a*]isoquinolin-10-yl)ethan-1-one (15qa). Orange solid (78 mg, 57%); R_f 0.40 (hexane/EtOAc, 8:2); m.p. 105.1–106.2 ºC; t_R 22.20 min; IR (neat) $\tilde{v}$ = 3020, 2952, 2923, 1656, 1384, 1303, 1245, 817, 735, 670 cm^{-1}; ^{1}H NMR (400 MHz, CDCl$_3$) δ = 8.28 (m, 1H; ArH), 7.86–7.83 (m, 2H; ArH), 7.37–7.25 (m, 4H; 4 × ArH), 4.22 (t, J = 6.2 Hz, 2H; CH$_2$N), 3.13 (t, J = 6.2 Hz, 2H; CH_2CH$_2$N), 2.68, 2.65 (2s, 6H; 2 × CH$_3$); ^{13}C NMR (101 MHz, CDCl$_3$) δ = 198.2 (CO), 137.8, 133.4, 132.2, 129.6, 129.1, 128.9, 108.9 (7 × ArC), 128.4, 127.2, 127.1, 125.7, 122.4, 121.0, 108.3 (7 × CH), 40.4, 30.0 (2 × CH$_2$), 26.7, 10.7 (2 × CH$_3$); GC-MS (EI) *m/z* (%) = 276 (M$^+$+1, 24), 275 (M$^+$, 100), 274 (30), 261 (25), 260 (61), 232 (28), 230 (32), 228 (13), 217 (23), 216 (12), 207 (16), 130 (20), 129 (17), 115 (18), 114 (13), 108 (11). HRMS (EI) *m/z* calcd. for C$_{19}$H$_{17}$NO 275.1310, found 275.1297.
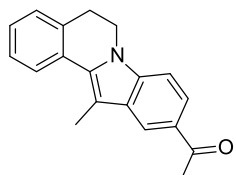
10-Fluoro-12-methyl-5,6-dihydroindolo[2,1-*a*]isoquinoline (15sa). Light yellow solid (113 mg, 90%); R_f 0.62 (hexane/EtOAc, 8:2); m.p. 136.1–136.9 ºC; t_R 17.41 min; IR (neat) $\tilde{v}$ = 3021, 2952, 2923, 1601, 1572, 1458, 1168, 1157, 1118, 849, 797, 763, 738 cm^{-1}; ^{1}H NMR (400 MHz, CDCl$_3$) δ = 7.83 (d, J = 7.8 Hz, 1H; ArH), 7.34–7.14 (m, 5H; 5 × ArH), 6.97–6.93 (td, J = 9.1,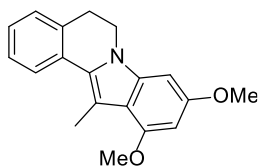 2.5 Hz, 1H; ArH), 4.14 (t, J = 6.3 Hz, 2H; CH$_2$N), 3.09 (t, J = 6.3 Hz, 2H; CH_2CH$_2$N), 2.56 (s, 3H; CH$_3$); ^{13}C NMR (101 MHz, CDCl$_3$) δ = 159.4, 156.3, 133.4 (3 × ArC), 132.2 (d, J_{C-F} = 24.5 Hz, ArC), 130.0 (ArC), 129.7 (d, J_{C-F} = 9.5 Hz, ArC), 107.1 (d, J_{C-F} = 5.0 Hz, ArC), 128.5, 127.2, 127.0, 125.7 (4 × CH), 110.2 (d, J_{C-F} = 26.5 Hz, CH), 109.2 (d, J_{C-F} = 9.6 Hz, CH), 103.7 (d, J_{C-F} = 23.3 Hz, CH), 40.4, 30.2 (2 × CH$_2$), 10.9 (CH$_3$); GC-MS (EI) *m/z* (%) = 252 (M$^+$+1, 16), 515 (M$^+$, 99), 250 (100), 249 (12), 248 (21), 235 (27), 118 (13). HRMS (EI) *m/z* calcd. for C$_{17}$H$_{14}$NF 251.1101, found 251.1095.
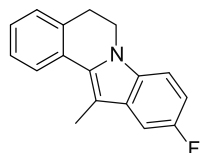
9,11-Dimethoxy-12-methyl-5,6-dihydroindolo[2,1-*a*]isoquinoline (15ta). Light yellow solid (63 mg, 43%); R_f 0.65 (hexane/EtOAc, 8:2); m.p. 77.6–78.2 ºC; t_R 22.09 min; IR (neat) $\tilde{v}$ = 3000, 2920, 2846, 1584, 1456, 1307, 1249, 1203, 1139, 1051, 761, 743 cm^{-1}; ^{1}H NMR (300 MHz, CDCl$_3$) δ = 7.70 (d, J = 7.8 Hz, 1H; ArH), 7.27–7.21 (m, 1H; ArH), 7.19–7.17 (m, 1H; ArH), 7.11–7.09 (m, 1H; ArH), 6.27 (s, 1H; ArH), 6.09–6.08 (m, 1H; ArH), 4.03 (t, J = 6.3 Hz, 2H; CH$_2$N), 3.83, 3.79 (2s, 6H; 2 × CH$_3$O), 3.01 (t, J = 6.3 Hz, 2H; CH_2CH$_2$N), 2.70 (s, 3H; CH$_3$); ^{13}C NMR (75 MHz, CDCl$_3$) δ = 157.5, 156.0, 136.9, 133.0, 130.7, 113.6, 108.5, 91.4 (8 × C), 128.3, 127.0, 125.8, 125.0, 84.5 (6 × CH), 55.8, 55.4 (2 × CH$_3$O), 40.4, 30.5 (2 × CH$_2$), 12.8 (CH$_3$); GC-MS (EI) *m/z* (%) = 294 (M$^+$+1, 16), 293 (M$^+$, 100), 279 (18), 278 (85), 235 (32), 234 (15), 207 (13), 206 (13), 147 (27), 139 (13). HRMS (EI) *m/z* calcd. for C$_{19}$H$_{19}$NO$_2$ 293.1416, found 293.1412.
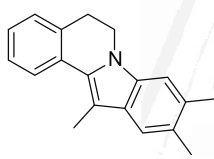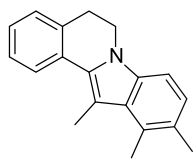
12-Methyl-9,11-bis(trifluoromethyl)-5,6-dihydroindolo[2,1-*a*]isoquinoline (15ua).
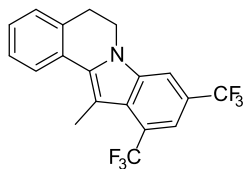
Bright yellow solid (66 mg, 36%); R_f 0.60 (hexane/EtOAc, 8:2); m.p. 88.3–89.7 ºC; t_R 16.71 min; IR (neat) $\tilde{v}$ = 3000, 2952, 2884, 1624, 1546, 1402, 1274, 1147, 1095, 1081, 1039, 874, 764 cm^{-1}; ^{1}H NMR (400 MHz, CDCl$_3$) δ = 7.90 (d, J = 7.8 Hz, 1H; ArH), 7.80 (s, 1H; ArH), 7.73 (s, 1H; ArH), 7.45–7.41 (m, 1H; ArH), 7.37–7.33 (m, 2H; 2 × ArH), 4.29 (t, J = 6.1 Hz, 2H; CH$_2$N), 3.17 (t, J = 6.1 Hz, 2H; CH_2CH$_2$N), 2.71 (d, J = 1.7 Hz, 3H; CH$_3$); ^{13}C NMR (101 MHz, CDCl$_3$) δ = 136.3, 135.6, 134.5, 128.7 (4 × C), 128.4, 128.2, 127.4, 127.0 (4 ×CH), 126.0 (q, $J_{C\text{-}F}$ = 270.1 Hz, CF$_3$), 125.7 (q, $J_{C\text{-}F}$ = 269.7 Hz, CF$_3$), 122.1 (q, $J_{C\text{-}F}$ = 31.7 Hz, *C*CF$_3$), 121.7 (q, $J_{C\text{-}F}$ = 31.5 Hz, *C*CF$_3$), 114.5 (q, $J_{C\text{-}F}$ = 2.7 Hz, *C*HCCF$_3$), 109.9 (q, $J_{C\text{-}F}$ = 2.7 Hz, *C*HCCF$_3$), 107.2 (C), 40.6, 30.0 (2 × CH$_2$), 12.0 (q, J = 2.0 Hz, CH$_3$); GC-MS (EI) *m/z* (%) = 370 (M$^+$+1, 19), 369 (M$^+$, 89), 368 (100), 353 (25), 350 (12), 298 (12), 207 (12), 167 (10), 69 (14). HRMS (EI) *m/z* calcd. for C$_{19}$H$_{13}$F$_6$N 369.0952, found 369.0943.

10,11,12-Trimethyl-5,6-dihydroindolo[2,1-*a*]isoquinoline and 9,10,12-trimethyl-5,6-dihydroindolo[2,1-*a*]isoquinoline (15va, 15va').

Light yellow solid (83 mg, 64%); 50:50 regioisomeric mixture; R_f 0.80 (hexane/EtOAc, 8:2); m.p. 82.1–82.8/87.9–88.7 ºC; t_R 18.84 and 19.28 min; IR (neat) $\tilde{v}$ = 3021, 2919, 2851, 1601, 1542, 1455, 1333, 1255, 991, 874, 838, 792, 761, 742, 792 cm^{-1}; ^{1}H NMR (300 MHz, CDCl$_3$) δ = 7.83 (t, J = 8.4 Hz, 2H; 2 × ArH), 7.38–7.21 (m, 7H; 7 × ArH), 7.10 (s, 1H; ArH), 7.06, 7.02 (AB system, J = 8.4 Hz, 2H; 2 × ArH), 4.17 (t, J = 6.3 Hz, 2H; CH$_2$N), 4.14 (t, J = 6.0 Hz, 2H; CH$_2$N), 3.13 (t, J = 6.3 Hz, 2H; CH_2CH$_2$N), 3.08 (t, J = 6.0 Hz, 2H; CH_2CH$_2$N), 2.86, 2.72, 2.61, 2.42, 2.40, 2.39 (6s, 18H; 6 × CH$_3$); ^{13}C NMR (101 MHz, CDCl$_3$) δ = 134.6, 134.4, 134.2, 133.3, 131.2, 131.1, 130.7, 130.4, 130.0, 129.2, 128.1, 127.9, 127.7, 126.6, 107.8, 106.7 (16 × C), 128.4, 128.3, 127.1, 127.0, 126.5, 126.2, 126.1, 125.3, 124.9, 119.0, 109.2, 106.0 (12 × CH), 40.1, 40.0 (2 × CH$_2$N), 30.6, 30.4 (2 × CH_2CH$_2$N), 20.8, 20.3, 20.0, 16.3, 14.1, 10.9 (6 × CH$_3$); GC-MS (EI) *m/z* (%) = 262 (M$^+$+1, 20), 261 (M$^+$, 100), 260 (79), 258 (11), 245 (10). HRMS (EI) *m/z* calcd. for C$_{19}$H$_{19}$N 261.1517, found 261.1499.

9,10-Dimethoxy-12-methyl-5,6-dihydroindolo[2,1-*a*]isoquinoline (15wa).
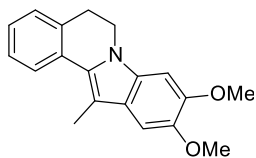
Yellow solid (133 mg, 91%); R_f 0.22 (hexane/EtOAc, 8:2); m.p. 142.5–143.9 ºC; t_R 21.17 min; IR (neat) $\tilde{v}$ = 2923, 1463, 1342, 1247, 1224, 1201, 1156, 1034, 764 cm^{-1}; ^{1}H NMR (400 MHz, CDCl$_3$) δ = 7.79–7.77 (m, 1H; ArH), 7.34–7.30 (m, 1H; ArH), 7.27–7.24 (m, 1H; ArH), 7.19–7.15 (m, 1H; ArH), 7.08 (s, 1H; ArH), 6.78 (s, 1H; ArH), 4.15 (t, J = 6.3 Hz, 2H; CH$_2$N), 3.96 (2s, 6H; 2 × CH$_3$O), 3.11 (t, J = 6.3 Hz, 2H; CH_2CH$_2$N), 2.59 (s,

3H; CH$_3$); ^{13}C NMR (101 MHz, CDCl$_3$) δ = 147.3, 144.8, 132.6, 130.6, 129.8, 129.4, 122.0, 106.9 (8 × C), 128.3, 127.0, 125.9, 124.8, 100.6, 92.1 (6 × CH), 56.5, 56.3 (2 × CH$_3$O), 40.3, 30.2 (2 × CH$_2$), 11.0 (CH$_3$); CG-MS (EI) *m/z* (%) = 294 (24), 293 (M$^+$, 100), 281 (13), 278 (56), 250 (15), 236 (13), 235 (47), 234 (11), 207 (36), 147 (26). HRMS (EI) *m/z* calcd. for C$_{19}$H$_{19}$NO$_2$ 293.1416, found 293.1431.
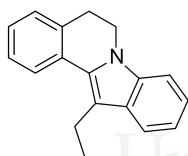
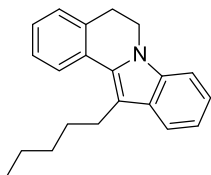**2,3-Dimethoxy-12-methyl-5,6-dihydroindolo[2,1-*a*]isoquinoline (15xa).**[156e] Yellow solid (97 mg, 66%); R_f 0.35 (hexane/EtOAc, 8:2); m.p. 149.6–150.0 ºC [lit.[156e] 148.1–151.8 ºC]; t_R 25.36 min; IR (neat) $\tilde{u}$ = 2922, 2852, 1605, 1551, 1503, 1461, 1248, 1225, 1143, 1070, 858, 822, 742 cm^{-1}; ^{1}H NMR (300 MHz, CDCl$_3$) δ = 7.84 (d, *J* = 7.8 Hz, 1H; ArH), 7.37–7.35 (m, 1H; ArH), 7.29–7.26 (m, 1H; ArH), 7.24–7.22 (m, 1H; ArH), 6.40 (m, 1H; ArH), 6.23 (m, 1H; ArH), 4.15 (t, *J* = 6.3 Hz, 2H; CH$_2$N), 3.96, 3.92 (2s, 6H; 2 × CH$_3$O), 3.13 (t, *J* = 6.3 Hz, 2H; C*H*$_2$CH$_2$N), 2.85 (s, 3H; CH$_3$); ^{13}C NMR (75 MHz, CDCl$_3$) δ = 157.4, 155.9, 136.8, 132.9, 130.6, 128.4, 113.5, 108.3 (8 × ArC), 128.2, 126.9, 125.7, 124.9, 91.3, 84.3 (6 × CH), 55.6, 55.2 (2 × CH$_3$O), 40.3, 30.3 (2 × CH$_2$), 12.7 (CH$_3$); GC-MS (EI) *m/z* (%) = 294 (M$^+$, 5), 293 (21), 281 (24), 208 (19), 207 (100), 133 (10).
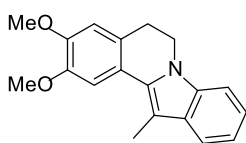
12-Ethyl-5,6-dihydroindolo[2,1-*a*]isoquinoline (15hb).[156e] White solid (106 mg, 86%); R_f 0.70 (hexane/EtOAc, 8:2); m.p. 133.9–135.2 ºC [lit.[156e] 134.5–135.7 ºC]; t_R 17.43 min; IR (neat) $\tilde{u}$ = 3040, 1596, 1536, 1456, 1355, 1341, 1127, 848, 759 cm^{-1}; ^{1}H NMR (300 MHz, CDCl$_3$) δ = 7.84 (d, *J* = 7.8 Hz, 1H; ArH), 7.64 (d, *J* = 7.8 Hz, 1H; ArH), 7.37–7.29 (m, 4H; 4 × ArH), 7.25–7.20 (m, 1H; ArH), 7.14–7.12 (m, 1H; ArH), 4.23 (t, *J* = 6.3 Hz, 2H; CH$_2$N), 3.16–3.08 (m, 4H; C*H*$_2$CH$_2$N, C*H*$_2$CH$_3$), 1.40 (t, *J* = 7.5 Hz, 3H; CH$_3$); ^{13}C NMR (75 MHz, CDCl$_3$) δ = 135.4, 133.6, 130.1, 130.0, 128.5, 114.2 (6 × C), 128.4, 127.2, 126.6, 125.3, 121.9, 118.9, 118.8, 108.6 (8 × CH), 40.0, 30.2, 18.4 (3 × CH$_2$), 15.2 (CH$_3$); GC-MS (EI) *m/z* (%) = 247 (M$^+$, 35), 233 (18), 232 (100), 230 (16), 217 (13).

12-Pentyl-5,6-dihydroindolo[2,1-*a*]isoquinoline (15hc).[229] Light yellow solid (91 mg, 63%); R_f 0.75 (hexane/EtOAc, 8:2); m.p. 92.7–93.8 ºC; t_R 19.19 min; IR (neat) $\tilde{u}$ = 3040, 2952, 1605, 1456, 1326, 1255, 1008, 797, 768, 754 cm^{-1}; ^{1}H NMR (500 MHz, CDCl$_3$) δ = 7.83 (d, *J* = 7.8 Hz, 1H; ArH), 7.63 (d, *J* = 7.8 Hz, 1H; ArH), 7.35–7.19 (m, 5H; 5 × ArH), 7.10 (t, *J* = 7.1 Hz, 1H; ArH), 4.22 (t, *J* = 6.3 Hz, 2H; CH$_2$N), 3.16–3.06 (m, 4H; C*H*$_2$CH$_2$N, CH$_2$C), 1.77–1.74 (m, 2H; C*H*$_2$CH$_2$C), 1.53–1.38 (m, 4H; C*H*$_2$C*H*$_2$CH$_3$),

[229] Chen, Y.-Y.; Chen, J.-H.; Zhang, N.-N.; Ye, L.-M.; Zhang, X.-J.; Yan, M. *Tetrahedron Lett.* **2015**, *56*, 478-481.

0.93 (t, J = 7.2 Hz, 3H; CH$_3$); ^{13}C NMR (125 MHz, CDCl$_3$) δ = 135.4, 133.6, 130.3, 130.2, 129.0, 113.1 (6 × C), 128.4, 127.2, 126.6, 125.3, 121.9, 119.0, 118.9, 108.6 (8 × CH), 40.1, 32.3, 30.5, 30.2, 25.3, 22.6 (6 × CH$_2$), 14.1 (CH$_3$); GC-MS (EI) m/z (%) = 290 (M$^+$+1, 5), 289 (M$^+$, 24), 233 (19), 232 (100), 230 (11).

1-(1-Nitroethyl)-2-(perfluorophenyl)-1,2,3,4-tetrahydroisoquinoline (16ya). Colourless oil (97 mg, 52%); 71:29 *dr*; $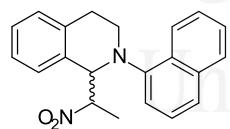R_f$ 0.42 (hexane/EtOAc, 8:2); t_R 16.86 min; IR (neat) $\tilde{υ}$ = 3020, 2982, 1550, 1516, 1500, 1455, 1361, 1054, 1026, 990, 973, 770, 750 cm^{-1}; *NMR data of the major diastereomer*: ^{1}H NMR (500 MHz, CDCl$_3$) δ = 7.32–7.21 (m, 4H; 4 × ArH), 4.81–4.72 (m, 2H; CHNO$_2$, CHN), 3.74–3.65 (m, 1H; C*H*HN), 3.13–3.06 (m, 1H; CH*H*N), 2.94–2.84 (m, 2H; C*H$_2$*CH$_2$N), 1.44 (d, J = 6.3 Hz, 3H; CH$_3$); *NMR data of the minor diastereomer*: ^{1}H NMR (500 MHz, CDCl$_3$) δ = 7.16–7.12 (m, 4H, 4 × ArH), 5.14–5.12 (m, 1H, CHNO$_2$), 4.81–4.72 (m, 1H; CHN), 3.57–3.49 (m, 1H; C*H*HN), 3.24–3.16 (m, 1H; CH*H*N), 3.01–2.97 (m, 2H; C*H$_2$*CH$_2$N), 1.57 (d, J = 6.7 Hz 3H; CH$_3$). *NMR data of the major diastereomer*: ^{13}C NMR (125 MHz, CDCl$_3$) δ = 135.6, 132.2, 125.5 (3 × C), 126.6, 128.2, 128.4, 129.0 (4 × CH), 87.5 (CHNO$_2$), 65.03 (CHN), 47.9, 28.6 (2 × CH$_2$), 17.1 (CH$_3$); *selected NMR data of the minor diastereomer*: ^{13}C NMR (125 MHz, CDCl$_3$) δ = 135.2, 132.9, 125.5 (3 × C), 129.2, 128.0, 127.0, 126.9 (4 × CH), 88.7 (CHNO$_2$), 63.4 (CHN), 48.9, 28.8 (2 × CH$_2$), 17.1 (CH$_3$); *NMR data of the mixture*: 146.3, 142.9, 139.8, 137.0, 136.9, 136.5 (6m, 6 × CF); GC-MS (EI) m/z (%) = 372 (M$^+$, 0.1), 299 (17), 298 (100), 115 (13). HRMS (EI) m/z calcd. for C$_{17}$H$_{13}$N$_2$O$_2$F$_5$ 372.0897, found 372.0883.
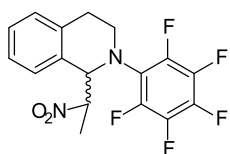
2-(Naphthalen-1-yl)-1-(1-nitroethyl)-1,2,3,4-tetrahydroisoquinoline (16za). Yellow oil (33 mg, 20%); 70:30 *dr*; R_f 0.63 (hexane/EtOAc, 8:2); IR (neat) $\tilde{υ}$ = 3050, 2923, 1548, 1398, 1083, 947, 774, 750 cm^{-1}; *NMR data of the major diastereomer*: ^{1}H NMR (500 MHz, CDCl$_3$) δ = 8.11 (d, J = 8.0 Hz, 1H; ArH), 7.84–7.80 (m, 1H; ArH), 7.61–7.45 (m, 4H; 4 × ArH), 7.33–7.27 (m, 2H; 2 × ArH), 7.24–7.16 (m, 2H; 2 × ArH), 6.87 (d, J = 6.9 Hz, 1H; ArH), 5.14–5.07 (m, 1H; CHNO$_2$), 5.03–4.92 (m, 1H; CHN), 3.90–3.82 (m, 1H; C*H*HN), 3.51–3.43 (m, 1H; CH*H*N), 2.78–2.67 (m, 2H; C*H$_2$*CH$_2$N), 1.63 (d, J = 6.6 Hz, 3H; CH$_3$); *selected NMR data of the minor diastereomer*: ^{1}H NMR (500 MHz, CDCl$_3$) δ = 8.22 (d, J = 8.0 Hz, 1H; ArH), 6.92 (d, J = 7.1 Hz, 1H; ArH), 3.66–3.57 (m, 1H; C*H*HN), 1.74 (d, J = 6.6 Hz, 3H; CH$_3$). *NMR data of the major diastereomer*: ^{13}C NMR (125 MHz, CDCl$_3$) δ = 147.3, 136.3, 134.8, 132.7, 118.5 (5 × C), 129.7, 128.3, 128.1, 127.9, 126.2, 126.0, 125.5, 124.6, 123.6 (11 × CH), 86.6 (CHNO$_2$), 64.5 (CHN), 46.0, 25.4 (2 × CH$_2$), 17.0 (CH$_3$); *selected NMR data of the minor diastereomer*: ^{13}C NMR (125 MHz, CDCl$_3$) δ = 147.9, 135.6, 133.6, 119.2 (C), 129.5, 128.6, 127.8, 126.8, 126.7, 125.69, 125.7, 124.7, 123.5 (CH), 88.4 (CHNO$_2$), 64.1 (CHN), 47.2, 29.7 (2 × CH$_2$),

16.3 (CH$_3$); MS (DIP) *m/z* (%) = 332 (M$^+$, 3), 259 (21), 258 (100), 256 (10), 127 (10). HRMS (EI) *m/z* calcd. for C$_{21}$H$_{20}$N$_2$O$_2$ 332.1525, found 332.1510.

4.5. General procedure for the synthesis of 5,6-dihydroindolo[2.1-*a*]isoquinoline-12-carbaldehyde (17)

A mixture of 12-methyl-5,6-dihydroindolo[2,1-*a*]isoquinoline (**15ha**, 0.3 mmol) and MnO$_2$ (3 equiv.) in toluene-HOAc (3:0.3 mL) was heated at 110 ºC for 1.5 h. The reaction crude was diluted with EtOAc (5 mL) and filtered through a pad of silica, Celite and MgSO$_4$. The filtrate was washed with brine (5 mL) and the organic phase was dried with MgSO$_4$, followed by filtration and solvent evaporation under vacuum. The residue was purified by column chromatography (hexane/EtOAc) to afford the pure product **17**.

4.6. Physical and spectroscopic data

5,6-Dihydroindolo[2,1-*a*]isoquinoline-12-carbaldehyde (17ha).[230] White solid (67 mg, 90%); R_f 0.20 (hexane/EtOAc, 8:2); m.p. 121.8–122.6 ºC [lit.[230] 122.0 ºC]; t_R 20.23 min; IR (neat) $\tilde{v}$ = 3045, 3013, 2830, 1636, 1468, 1453, 1391, 1366, 1329, 1134, 1042, 741, 673 cm^{-1}; ^{1}H NMR (300 MHz, CDCl$_3$) δ = 10.52 (s, 1H; CHO), 8.47–8.44 (m, 1H; ArH), 7.96 (dd, *J* = 5.4, 3.7 Hz, 1H; ArH), 7.45–7.31 (m, 6H; 6 × ArH), 4.25 (t, *J* = 6.5 Hz, 2H; CH$_2$N); 3.18 (t, *J* = 6.5 Hz, 2H; C*H*$_2$CH$_2$N); ^{13}C NMR (75 MHz, CDCl$_3$) δ = 185.7 (C=O), 143.1, 135.7, 135.1, 127.1, 126.8, 113.5 (6 × C), 130.0, 129.1, 128.6, 127.9, 124.1, 123.4, 122.5, 109.3 (8 × CH), 40.2, 29.3 (2 × CH$_2$); GC-MS (EI) *m/z* (%) = 248 (M$^+$+1, 12), 247 (M$^+$, 69), 246 (M$^+$−1, 100), 218 (7), 217 (24), 216 (12), 207 (12)
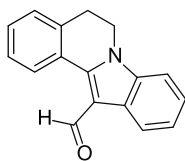
Experimental part of Chapter 5

General procedure for the oxidation of 1,2,3,4,-tetrahydroisoquinoline (18a)

1,2,3,4-Tetrahydroisoquinoline (**18**, 0.5 mmol), was added to a reactor tube containing TiO$_2$ P25 D-E (10 mg) in water or acetonitrile (2 mL) under air. The reaction mixture was irradiated with a LED of 369 nm (0.14 W/cm^2) during 20 h at room temperature. The resulting mixture was extracted or diluted with EtOAc (2 mL), filtered through Celite/MgSO$_4$ and the resulting reaction crude was subjected to GLC analysis.

---

[230] Pintori, D. G.; Greaney, M. F. *J. Am. Chem. Soc.* **2011**, *133*, 1209-1211.

Selected NMR spectra
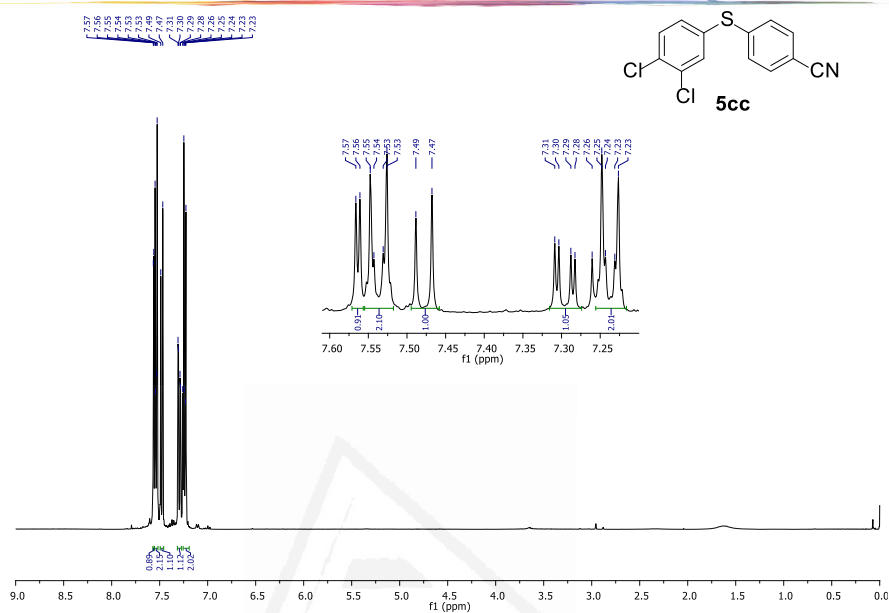
^{1}H NMR (300 MHz, CDCl$_3$)
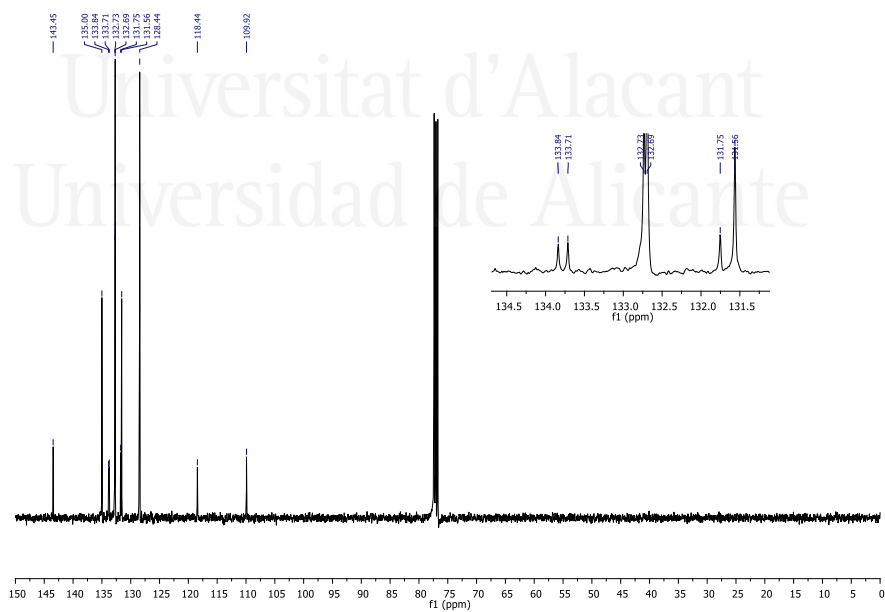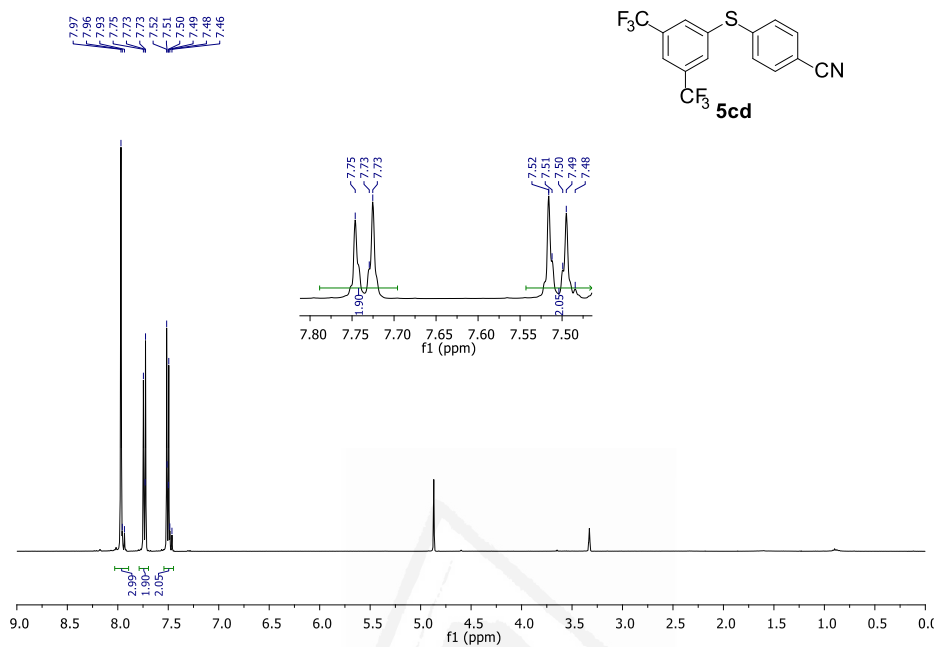
^{13}C NMR (75 MHz, CDCl$_3$)

^{1}H NMR (300 MHz, CD$_3$OD)

^{13}C NMR (75 MHz, CD$_3$OD)
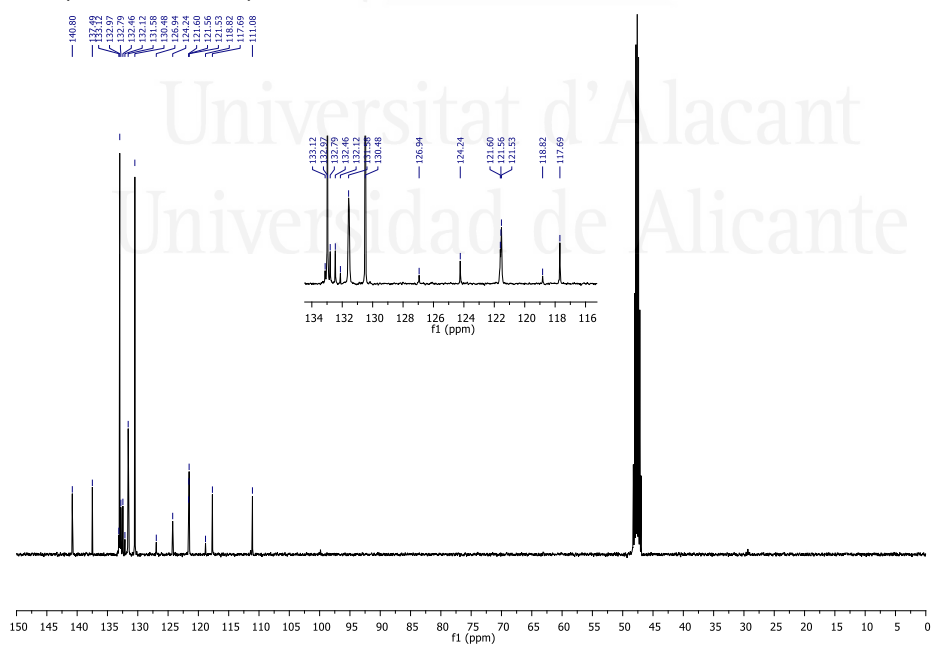
5ce

^{1}H NMR (300 MHz, CDCl$_3$)

^{13}C NMR (75 MHz, CDCl$_3$)

5cf
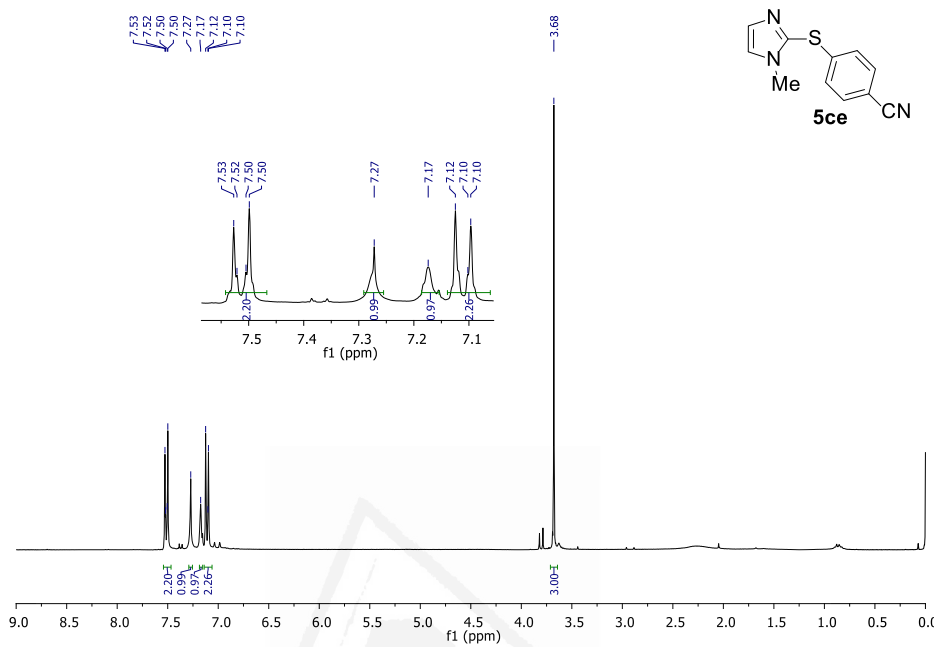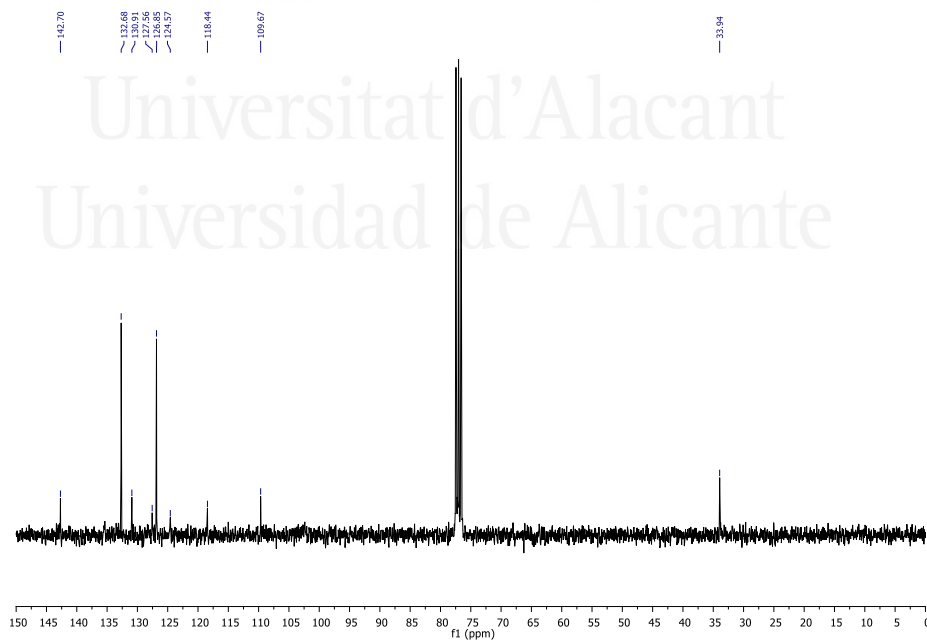
^{1}H NMR (300 MHz, CDCl$_3$)
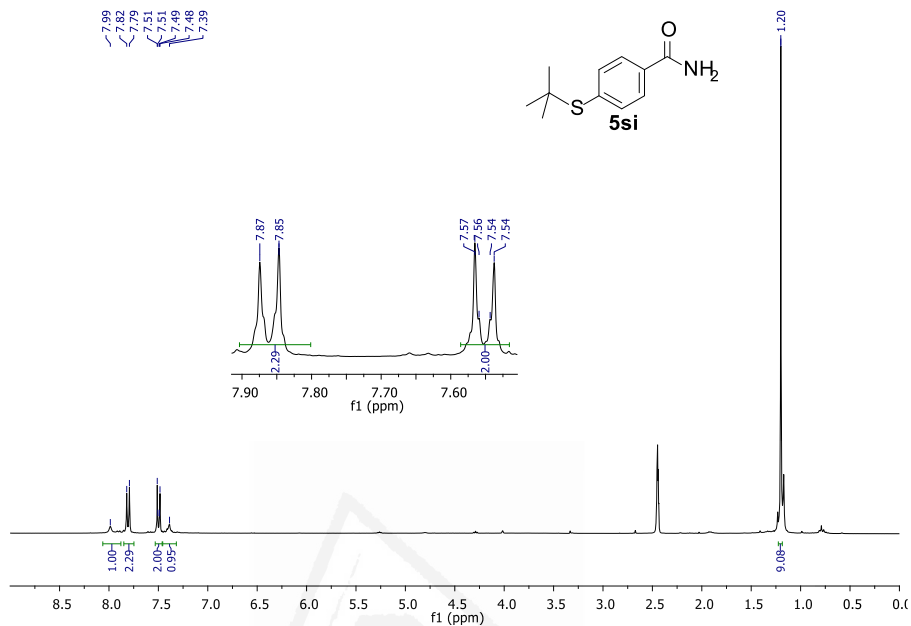
^{13}C NMR (75 MHz, CDCl$_3$)

^{1}H NMR (300 MHz, (CD$_3$)$_2$SO)

^{13}C NMR (75 MHz, (CD$_3$)$_2$SO)

^{1}H NMR (300 MHz, CDCl$_3$)

^{13}C NMR (75 MHz, CDCl$_3$)

^{1}H NMR (300 MHz, CDCl$_3$)

^{13}C NMR (75 MHz, CDCl$_3$)

^{1}H NMR (300 MHz, CDCl$_3$)

^{13}C NMR (75 MHz, CDCl$_3$)

¹H NMR (300 MHz, CDCl₃)

¹³C NMR (75 MHz, CDCl₃)

^{1}H NMR (300 MHz, CDCl$_3$)

^{13}C NMR (75 MHz, CDCl$_3$)

¹H NMR (400 MHz, CDCl₃)

¹³C NMR (101 MHz, CDCl₃)

15va 15va'
(50:50)

^{1}H NMR (300 MHz, CDCl$_3$)

^{13}C NMR (75 MHz, CDCl$_3$)

^{1}H NMR (400 MHz, CDCl$_3$)

^{13}C NMR (101 MHz, CDCl$_3$)

^{1}H NMR (300 MHz, CDCl$_3$)

^{13}C NMR (75 MHz, CDCl$_3$)

15hc
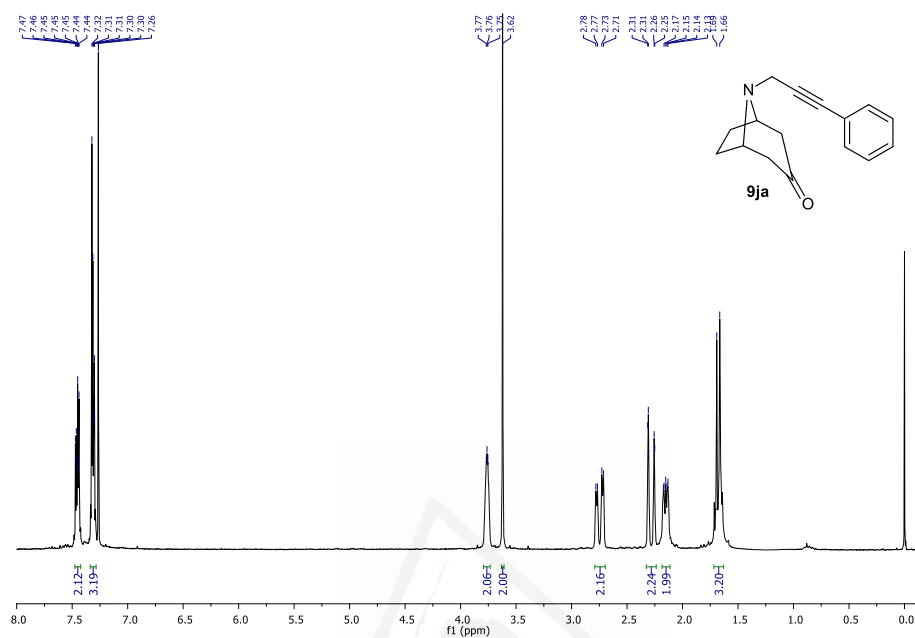
^{1}H NMR (500 MHz, CDCl$_3$)

^{13}C NMR (125 MHz, CDCl$_3$)
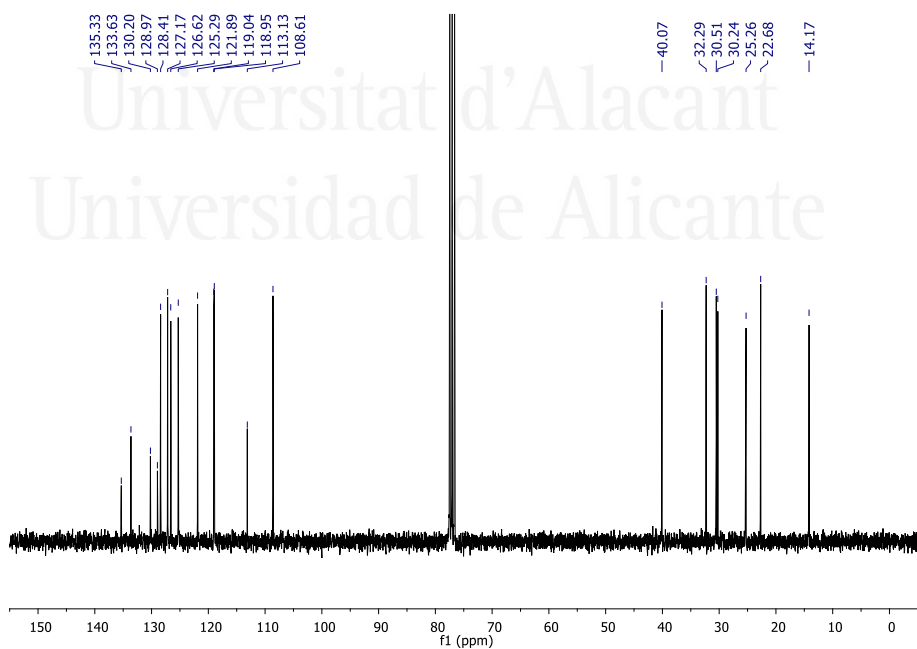
Resumen (Spanish summary)

Resumen (Spanish summary)

En esta tesis se presenta un estudio de carácter multidisciplinar, siendo de interés para una amplia variedad de investigadores en el campo de la Química. Los resultados fruto de este estudio han sido publicados en revistas de carácter internacional y presentados en diferentes simposios. A continuación, se resumen los aspectos más importantes y los resultados desarrollados en esta memoria.

Nanocatálisis y preparación de catalizadores

Actualmente, la nanocatálisis se presenta como una alternativa competitiva y sostenible a la catálisis convencional. Las nanopartículas (NPs) de metales de transición han surgido en los últimos años como una nueva familia de catalizadores capaces de promover de forma eficiente una gran variedad de reacciones de interés en síntesis orgánica. Las propiedades físico-químicas de las nanopartículas metálicas son muy diferentes a las propiedades de partículas condensadas de mayor tamaño. Al producirse cambios en la forma física, también se producen cambios en las propiedades ópticas, electrónicas, magnéticas y catalíticas de los metales. Una de las características que destaca de estos materiales es su elevada relación superficie/volumen, la cual provoca un exceso de energía libre en su superficie haciéndolas termodinámicamente inestables. Por tanto, un aspecto crucial en la formación de NPs es su estabilización.

Además, en muchos casos poseen los requisitos que hoy en día demanda la llamada "catálisis verde", es decir, la síntesis de catalizadores de bajo impacto ambiental, de fácil preparación y con la posibilidad de ser reutilizados sin pérdida de eficiencia.

Existen diversas estrategias para la preparación de nanopartículas metálicas. Estas se pueden clasificar en tres grandes bloques: físicas, químicas y biológicas. Siendo las estrategias químicas las más empleadas para este propósito.

Dentro de los métodos químicos se pueden encontrar la coprecipitación, la reducción química de sales metálicas, la electrólisis, microemulsiones, pirólisis, fitoquímicos y métodos solvo-termales, entre otros. Entre estas estrategias, la reducción química de sales metálicas es una de las más estudiadas. Esta reducción se puede llevar a cabo con diferentes agentes de reducción tales como metales alcalinos activados, disolventes oxidables (alcoholes), hidrógeno, monóxido de carbono e hidruros.

La síntesis de nanopartículas metálicas (NPsM) basada en la reducción de sales con metales alcalinos activados ha sido ampliamente desarrollada en nuestro grupo de investigación. En esta metodología se emplea litio metálico y un areno como agente de

transferencia electrónica. A través de este método se generan metales altamente reactivos, conocidos como metales Rieke. Este método de síntesis ha permitido la obtención de NPsM, tales como de Ni, Cu y de Fe, de tamaño uniforme y con elevada reactividad. La principal ventaja de este método es que la síntesis se hace a temperatura ambiente y en tiempos cortos de reacción, sin la necesidad de añadir agentes de nucleación o estabilizantes. Nuestro grupo de investigación tiene una vasta experiencia en este campo, especialmente en la formación de NPsCu soportadas y su aplicación en síntesis orgánica.

El especial interés en el uso del cobre se debe a que éste presenta muchas ventajas comparado con otros metales de transición. Una de estas es su precio, el cobre es mil veces más barato que el rutenio (el metal noble más económico). Además, el cobre presenta baja toxicidad en el cuerpo humano. Otra ventaja, y la que más interesa en química orgánica, es que el cobre presenta varias especies catalíticamente activas con diferente estado de oxidación. Al mismo tiempo, es compatible con la presencia de otros metales en el medio de reacción debido a su alta resistencia a la corrosión.

Teniendo en cuenta los antecedentes y la experiencia previa de nuestro grupo de investigación en este campo, en el **Capítulo 1** se describe la preparación de catalizadores basados en nanopartículas de cobre soportadas en titania (TiO_2), zeolita NaY (ZY) y carbón activo (C) empleando metales Rieke.

Esta estrategia consiste en la reducción de cloruro de cobre (II) anhidro con litio metálico en polvo y una cantidad catalítica del areno 4,4'-di-*terc*-butilbifenilo (DTBB), el cual se emplea como transportador de electrones. Las condiciones de reacción que se emplearon fueron: THF seco, temperatura ambiente y atmósfera de argón. En el proceso tiene lugar una transferencia electrónica del litio al areno, provocando la formación de un anión radical y/o del dianión correspondiente, generando una suspensión de tonalidad verde oscura. A continuación, se produce una transferencia electrónica por parte de estas especies hacia la sal metálica. Esta transferencia, que es muy rápida (10^6-10^9 $M^{-1}s^{-1}$), provoca la reducción de la sal y, como consecuencia, la formación de nanopartículas de cobre. La presencia de estas nanopartículas hace que la suspensión adquiera una coloración negra. Es en este momento en el que se adiciona el soporte inorgánico a la mezcla, seguido de filtrado, lavado y secado.

Una vez sintetizados, los catalizadores se caracterizaron empleando diferentes técnicas espectroscópicas y analíticas como: [a] plasma de acoplamiento inductivo con espectrometría de emisión óptica (ICP-OES), para conocer el contenido de cobre presente en el catalizador; [b] fisisorción de nitrógeno, aplicando la teoría de BET, para saber el área superficial; [c] espectroscopía de fotoelectrones emitidos por rayos X (XPS), para conocer la composición química y los estados de oxidación de las especies en superficie; [d]

fluorescencia de rayos X por energía dispersiva (EDX), para conocer la composición química en la superficie del catalizador; [e] microscopía electrónica de transmisión (TEM), a fin de conocer la distribución, el tamaño y la morfología de las nanopartículas metálicas en la superficie; y [f] difracción de rayos X (XRD), para conocer la composición del material y su estructura cristalográfica.

Los resultados obtenidos de los experimentos de EDX sobre varias regiones permitió confirmar la presencia de cobre en los diferentes soportes, con bandas de energía de 8.04, 8.90 KeV (líneas K) y 0.92 (línea L), además de las bandas características de cada soporte. En el caso de XRD, exclusivamente se observaron picos característicos de los soportes. Los resultados obtenidos a través del resto de técnicas se resumen en las Tablas 1 y 2.

Tabla 1. Resultados de los experimentos de TEM, ICP-OES y BET.

Entrada	Catalizador	Tamaño (nm)	Wt % Cu	BET (m^2/g)
1	NPsCu/TiO$_2$	0.98±0.42	1.90	119
2	NPsCu/C	5.95±0.95	3.50	1224
3	NPsCu/ZY	1.71±0.35	3.00	621

Tabla 2. Resultados de los experimentos de XPS.

Entrada	Catalizador	Energía de enlace (eV) Cu $2p_{3/2}$			relación
		Cu$_2$O	CuO	Satélites de Cu(II)	
1	NPsCu/TiO$_2$	932.6	934.4	940.3/943.8	Cu$_2$O > CuO
2	NPsCu/C	931.7	934.0	943.3	Cu$_2$O = CuO
3	NPsCu/ZY	932.6	934.6	941.5/944.1	Cu$_2$O = CuO

Toxicidad de los catalizadores

Para evaluar la citotoxicidad de nuestros sistemas catalíticos, se realizó un estudio comparativo con nanopartículas de cobre sin soportar. Este estudio biológico se llevó a cabo en colaboración con el grupo de investigación del Prof. Alexander V. Sirotkin (Constantine the Philosopher University in Nitra, Eslovaquia)

En este estudio se evaluó tanto el efecto de las nanopartículas no soportadas, como de las nanopartículas soportadas, en las funciones básicas de células ováricas de tejido porcino. En ese sentido, se analizó el efecto de la morfología (esféricas, triangulares y hexagonales) de las no soportadas y el sólido inorgánico (titania, zeolita y carbón activo) de las soportadas. Para ello, se llevaron a cabo experimentos de viabilidad celular, acumulación de PCNA (marcador de proliferación) y acumulación de BAX (marcador de muerte celular) empleando

microscopía y el test "Trypan blue". Por otro lado, se analizó la liberación de hormonas sexuales esteroideas (progesterona, testosterona y 17β-estradiol) empleando la técnica ELISA (acrónimo del inglés *Enzyme-Linked ImmunoSorbent Assay*: ensayos por inmunoabsorción de unión a enzimas).

Los resultados obtenidos a través de estas técnicas son bastantes prometedores en el campo de la reproducción. La viabilidad celular aumenta con la presencia de NPsCu, con la única excepción de las NPs hexagonales no soportadas. Las nanopartículas no soportadas con morfología triangular y las NPsCu/ZY mejoran la proliferación celular, mientras que las esféricas y hexagonales (no soportadas), junto con las NPsCu/TiO$_2$, no favorecen la acumulación de PCNA. En el caso de la apoptosis celular, todas las NPsCu reducen la acumulación de BAX, excepto las NPsCu/ZY y las hexagonales no soportadas. En general, la liberación de hormonas sexuales se ve favorecida por las NPsCu soportadas en ZY y C, mientras que se inhiben con TiO$_2$.

Las funciones básicas de las células ováricas de cerdo se vieron afectadas directamente por la morfología y el soporte de las NPsCu, por lo que un buen diseño de las NPsCu puede ser una herramienta útil para el control de procesos reproductivos.

Aplicación de metales de transición en química orgánica

En las últimas décadas, la catálisis con metales de transición para la formación de enlaces carbono-carbono (C-C) y carbono-heteroátomo (C-Het), a través de reacciones de acoplamiento cruzado, ha permitido superar muchas de las limitaciones que presentaban las reacciones clásicas. La importancia de este tipo de reacción se vio refrendada con la concesión del Premio Nobel de Química en 2010 a los profesores Heck, Negishi y Suzuki, por sus trabajos sobre las reacciones de acoplamiento cruzado catalizadas por paladio.

Dentro de las reacciones catalizadas por metales de transición, la formación de este tipo de enlaces es un área donde el cobre y el paladio compiten. Existen varios ejemplos en la bibliografía que emplean la catálisis heterogénea basada en complejos de cobre soportados, a través de la presencia de ligandos funcionalizados en la superficie, para reacciones de acoplamiento cruzado. Este tipo de sistemas catalíticos requieren la síntesis de ligandos especiales, una etapa de inmovilización de estos ligandos en la superficie del soporte y, finalmente, la formación del complejo con el cobre para obtener el catalizador final. En este sentido, el uso de NPsCu para catalizar este tipo de reacciones es una buena alternativa a los complejos inmovilizados, por la elevada relación superficie/volumen que poseen. Debido a su tamaño nanométrico es complicado separar estas NPsCu del medio de reacción. Por ese

motivo, soportarlas en sólidos inorgánicos no sólo favorece su estabilización y dispersión, si no que hace que sea sencillo poder recuperar el catalizador y reutilizarlo.

Acoplamiento cruzado catalizado por NPsCu para la formación de enlaces C-C, C-S y C-N

En el **Capítulo 2**, se emplearon los sistemas catalíticos descritos en el capítulo anterior para el estudio de reacciones de acoplamiento cruzado para la formación de enlaces C-C (reacción de Sonogashira-Hagihara), C-S (arilación de tioles) y C-N (arilación de azoles). Este trabajo se llevó a cabo en colaboración con el grupo de investigación de la Prof. Irina P. Beletskaya (Universidad Estatal de Moscú, Rusia).

Para evaluar la efectividad de nuestros catalizadores se estudió la influencia de los diferentes parámetros en las reacciones modelo de: 4-yodoanisol (**1a**) y fenilacetileno (**2a**) para la reacción de Sonogashira, 4-yodobenzonitrilo (**1c**) y tiofenol (**4a**) para la arilación de tioles y 4-yodobenzonitrilo (**1c**) e imidazol (**6a**) para la arilación de azoles. Con todos los resultados obtenidos se llegó a la conclusión de que las condiciones óptimas determinadas para cada reacción son:

- o Reacción de Sonogashira: NPsCu/ZY (4 mol%), alquino (1.50 equiv.), K_2CO_3 (2.00 equiv.), DMF (1 mL) a 120 ºC en argón.
- o Arilación de tioles: NPsCu/ZY (0.7 mol%), tiol (1.50 equiv.), en DMF (1 mL) y argón. Respecto a la temperatura, se utilizó 120 ºC para tiofenoles y 100 ºC para el resto de tioles. En el caso de la base, los mejores resultados se obtuvieron con K_2CO_3 (2.00 equiv.) para aromáticos y KOH (2.00 equiv.) para tioles alifáticos.
- o Arilación de azoles: NPsCu/TiO_2 (1.6 mol%), azol (1.20 equiv.), Cs_2CO_3 (2.00 equiv.), DMF (1 mL) a 120 ºC en argón.

Tras la optimización de las condiciones de reacción, los tres tipos de acoplamientos se han aplicado de manera exitosa a una gran variedad de productos de partida de diferente naturaleza. Además, un estudio comparativo reveló que nuestros catalizadores presentan mayor actividad catalítica que los catalizadores de cobre comerciales, empleando menor carga de metal.

La bioactividad que presentan los compuestos sintetizados en la arilación de tioles se está analizando actualmente a través de una colaboración con GlaxoSmithkline España, realizando pruebas *in-silico* e *in-vitro* en diferentes líneas celulares.

Resumen (Spanish summary)

En relación con la reciclabilidad de los sistemas, en todos los casos los catalizadores se han podido recuperar fácilmente y reutilizar en varios ciclos catalíticos sin pérdida aparente de la actividad catalítica.

Hay que tener en cuenta que la nanocatálisis se encuentra en la frontera entre la catálisis homogénea y heterogénea, lo cual hace más difícil determinar la naturaleza de esta. Para clarificar la naturaleza de nuestros catalizadores, se llevaron a cabo tests de filtración en caliente para ver si existía lixiviado del metal durante la reacción. Para ello se emplearon las reacciones modelos, descritas anteriormente, en cada uno de los acoplamientos. En esta ocasión, el calentamiento de la reacción se detuvo cuando la conversión al correspondiente producto final era menor del 20%. A continuación, se filtró el catalizador y el crudo de reacción resultante se volvió a calentar. En los tres acoplamientos, la conversión a producto final se mantuvo constante, y los crudos de reacción fueron analizados por ICP-MS dando una cantidad insignificante de cobre en disolución de 0.14%, 0.12%, 0.02%, para Sonogashira, arilación de tioles y de azoles, respectivamente.

Aunque estos experimentos apuntan a un proceso de naturaleza heterogénea, no se puede descartar del todo la posibilidad de que las especies metálicas que están en el soporte pasen a la disolución, catalicen la reacción y después se readsorban en el soporte. Este tipo de proceso se ha demostrado, sobre todo, en suspensiones de nanopartículas de metales de transición catalíticamente activos del grupo VIII. No obstante, recientemente, Scaiano y col. han utilizado la técnica de espectroscopía unimolecular para monitorizar una reacción de tipo click catalizada por NPsCu (que también involucra alquinos terminales) y han demostrado que la catálisis tiene lugar sobre la superficie de las NPs.

En base a los resultados obtenidos, se puede concluir que las NPsCu soportadas son catalizadores heterogéneos alternativos a los descritos de paladio. Además, son más baratos que éstos últimos y muestran comportamientos similares en este tipo de transformaciones.

Sin embargo, a pesar de este gran avance en la formación de enlaces C-C a través de acoplamientos cruzados, en general, estas metodologías implican una funcionalización previa de los materiales de partida y, por tanto, pasos adicionales de reacción. Además, comúnmente, durante el proceso de formación de los nuevos enlaces, los grupos funcionalizados preformados se pierden de manera simultánea, todo lo cual incrementa la cantidad de residuos y reduce la economía atómica y eficiencia del proceso.

Acoplamiento deshidrogenante cruzado catalizado por NPsCu para la síntesis de aminas propargílicas

Idealmente, un enlace C-C debería poderse generar por activación adecuada de dos enlaces C-H, lo cual se ha conseguido con catalizadores metálicos en presencia de un oxidante. Históricamente, la primera reacción que representa la formación de un enlace C-C a partir de dos enlaces C-H fue el homoacoplamiento de alquinos promovido por cobre, descrito por Glaser en 1869, y mejorado casi un siglo después por Eglinton y Hay. En 1993, Miura y col. publicaron la síntesis de *N*-metil-*N*-propargilanilinas por reacción de *N,N*-dimetilanilinas y alquinos terminales en presencia de cobre bajo atmósfera de oxígeno. Sin embargo, la reacción era poco selectiva, obteniéndose cantidades sustanciales de subproductos. Esta metodología fue mejorada por el grupo de Li utilizando hidroperóxido de *terc*-butilo como oxidante. Este grupo introdujo, en 2004, el concepto de acoplamiento deshidrogenante cruzado (CDC) como una poderosa herramienta sintética para el diseño de nuevas moléculas orgánicas por formación de enlaces C-C a partir de dos enlaces C-H de distintos sustratos de partida.

La inexistencia de estudios sobre catálisis heterogénea para llevar a cabo el CDC de alquinos y aminas en 2012 motivó al grupo del Prof. Alonso a estudiar la actividad catalítica de catalizadores basados en nanopartículas de cobre y su posible reutilización en este tipo de transformaciones.

Las aminas propargílicas son compuestos interesantes debido a la bioactividad que estas presentan. Se ha observado que muchas de ellas son activas como medicamentos para combatir los síntomas de la enfermedad de Parkinson, presentando una actividad neuroprotectora que provoca una desaceleración en la degeneración neurológica, a través de la inhibición de la monoamina oxidasa B. Algunos ejemplos de estos fármacos son la selegilina (Anipril ®) y la rasagilina (Azilect®), que se prescriben a pacientes para el tratamiento sintomático de la enfermedad en una etapa temprana o como terapia adyuvante en los casos más avanzados.

Para evaluar la efectividad de nuestros catalizadores en esta transformación, en el **Capítulo 3** se estudió la influencia de los diferentes parámetros en la reacción modelo de CDC de *N,N*-dimetilanilina (**8a**) y fenilacetileno (**2a**). Con todos los resultados obtenidos se llegó a la conclusión de que las condiciones óptimas determinadas para esta reacción son: NPsCu/ZY (1.5 mol%), alquino (1.2 equiv.), TBHP-H_2O (2 equiv.) a 70 ºC en aire. Estas condiciones se han aplicado con éxito a diferentes tipos de aminas y alquinos terminales, tanto aromáticos como alifáticos de diferente naturaleza electrónica. En general, los rendimientos han sido de moderados a excelentes, estando los primeros relacionados con la

presencia de grupos atrayentes de electrones en la amina de partida. Además, se ha propuesto el mecanismo de reacción en base a ensayos previos.

Por otra parte, la naturaleza heterogénea de este catalizador (con un lixiviado de cobre de 0.78 ppb) ha favorecido la reutilización del mismo en varios ciclos, sin pérdida aparente de la actividad catalítica. Además, el proceso se ha podido escalar con éxito (12 mmol).

Un estudio comparativo ha permitido concluir que el catalizador de NPsCu/ZY es superior a una serie de catalizadores de cobre comerciales, dando una mayor conversión del producto final y minimizando el homoacoplamiento del alquino.

La bioactividad que presentan estos compuestos se estudió a través del programa Lilly Open Innovation Drug Discovery (OIDD), realizando pruebas *in-silico* e *in-vitro* en diferentes líneas celulares. Se encontró que los productos **9da**, **9ea** y **9ia** son activos en diferentes líneas, siendo especialmente activos en la inhibición de la Arginasa.

Finalmente, se puede decir que el catalizador NPsCu/ZY es una alternativa interesante para la síntesis de aminas propargílicas a través de la reacción de CDC. Además, la facilidad de preparación del catalizador, la menor carga de metal, menor temperatura de reacción, no necesidad de atmósfera inerte y que la reacción se produzca en ausencia de disolvente, son algunas ventajas claras con respecto a otros catalizadores.

Acoplamiento deshidrogenante cruzado catalizado por NPsCu para la síntesis de dihidroindoloisoquinolinas

El interés en las dihidroindoisoquinolinas reside en sus aplicaciones en medicina. Estos compuestos son efectivos para el tratamiento de cáncer de pecho, debido a que inhiben la polimerización de la tubulina y ralentizan el crecimiento de las células cancerígenas. Además, estas moléculas se pueden encontrar en productos naturales como la cryptausolina y derivados, los cuales actúan como antifúngicos y agonistas melatoninérgicos.

En general, la síntesis de 5,6-dihidroindolo[2,1-*a*]isoquinolinas se lleva a cabo a través de ciclaciones intramoleculares de *N*-aril-1,2,3,4-tetrahidroisoquinolinas previamente funcionalizadas. Nuestro grupo de investigación decidió llevar a cabo la síntesis de estos compuestos a través del acoplamiento deshidrogenate cruzado entre *N*-aril-1,2,3,4-tetrahidroisoquinolinas y nitroalcanos, activando tres enlaces C-H para la formación de dos enlaces C-C en un único paso.

Para evaluar la efectividad de nuestros catalizadores, en el **Capítulo 4** se estudió la influencia de los diferentes parámetros en la reacción modelo de CDC de *N*-fenil-1,2,3,4-tetrahidroisoquinolina (**8h**) y nitroetano (**14a**). Con todos los resultados obtenidos se llegó a

la conclusión de que las condiciones óptimas determinadas para esta reacción son: NPsCu/TiO$_2$ (1.5 mol%), nitroalcano (2.4 equiv.) a 70 ºC en aire. Estas condiciones se aplicaron de manera exitosa a una gran variedad de materiales de partida de diferente naturaleza electrónica. Además, se propuso un mecanismo de reacción en base a varios experimentos de control.

Se llevaron a cabo estudios de recuperación y reutilización del catalizador, sin embargo, a diferencia de los acoplamientos anteriores, la reutilización de NPsCu/TiO$_2$ no fue eficiente. Para entender este comportamiento, se realizaron experimentos de XPS al catalizador reutilizado, pudiendo observar especies nitrogenadas adsorbidas en la superficie del catalizador, que pueden envenenar el catalizador y disminuir su actividad catalítica.

Un estudio comparativo con catalizadores de cobre comerciales pudo confirmar la superioridad de nuestro catalizador, corroborando que el tamaño nanométrico de las NPsCu/TiO$_2$ tiene un papel importante en esta transformación.

La bioactividad que presentan estos compuestos se está analizando actualmente en colaboración con GlaxoSmithkline España, realizando pruebas *in-silico* e *in-vitro* en diferentes líneas celulares.

Oxidación deshidrogenante de aminas cíclicas empleando fotocatálisis heterogénea

En el último año de la tesis, nuestra atención se fijó en el campo de la fotocatálisis heterogénea. Teniendo en cuenta la experiencia de nuestro grupo de investigación en la preparación de catalizadores de NPsCu/TiO$_2$, se decidió explorar su potencial para ser usados como fotocatalizadores en la oxidación de aminas cíclicas para la formación de sus correspondientes iminas.

Entre la amplia gama de aminas disponibles, nuestro grupo de investigación se centró en las 1,2,3,4-tetrahidroisoquinolinas (THIQs), debido a la estructura privilegiada que estas presentan y sus múltiples aplicaciones en química médica. Estos compuestos son efectivos en el tratamiento de enfermedades cardiovasculares, del sistema nervioso central, oncológicas y metabólicas, entre otras. Existen varios fármacos comercializados basados en estas moléculas como son: (a) Accupril™, que se utiliza en el tratamiento de la hipertensión; (b) Vesicare™ que actúa en el receptor muscarínico para el tratamiento de vejiga hiperactiva; (c) Merital/Alival™ que se utilizan como antidepresivos; (d) Yodelis™ para el tratamiento del sarcoma; y (e) Xiidra™ para el tratamiento de la enfermedad del ojo seco.

Resumen (Spanish summary)

Las iminas cíclicas derivadas de estas aminas han mostrado cierta actividad biológica como antimaláricos (como, por ejemplo, la Ancistrocladidina) y, además, son intermedios muy versátiles para la síntesis de THIQs con actividad biológica.

Respecto a la titania, ésta presenta tres estructuras activas en fotocatálisis; brookita (estructura ortorrómbica), anatasa (estructura tetragonal) y rutilo (estructura octaédrica). Estas dos últimas son las más estudiadas en fotocatálisis, empleando lo que se conoce como TiO_2 P25, que es una mezcla entre las estructuras anatasa y rutilo en una proporción 75/25, respectivamente. La interfase generada entre estructuras hace que la fase rutilo actúe como receptor de electrones, aumentando la distancia entre el electrón y el hueco generado, evitando la recombinación de estos. Evitar este proceso aumenta la capacidad catalítica del correspondiente fotocatalizador y por ese motivo la TiO_2 P25 es de las más utilizadas.

Para mejorar las propiedades de la titania, ésta se puede dopar con moléculas orgánicas o con metales. En base a la experiencia previa de nuestro grupo de investigación, se vio de interés el dopaje con metales. Este tipo de catalizadores puede ser útil en transformaciones orgánicas porque: (a) se preparan fácilmente a partir de materiales económicos; (b) presentan alta estabilidad al aire; (c) la elevada área superficial de estas NPs favorece los procesos SET (acrónimo del inglés *Single Electron Transfer*) en la superficie del catalizador; y (d) la variación en la morfología del soporte y el método de síntesis de las NPsCu permitirán modular los valores de "band gap".

En el **Capítulo 5**, se describe la oxidación deshidrogenante de 1,2,3,4-tetrahidroisoquinolinas (THIQs) para la formación de 3,4-dihidroisoquinolinas (DHIQs), empleando nuestros sistemas basados en nanopartículas metálicas soportadas en titania. Para llevar a cabo este estudio, se decidió realizar una estancia breve de tres meses en los laboratorios del Prof. J. C. Scaiano en la Universidad de Ottawa (Canadá), con el fin de adquirir experiencia en la aplicación de la fotocatálisis a nuestros sistemas catalíticos.

En primer lugar, se llevó a cabo la medida de los valores de "band gap" de nuestros sistemas empleando la espectroscopía de reflectancia difusa (DR, del acrónimo en inglés: *Diffuse Reflectance*). Los valores obtenidos a través de estos experimentos se resumen en la Tabla 3.

Tabla 3. Valores de "band gap" de los catalizadores basado en nanopartículas metálicas soportadas en titania.

Entry	Catalyst	λ (nm)	E_g (eV)
1	TiO_2 (P25 D-E)	397	3.20
2	NPsCu/TiO_2 (P25 D-E)	441	2.88
3	NPsCu/TiO_2 (P25 no D-E)	460	2.76
4	NPsCu/TiO_2 (anatasa 15 nm)	412	3.08
5	NPsCu/TiO_2 (anatasa 4 nm)	445	2.85
6	NPsMn/TiO_2 (P25 D-E)	441	2.88
7	NPsCuMn/TiO_2 (P25 D-E)	400	3.17
8	NPsCuNi/TiO_2 (P25 D-E)	475	2.67
9	NPsCuFe/TiO_2 (P25 D-E)	420	3.02

D-E = Degussa-Evonik.

Para evaluar la efectividad de nuestros catalizadores se estudió la influencia de los diferentes parámetros en la oxidación de 1,2,3,4-tetrahidroisoquinolina (**18a**). Con todos los resultados obtenidos se llegó a la conclusión de que la presencia de metal en el catalizador es innecesaria para esta transformación. Las condiciones óptimas determinadas para esta reacción son: TiO_2 (P25 D-E) (0.06 M), LED de 369 nm (0.14 W/cm^2), agua o acetonitrilo (2 mL) en aire. Actualmente se sigue estudiando el alcance, el mecanismo de la reacción y la reutilización del catalizador.

En base a estos resultados, se vio de interés estudiar la interacción existente entre la THIQ (**18a**) y la TiO_2. Para ello, se llevaron a cabo distintos experimentos de DR y de espectroscopía de infrarrojo por transformada de Fourier de reflectancia total atenuada (ATR-FTIR, acrónimo del inglés: *Attenuated Total Reflectance Fourier-Transform InfraRed Spectroscopy*), confirmando la presencia de **18a** en la superficie del catalizador. Cuando se analizaron los resultados de DR de los catalizadores, se pudo observar que el "band gap" más bajo, cuando se dopa con metales, era de 2.53 eV. Estos datos apuntan a la posible formación de un complejo de transferencia electrónica entre la THIQ y el TiO_2.

Debido a la posible formación de este complejo, se realizaron experimentos de control confirmando la fuerte interacción entre THIQ (**18a**) y la titania. Para saber qué cantidad de **18a** quedaba en la superficie del catalizador se realizaron experimentos de absorción y, con ayuda de la ecuación de Lambert-Beer, se pudo concluir que 0.009 de los 0.5 mmoles iniciales de **18a** se quedaban anclados en la TiO_2 tras finalizar la reacción.

Finalmente, se decidió evaluar las propiedades foto-físicas de las especies excitadas generadas en el medio de reacción. Para ello se empleó la técnica de fotólisis de destello láser conocido como LFP (acrónimo del inglés: *Laser Flash Photolysis*).

Resumen (Spanish summary)

LFP se engloba en las técnicas conocidas como "pump-probe", a través de las cuales se evalúa el comportamiento dinámico de intermedios reactivos y de estados excitados de los diferentes sustratos. En estas técnicas el "pump" es un láser que aplica un pulso corto (nanosegundos) que excita la molécula inicial generando las especies de interés, mientras que el "probe" permite realizar el seguimiento del comportamiento de las moléculas excitadas. Se puede pensar en los equipos LFP como espectrómetros UV-Visible con una respuesta rápida en la que la muestra se puede irradiar *in situ* a través de un haz de láser.

En primer lugar, se llevó a cabo la calibración del equipo utilizando una muestra conocida. En nuestro caso se utilizó 1-azaxantona. Una vez calibrado el equipo, se comprobó que la absorbancia de la muestra de THIQ (**18a**) estaba entre 0.3-0.4, para asegurarnos unos resultados fiables. Si la muestra estuviera más concentrada, veríamos las especies excitadas del estado basal y no estaríamos observando las transiciones deseadas.

Por otro lado, para saber qué longitud de onda emplear al analizar nuestra muestra, primero se llevaron a cabo experimentos de fluorescencia, obteniendo los correspondientes espectros de excitación y emisión. En estos espectros se pudo observar que el de emisión mostraba dos picos a 280 y 330 nm, correspondientes a los dos confórmeros que presenta esta molécula (axial y ecuatorial, en función de dónde se encuentre el hidrógeno), mientras que en el espectro de excitación solamente genera un pico cerca de 380 nm.

Con LFP también se llevó a cabo el estudio de fluorescencia de emisión, observando dos señales como en el caso de los experimentos realizados en el espectrofluorímetro. En base a los resultados obtenidos en ambos experimentos de fluorescencia, se decidió emplear 380 nm como longitud de onda de seguimiento.

Los experimentos de LFP se llevaron a cabo empleando el harmónico de 355 nm (Nd/YAG) como longitud de onda de excitación, con una potencia de 30 mJ y con las muestras previamente desgasificadas. La importancia de desgasificar las muestras reside en que las especies excitadas presentan una mayor vida media en atmósfera inerte, ya que el oxígeno singlete no colapsa el radical generado.

Finalmente, se obtuvo una cinética de pseudo-primer orden, obteniendo una constante de $1.03 \cdot 10^5$ s^{-1} y una vida media de las especies excitadas de la THIQ (**18a***) de 9730.1 ns. Sin embargo, los datos obtenidos no cuadran con los descritos en la bibliografía y esto puede deberse a que, en realidad, no estamos observando la especie triplete del sistema. Quizá, debido a la potencia del láser (30 mJ), se generan nuevas especies que han reaccionado entre ellas y el producto de esta reacción es lo que realmente se detecta o, simplemente, se está observando la especie singlete del material de partida.

Aparte de este experimento, se quiso evaluar el medio real de reacción, por lo que se estudió la suspensión generada en la reacción estándar (en presencia de TiO_2). Desgraciadamente, no se obtuvo ninguna señal en este caso, ni empleando la modalidad de transmisión (con una suspensión muy fina) ni la de DR (con una muestra sólida). La falta de señal se podría explicar por la capacidad de la titania para atrapar las especies excitadas generadas.

En base a estos resultados, es necesario realizar más experimentos para poder concluir de manera inequívoca qué especies están involucradas en el medio de reacción y cuáles son las propiedades foto-físicas de estas.

Conclusión general

A lo largo de esta tesis se ha podido observar que, en general, las nanopartículas de cobre se pueden considerar como catalizadores heterogéneos eficientes en diferentes reacciones orgánicas. En general, estos sistemas catalíticos han demostrado ser eficaces en la formación de enlaces C-C, C-S y C-N, a través de reacciones de acoplamiento, en la síntesis de aminas propargílicas y de dihidroindoloisoquinolinas, a través de reacciones de acoplamiento deshidrogenante cruzado.

Nuestros catalizadores de cobre soportados son fáciles de preparar, no son tóxicos, funcionan con baja carga de metal, la mayoría de ellos en aire y sin disolvente, suelen ser reciclables y siempre muestran mejor actividad catalítica que los catalizadores de cobre comerciales. Respecto al ultimo punto, este estudio respalda la extraordinaria actividad catalítica de las especies metálicas de tamaño nanométrico.

Además, empleando titania como soporte, se ha estudiado la oxidación deshidrogenante de tetrahidroisoquinolinas a dihidroisoquinolinas empleando activación fotoquímica. Sin embargo, en este caso parece que la transformación se ve promovida principalmente por el papel de la titania más que por el metal. En ese sentido, se necesita realizar más estudios para evaluar el alcance de estos sistemas nanométricos como fotocatalizadores heterogéneos en síntesis orgánica.

Finalmente, estas nanopartículas metálicas han demostrado ser herramientas útiles para la modulación de las funciones ováricas básicas, con una posible aplicación en el tratamiento de trastornos en reproducción.

Annex

Abbreviations list

Abs.	absorbance
AFM	Atomic Force Microscopy
ATR-FTIR	Attenuated Total Reflectance Fourier-Transform Infrared Spectroscopy
BAX	bcl-2-associated X protein
BDC	1,4-benzenedicarboxylate
BET	Brunauer-Emmett-Teller analysis
bpy	2,2-bipyridine
C	active carbon
Cat.	catalyst
CDC	cross-dehydrogenative coupling
CFL	compact fluorescent lamp
CNFs	carbon nanofibers
COD	cyclooctadiene
Cryo-TEM	Cryo-Electron Microscopy
CuNRs	copper nanorods
DAB	3,3'-diaminobenzidine
DABCO	1,4-diazabicyclo[2.2.2]octane
DDQ	2,3-dichloro-5,6-dicyano-1,4-benzoquinone
DHEA-S	dehydroepiandrosterone sulfate
DHIQ	3,4-dihydroisoquinoline
DMA/DMAc	*N,N*-dimethylacetamide
DMEM/F12	Dulbecco's modified eagle medium: nutrient mixture F-12

DMF	*N,N*-dimethylformamide
DMSO	dimethyl sulfoxide
DNA	deoxyribonucleic acid
DNPH	2,4-dinitrophenylhydrazine
DOPA	dopamine
dppe	1,2-bis(diphenylphosphine)ethane
DR	Diffuse Reflectance
DTBB	4,4'-di-*tert*-butylbiphenyl
dtbbpy	4,4'-di-*tert*-butyl-2,2'-dipyridyl
EDX	Energy-Disperse X-Ray Spectroscopy
Equiv.	equivalents
EXAFS	X-Ray Absorption Fine Structure
F(R)	function of reflectance
FTIR	Fourier-Transform Infrared Spectroscopy
GLC	Gas Liquid Chromatography
GO	graphene oxide
H$_2$TPP	tetraphenylporphirin
HAADF-STEM	High-Angle Annular Dark-Field Imaging
HAT	hydrogen atom transfer
HCS	hydrochar
HRTEM	High-Resolution Transmission Electron Microscopy
IBM	International Business Machines corporation
ICP	Inductively Coupled Plasma Spectroscopy
IgG	immunoglobulin G

IQ	isoquinoline
IRED	imine reductase
LDL	low-density lipoprotein
LDLR	low-density lipoprotein receptor
LED	light emitting diode
LFP	Laser Flash Photolysis
M	metal
MA	maleic acid
MAO	monoamine oxidase
MK-10	montmorillonite K10
MOF	metal organic framework
MS	Mass Spectrometry
MW	microwaves
MWCNTs	multiwalled carbon nanotubes
Nd:YAG	neodymium-doped yttrium aluminium garnet
NFkB	nuclear factor kappa B
NHC	N-heterocyclic carbene
NMR	Nuclear Magnetic Resonance
NPs	nanoparticles
OD	optical density
OES	Optical Emission Spectroscopy
OIDD	Open Innovation Drug Discovery
PANI	polyaniline
PBS	phosphate-buffered saline

PCN-222	2,7-bis-(*N*-carbazolyl)-9-fluorenone hypercrosslinked polymer
PCNA	proliferating cell nuclear antigen
PCSK9	proprotein convertase subtilisin kexin type 9
PP	2-{[(piperazin-1-ylmethyl)imino]methyl}phenol
ppb	parts per billion
ppy	2-phenylpyridine
RGO	reduced graphene oxide
RIA	radioimmunoassay
SAED	Selected Area Electron Diffraction
SD	standard deviation
SEM	Scanning Electron Microscopy
SET	single-electron-transfer
SMNP	solid microporous nanoparticle
STEM	Scanning Transmission Electron Microscopy
STEM-EELS	Electron-Energy Loss Spectroscopy
TBHP	*tert*-butyl hydroperoxide
TEM	Transmission Electron Microscopy
TEMPO	2,2,6,6-tetramethylpiperidine-1-oxyl
THF	tetrahydrofuran
THIQ	tetrahydroisoquinoline
TiO$_2$	titania
TiO$_2$ P25	titania anatase/rutile 75/25
TMEDA	*N,N,N',N'*-tetramethylethylenediamine
WHO	The World Health Organisation's

XANES	X-Ray Absorption Near Edge Structure
XAS	X-Ray Absorption Spectroscopy
XPS	X-Ray Photoelectron Spectroscopy
XRD	powder X-Ray Diffraction
ZY	sodium zeolite-Y
IL-17 PPI	interleukin 17 protein-protein interaction
MTB	mycrobacterium tuberculosis
NNMT	nicotinamide *N*-methyltransferase